UNIVERSITÀ DEGLI STUDI FIRENZE

PhD in
Physics and Astronomy

CYCLE XXXVIII

COORDINATOR Prof. Giovanni Modugno

Applications of the holographic correspondence to QCD-like theories

Academic Discipline (SSD) FIS/02, PHYS-02/A

Doctoral Candidate
Dr. Andrea Olzi

Andrea Olzi

Supervisor
Prof. Aldo L. Cotrone

Aldo Lorenzo Cotrone

Co-supervisor
Prof. Francesco Bigazzi

Francesco Bigazzi

Coordinator
Prof. Giovanni Modugno

Giovanni Modugno

To my family,
in all the people who embody it for me.

Acknowledgments

I would like to express my deepest gratitude to my supervisors, Aldo and Francesco. Much of what I have learned, and whatever value this work may hold, I owe to them. Since the time of my master's thesis, they have guided me with unwavering support, kindness, and patience. Working with them has been a privilege not only from a scientific perspective but also from a personal one. I feel truly fortunate to have met them, and I am confident that the bond we have built will endure well beyond my time in Florence.

I am also profoundly grateful to Carlos Hoyos, who, especially in the past year, has become like an additional supervisor to me. Thanks to him, I had the opportunity to visit the University of Oviedo and collaborate closely with him. From our very first meeting, he made me feel at ease, sharing not only his ideas but also his enthusiasm for research. Over time, I have learned an enormous amount from him, not only in terms of physics but also in how to approach problems with patience and clarity. I will always value his generosity, his guidance, and the time he dedicated to answering my countless (and often rather naïve) questions.

I am indebted to Carlos as well for introducing me to Niko Jokela, who warmly welcomed me in Helsinki. Despite the harsh winter cold, my time there was deeply enriching, both scientifically and personally. Working with Niko and being part of such a vibrant academic environment was a truly valuable experience.

I also had the pleasure of spending two months at King's College London, thanks to the kind hospitality of Damian Galante. He offered me the opportunity to engage in active research on a topic outside my main expertise, generously sharing his vast knowledge with me.

Finally, I wish to thank all the colleagues with whom I have exchanged ideas along the way, as each of them has contributed to shaping me into a better researcher. Among them, Federico Castellani holds a very special place. Since our bachelor's studies, we have walked side by side on this academic journey. It has truly been a wonderful adventure.

Then, in alphabetical order, I want to thank Evangelos Afxonidis, Dionysios Anninos, Alvaro Arboleya, Giulio Barni, Alice Bernamonti, Ignacio Carreño Bolla, Alessio Caddeo (best postdoc ever), Stefania Caggioli, Andrea Cappelli, Andrea Conti, Stefano Gagliani, Federico Galli, Mauro Giliberti, Lorenzo Giombi, Eduardo Grossi, Adolfo Guarino, Oscar Henriksson, Matti Jarvinen, Patrick Messen, Marina Moleti, Matteo Morittu, Daniele Musso, Niall Macpherson, José Manuel Penin, Aleksi Piispa, Natalia Pinzani Fokeeva, David Rodríguez Fernández, Daniele Roselli, Jean-Loup Raymond, Michele Redi, Lorenzo Russo, Domenico Seminara, Andrea Tesi, and Riccardo Villa.

To all, I look forward to seeing you again along the way.

Abstract

Quantum chromodynamics (QCD) is the fundamental theory describing the strong interactions between quarks and gluons. Its distinctive properties, asymptotic freedom at high energies and confinement at low energies, make it a paradigmatic example of a theory whose ultraviolet and infrared regimes require qualitatively different tools. While perturbation theory and lattice simulations have provided powerful insights, many questions remain unsolved in regimes of strong coupling, finite temperature and density, and real-time dynamics. In this context, holography offers a complementary approach: by mapping certain strongly coupled field theories to weakly coupled gravitational descriptions, it provides a controlled framework to explore non-perturbative dynamics.

This thesis addresses two problems at the intersection of QCD and holography. The first concerns the description of baryons in one-flavored QCD. Unlike the multi-flavor case, where baryons emerge as solitons of the chiral Lagrangian, the single-flavor theory lacks the symmetry structure required for this construction. Building on proposals that interpret baryons as quantum Hall droplets, *i.e.* (2+1)-dimensional excitations of the η' meson charged under the baryonic symmetry, we provide an explicit realization within the Witten-Sakai-Sugimoto (WSS) model. These extended objects, namely *Hall droplet sheets*, are constructed as D6-branes embedded in the WSS model. Their charged configurations yield a holographic description of single-flavor baryons, whose masses, radii, and spin-baryon number relations can be computed. We further extend this framework to related topological defects such as axionic strings, domain walls, vortons, and exotic composite configurations, some of which have potential cosmological implications, including novel dark matter candidates.

The second problem addressed in this thesis concerns weak interaction rates in dense, strongly coupled quark matter, which is expected to be present in neutron star cores. These rates determine how quickly dense quark matter restores equilibrium and dissipates energy, which is crucial for the damping of stellar oscillations and for the long-term stability of rapidly rotating stars. Conventional perturbative estimates are restricted to weak coupling and uncertain in astrophysical regimes. We derive a non-perturbative expression for the weak rates in terms of correlators of gauge-invariant operators. Within a bottom-up holographic model of massless quark matter, we compute their leading low-temperature behavior at large density, uncovering qualitative deviations from perturbative predictions, including logarithmic suppression at high chemical potential.

In summary, this thesis demonstrates how holography can shed new light on open problems in QCD. On the one hand, it provides a framework for the low-energy description of baryons in one-flavor QCD and their potential dark sector relatives. On the other hand, it provides a first step toward non-perturbative determinations of weak interaction rates in dense quark matter, relevant for neutron star phenomenology. Together, these results highlight the versatility of holographic methods in addressing strongly coupled phenomena beyond the reach of traditional approaches.

Contents

Introduction

This thesis is based on the original research results obtained in [1, 2, 3, 4, 5, 6]. Before focusing on the latter, we will provide the reader with an introduction to the related scientific context and tools, with the further aim to situate our research works in the modern landscape of high-energy theory. We begin from first principles and progressively move towards the specific problems that motivated our research. The two problems treated in the original papers collected in this thesis are

- the low-energy description of baryons in single-flavor quantum chromodynamics (QCD),
- the computation of weak interaction rates in strongly coupled cold quark matter.

In order to motivate these problems and explain the methods used in our works, it is necessary to recall several central ideas in QCD, the physics of matter at finite temperature and baryon density, and several core ideas from string theory and gauge/gravity duality.

Quantum chromodynamics is the quantum field theory describing the strong interactions between quarks and gluons. The theory is asymptotically free [7, 8, 9, 10]: at high energies, the gauge coupling becomes small and perturbative techniques are applicable. The same theory is, however, confining at low energies [11, 12]: asymptotic states are always color singlets. As a consequence, quarks and gluons cannot exist freely but are confined into color singlets: hadrons (mesons and baryons). Asymptotic freedom and confinement together make QCD an example of a theory whose ultraviolet (UV) and infrared (IR) behaviors are qualitatively different, and which therefore requires very different theoretical tools in the two regimes. Moreover, many of the most interesting phenomena of QCD, like mass gaps, chiral symmetry breaking, hadron structure, and bound states, are inherently non-perturbative and require methods beyond perturbation theory.

In the last decades, several non-perturbative methods were developed to study QCD at low energies, where it becomes strongly coupled. Lattice gauge theory, *i.e.* Wilson's formulation of gauge theories on an Euclidean spacetime lattice [11], provides a first-principles, systematically improvable tool to compute the static properties of QCD and its equilibrium thermodynamics using Monte Carlo simulations; it has been extremely successful at computing hadron spectra, the QCD equation of state at vanishing baryon density, and many thermodynamic observables. Effective field theories and model approaches, *e.g.* chiral perturbation theory, capture the low-energy and symmetry aspects of QCD and provide analytic control in particular regimes [13, 14]. Large-N methods provide a systematic framework to study non-perturbative aspects of QCD by considering a generalization of the theory in which the number of colors, N, is treated as a (large) free parameter [15]. In the large-N limit, one can identify a natural organization of hadronic spectra and interactions in powers of $1/N$, providing both qualitative and quantitative insights into the spectrum of mesons and baryons, and the emergence of topological structures, *e.g.* solitons. For instance, baryons can be interpreted as solitonic objects in the large-N limit, and meson couplings scale with definite powers of $1/N$ (for instance, meson decay amplitudes scale as $1/\sqrt{N}$ and meson–meson scattering amplitudes as $1/N$), giving a controlled approximation scheme for otherwise strongly coupled dynamics [16, 17].

Despite these successes, several serious limitations remain. Perturbation theory breaks down (well) above the QCD dynamical scale $\Lambda_{\mathrm{QCD}} \approx 200$ MeV since the gauge coupling constant becomes large. Lattice techniques are very powerful for Euclidean (imaginary-time) observables at zero chemical potential, but they confront severe obstacles when one attempts to simulate QCD at non-zero baryon chemical potential due to the infamous sign problem [18]. The sign problem is not merely a technicality, but a fundamental obstruction to Monte Carlo approaches, and no general solution is currently known. Effective models can capture aspects of the QCD phase diagram and hadronic physics, but they necessarily involve model-dependent assumptions and parameters that cannot be systematically improved from first principles.

String theory was first introduced in the late 1960s as an attempt to describe the strong interactions, inspired by the pattern of hadronic resonances observed experimentally. In particular, the masses and spins of mesons and baryons were found to approximately lie on linear Regge trajectories, hence indicating the occurrence of a linear relation between the angular momentum and the squared mass of these particles. The Veneziano amplitude [19] provided an explicit analytic expression for a four-point scattering amplitude that exhibited crossing symmetry and the expected Regge behavior, effectively reproducing the spectrum of observed resonances. This success led to the interpretation of hadrons as excitations of one-dimensional extended objects, *i.e.* strings, and to the development of the bosonic string model.

In spite of these initial successes, bosonic string theory encountered severe theoretical problems. The spectrum included an unphysical tachyon, signaling an instability, and the consistency of the quantum theory required 26 spacetime dimensions. Moreover, the subsequent formulation of QCD as the fundamental theory of strong interactions in the early 1970s provided a more accurate and predictive description of hadronic physics. As a result, string theory was no longer pursued as a model of hadrons, but the mathematical structures developed in this context became the foundation of modern string theory, which includes gravity and gauge interactions in a unified quantum-consistent framework; see *e.g.* [20, 21].

In its modern formulation, string theory is a consistent quantum theory of one-dimensional extended objects (strings) whose vibrational modes correspond to particles of different spins and charges. Remarkably, the spectrum automatically contains a massless spin-2 excitation, which can be interpreted as the graviton, thereby providing a quantum-consistent framework for gravity. Together with the other modes corresponding to gauge fields and matter fields, this makes string theory a candidate for a unified theory of all fundamental interactions.

Holography emerged from this string-theoretic framework as a realization of the idea that a quantum field theory in flat spacetime can be equivalently described in terms of a quantum gravity theory in at least one higher dimension. This correspondence is perhaps one of the strongest realizations of the *holographic principle*, first proposed in [22, 23], which states that the information about the spectrum and dynamics of a theory of quantum gravity inside a volume V is encoded in the degrees of freedom residing on the boundary ∂V. The first (and best understood) concrete example of holography is provided by the AdS/CFT correspondence first proposed by Maldacena in [24], and further elucidated in [25, 26]. This correspondence establishes a duality between (a certain version of) string theory on Anti-de Sitter spacetime (AdS) and a Conformal Field Theory (CFT) on the boundary of the AdS spacetime. Subsequent works established the explicit dictionary between boundary field theory operators and bulk fields, relating correlation functions, symmetries, and a variety of non-perturbative phenomena to corresponding objects on the gravity side.

The holographic correspondence realizes a strong-weak duality: certain strongly coupled regimes in the quantum field theory side turn out to be mapped into weakly interacting, low-energy regimes of the dual string description, where the latter effectively reduces to a classical theory of gravity. This makes holography particularly appropriate to attack the problems outlined at the beginning of this introduction. On the one hand, holographic models provide a framework in which strongly coupled phenomena of quantum field theories, like hadronic physics, can be studied using geometric and semiclassical tools. In particular, baryons appear as localized topological configurations whose properties, such as masses and couplings, can be computed within the holographic setup [27, 28]. On the other hand, holography gives direct access to *e.g.* spectral functions and real-time response, at finite temperature and finite density, by solving linearized fluctuation equations in a black hole geometry, which is often much simpler than analytically continuing noisy Euclidean lattice data [29, 30].

The original AdS/CFT correspondence applies strictly to supersymmetric and conformal theories, which differ substantially from QCD. The latter is neither supersymmetric nor conformal, and instead displays phenomena such as confinement, chiral symmetry breaking, and the emergence of a rich hadronic spectrum. To approach such a theory holographically, various extensions of the original correspondence have been developed. On the one hand, "top-down" constructions [31, 32, 33] are derived from explicit string theory backgrounds and can incorporate ingredients such as flavor degrees of freedom or deformations that break conformal invariance, producing models with confinement and chiral symmetry breaking. On the other hand, "bottom-up" approaches [34, 35, 36, 37] adopt a more phenomenological perspective, in which effective gravitational actions are engineered to reproduce the salient features of QCD, such as confinement, phase diagram, or hadronic spectra. Generally, one considers holographic theories dual to "QCD-like theories" intended as non-Abelian gauge theories with fundamental flavors that share non-perturbative features with QCD, even if they do not reproduce all of its quantitative details. In both top-down and bottom-up frameworks, the large N (with N being the rank of the non-Abelian gauge group of the dual QCD-like theory) and large gauge coupling limits play a central role, allowing for the validity of the classical gravitational dual and providing a natural organizing principle for the strongly coupled dynamics.

Through these developments, holography has evolved into a powerful toolkit for investigating QCD-like theories beyond the reach of perturbation theory or lattice simulations.

The first part of the thesis collects the original contributions from [1, 2, 3, 5, 6]. These research works are motivated by the following puzzle in low-energy QCD. In the standard low-energy description valid for N_f light flavors, baryons can be described as topological solitons (Skyrmions) of the chiral Lagrangian. However, in the case of one flavor, $N_f = 1$, this description fails: there are no pionic $\mathrm{SU}(N_f)$ degrees of freedom to support a Skyrmion, and it is not possible to write down a conserved baryon current. Therefore, an alternative low-energy description of the baryon is required.

At low energies, in the large-N limit, one-flavored QCD is not a trivial theory: there is a light particle, namely the η' meson. It is a periodic field, being the phase of the chiral condensate, and its physics is described by the chiral Lagrangian. In [38], it has been shown that in the infrared of one-flavored QCD, there are extended, (2+1) dimensional excitations of the η' particle, charged under a topological generalized symmetry. These objects are called *sheets* and they are metastable in the large-N limit, so it makes sense to study the effective field theory living on their worldvolume. In [38], following the ideas of [39], it has been argued that the effective field theory living on their worldvolume is a $\mathrm{U}(1)_N$ Chern-Simons (CS) theory. Remarkably, this is the effective field theory that describes the bulk physics of a fractional quantum Hall state. Then, the sheets (with finite radius) can be interpreted as baryons by coupling the baryon gauge field to the CS theory on the sheet. Indeed, this coupling is precisely like the coupling of the electromagnetic gauge field to the emergent gauge field in the fractional quantum Hall effect (FQHE). This way, the so-called *Hall droplet sheets* provide an alternative description of one-flavored baryons in low-energy QCD at large N. Several expected properties of baryons have been derived from these premises, yet precise quantitative statements are, as usual, difficult to achieve from purely effective descriptions [40, 41, 42, 43, 44, 38, 45, 46, 47, 48, 49, 50, 51, 52]. In particular, the η' potential arises non-perturbatively from gluon dynamics and is generally non-analytic, which makes semiclassical approximations subtle and potentially unreliable.

In this thesis, we provide an explicit realization of this idea within the Witten-Sakai-Sugimoto (WSS) model [31, 32, 33], which is the top-down holographic model that better resembles QCD in the planar limit and in the low-energy, strongly coupled regime. It is constructed by compactifying type IIA string theory with N D4-branes on a spatial circle with antiperiodic boundary conditions for fermions, which breaks supersymmetry and generates confinement at low energies. Chiral quark flavors are introduced via pairs of D8 and $\overline{\mathrm{D8}}$ branes, whose geometric embedding in the background enforces spontaneous chiral symmetry breaking. The resulting set-up provides a unified holographic framework that naturally incorporates mesons, baryons, and glueballs, and has been widely used as a qualitative laboratory for non-perturbative QCD phenomena. First, we constructed the Hall droplet sheets in terms of D6-branes embedded in the one-flavored WSS model [1]. These are wrapped on the background S^4, and extended along (2+1) Minkowski directions. After the reduction on the four-sphere, the expected $\mathrm{U}(1)_N$ CS theory naturally arises on the D6-brane worldvolume. We focused on two relatively simple configurations: the infinite sheet and the semi-infinite sheet with a straight boundary on the flavor brane. The holographic framework allowed us to compute several properties of the sheets, like their tension and thickness. Moreover, the spatial profile of the η' meson, associated with the flavor gauge field sourced by the D6-brane, has been determined for both configurations.

In [6], we provided a first-principle construction of baryons as quantum Hall droplets in the WSS model. These are described again in terms of a wrapped D6-brane, which now has a circular boundary on the flavor brane and, therefore, has a disk-like profile in the Minkowski directions. In order to describe a (meta)stable baryon as a quantum Hall droplet, it is necessary to consider charged configurations under the baryonic symmetry. This corresponds to considering a D6-brane with a non-trivial electromagnetic field on its worldvolume. Such a configuration carries a non-zero baryon number n_B, and a non-zero spin J. In particular, we focused on configurations such that $J = N\, n_B^2/2$ (as in the standard FQHE), which reduces to the expected relation $J = N/2$ for the elementary $n_B = 1$ one-flavored baryon made by N quarks with aligned spins. The baryon physical properties, like the energy and the stability radius, were computed within the holographic model, revealing agreement with the field theory expectations.

In [2, 5, 6], we employed a similar brane setup to describe models of so-called cosmic topological defects. We considered the WSS model at high temperature as the holographic dual of a completely hidden sector composed of an $\mathrm{SU}(N)$ gauge theory coupled with a single massless flavor in a cosmological scenario. At low energies, the effective theory is described by an axion-like particle resulting from the spontaneous breaking of the axial $\mathrm{U}(1)_A$ flavor symmetry. As the Universe cools below a critical temperature, the chiral symmetry is broken, and non-trivial vacuum configurations form, resulting in the creation of topological defects such as cosmic strings and domain walls. In the above-mentioned works, we realized in terms of D6-branes various topological defects: the straight axionic string, the string loop, and the domain wall. In particular, we showed the presence of a first-order phase transition separating the string loop from the domain wall solution. Then, we studied their charged version by turning on an electromagnetic field on the D6-brane worldvolume, and imposing the anyonic relation $J = N\, n_B^2/2$. The charged string loop, *i.e.* the vorton, has been studied in terms of fields living on the D6-brane worldvolume, finding that there are no metastable vortons unless they carry a huge charge in terms of the parameters of the theory ($n_B \sim \lambda$, with λ the 't Hooft coupling). The charged domain wall, described by a D6-brane with a circular boundary on the flavor brane, corresponds to a dark Hall droplet baryon and in this cosmological scenario represents a new candidate of dark matter recently predicted in [2] as the *axionic-baryon* (a-baryon). In [6], we enriched the zoo of topological defects by studying more exotic objects like the “sandwich vortons”, described by a D6-brane ending, with a circular boundary, on two flavor branes; and the infinite domain walls with a hole. In addition, in [2, 5], we provided an effective description in terms of degrees of freedom living on the flavor brane, *i.e.* mesonic modes, of the charged straight string and vorton.

The second part of the original content of the thesis is devoted to presenting the original work [4]. The physical systems that motivated this study are the neutron stars, which are the remnants of old massive stars that undergo a supernova explosion and a subsequent gravitational collapse [53]. They provide a unique laboratory to study matter under extreme conditions. As a matter of fact, neutron stars probe the high-density and low-temperature portion of the QCD phase diagram, as they are made of cold nuclear matter and (perhaps), in the core, cold quark matter [54, 55, 56]. Among all the interesting aspects to study, we focused on the role played by the weak interactions.

Weak interactions are essential in shaping the physics of neutron stars and their binary mergers. The stellar equation of state, which governs the mass–radius relation, is constrained by the requirement of beta-equilibrium. This condition fixes the balance among the abundances of different quark (or baryon) and lepton species. If the density of the star is perturbed so that matter is driven out of beta-equilibrium, weak processes act to restore equilibrium and, in doing so, damp the perturbation. The associated dissipation manifests itself as an effective bulk viscosity, which is strongly amplified when the oscillation period of the perturbation matches the relaxation timescale set by the weak interaction rates at a given density [57, 58, 59, 60, 61, 62, 63, 64, 65, 66, 67]; see [68] for a review of transport in neutron stars. Oscillations of a rotating neutron star produce gravitational waves that cause the star to lose angular momentum and spin down, a process that is more pronounced for rapidly rotating stars. Despite this, fast-rotating pulsars with periods on the order of milliseconds are observed within a limited range of temperatures. Bulk viscosity induced by beta equilibration is a leading candidate to explain this "stability window" [69, 70, 71]. Moreover, this viscosity influences not only the continuous gravitational wave emission of isolated stars [72], but also the gravitational wave signal from binary neutron star inspirals [73] and the complex post-merger dynamics [74, 75, 76, 77, 78, 79, 80].

At the densities involved in the core of neutron stars, where quark matter is expected to be present, QCD cannot be reliably treated within perturbation theory, and lattice simulations are obstructed by the sign problem. This motivates the use of alternative non-perturbative methods. Holographic approaches provide one such framework and have been applied to the study of dense matter in neutron stars (see [81, 82] for recent reviews). In particular, the bulk viscosity generated by weak interactions was investigated holographically in [83]. However, the bulk viscosity formula involves weak interaction rates, which so far have been computed only perturbatively. As a result, the approach is not fully self-contained. Moreover, existing perturbative formulas are based on tree-level scattering amplitudes of quarks and leptons [84, 85, 86], and a key property of the bulk viscosity, that is its temperature dependence, is especially sensitive to the microscopic behavior of these rates. This introduces a significant source of uncertainty in current estimates. In [4], we proposed a step toward reducing this uncertainty by providing a non-perturbative expression for the weak rates in terms of correlators of gauge-invariant operators. Using this formalism, we evaluated the temperature dependence of the rates in a simple bottom-up holographic model of unpaired (massless) quark matter [34]. Within this framework, we obtained the leading-order low-temperature behavior of the weak reaction rate in dense, strongly coupled matter at beta-equilibrium. A comparison with perturbative results [84, 85, 86] revealed qualitative differences, most notably a logarithmic suppression of the rate at large μ_q/T, where μ_q denotes the quark chemical potential.

The thesis is organized as follows. In the first part, we provide an introduction to the relevant topics covered in this manuscript. In chapter 1, we discuss some aspects of QCD in the non-perturbative regime. In particular, we show that at low energies, in the large-N limit, the theory can be described in terms of weakly interacting mesons, where baryons arise as topological solitons. Then, we briefly discuss the phase diagram of QCD at finite temperature and finite baryon chemical potential. Finally, we introduce neutron stars and their main characteristics, focusing on the role played by weak interactions.

In chapter 2, we present in more detail the problem of finding a low-energy description of baryons in one-flavored QCD. This chapter is mainly based on the article [38].

Chapter 3 gives a short introduction to string theory and the holographic correspondence, focusing on applications to large-N models of QCD. This is far from being a comprehensive review of the topic, but rather a summary of the key points we will use in the following.

The thesis is then divided into two parts associated with the two topics presented at the beginning of this introduction. The first part, covered by the chapters 4, 5, 6, and 7, addresses the problem of finding a holographic description of the one-flavored baryon in terms of a Hall droplet sheet. The second part, which contains the chapters 8 and 9, focuses on the computation of the weak rates in strongly coupled cold quark matter using a bottom-up holographic model.

Chapter 4 represents the first step of the quest for finding the holographic dual of the Hall droplet baryon, and is based on [1]. The holographic construction of the Hall droplet sheet in terms of a D6-brane is presented, and two explicit configurations (the infinite sheet and the semi-infinite sheet with a straight boundary) are analyzed in detail. Chapter 5 is based on [2, 5] and discusses the holographic realization, within the WSS model, of topological defects such as cosmic strings and domain walls. This part of the thesis ends with chapter 6, based on [6]. Here, we present the construction of baryons as quantum Hall droplets as D6-branes in the single-flavor WSS model, both in the confined and in the deconfined phase. The holographic description allows us to calculate precisely their properties, such as mass and size. We also consider other objects with baryonic charge, such as vortons, domain walls with holes, and "sandwich vortons". We conclude by discussing the relative (meta)stability of the various configurations.

Chapter 7 provides a summary and some concluding remarks regarding the original contributions collected in the chapters 4, 5, and 6. We conclude with some future directions.

In chapter 8, based on [4], we derive the formulas for the weak equilibration rate of quark flavor densities to leading order in the Fermi coupling. Then we use the holographic model [34] to compute explicitly the leading order low-temperature behavior of the weak reaction rate in a large-density state of strongly coupled (massless) matter at beta-equilibrium.

Finally, in chapter 9, we summarize the results of chapter 8 and we compare them with the perturbative result for weak rates already present in the literature. We conclude with a few possible outlooks.

Supplementary material, together with technical details, can be found in the appendices A, B, C, D, E, F, and G.

Chapter 1

Some non-perturbative aspects of QCD

In this chapter, we are going to briefly review some important aspects of Quantum chromodynamics in its non-perturbative regime. After a short introduction to the theory in section 1.1, we discuss the low-energy limit of QCD, showing that in the large-N limit, it reduces effectively to a theory of weakly interacting mesons. This is the content of section 1.2. Then, in section 1.3, we discuss the appearance of baryons as solitons in the meson effective field theory. In section 1.4, we discuss the role of axion particles in low-energy QCD and in QCD-like theories where they are usually called axion-like particles (ALPs). We conclude with section 1.5 in which we review the QCD phase diagram and explain the importance of neutron stars in this context.

1.1 The theory of strong interactions

Quantum chromodynamics is the quantum field theory that describes the interaction, mediated by particles known as gluons, between elementary particles called quarks. At sufficiently low energies, it is responsible for the force that makes hadrons (baryons and mesons) bound states of quarks.

QCD is a Yang-Mills theory, a SU(3) gauge theory, with fermionic matter fields, Dirac fermions, transforming in the fundamental representation of the gauge group. The gauge bosons of the theory are identified with the gluons, while the Dirac fermions are known as the quarks, and they can be in N_f different species, called flavors. In real-world QCD, there are $N_f = 6$ different flavors known as *up, down, charm, strange, top, and bottom.*

The QCD Lagrangian, up to gauge fixing terms, reads

$$\mathcal{L}_{\text{QCD}} = -\frac{1}{2g_{\text{YM}}^2}\text{tr}\left(F^{\mu\nu}F_{\mu\nu}\right) + \sum_{i=1}^{N_f}\bar{q}_i\left(i\not{D} - m_i\right)q_i, \tag{1.1}$$

where $F_{\mu\nu} = \partial_\mu A_\nu - \partial_\nu A_\mu + i[A_\mu, A_\nu]$ is the SU(3) field strength, $D_\mu = \partial_\mu + iA_\mu$ is the covariant derivative in the fundamental representation of the gauge group, acting on the quark fields q_i, and $\not{D} = \gamma^\mu D_\mu$, with γ^μ is the four-dimensional Dirac matrix.

The SU(3) gauge connection A is the gluon field and, like a Lie algebra-valued one-form, it transforms under the adjoint representation of the gauge group: $A_\mu = A_\mu^a T^a$ where $a = 1, \dots, 8$ is the color index and T^a are the generators of the group. The QCD Lagrangian is invariant under the SU(3) color gauge transformations

$$q_i \to \mathcal{U}(x) q_i, \qquad A_\mu \to \mathcal{U}(x) A_\mu \mathcal{U}^\dagger(x) + i\, g_{\mathrm{YM}} \partial_\mu \mathcal{U}(x) \mathcal{U}^\dagger(x), \tag{1.2}$$

where $\mathcal{U}(x) \in \mathrm{SU}(3)$.

The theory of strong interactions is renormalizable, and we can compute the beta function of the theory at small coupling (one-loop)

$$\beta(g_{\mathrm{YM}}) = \mu \frac{d}{d\mu} g_{\mathrm{YM}} = -\frac{g_{\mathrm{YM}}^3}{(4\pi)^2}\left(11 - \frac{2N_f}{3}\right) + \mathcal{O}(g_{\mathrm{YM}}^4), \tag{1.3}$$

where μ is the energy scale. This leads to the well-known running of the strong coupling constant, defined as $\alpha_s = g_{\mathrm{YM}}^2/(4\pi)$

$$\alpha_s(\mu) = \frac{\alpha_s(\Lambda_{\mathrm{UV}})}{1 + b_0\, \alpha_s(\Lambda_{\mathrm{UV}}) \log\left(\mu^2/\Lambda_{\mathrm{UV}}^2\right)}\,, \tag{1.4}$$

where Λ_{UV} is the UV cutoff scale and $b_0 = 11 - 2N_f/3$, which is positive for $N_f = 6$. This expression of the running coupling constant accounts for a key feature of QCD, known as *asymptotic freedom* [7, 8, 9, 10]: the coupling constant approaches zero at high energies (or short distances), implying that the theory is weakly coupled in such a regime. Therefore, it is consistent to use perturbative methods to study quantum corrections. On the contrary, it is much more difficult to study the theory at large distances where the coupling constant becomes very large, since the beta function (1.3) is valid only when the coupling constant is small compared to one.

We can estimate the energy scale at which $\alpha_s(\mu)$ diverges. This happens at a finite energy, known as the *QCD dynamical scale* given by

$$\Lambda_{\mathrm{QCD}} = \Lambda_{\mathrm{UV}} \exp\left(-\frac{1}{2b_0\, \alpha_s(\Lambda_{\mathrm{UV}})}\right) \approx 200\mathrm{MeV}. \tag{1.5}$$

We can interpret this scale as the energy at which QCD makes the transition between the weakly coupled and the strongly coupled regime.

At low energies, where QCD is strongly coupled, it shows another key property known as *color confinement*, meaning that asymptotic states are always color singlets. As a consequence, quarks and gluons cannot exist freely but are confined into color singlets: hadrons. These particles are classified into two families, depending on their quark composition. The first family goes under the name of *mesons*: particles made out of a quark and an antiquark, strongly interacting. Then, there are the *baryons* which are made out of three interacting quarks. These are the only hadronic bound states[1] that respect color confinement, and their wavefunction is schematically given by

$$\Psi_{\mathrm{mesons}} \sim q_i \bar{q}_i, \qquad \Psi_{\mathrm{baryons}} \sim \epsilon^{ijk} q_i q_j q_k, \qquad i,j,k = 1,2,3. \tag{1.6}$$

[1] We do not consider *exotic* hadrons like the tetraquarks, the pentaquarks or the hexaquarks.

Wilson loops as a probe for confinement

In a gauge theory, a special role is played by non-local operators, like the *Wilson loops*. These are non-local gauge-invariant operators that describe the parallel transport for a quark field along a closed path. If the path is not closed, the operators are referred to as Wilson lines. Let us consider a Yang-Mills theory with the quark as an infinitely heavy (non-dynamical) test particle not sourcing the gauge field.

As first pointed out in [11], the vacuum expectation value of the Wilson loop operator, denoted as $\mathcal{W}$, provides an order parameter for the confinement/deconfinement phase transition in pure Yang-Mills. We can compute such an expectation value by performing the path integral over the gauge connection configurations A:

$$\langle \mathcal{W}(\mathcal{C}) \rangle = \int \mathcal{D}A \, \mathrm{tr} \left(\mathcal{P} \, \exp \left[i \oint_{\mathcal{C}} dx^{\mu} A_{\mu} \right] \right) \exp(i \, S_{\mathrm{YM}}), \tag{1.7}$$

where $\mathcal{C}$ is the closed contour, $S_{\mathrm{YM}} = -(2g_{\mathrm{YM}}^2)^{-1} \, \mathrm{tr} \left(F_{\mu\nu} F^{\mu\nu} \right)$ is the Yang-Mills action.

Consider, as an example, the contour $\mathcal{C}$ to be a $R \times T$ rectangular closed path in the (t, x^1)-plane as in figure 1.1. In the limit $T \gg R$, this configuration corresponds to a static quark-antiquark pair at a fixed spatial distance R where the temporal sides of the rectangle can be interpreted as the worldlines of the two particles. Because of the path orientation, one is a particle and the other, the one propagating backward in time, is an antiparticle.

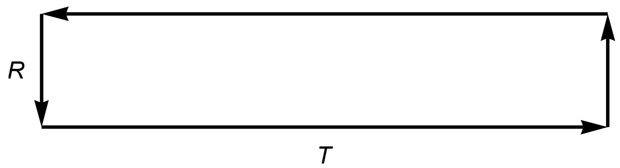

Figure 1.1. Rectangular-shaped Wilson loop in the (t, x^1)-plane with sides T, and R. We consider the limit $T \gg R$.

One can show that, in this limit,

$$\langle \mathcal{W}(\mathcal{C}) \rangle = B(R) \exp \left(-T \, V(R) \right), \tag{1.8}$$

with $V(R)$ being the quark-antiquark potential and $B(R)$ an R-dependent prefactor. We can invert this formula to formally extract $V(R)$ in terms of the Wilson loop expectation value:

$$V(R) = -\lim_{T \to \infty} \frac{\log \langle \mathcal{W}(\mathcal{C}) \rangle}{T}. \tag{1.9}$$

For a confining theory, like Yang-Mills theory with probe quarks, the potential scales linearly with the quark-antiquark spatial distance:

$$V(R) \sim T_{\mathrm{tube}} \, R, \tag{1.10}$$

where T_{tube} is the tension (energy per unit length) of the flux tube (or string) that forms between the quark and the antiquark. In this case, the expectation value of the Wilson loop behaves as

$$\langle \mathcal{W}(\mathcal{C}) \rangle \sim \exp\left(-T_{\text{tube}}\text{Area}(\mathcal{C})\right), \tag{1.11}$$

where $\text{Area}(\mathcal{C}) = T \cdot R$. The exponential decay of the Wilson loop expectation value with the area enclosed by the loop $\mathcal{C}$ itself is known as *area-law criterion* to determine if a quantum field theory is confining.

In QCD with dynamical quarks, the notion of confinement is more subtle than in pure Yang-Mills theory [12, 87]. The Wilson loop no longer shows an exact area law at large distances, since the string connecting static quarks can break through the creation of light quark-antiquark pairs. Nevertheless, confinement manifests in the absence of colored asymptotic states: only color-neutral hadrons are observed experimentally. Effective order parameters, such as the Polyakov loop and the behavior of chiral symmetry, are often used to study the confinement–deconfinement transition. Thus, while the strict area law is lost, the physical principle of confinement remains a defining feature of QCD with dynamical quarks.

The symmetries of QCD

The analysis of the symmetry pattern of QCD is a powerful tool to investigate how the theory behaves at low energies, in the regime where it is strongly coupled. We have already noticed that the QCD Lagrangian is invariant under the SU(3) color gauge transformations.

Real-world QCD has 6 massive flavors (up, down, strange, charge, bottom, top) whose masses are approximately $m_u \approx 2$ Mev, $m_d \approx 5$ Mev, $m_s \approx 95$ Mev, $m_c \approx 1.2$ Gev, $m_b \approx 4$ Gev, and $m_t \approx 173$ Gev. Among them, it is possible to distinguish between *light* quarks (up, down, and strange) and *heavy* quarks (charm, bottom, and top), with respect to the QCD dynamical scale. The lightest hadrons are made out of the lightest quarks, and therefore, we forget about the heavy ones if we want to study the most stable bound states of QCD. Moreover, we know that the QCD scale, at which QCD confines, is around 200 MeV, so a reasonable approximation is to neglect also the mass of the light quarks since $m_{u,d,s} < \Lambda_{\text{QCD}}$.[2]

The massless limit for the quark fields is known as the *chiral* limit, because now the QCD Lagrangian with N_f massless flavors enjoys chiral symmetry, with group

$$\text{U}(N_f)_L \times \text{U}_\text{R}(N_f)_R. \tag{1.12}$$

This is evident if we decompose the Dirac fermion into the left-handed and right-handed parts $q_i = q_i^L + q_i^R$, which transform as

$$q_i^L \to \mathcal{U}_{ij}^L q_j^L, \qquad\qquad q_i^R \to \mathcal{U}_{ij}^R q_j^R, \tag{1.13}$$

with $\mathcal{U}^{L,R} \in \text{U}(N_f)_{L,R}$. The chiral symmetry group can be written in terms of its vectorial subgroup $\text{U}(N_f)_V$ and the axial subgroup $\text{U}(N_f)_A$:

$$\text{U}(N_f)_L \times \text{U}(N_f)_R \simeq \frac{\text{SU}(N_f)_V \times \text{U}(1)_V}{\mathbb{Z}_{N_f}} \times \frac{\text{SU}(N_f)_A \times \text{U}(1)_A}{\mathbb{Z}_{N_f}}, \tag{1.14}$$

[2] Clearly, this approximation is more reliable for the up and the down quark than the strange quark.

where $\simeq$ indicates the isomorphism relation since we have used the well-known mathematical result $\mathrm{U}(N) \simeq \mathrm{SU}(N) \times \mathrm{U}(1)/\mathbb{Z}_N$.

Every exact symmetry of the QCD Lagrangian corresponds to a conserved quantity, as dictated by Noether's theorem. In quantum mechanics, this implies that physical states can be organized according to the irreducible representations of these symmetry groups. In the case of chiral QCD, the $\mathrm{SU}(N_f)_V$ symmetry is an exact symmetry and leads to the conservation of *isospin*. Hadrons, the physical states of the theory, can be classified by the irreducible representations of $\mathrm{SU}(N_f)_V$. Although this classification arises from an approximate model, it agrees reasonably well with experimental observations.

Another exact symmetry of QCD is the $\mathrm{U}(1)_V$ symmetry, which corresponds to the conservation of the *baryon number*. In contrast, the axial symmetry $\mathrm{SU}(N_f)_A$ is not an exact symmetry. It is spontaneously broken, meaning that while it is a symmetry of the Lagrangian, it is not preserved by the vacuum state. This leads to the emergence of $N_f^2 - 1$ massless particles known as *Goldstone bosons*, as predicted by Goldstone's theorem. In the real world, these correspond approximately to the three pions (for $N_f = 2$) or the octet of light pseudoscalar mesons (for $N_f = 3$). These particles are not exactly massless because the up, down, and strange quarks have small but nonzero masses.

Finally, the axial $\mathrm{U}(1)_A$ symmetry is *anomalous*, meaning it is a classical symmetry of the Lagrangian but is broken at the quantum level due to the axial anomaly. The presence of an anomaly explains why there is no light singlet (under $\mathrm{SU}(N_f)_V$) pseudoscalar meson with mass comparable to that of pions. This has been known as the η' or U(1) *problem* because the measured experimental mass of the η' meson was incompatible with it being a Goldstone boson of the $\mathrm{U}(1)_A$ spontaneous breaking.

θ term in QCD

In the Yang-Mills sector of the theory, there is a Lagrangian term consistent with gauge symmetry, Lorentz invariance, and renormalizability that we did not mention. It can be written as

$$S_\theta = \frac{\theta}{32\pi^2} \int d^4x \, \epsilon^{\mu\nu\rho\sigma} \, \mathrm{tr}(F_{\mu\nu} F_{\rho\sigma}). \tag{1.15}$$

The parameter θ has to be an angular variable, $\theta \in [0, 2\pi)$ because the path integral of the theory is invariant under $\theta \to \theta + 2\pi k$ with $k \in \mathbb{Z}$. The theta term is topological and therefore it does not enter the equations of motion for the fields. However, it can affect some physical quantities [88, 89]. For example, one can show that the vacuum energy density of a Yang-Mills theory $\varepsilon(\theta)$ depends on θ. A relevant quantity in this context is the topological susceptibility, defined as

$$\chi_g = \left.\frac{d^2\varepsilon(\theta)}{d\theta^2}\right|_{\theta=0} . \tag{1.16}$$

This quantity can also be written as

$$\chi_g = \int d^4x \, \langle \mathcal{Q}(x) \mathcal{Q}(0) \rangle, \tag{1.17}$$

where $\mathcal{Q} = \epsilon^{\mu\nu\rho\sigma}\,\mathrm{tr}(F_{\mu\nu}F_{\rho\sigma})/(32\pi^2)$ is the topological charge density. This expression shows that χ_g measures the fluctuation of the topological charge in the vacuum: a non-zero χ_g implies that topologically non-trivial configurations contribute significantly to the QCD vacuum energy.

The presence of quarks creates an interplay with the theta term. In particular, if at least one quark is massless, a $\mathrm{U}(1)_A$ transformation can rotate away the presence of θ and therefore there are no physical quantities which depend on θ. However, if all the quarks are massive, as in real-world QCD, then the theta angle cannot be rotated away. Therefore, when quarks are taken into account, the full QCD topological susceptibility is modified, and it goes to zero in the limit of massless quarks since the theory does not depend on θ.

1.2 Large-N limit of low-energy QCD

As mentioned in the introduction, the perturbative approach to QCD works only at energies much greater than Λ_{QCD}. If we are interested in the low-energy limit of QCD, we have to employ alternative approaches. A very useful tool in the low-energy regime is the *large-N expansion*, with N number of colors, first introduced by Gerard 't Hooft [15]. Now we will promote the number of colors N to be a large number, even if real-world QCD has $N = 3$.

Let us go back to our definition of the QCD scale (1.5). If we directly take the limit $N \to \infty$, $b_0 \propto N$, and there is no parametric separation between the physical scale Λ_{QCD} and the cutoff Λ_{UV}. To rectify this, and not change the theory at the QCD scale, we define the 't Hooft coupling constant

$$\lambda \equiv g_{\mathrm{YM}}^2 N, \tag{1.18}$$

and require that in the limit, known as 't Hooft limit, $N \to \infty$ and $g_{\mathrm{YM}}^2 \to 0$, we keep $\lambda =$ constant.

In the large-N limit, there is a new coupling constant which is small and allows for a perturbative expansion $\sim 1/N$. It is a known result that Feynman diagrams in the large-N limit can be ordered by relevance according to their $1/N$ dependence. This expansion has a close connection with topology since one can show that the N-dependence of a diagram goes like N^{χ_E}, where χ_E is the Euler characteristic of the diagram inscribed on the Riemann surface of a two-dimensional manifold of a given topology.

In this work, we are mainly interested in the low-energy regime of QCD, where the theory confines, and therefore, we focus on hadron degrees of freedom that we have at large-N. The naive wave-function of baryons in this case is

$$\Psi^{\mathrm{large}-N}_{\mathrm{baryons}} \sim \epsilon^{i_1 i_2 \ldots i_N} q_{i_1} q_{i_2} \ldots q_{i_N}, \qquad i_1, i_2 \ldots i_N = 1, \ldots, N. \tag{1.19}$$

This means that baryons are made out of N quarks, and therefore it is reasonable to deduce that the baryon mass scale linearly with N. Their radius is fixed by an energy scale $\propto \Lambda_{\mathrm{QCD}} \sim N^0$ (see [16]). This very specific behavior, where the mass of a particle scales with the inverse of the coupling constant, and the size does not scale with it, is the typical behavior of *solitonic solutions*. This strongly suggests that baryons should emerge as solitons in the large-N effective field theory [16, 90].

On the other side, the naive meson wave-function at large-N is

$$\Psi_{\text{mesons}}^{\text{large}-N} \sim q_i \bar{q}_i, \qquad i = 1, \ldots, N. \tag{1.20}$$

Their structure does not change with N and therefore their mass scales $\sim N^0$. Also in this case, the only dimensionful energy scale that can set their radius is $\Lambda_{\text{QCD}} \sim N^0$.

In the limit of large-N, baryons cease to be dynamical degrees of freedom because their mass diverges. Consequently, the low-energy QCD Lagrangian simplifies and effectively describes only mesonic fields:[3]

$$\mathcal{L}_{\text{QCD}}^{\text{large}-N} = \mathcal{L}_{\text{mesons}}. \tag{1.21}$$

In this regime, the interactions among mesons are suppressed, since the interaction coupling constant scales as $\sim 1/N$. This implies that as N increases, mesons become increasingly non-interacting. In this theory, baryons emerge as solitons as we will see in section 1.3.

1.2.1 An effective field theory for mesons

We have seen how, in the large-N limit, low-energy QCD reduces to a theory of weakly-interacting mesons. In this section, we review how the meson effective field theory can be constructed. First of all, this is a low-energy theory, valid for energies lower than some putative cutoff Λ, therefore, the fields of this theory will be hadrons with $m < \Lambda$. Moreover, the symmetries of the Lagrangian have to be ones of the QCD Lagrangian. The theory will come with some free parameters that have to be fixed by comparing observables, derived within this theory, with experimental data.

For energies lower than Λ, the relevant degrees of freedom of QCD are the $N_f^2 - 1$ Nambu-Goldstone bosons associated with chiral symmetry breaking. They can be cast in the matrix-valued field

$$\mathcal{U}(x) = \exp\left(\frac{i}{f_\pi} \sum_{a=1}^{N_f^2-1} \pi^a(x) T^a\right), \tag{1.22}$$

where T^a are the generators of $\text{SU}(N_f)$, normalized so that $\text{Tr}(T^a T^b) = \delta^{ab}/2$. We have not included a $N_f{}^{\text{th}}$ generator matrix proportional to the identity, since the corresponding field would be the Goldstone boson for the $\text{U}(1)_A$ symmetry, which is eliminated by the chiral anomaly. We will come back to this point later in this section. We have also introduced a dimensionful constant f_π. This ensures that pion fields have canonical dimensions for scalar fields in four dimensions. It is called the pion decay constant, although this name makes very little sense in our current theory because the pions are stable excitations and do not decay. However, they can decay when they are coupled to the electroweak sector. The scale f_π determines the pion's decay width, whence its name. In the large-N limit, it can be shown that $f_\pi \sim \sqrt{N}$.

[3]The large-N is not necessary to study pions using the effective field theory. However, in the large-N limit this becomes more reliable.

The Lagrangian describing the meson effective field theory will be constructed as an expansion in the derivatives of the meson field $\mathcal{U}$. Moreover, in the massless limit, the Lagrangian must be invariant under the global chiral symmetry group $\mathrm{U}(1)_V \times \mathrm{SU}(N_f)_L \times \mathrm{SU}(N_f)_R$. Then, it is easy to show that the leading-order term in the meson Lagrangian is

$$\mathcal{L}_{\text{mesons}} = \frac{f_\pi^2}{4} \mathrm{Tr}\left(\partial_\mu \mathcal{U}\, \partial^\mu \mathcal{U}^\dagger\right) + \mathcal{O}\left((\partial\mathcal{U})^4\right). \tag{1.23}$$

This is known as the *chiral Lagrangian* and it describes the dynamics of the meson field. The normalization constant has been fixed to reproduce the canonical form of the kinetic term. In fact, we can expand in a power series of π^a/f_π to get

$$\mathcal{L}_{\text{mesons}} = \frac{1}{2}\partial_\mu \pi^a(x)\partial^\mu \pi^a(x) + \mathcal{O}(\pi^4). \tag{1.24}$$

Let us now consider the effect of including masses for the quarks. If the masses are large compared to the QCD scale, then the quarks play no role in low-energy physics. Here we will be interested in the situation where the masses are small, compared to Λ_{QCD}. In this case, we still have an approximate chiral symmetry. We can incorporate the masses in the chiral Lagrangian by the $N_f \times N_f$ matrix $M = \mathrm{diag}(m_1, \ldots, m_{N_f})$ and adding to the chiral Lagrangian the term

$$\mathcal{L}_{\text{mass}} = \frac{f_\pi^2\, Y}{2} \mathrm{Tr}(M\, \mathcal{U} + \mathcal{U}^\dagger M^\dagger), \tag{1.25}$$

where Y has the dimension of a mass, and it is related to the chiral condensate Σ by $\Sigma = f_\pi^2\, N_f Y$. This term breaks explicitly the chiral symmetry, but for small masses it can be treated as a perturbation.

We conclude this section by discussing what happens to the chiral anomaly in the large-N limit. Let us recall that the presence of the chiral anomaly can be expressed in terms of the non-conservation of the $\mathrm{U}(1)_A$ axial current at the quantum level

$$\partial_\mu J^\mu_A = \frac{g^2_{\mathrm{YM}} N_f}{8\pi^2}\, \epsilon^{\mu\nu\rho\sigma} \mathrm{tr}(F_{\mu\nu} F_{\rho\sigma}). \tag{1.26}$$

In the large-N limit, the RHS of the above equation goes to zero, and $\mathrm{U}(1)_A$ is not anomalous anymore. As a consequence, the η', which was very massive compared to pions, appears as a Nambu-Goldstone boson. Therefore, the pion matrix $\mathcal{U}(x)$ takes now values in $\mathrm{U}(N_f)$, and the η' meson is identified as its phase

$$\det \mathcal{U} = \exp(i\eta'/f_\pi), \tag{1.27}$$

and it is said to be the phase of the chiral condensate.[4]

The chiral anomaly can be seen only going to the next leading order in $1/N$ and it gives rise to a mass term for η':

$$\mathcal{L}_{\text{mesons}} \supset -\frac{1}{2} f_\pi^2\, m^2_{\eta'}(-i \log \det \mathcal{U})^2, \tag{1.28}$$

[4] In the formula (1.27), we used that at leading order in $1/N$, $f_{\eta'} = f_\pi$.

where $m_{\eta'}$ is the η' mass which scales as $N^{-1/2}$. A long time ago, Witten and Veneziano [88, 89] found a relation between the topological susceptibility of pure Yang-Mills and the η' mass

$$m_{\eta'}^2 = m_{\mathrm{WV}}^2 = \frac{4N_f}{f_\pi^2}\,\chi_g\,. \tag{1.29}$$

To stress the paternity of this formula, the η' mass is often indicated as m_{WV}. This formula ends the famous $\mathrm{U}(1)_A$ problem, as it gives a non-vanishing mass to the η' also in the chiral limit, thus confirming that it cannot be interpreted as a Nambu-Goldstone boson.

1.3 The Skyrme model for baryons

We have presented an effective theory for the mesons, and we can ask which role is played by $\mathrm{U}(1)_V$ in this theory. This symmetry acts trivially on $\mathcal{U} \to \mathcal{U}$. As a consequence, there is no conserved charge coming from this vector symmetry. We remind that charged objects under this symmetry are the baryons, and therefore there is no reason to expect that the meson effective theory knows anything about the baryons, since we intentionally threw out all but the lightest excitations.

It is therefore surprising to learn that the baryons do arise in the Skyrme model, an extension of the chiral Lagrangian: they appear as solitonic objects in the meson effective field theory. Let us first show that the chiral Lagrangian has a hidden conserved current. The field $\mathcal{U}(x)$, at given time t, is a map from the space of coordinates to the space of fields

$$\mathcal{U}(x) : \mathbb{R}^3 \to \mathrm{SU}(N_f). \tag{1.30}$$

In order for this map to be physical, it must be continuous and with finite energy. The latter request implies that

$$\lim_{|x|\to\infty} \mathcal{U}(x) = \mathcal{U}_{\text{vacuum}}, \tag{1.31}$$

where $\mathcal{U}_{\text{vacuum}}$ is a constant value, and represents the minimum of the potential of the chiral Lagrangian. This is necessary to avoid singularities on the boundary of $\mathbb{R}^3$. Then, it follows from the stereographic projection that the $\mathbb{R}^3$ space with a single point at infinity (associated with the boundary) is equivalent to the three-sphere S^3. Therefore, we can rewrite

$$\mathcal{U}(x) : S^3 \to \mathrm{SU}(N_f). \tag{1.32}$$

Such field configurations are characterized by their winding

$$\pi_3(\mathrm{SU}(N_f)) = \mathbb{Z}. \tag{1.33}$$

This winding number, which we denote by $n_B \in \mathbb{Z}$, can be computed by the integral

$$n_B = \frac{1}{24\pi^2}\int d^3x\,\epsilon^{ijk}\,\mathrm{Tr}\left(\mathcal{U}^\dagger\,(\partial_i\mathcal{U})\,\mathcal{U}^\dagger\,(\partial_j\mathcal{U})\,\mathcal{U}^\dagger\,(\partial_k\mathcal{U})\right). \tag{1.34}$$

We can go further and write down a corresponding local conserved current

$$j^\mu_{n_B} = \frac{1}{24\pi^2}\epsilon^{\mu\nu\rho\sigma}\,\mathrm{Tr}\left(\mathcal{U}^\dagger\left(\partial_\nu\mathcal{U}\right)\mathcal{U}^\dagger\left(\partial_\rho\mathcal{U}\right)\mathcal{U}^\dagger\left(\partial_\sigma\mathcal{U}\right)\right), \tag{1.35}$$

which obeys $\partial_\mu j^\mu_{n_B} = 0$. The winding number is given, as usual, by $n_B = \int d^3x\, j^0_{n_B}$. It is natural to search for an interpretation of this conserved current $j^\mu_{n_B}$, in terms of the microscopic theory. The only symmetry group candidate for this symmetry is $\mathrm{U}(1)_V$, strongly suggesting that we have to identify n_B as the baryon number and, correspondingly, these solitonic configurations with baryons.

However, even if the meson effective field theory with only two-derivative terms has the topology to support solitons, no static solutions exist. This comes from Derrick's theorem [91], which in our case can be understood as follows. Taking into account only two-derivative terms, the energy for a static configuration $\mathcal{U}$ is

$$E = \frac{f_\pi^2}{4}\int d^3x\,\mathrm{Tr}\left(\partial_i\mathcal{U}^\dagger\partial_i\mathcal{U}\right). \tag{1.36}$$

Solutions to the equations of motion are minima (or, more generally, saddle points) of this energy functional. A simple scaling argument tells us that these do not exist. To see this, consider a putative solution $\mathcal{U}_*(x)$ with energy E_*. Then, the new configuration $\mathcal{U}_\lambda(x) = \mathcal{U}_*(\lambda x)$ has energy $E_\lambda = E_*/\lambda$ so that we can always lower the energy of any configuration just by rescaling its size. The reason for this is that the classical theory is scale invariant, so there is nothing to set the size of the soliton. Indeed, the only dimensionful quantity, f_π, multiplies the whole action and so does not affect the classical equations of motion. The way out of this problem is to introduce a higher derivative term so that the scale invariance is broken, and the solution is stabilized. The effective Lagrangian, cured with the higher derivative term, reads

$$\mathcal{L}_{\mathrm{Skyrme}} = \frac{f_\pi^2}{4}\mathrm{Tr}\left(\partial_\mu\mathcal{U}\,\partial^\mu\mathcal{U}^\dagger\right) + \frac{1}{32e^2}\mathrm{Tr}\left(\left[\mathcal{U}^\dagger\partial^\mu\mathcal{U},\mathcal{U}^\dagger\partial_\mu\mathcal{U}\right]\right), \tag{1.37}$$

where e^2 is a dimensionless coupling constant. This is known as the *Skyrme model* [92].

We conclude this section by presenting a solution to the equations of motion that carries a non-zero baryon number. We consider $N_f = 2$ in which case, a convenient parametrization of $\mathcal{U} \in \mathrm{SU}(2)$ is

$$\mathcal{U} = \rho + i\,\sigma^a\pi_a, \qquad\qquad \rho^2 + \pi_a^2 = 1, \tag{1.38}$$

where σ^a are the Pauli matrices. The so-called *hedgehog* ansatz describes a single Skyrmion wrapping around the target space S^3

$$\mathcal{U} = \exp\left(i\frac{f(r)}{r}\sigma^a x_a\right) = \cos f(r) + \frac{i\sigma^a x_a}{r}\sin f(r), \tag{1.39}$$

where r here is the radius of the manifold where $\mathcal{U}$ is defined. The condition $\mathcal{U}(r\to\infty) = 1$ is achieved by $f(r\to\infty) = 0$. In order for $\mathcal{U}$ to be well-defined at the origin $r = 0$, we have to require $f(0) = \pi\, m$, with $m \in \mathbb{Z}$. It is a simple exercise to show that

$$n_B = m. \tag{1.40}$$

With our ansatz, the equation of motion becomes an ordinary differential equation for $f(r)$

$$\left(r^2 + 2\sin^2 f(r)\right) f''(r) + 2rf'(r) + \sin(2f(r))(f'(r))^2 - \sin^2 f(r)\sin(2f(r)) = 0, \tag{1.41}$$

which can be solved numerically. The solution corresponding to $m = 1$ is interpreted as a classical baryon.

1.4 Axions and ALPs

The strong $\mathcal{CP}$ problem and the Peccei-Quinn mechanism

As we discussed in section 1.1, the QCD action admits the presence of a topological term S_θ, see equation (1.15). This term breaks parity $\mathcal{P}$ and time reversal $\mathcal{T}$ since under $\mathcal{P}$ or $\mathcal{T}$ transformation, $\theta \to -\theta$, while the charge conjugation is a symmetry. Thus, the transformation $\mathcal{CP}$: $\theta \to -\theta$ is not a symmetry unless $\theta = 0, \pi$. In the presence of massive quarks, the physically relevant $\mathcal{CP}$-violating parameter is not simply θ, but the combination

$$\bar{\theta} = \theta + \arg\det M, \tag{1.42}$$

with M the quark mass matrix. Since $\bar{\theta}$ cannot be rotated away through chiral field redefinitions if all quarks are massive, it represents a genuine physical parameter of QCD. Its presence violates both $\mathcal{P}$ and $\mathcal{CP}$ symmetries.

A particularly sensitive observable to $\bar{\theta}$ is the electric dipole moment (EDM) of the neutron. Current experimental bounds on the neutron EDM constrain $\bar{\theta}$ to be extraordinarily small:

$$|\bar{\theta}| \lesssim 10^{-10}, \tag{1.43}$$

which corresponds to a level of $\mathcal{CP}$ violation in the strong sector that is many orders of magnitude below the naive expectation. This extremely small value lacks a natural explanation within the Standard Model and constitutes what is known as the *strong $\mathcal{CP}$ problem*.

A compelling solution was proposed by Peccei and Quinn (PQ) [93], who introduced a new global chiral symmetry $\mathrm{U}(1)_{\mathrm{PQ}}$, which is anomalous when coupled to QCD. When this symmetry is spontaneously broken at some high scale f_a, it gives rise to a pseudo-Nambu–Goldstone boson, the *axion*, which dynamically cancels the effective $\bar{\theta}$ angle. The scale f_a is known as the Peccei–Quinn symmetry-breaking scale, and it sets the axion decay constant, which also governs the strength of axion interactions with Standard Model fields. The axion field $a(x)$ couples to the QCD topological charge density $\mathcal{Q}(x)$ and shifts under PQ transformations as $a/f_a \to a/f_a + \alpha$, allowing the QCD vacuum energy to be minimized dynamically at $\bar{\theta} + a/f_a = 0$. As a result, the axion field relaxes to cancel any $\mathcal{CP}$-violating effects from the QCD θ-term, thus solving the strong $\mathcal{CP}$ problem naturally.

At energies well below the PQ symmetry-breaking scale f_a, the axion can be described within the framework of an effective field theory. Since it arises as a pseudo-Nambu–Goldstone boson, its interactions are suppressed by f_a, and it couples derivatively to matter fields and anomalously to gauge bosons.

The effective Lagrangian for the axion in the presence of QCD and electromagnetic fields takes the form [94]

$$\begin{aligned}\mathcal{L}_{\text{axion}} =& \frac{1}{2}\partial_\mu a\, \partial^\mu a + \frac{a}{f_a}\frac{g_{\text{YM}}^2}{32\pi^2}\epsilon^{\mu\nu\rho\sigma}\text{tr}(F_{\mu\nu}F_{\rho\sigma}) + \\ &+ \frac{C_\gamma}{4}\frac{a}{f_a}\epsilon^{\mu\nu\rho\sigma}F^{\text{em.}}_{\mu\nu}F^{\text{em.}}_{\rho\sigma} + \sum_i \frac{C_i}{2f_a}\partial_\mu a\, \bar{q}_i\gamma^\mu\gamma^5 q_i,\end{aligned} \tag{1.44}$$

where $F^{\text{em.}}_{\mu\nu}$ is the electromagnetic field strength tensor, and q_i is the quark field. The constants C_γ and C_i are model-dependent dimensionless coefficients that arise from the details of the UV completion.

QCD instanton effects generate a potential for the axion:

$$V(a) \approx m_a^2 f_a^2 \left[1 - \cos\left(\frac{a}{f_a}\right)\right], \tag{1.45}$$

where the axion mass, in the two-flavored case, is approximately

$$m_a \approx \frac{\sqrt{m_u m_d}}{m_u + m_d}\frac{f_\pi m_\pi}{f_a} \approx 5.7\,\mu\text{eV}\left(\frac{10^{12}\ \text{GeV}}{f_a}\right). \tag{1.46}$$

Thus, the axion acquires a small mass from QCD effects, with its mass inversely proportional to the PQ scale. For $f_a \gg \Lambda_{\text{QCD}}$, the axion is extremely light and weakly coupled, making it an excellent *dark matter* candidate and a prime target for experimental searches.

Axion-like particles (ALPs)

Axion-like particles are hypothetical pseudoscalar bosons that arise in a broad class of theories beyond the Standard Model. While the QCD axion is specifically tied to the solution of the strong $\mathcal{CP}$ problem via the Peccei–Quinn mechanism, ALPs generalize the concept by relaxing this connection. In particular, ALPs do not necessarily couple to gluons or solve the strong $\mathcal{CP}$ problem. Still, they retain the pseudo-Nambu–Goldstone boson character and share many properties with the axion.

By definition, an ALP is typically a pseudoscalar particle that couples to Standard Model fields via higher-dimensional operators, most notably through an anomalous coupling to the photon field. The pseudoscalar nature ensures that its leading interactions are derivative or involve dual field strengths, preserving shift symmetry at the classical level. The low-energy effective Lagrangian takes a similar form to (1.44). However, in this case, the ALP mass m_a and the decay constants C are largely independent. This decoupling from QCD dynamics allows for a wide range of possible masses and interaction strengths, leading to a much richer phenomenology and connection with dark matter.

As we will discuss in detail in chapter 5, in this work, we are going to use the name ALPs for pseudoscalar particles that do not necessarily have a coupling with the photon field.

Composite axion models

Axion models can be broadly divided into two classes, depending on the ultraviolet origin of the axion field. In *elementary* models, the axion arises as the phase of a fundamental scalar field, whose vacuum expectation value spontaneously breaks the PQ symmetry. In contrast, in *composite* models, the axion is realized as a pseudo-Nambu-Goldstone boson of a new confining gauge theory, in close analogy to the pions of QCD. In this case, the PQ symmetry is an approximate global chiral symmetry of the strong dynamics, and its spontaneous breaking by fermion condensation generates the axion without invoking a fundamental PQ scalar.

A well-known benchmark for elementary axions is the *Kim-Shifman-Vainshtein-Zakharov (KSVZ)* model [95, 96]. In its minimal form, a new heavy vector-like fermion Ψ is introduced, charged under QCD and under the global anomalous $\mathrm{U}(1)_{\mathrm{PQ}}$ symmetry. The axion field arises as the phase of a complex scalar Φ whose vacuum expectation value breaks the PQ symmetry spontaneously:

$$\Phi = \frac{f_a}{\sqrt{2}} \exp\left(\frac{i\,a}{f_a}\right), \qquad \langle \Phi \rangle = \frac{f_a}{\sqrt{2}}.$$

The fermion Ψ couples to Φ via a Yukawa interaction,

$$\mathcal{L} \supset y\,\Phi\,\bar{\Psi}_L \Psi_R + \mathrm{h.c.},$$

acquiring a mass after PQ breaking. Upon integrating out Ψ, a one-loop triangle anomaly generates the effective axion-gluon coupling, dynamically canceling the QCD $\bar{\theta}$-term. Variants of this construction can also accommodate ALPs, in which case the pseudoscalar does not necessarily couple to gluons.

While the minimal KSVZ axion is elementary, one can envision composite realizations of the same idea, where the role of the PQ scalar Φ is played by a fermion bilinear condensate in a new confining gauge theory. More generally, one may construct models where both the PQ-charged fermions and the confining gauge group belong to a hidden "dark" sector neutral under the Standard Model. In such cases, an asymptotically free gauge group G_{dark} confines at a scale Λ_{dark}, generating a condensate

$$\langle \bar{\psi}\psi \rangle \sim \Lambda_{\mathrm{dark}}^3, \tag{1.47}$$

which spontaneously breaks the global PQ symmetry, $\mathrm{U}(1)_{\mathrm{PQ}} \to \emptyset$, and gives rise to a composite axion. This is the situation we will consider in Chapter 5.

1.5 Phases of QCD

Quantum chromodynamics can be studied at finite temperature, finite baryon chemical potential, and finite isospin chemical potential. These ingredients are necessary to study QCD in a "real-world" scenario. Varying the values of the temperature T, and the chemical potential μ_B (as well as the isospin chemical potential μ_{ISO}), one can construct the phase diagram of QCD. See *e.g.* [97] for a review on the topic. For the purposes of our discussion, we can set the isospin chemical potential to zero, and discuss the QCD phase diagram as a function of T and μ_B, whose schematic representation is reported in figure 1.2. The reader should

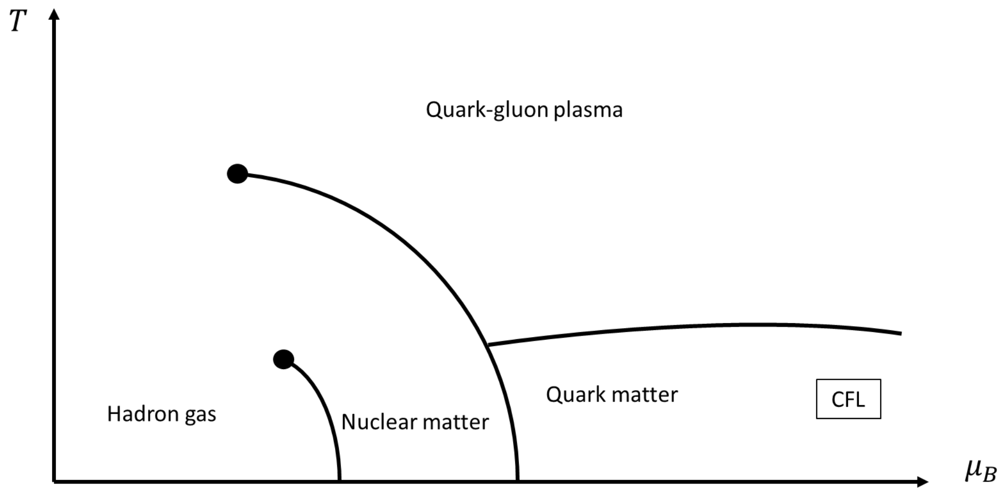

Figure 1.2. A schematic view of the QCD phase diagram as a function of the temperature T and the baryon chemical potential μ_B.

keep in mind that there is broad consensus about the behavior of QCD matter only in two limiting regimes: at vanishing baryon chemical potential ($\mu_B = 0$), where lattice QCD calculations are reliable, and at asymptotically large μ_B and low temperature, where perturbative QCD provides guidance. In contrast, the intermediate region of the QCD phase diagram, which is most relevant for the physics of neutron stars and heavy-ion collisions, remains highly uncertain. Our current understanding of this domain is largely conjectural, based on effective models, phenomenological approaches, and indirect constraints from astrophysical observations and experimental data from relativistic heavy-ion collisions.

At low densities and low temperatures, QCD is in the *hadron gas* phase. In this phase, quarks (and gluons) are confined into color-neutral states.

At sufficiently high temperatures, quarks are no longer confined into color-neutral hadrons, and the QCD matter enters a *plasma state of quarks and gluons*. There is no net separation (*i.e* no first-order transition line) between the latter and the hadron gas phase (at sufficiently low densities), but just a crossover. The quark-gluon plasma can be studied using hydrodynamics as the temperature decreases, and since it becomes strongly coupled, it cannot be described in terms of quasiparticles.

At high baryon density and low temperature, the situation is far less accessible. Because of the sign problem, lattice QCD cannot directly address this regime. Moreover, unless we consider asymptotically large densities, QCD cannot be treated using perturbation theory. See [98, 99] for more details.

If the baryon chemical potential is less than the mass of a nucleon ($\approx$ 939 MeV), it is not possible to create neutrons and protons at zero temperature. In this regime, the ground state of QCD contains no baryons and corresponds to the vacuum. However, when μ_B approaches the mass of a nucleon, the system undergoes a transition to uniform nuclear matter, where baryons begin to populate the ground state. Nuclear matter is a liquid with neutron and proton quasiparticles. They are equal in number as long as $\mu_{\text{ISO}} = 0$. In contrast with the hadron gas phase, now protons and neutrons interact with each other via the strong force. There are many attempts in the literature to construct models of nuclear matter, see *e.g.* [100]. At sufficiently low temperatures, the motion of nucleons in nuclear matter is governed primarily by the Pauli exclusion principle, since almost all states up to the Fermi surface are occupied. In this regime, the excitations of the system can be understood in terms of a relativistic Fermi liquid theory. This framework allows us to treat neutrons and protons as long-lived quasiparticles with effective masses and interactions. In addition to this quasiparticle picture, attractive components of the nucleon–nucleon interaction lead to the formation of Cooper pairs, much like in conventional superconductors where electrons pair due to an effective attraction mediated by phonons. The onset of pairing implies that nuclear matter is not just a Fermi liquid, but a superfluid at low temperatures. This superfluidity is expected in regions of the QCD phase diagram where densities are comparable to nuclear saturation density n_s and temperatures are low compared to the pairing gap ($T \approx (10^9 - 10^{10})$ K).

At higher densities, the common understanding is that quark matter becomes the relevant phase of QCD, with quarks being the relevant degrees of freedom. Despite little being known about the transition from hadronic to quark matter, we expect that at high enough densities, quark matter is a Fermi liquid, with quark quasiparticles. Increasing the density even more, the momentum transfer between quarks near the Fermi surface leads to a weakly-interacting theory of quarks. Moreover, since the interaction between quarks is attractive, below some critical temperature, quarks will form Cooper pairs, creating a superconducting state called *color superconductor*. Among the possible superconducting phases, one of the simplest is the Color-Flavor-Locking (CFL) phase (where all quarks participate in Cooper pairing), which is believed to dominate for asymptotically large values of μ_B [101].

As we will discuss in the next section, neutron stars probe the high-density and low-temperature portion of the QCD phase diagram, as they are made of cold nuclear matter and (perhaps), in the core, cold quark matter. Neutron stars, like all astrophysical objects, are governed not only by the strong interaction but also by the weak and electromagnetic interactions. Weak interactions work to maintain the beta-equilibrium in the star, *i.e.* the condition that fixes the balance among the abundances of different baryon (or quark) and lepton species, and are responsible for various transport properties. This aspect plays a major role in this thesis, as we are going to discuss in chapter 8.

1.5.1 Neutron stars in a nutshell

In this section, we introduce the physical system which will play a relevant role in chapter 8: the neutron star. Neutron stars are the remnants of old *massive* stars that undergo a supernova explosion and a subsequent gravitational collapse [53]. For this to happen, the mass of the progenitor star, *i.e.* the original hydrogen-burning star, has to be sufficiently large ($M \gtrsim 10M_\odot$) for a supernova explosion to take place, but not too large ($M \lesssim 25M_\odot$) so that its core does not collapse directly to a black hole.[5] As the stellar material collapses, its density increases and eventually it

[5]The symbol $M_\odot$ refers to the mass of the Sun, which is measured to be approximately $M_\odot = (1.988475 \pm 0.000092) \times 10^{30}$ Kg.

reaches a density comparable with the nuclear saturation density $n_s \approx 0.16\,\mathrm{fm}^{-3}$. This is the equilibrium density of nuclear matter, *i.e.* the density at which nucleons (protons and neutrons) arrange themselves inside nuclei. At this stage, the nucleons created during the collapse are packed as tightly as possible, leaving no room for further compression. The short-range hard-core repulsion of the strong nuclear force between nucleons, together with the neutron degeneracy pressure that arises from the Pauli exclusion principle, makes the stellar matter stiff enough to stop the gravitational collapse. The result of this process is a compact object with a mass of approximately $\approx (1-2)M_\odot$, and radius $\approx (11-13)$ Km. The average density is comparable with the nuclear saturation density $n_s \approx 0.16\,\mathrm{fm}^{-3}$. However, the density inside a neutron star is not uniform throughout its structure. In the outer layers, or crust, the density is much lower, beginning at values comparable to those of ordinary atomic nuclei and gradually decreasing toward zero at the surface. In contrast, toward the inner core, the gravitational pressure becomes far more intense, and in more massive neutron stars, the weight of the overlying layers compresses the central region even further. As a result, the density at the core can exceed the nuclear saturation density by several factors, typically reaching values in the range of $(2-5)n_s$ for stable neutron stars, and possibly even higher for the most massive ones on the verge of collapsing into a black hole.

At the densities corresponding to neutron star cores, QCD is strongly coupled. Modern chiral effective field theory [13] (based on perturbative treatment of nuclear interactions via meson exchange) can describe quantitatively nuclear matter at densities only slightly above n_s, while perturbative QCD is accurate only around $40n_s$. Moreover, as we already said in the previous section, at high densities, lattice QCD suffers from the sign problem and therefore cannot be trusted. In this scenario, holography provides a powerful tool for tackling the strongly coupled nature of matter inside neutron stars. See [102] for a comprehensive review on the application of holography to compact objects.

In this thesis, we will focus on the role played by weak interactions, since they affect many properties of neutron stars and their binary mergers.

Weak interactions and effective bulk viscosity

Weak interactions enforce beta-equilibrium in the star, *i.e.* the system is in chemical equilibrium thanks to weak processes. For a compound of neutrons, protons, electrons, and muons, one has

$$\mu_n = \mu_p + \mu_l, \qquad\qquad \mu_l = \mu_e = \mu_\mu, \tag{1.48}$$

where l stands for electrons e, and muons μ, so μ_n, μ_p, μ_e, and μ_μ are respectively the neutron, proton, electron, and muon chemical potentials. We have assumed that neutrinos are not trapped. As we have discussed, in the core of neutron stars, matter is expected to be in the deconfined phase, and therefore, the beta-equilibrium condition transferred to quark matter reads[6]

$$\mu_u + \mu_l = \mu_s, \qquad\qquad \mu_l = \mu_e = \mu_\mu, \tag{1.49}$$

[6] At the densities expected in the core of neutron stars, quark matter can exist only in terms of the three lightest flavors: up, down, and strange.

where μ_u and μ_s are respectively the up and strange quark chemical potentials. As before, we assume that neutrinos are not trapped here.

A perturbation can drive the system out of equilibrium, and weak processes will try to restore the balance and dampen the perturbation. This generates an effective *bulk viscosity* ζ. We remember that in standard hydrodynamics, the bulk viscosity is a transport coefficient associated with the ability of a fluid to counteract a compression or an expansion. Bulk viscosity becomes important when a fluid's density is changing over time, such as in oscillations or waves within a star. When a neutron star undergoes oscillations - say, due to rotation or stellar quakes - its density fluctuates. This changes the relative abundances of neutrons, protons, (or up, down, and strange quarks in the core), and electrons, pushing the system out of chemical equilibrium. The weak interactions try to restore equilibrium, but they take time. This delay between the change in density and the system's chemical response causes a phase lag in pressure. As a consequence, the pressure response is no longer perfectly in sync with the volume change. This mismatch leads to dissipation of mechanical energy into heat: this is exactly what bulk viscosity does.

Let us review the derivation of the bulk viscosity in the context of neutron stars, as described in the review [68], where more details can be found. We indicate with ω the angular frequency of the volume oscillation so that we can write the volume as $V(t) = V_0[1 + \delta v(t)]$, with a dimensionless volume perturbation $\delta v(t) = \delta v_0 \cos(\omega t) \ll 1$. On the one hand, the dissipated energy density, averaged over one oscillation period $\tau = 2\pi/\omega$, can be written as

$$\langle \dot{\varepsilon} \rangle_\tau = -\frac{\zeta}{\tau} \int_0^\tau dt\, (\nabla \cdot \mathbf{v}) \approx -\frac{\zeta\, \omega^2 \delta v_0^2}{2}, \tag{1.50}$$

where the upper dot indicates the time derivative, and $\mathbf{v}$ is the velocity field of the fluid. On the other hand, the dissipated energy density can be expressed in terms of the mechanical work done by the induced pressure oscillation

$$\langle \dot{\varepsilon} \rangle_\tau = \frac{1}{\tau} \int_0^\tau dt\, P(t) \frac{d\delta v}{dt}, \tag{1.51}$$

where the pressure is given by

$$P(t) = P_0 + \frac{\partial P}{\partial V} V_0\, \delta v + \sum_{x=\text{species}} \frac{\partial P}{\partial n_x} \delta n_x. \tag{1.52}$$

The oscillation in the pressure is, in general, out of phase compared to the volume oscillation because of the microscopic re-equilibration processes which induce changes in the number densities of the particle species n_x. In the case of unpaired quark matter, the oscillations in density occur for the three quark flavors and the electron, δn_u, δn_d, δn_s, and δn_e.

From (1.50), and (1.51), it follows that

$$\zeta = -\frac{2}{\omega^2 \delta v_0^2} \frac{1}{\tau} \int_0^\tau dt\, P(t) \frac{d\delta v}{dt}. \tag{1.53}$$

The weak processes responsible for restoring beta-equilibrium are produced by a W-boson exchange or emission:

$$u+d \rightleftharpoons u+s, \quad u+\ell^- \to d,s+\nu_\ell, \quad d,s \to u+\ell^-+\bar{\nu}_\ell, \quad \ell_1^- \to \ell_2^- + \nu_{\ell_1} + \bar{\nu}_{\ell_2}\,, \tag{1.54}$$

where $\ell = e, \mu$. Among them, the non-leptonic process $u + d \leftrightarrow u + s$ will turn out to be the dominant one. In chapter 8, we will give general expressions for the decay rates of these processes, keeping the leptonic processes as well.

Referring to [68] for details, it turns out that the final result for the bulk viscosity in the limit where leptonic processes can be neglected, is

$$\zeta \approx \frac{\lambda_{ds} B^2}{\lambda_{ds}^2 B^2 + \omega^2}, \tag{1.55}$$

where

$$B \equiv n_d \frac{\partial \mu_d}{\partial n_d} - n_s \frac{\partial \mu_s}{\partial n_s}, \qquad C \equiv \frac{\partial \mu_d}{\partial n_d} + \frac{\partial \mu_s}{\partial n_s}. \tag{1.56}$$

The parameter λ_{ds} is the decay rate of the process $u + d \leftrightarrow u + s$, in unpaired quark matter [103]

$$\lambda_{ds} \approx G_F^2 \sin^2 \theta_C \cos^2 \theta_C \frac{64}{4\pi^2} \mu_d^5 T^2 \left(1 + \frac{4\alpha_s}{9\pi} \log \frac{\kappa\, \alpha_s \mu_d}{T}\right)^4, \tag{1.57}$$

where $\kappa \approx 0.28(2/3\pi)^{1/2} \approx 0.13$, G_F is the Fermi's constant, θ_C the Cabibbo angle giving the change of basis between quark mass and flavor eigenstates. This result for λ_{ds} is obtained using perturbative QCD and therefore cannot be trusted completely for the densities inside of a neutron star, where non-perturbative effects of QCD can become important. In chapter 8, we will employ holography to perform a non-perturbative computation of λ_{ds}.

Bulk viscosity is particularly important for the stability of r-modes, global oscillations of rotating neutron stars that are driven unstable by gravitational wave emission. The competition between this driving mechanism and viscous damping determines the instability window in the plane of stellar rotation frequency and core temperature. Observational data on spin distributions of young pulsars and of accreting systems can therefore provide indirect information on the magnitude and microphysical origin of bulk viscosity in dense matter, thus linking microscopic QCD processes to astrophysical observations. In this sense, neutron stars act as unique laboratories where the interplay between fundamental particle physics and macroscopic astrophysical dynamics can be explored. The study of bulk viscosity, together with other transport coefficients such as shear viscosity and thermal conductivity, remains central in bridging QCD-inspired microphysics with the phenomenology of compact stars. Future observations with improved gravitational wave detectors and X-ray telescopes are expected to provide further constraints on the damping timescales of oscillation modes, thereby refining our knowledge of the properties of dense QCD matter and its various phases.

Chapter 2

Baryons as quantum Hall droplets

In section 1.3, we have seen that baryons can be described as solitons of the chiral Lagrangian called Skyrmions. However, in the special case of $N_f = 1$, the group manifold SU(N_f) trivializes, and it is not possible to write down a conserved baryon current. It seems that a low-energy description of the one-flavored baryon is not available, even if we know that the one-flavored baryon must exist: it is the bound state of N quarks with total spin $N/2$. In this chapter, we present the idea, proposed in [38], according to which one-flavored baryons can be described at low energy in terms of another kind of solitons.

In section 2.1 we will review the one-flavored QCD theory showing that it does not admit a low-energy description of baryons in terms of Skyrmions. In section 2.2, we will show that, in the IR of one-flavored QCD, there are extended, (2+1)-dimensional excitations of the η' particle, charged under a topological generalized symmetry. We will call these objects *sheets* and discuss their features. As we will see, these sheets are metastable and hence it makes sense to study the effective field theory living on their worldvolume which we will present in section 2.3. Finally, in section 2.4 we will explain how these sheets can be charged under the baryon symmetry following a close analogy with the fractional quantum Hall effect. This way, they provide an alternative description of one-flavored baryons in low-energy QCD at large-N.

2.1 One-flavored QCD

It has been known for several decades that in the 't Hooft limit, baryons should be viewed as solitons [16, 90]. As we discussed in 1.2, this statement is explicitly realized when we consider QCD at low energy in the large-N limit, since their mass scales linearly with N, the inverse coupling constant $1/N$ of the effective field theory, while their size does not scale with N.

At low energy, QCD is effectively described by a theory of weakly interacting mesons described by the pion matrix $\mathcal{U}$, which takes values in SU(N_f). Within this theory, baryons arise as solitonic objects known as Skyrmions constructed out of $\mathcal{U}$. The baryon number is identified with the winding (1.34) of the configuration and, as we have seen, it is classified by $\pi_3(\mathrm{SU}(N_f)) = \mathbb{Z}$.

Let us comment on this general result. The baryon charge is identified with the third homotopy group π_3 of the *entire* space of fields. However, we have just seen that it is enough to consider the π_3 of mesons $\mathcal{U}$, the (pseudo-) Nambu-Goldstone boson of chiral symmetry breaking. It is not guaranteed that this prescription correctly describes all the baryons.[1] This is the central idea in [38][2]: there are situations where the baryons are not captured by the mesonic degrees of freedom alone. One of these situations appears when we consider the case of $N_f = 1$. The one-flavored QCD Lagrangian reads

$$\mathcal{L}_{\mathrm{QCD}}^{N_f=1} = -\frac{1}{2g_{YM}^2}\mathrm{tr}\left(F^{\mu\nu}F_{\mu\nu}\right) + \frac{\theta}{32\pi^2}\,\epsilon^{\mu\nu\rho\sigma}\,\mathrm{tr}\left(F_{\mu\nu}F_{\rho\sigma}\right) + \bar{q}(i\not{D} - m)q, \tag{2.1}$$

where m is the quark mass, and we will take it real and positive. In this chapter, we will consider the limit where $m \ll \Lambda_{\mathrm{QCD}}$, so that the chiral limit makes sense. Moreover, we will work at $\theta = 0$. See [39, 105] for a beautiful discussion about the one-flavored QCD at $\theta = \pi$ and associated domain walls in this theory.

From a microscopic point of view, this theory admits only one baryonic object, whose naive wavefunction is given by

$$(\Psi_{N_f=1\,\mathrm{baryon}})_{s_1\dots s_N} = \epsilon_{a_1\dots a_N}\, q_{s_1}^{a_1} \dots q_{s_N}^{a_N}\,, \tag{2.2}$$

where the indices a_i, with $i = 1 \dots N$, are the color indices and s_i are the spin indices, taking two values. Due to the anti-symmetrization over color indices, and the fermionic nature of the quark fields q_s^a, the spin indices must be symmetrized over to get a non-zero combination. Therefore, there exists only one $N_f = 1$ baryon, and its spin is $N/2$. However, the Skyrme model fails to describe this one-flavored baryon. This is because the group manifold $\mathrm{SU}(N_f)$ trivializes for $N_f = 1$ and the baryon charge can no longer be identified with the π_3 of mesons. It seems that there is no longer a low-energy description of this baryon. This opens a *puzzle* since the baryon does exist in one-flavored QCD and therefore we should be able to describe it also from the IR point of view.

It is now that things get interesting! Remember that, if $m \ll \Lambda_{\mathrm{QCD}}$, at large N, there is a light particle: the η' meson. We have seen in section 1.2 how this particle arises in the chiral Lagrangian: the one-flavored QCD at finite N is gapped but if we take the large-N limit, $\mathrm{U}(1)_A$ becomes an exact symmetry and its spontaneous breaking leads to the (pseudo-) Nambu-Goldstone boson η'. The meson η' is a periodic scalar $\eta' \simeq \eta' + 2\pi$, being the value of the phase of the chiral condensate (1.27). The effective Lagrangian for the η' field at large N, including the $1/N$ correction reads

$$\mathcal{L}_{\eta'} = \frac{f_\pi^2}{2}\left(\partial\eta'\right)^2 - \frac{1}{2}m\, f_\pi^2\Lambda_{\mathrm{QCD}}\cos\left(\eta'\right) - \frac{1}{2}f_\pi^2 m_{\eta'}^2 \min\left(\eta' + 2\pi k\right)^2, \tag{2.3}$$

where we recall that $m_{\eta'} = m_{\mathrm{WV}}$. The first and the second terms of the Lagrangian are respectively the kinetic and mass terms for η'. They both scale with N in

[1] See [104] for a recent demonstration that enlarging the space of mesons may improve upon the predictions of the Skyrme model.

[2] This work develops some ideas already present in the literuature [40, 41, 42, 43, 44].

the large-N limit, since $f_\pi \sim \sqrt{N}$. The third term is the first $1/N$ correction to the chiral Lagrangian coming from the ABJ anomaly, and $m_{\eta'} \sim 1/\sqrt{N}$ is the Witten-Veneziano mass (1.29). Let us put it on the bench for the moment; we will go back to it in section 2.3. There is a unique trivially gapped ground state of the theory, which is $\eta' = 0 \bmod 2\pi$.

2.2 Extended configurations of the η' meson: the sheets

Let us study the symmetries of the Lagrangian (2.3). We have already observed that η' takes values on a circle S^1 and therefore the Lagrangian is invariant under $\eta' \to \eta' + 2\pi$. Moreover, if we set $m = 0$ we restore the exact chiral symmetry.

This model enjoys another symmetry which lies in a class of symmetries that go by the name of *generalized symmetries*. For the purposes of our discussion, we can limit ourselves to the basic definition of these symmetries following [106, 107]. We are accustomed to understanding global and gauge symmetries as acting on fields or, more generally, on local operators in a quantum field theory. These symmetries may be either discrete or continuous. Continuous symmetries are associated with conserved currents J^μ, satisfying the conservation equation $\partial_\mu J^\mu = 0$. In the language of differential forms, J is a one-form, and conservation law translates to $d \star J = 0$. Given such a current, one can define a conserved charge by integrating J over a codimension-one sub-manifold $X \subset \mathcal{M}$ of the whole spacetime $\mathcal{M}$:

$$Q = \int_X \star J. \tag{2.4}$$

This charge acts on local operators $\mathcal{O}^i$ defined at a point $x \in X$ via

$$e^{iQ}\mathcal{O}^i(x) = R^i_j \mathcal{O}^j(x), \tag{2.5}$$

where R^i_j represents the group action. In the case of a discrete symmetry, there is no associated conserved current, yet the generator can still be linked to a codimension-one manifold. We refer to both continuous and discrete symmetries of this sort as zero-form symmetries. These are the standard symmetries commonly encountered in quantum field theory.

The notion of *generalized symmetries* extends this framework to include higher-form symmetries. A q-form symmetry is defined such that its generator is associated with a co-dimension $(q+1)$ submanifold $X \subset \mathcal{M}$. For a continuous q-form symmetry, there exists a conserved $(q+1)$-form current J, and the corresponding conserved charge is given again by $Q = \int_X \star J$. For $q > 0$, these generalized symmetries are necessarily Abelian. This property arises from the structure of the group multiplication, $Q_{g_1}(X)Q_{g_2}(X)$, for group elements g_1 and g_2. In the $q = 0$ case, the associated manifolds are codimension-one, and we can define this product via time-ordering. However, for $q > 0$, such an ordering is not possible, implying that the symmetry generators must commute. A q-form symmetry acts on operators defined on q-dimensional manifolds $\mathcal{C}$. For instance, one-form symmetries act on line operators, such as Wilson lines.

Let us go back to the Lagrangian (2.3). As we anticipated, this model enjoys a generalized symmetry. This is a topological U(1) two-form symmetry, associated with the current

$$J^{\mu\nu\rho} = \frac{1}{2\pi}\epsilon^{\mu\nu\rho\sigma}\partial_\sigma \eta'. \tag{2.6}$$

In the language of differential forms, J is a (2+1)-form current, and it is topologically conserved, as one can easily see from

$$\partial_\mu J^{\mu\nu\rho} = \frac{1}{2\pi}\epsilon^{\mu\nu\rho\sigma}\partial_\mu\partial_\sigma \eta' = 0. \tag{2.7}$$

The associated conserved number is classified by the fundamental group of U(1): $\pi_1(\mathrm{U}(1)) = \pi_1(S^1)$, where we used $\mathrm{U}(1) \sim S^1$. Charged objects under this symmetry are infinitely extended, $(2+1)$-dimensional objects that interpolate from $\eta' = 0$ on one side to $\eta' = 2\pi$ on the other. Through this work, we will call these objects *sheets*. In order to visualize an infinite sheet, consider the simple configuration

$$\eta' = f(x_3), \qquad \lim_{x_3\to-\infty} f(x_3) = 0, \qquad \lim_{x_3\to+\infty} f(x_3) = 2\pi, \tag{2.8}$$

in the Minkowski spacetime spanned by the coordinate (t, x_1, x_2, x_3), where η' is some function f of the spatial coordinate orthogonal to the sheet solely, which we called x_3. This configuration satisfies

$$Q = \int d^3x\, J_{t\,x_1\,x_2} = 1 \tag{2.9}$$

An issue concerning these sheets is that they are not finite energy configurations because they have a divergent mass. However, things may change if the sheet has a *boundary* preventing it from being extended infinitely. Around the boundary, the η' field has the monodromy $\eta' \to \eta + 2\pi$ and as a consequence, the field η' cannot be smooth everywhere: it has to be singular somewhere in spacetime. It is easiest if we take advantage of figure 2.1. As one can see, the field can interpolate continuously between the two vacua $\eta' = 0$ and $\eta' = 2\pi$ through the sheet placed at $\eta' = \pi$. But what happens outside the sheet? We would like that $\eta' = 0 \mod 2\pi$ outside the sheet in order to construct finite energy configurations. However, this requirement violates the monodromy of η', because the field η' can stay in the 0-vacuum while avoiding the sheet, ending in a region where $\eta' = 2\pi$. Thus, we conclude that the η' field must be singular, and the minimal singularity that must exist is of the form of the boundary. One can interpret this monodromy violation with the presence of a higher-dimensional Dirac string through which η' has a jump discontinuity from 0 to 2π. We will call this object *Dirac sheet* and it will be investigated in detail in chapter 4.

Within the effective Lagrangian (2.3), the tension of these boundaries is incalculable. It diverges logarithmically in the ultraviolet, as one can see from a qualitative analysis [38]:

$$T_{\mathrm{bdry}} \sim N\Lambda^2_{\mathrm{QCD}} \log \Lambda_{\mathrm{cutoff}} \tag{2.10}$$

where T_{bdry} denotes the tension of the string-like boundary and it is of order N just because the effective Lagrangian (2.3) is of order N.

Before we study the effective field theory on the sheet and its boundary, we must pause for a moment and ask ourselves if this makes sense. Indeed, it seems that we have found a paradox: from the point of view of the infrared theory, there are objects,

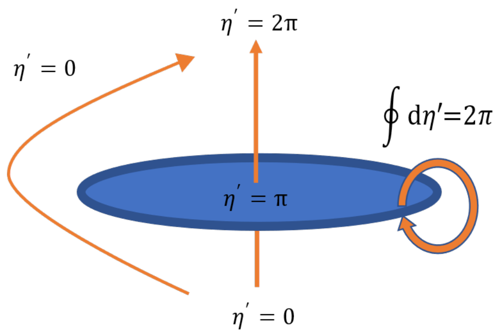

Figure 2.1. The figure shows schematically a sheet living in the field space at $\eta' = \pi$, with a circular boundary. The η' field has a $\eta' \to \eta' + 2\pi$ monodromy around the boundary.

the sheets, which carry a conserved charge and hence cannot decay, but there are no such unbreakable objects in the full QCD theory. Thus, these sheets must decay because they do not separate two distinct vacua and do not carry a conserved charge in the full theory. We said that the mass of the strings is incalculable in the infrared theory. This is why, from the point of view of the infrared observer, the sheets seem stable. Hence, we argue that the divergence in the energy will be regulated in the full theory.

We need to estimate the lifetime of the sheet. Since the tension of the boundary scales like N, and since the tension of the sheet itself also scales like N (both follow simply from the fact that the Lagrangian (2.3) is of order N), it immediately follows that the decay probability per unit volume and per unit time, Γ, obeys:

$$\log \Gamma \sim -N. \tag{2.11}$$

Thus, the sheet is metastable in the large N limit, and the question of finding the effective field theory on it makes sense.

2.3 The effective field theory on the sheets

So far, we have discussed some features of these new objects, the sheets, and yet there is no sign of baryons. The turning point in this discussion is the observation that the η' effective theory is incomplete: there is a *cusp singularity* in the potential, and it is because of this that we can reinterpret some excitations of the theory as baryons.

The cusp singularity appears when we include the $1/N$ correction through the potential term

$$\frac{f_\pi^2 m_{\eta'}^2}{2} \min_{k\in\mathbb{Z}} (\eta' + 2\pi k)^2, \tag{2.12}$$

which is a perfectly smooth and 2π-periodic function except for $\eta' = \pi \mod 2\pi$. Such a cusp singularity in an effective theory is quite mild. It does not signal the appearance of new light particles in $(3 + 1)$-dimensions, usually associated with branch cuts in the effective potential. The physical interpretation of the cusp is that at $\eta' = \pi$ some heavy fields jump from one vacuum to the other. These heavy fields are the glueballs, which are not taken into account in the chiral Lagrangian.

Before proceeding to study the effects of this cusp singularity on the effective theory on the sheet, we must make some cautionary remarks. Within an effective theory such as (2.3), for sufficiently small m, the sheet is guaranteed to be a metastable configuration in the theory, decaying through non-perturbative effects that scale like (2.11). However, due to the cusp singularity at the core of the sheet and the fact that some heavy fields are rearranged at the core of the sheet, we cannot prove that the sheet is a metastable configuration in the effective theory. It might disappear altogether. While one can give several qualitative arguments supporting the existence of the sheet despite the mild singularity that makes the effective field theory break down, at present, this is not proven and should be viewed as an assumption.

The effective field theory on the sheet always includes the center-of-mass degrees of freedom, typically described by the Dirac–Born–Infeld (DBI) action. This action captures the low-energy dynamics of the transverse fluctuations of the sheet. However, since we are primarily interested in the internal dynamics on the sheet, we will omit this term for the moment. The effective field theory that lives on the η'-sheet can be motivated using arguments presented in [39, 105, 38]. These arguments rely on sophisticated tools involving 't Hooft anomalies, especially mixed anomalies involving discrete symmetries. While a full account would require these advanced techniques, which are beyond the scope of this work, we aim to give a physical intuition for the emergence of the effective field theory.

To illustrate these ideas, let us begin with an instructive (though not minimal) example [108, 39, 105]. Pure SU(N) Yang-Mills theory admits multiple global formulations that differ in the global structure of the gauge group. Since the gauge bosons transform in the adjoint representation, they are invariant under the center symmetry $\mathbb{Z}_N \subset \mathrm{SU}(N)$:

$$\mathbb{Z}_N = \left\{ e^{2\pi i k/N} \cdot \mathbb{I}_N, \quad k = 0, 1, \ldots, N-1 \right\}. \tag{2.13}$$

This suggests that the gauge group could be taken to be either SU(N) or the quotient $\mathrm{SU}(N)/\mathbb{Z}_N$. However, this choice is not merely a matter of convenience: it defines distinct quantum field theories. More generally, for any subgroup $\mathbb{Z}_p \subset \mathbb{Z}_N$, one can consider a gauge group $G_p = \mathrm{SU}(N)/\mathbb{Z}_p$. The key point is that although these theories share the same Lie algebra $\mathfrak{su}(N)$, and hence the same local operator content and Lagrangian density, their global properties differ. In particular, they differ in their spectrum of non-local operators, such as Wilson and 't Hooft lines, and in how they respond to background gauge fields for global symmetries.

For instance, Wilson lines are labeled by representations of the gauge group. The representations of $G = \mathrm{SU}(N)/\mathbb{Z}_N$ form a strict subset of those of SU(N), as some representations, such as the fundamental, are not well-defined in the quotient group. Consequently, the theory with gauge group $G_N = \mathrm{SU}(N)/\mathbb{Z}_N$ does not allow Wilson lines in the fundamental representation. Only those representations invariant under the action of the center are permitted. Similarly, matter fields transforming in representations that are not center-invariant (such as fundamental matter) cannot be coupled to such a theory. Only adjoint or other center-blind representations are allowed.

Another crucial difference between the two theories arises in their behavior under shifts of the θ-angle. For $G = \mathrm{SU}(N)$, the theory is invariant under $\theta \to \theta + 2\pi$, owing to the fact that the instanton number is quantized in integers. However, when the gauge group is $G_N = \mathrm{SU}(N)/\mathbb{Z}_N$, the instanton number becomes fractional, taking values in $\frac{1}{N}\mathbb{Z}$, due to the presence of non-trivial bundles with a non-trivial second Stiefel–Whitney class. As a result, the theory is invariant only under $\theta \to \theta + 2\pi N$.

$$G = \mathrm{SU}(N) : \theta \in [0, 2\pi), \qquad G_N = \mathrm{SU}(N)/\mathbb{Z}_N : \theta \in [0, 2\pi N). \tag{2.14}$$

Let us now focus on discrete symmetries, in particular $\mathcal{CP}$ (or equivalently, time-reversal symmetry), under which $\theta \to -\theta$. Time-reversal invariant points then correspond to fixed points under this transformation:

$$\theta = 0, \pi \qquad \text{for} \qquad G = \mathrm{SU}(N), \tag{2.15}$$

$$\theta = 0, \pi N \qquad \text{for} \qquad G_N = \mathrm{SU}(N)/\mathbb{Z}_N. \tag{2.16}$$

These fixed points do not generally align across the two theories. For example, suppose we start with the $\mathrm{SU}(N)$ Yang–Mills theory at $\theta = \pi$, which is time-reversal invariant. Now consider gauging the $\mathbb{Z}_N$ one-form global symmetry: this effectively promotes the center symmetry to a gauge symmetry and transforms the theory into one with gauge group $G_N = \mathrm{SU}(N)/\mathbb{Z}_N$.

However, under this procedure, the θ-angle must be reinterpreted. In the new theory, the angle becomes

$$\theta_{\mathrm{SU}(N)/\mathbb{Z}_N} = (2p+1)\pi, \quad \text{for some } p \in \mathbb{Z}, \tag{2.17}$$

which is *not* a time-reversal invariant point when N is even.[3] Indeed, for even N, there exists no integer p for which $\theta_{\mathrm{SU}(N)/\mathbb{Z}_N} = 0$ or πN. This implies that the gauging of the one-form symmetry explicitly breaks time-reversal invariance.

This phenomenon reflects the presence of a *mixed 't Hooft anomaly* between the $\mathbb{Z}_N$ one-form symmetry and time-reversal symmetry. In essence, these two symmetries cannot be simultaneously preserved: gauging one necessarily breaks the other. Due to anomaly matching, this anomaly must manifest in the infrared effective theory.

At $\theta = \pi$, time-reversal is spontaneously broken, leading to two degenerate vacua related by $\mathcal{CP}$. Domain walls can then interpolate between these vacua. Since the two vacua differ by a discrete symmetry transformation, the theory on the domain wall must itself encode the anomaly. Remarkably, it can be shown [39] that the anomaly is saturated by a $(2+1)$-dimensional topological quantum field theory (TQFT) living on the domain wall. An appropriate theory turns out to be an $\mathrm{SU}(N)_1$ Chern–Simons theory:

$$\frac{1}{4\pi}\int_{M_3} \mathrm{tr}\left(\widetilde{a} \wedge d\widetilde{a} + \frac{2}{3}\widetilde{a} \wedge \widetilde{a} \wedge \widetilde{a}\right), \tag{2.18}$$

where M_3 denotes the (2+1)-dimensional worldvolume of the domain wall and $\widetilde{a}$ is an $\mathfrak{su}(N)$-valued gauge connection. This theory correctly reproduces the anomaly structure and hence provides the effective field theory on the domain wall.

[3] We can end up with the same conclusion also for N odd. In order to prove it, we would have to invoke a whole bunch of new machinery, and therefore we restrict ourselves to even N.

It is natural to conjecture that also for $N_f = 1$ QCD, the configuration that interpolates between $\eta' = 0$ to $\eta' = 2\pi$ carries a $\mathrm{SU}(N)_1$ Chern–Simons theory on the sheet at $\eta' = \pi$. Let us explain the heuristic reason for the appearance of this TFT in the one-flavored case, but please note that this is far from being a demonstration. If we perform an axial transformation with parameter α, this leads to $\theta \to \theta + 2\alpha$, accompanied by $q \to e^{i\alpha\gamma_5} q$. Taking $\alpha = \pi$, the shift $\theta \to \theta + 2\pi$ implements the transformation described in the example above. Thus, the sheet of the one-flavored QCD, and so the η' configuration, plays the role of a domain wall in pure Yang–Mills theory.

In summary, we have found that the Lagrangian (2.3) admits some extended excitations of the η' field, known as sheets. They are very long-lived in the large-N limit, so studying the effective field theory that lives on their world volume makes sense. It turns out that due to the rearrangement of some glueballs, the $\eta' = \pi$ sheet carries a non-trivial topological field theory.

Non-Abelian Chern–Simons theories are quite difficult to deal with, so we make use of the level-rank dualities [109], which are known exact dualities between Chern–Simons theories. In our case, we can use the following level-rank duality:

$$\mathrm{SU}(N)_1 \longleftrightarrow \mathrm{U}(1)_N. \tag{2.19}$$

Finally, we can write the theory on the sheet (again, we are omitting the DBI term) by the introduction of an Abelian connection a:

$$S_{\text{sheet}} = \frac{N}{4\pi} \int_{M_3} a \wedge da, \tag{2.20}$$

where now M_3 is the $(2+1)$-dimensional space spanned by the sheet worldvolume.

2.4 Baryons as quantum Hall droplets

We have all the ingredients to show how baryons arise in this framework. The theory on the sheet (2.20) is a $\mathrm{U}(1)_N$ Chern-Simons theory defined on a three-dimensional manifold M_3. As discussed in appendix A, this theory is intimately connected with the physics of the fractional quantum Hall effect (FQHE). In condensed matter physics, the FQHE describes a strongly correlated phase of electrons in two dimensions under a strong magnetic field, and at low temperature, characterized by a quantized Hall conductance:

$$\sigma_H = \frac{e^2}{h} \nu, \tag{2.21}$$

where e is the electron charge, h is the Planck constant and ν is a rational number known as the *filling fraction*. For certain values of ν, such as $\nu = 1/N$ with N odd, the low-energy effective field theory is given by a $\mathrm{U}(1)_N$ CS theory [110, 111].

This connection was first formalized by Zhang, Hansson, and Kivelson [110] in the context of the effective field theory for the FQHE. The electrons form an incompressible quantum fluid with topological order, where individual particle identities are lost and only collective excitations (anyons) survive at low energies.

The emergent gauge field a in the CS theory encodes the dynamics of these collective modes. Coupling a to an external electromagnetic field A via the term

$$S_{\text{int}} = \frac{1}{2\pi}\int a \wedge dA, \tag{2.22}$$

yields a total action

$$S = \frac{N}{4\pi}\int a \wedge da + \frac{1}{2\pi}\int a \wedge dA. \tag{2.23}$$

Integrating out a leads to the Hall response with filling fraction $\nu = 1/N$, reproducing the correct Hall conductance.

Let us go back to the theory on the sheet. We want to couple it with the $\mathrm{U}(1)_B$ baryonic background gauge field, namely A_B, which plays the role of the external electromagnetic field in the standard FQHE. The minimal coupling is

$$\frac{1}{2\pi}\int_{M_3} a \wedge dA_B, \tag{2.24}$$

as in the FQHE with $A \to A_B$. In the language of level-rank duality, the baryon symmetry is now a magnetic symmetry in the description based on the $\mathrm{U}(1)_N$ theory. The effective field theory on the sheet (without the DBI term) is

$$S_{\text{sheet}} = \frac{N}{4\pi}\int_{M_3} a \wedge da + \frac{1}{2\pi}\int_{M_3} a \wedge dA_B. \tag{2.25}$$

We can go on with the parallelism between our model and the fractional quantum Hall physics. Our sheet is, in fact, a droplet realizing the fractional quantum Hall effect. It is an Abelian quantum Hall state, and for this reason, we refer to the sheet as a *Hall droplet*. The presence of the boundary is crucial to claim the stability of these objects, even at finite N. It can be shown that, if the action (2.25) is defined on a manifold with boundary, the gauge degrees of freedom become dynamical at the edge. This is the *bulk-boundary correspondence*, briefly discussed in appendix A: the universal physics of the bulk, including the electromagnetic (baryonic) response, is encoded in the edge theory. For a circular boundary of radius R, the edge physics is described by the Floreanini-Jackiw [112] action:

$$S_{\text{edge}} = \frac{N}{4\pi}\int dt dx\, (\partial_t \chi + v\, \partial_x \chi)\, \partial_x \chi, \tag{2.26}$$

where $x = R\varphi$ is the coordinate along the boundary, and R is the radius of the circular boundary. The field χ, related to the gauge connection a through $a = d\chi$, is the chiral edge mode moving at a velocity v along the compact boundary, and hence χ is called the compactified chiral boson.[4] It is a periodic field $\chi \sim \chi + 2\pi n$ with $n \in \mathbb{Z}$. The total baryon charge is given by the winding of the chiral boson along the boundary

$$n_B = \frac{1}{2\pi}\int d\chi. \tag{2.28}$$

[4]The chirality of the field χ, can be read from the Floreanini-Jackiw action, and the associated Euler-Lagrange equation, which reads

$$(\partial_t + v\, \partial_x)\partial_x \chi = 0. \tag{2.27}$$

Thus, the operator carrying one unit of baryon charge is the vertex operator

$$\mathcal{V}_1 =: e^{iN\chi} :, \tag{2.29}$$

where the subscript indicates the baryon number of the operator $\mathcal{V}$.

The energy of the state corresponding to the operator $\mathcal{V}_1$ over the ground state is $\sim N/R$. The scaling with N follows from the fact that the action is proportional to N, while the $1/R$ follows from the energy dependence on the geometry of a chiral edge state. The spin of this operator is $N/2$ (see formula (A.19) of the appendix A), which is the spin of the one-flavored baryon. This construction bridges the gap between the UV baryons and the IR effective theory: we now have a description of the baryons in terms of objects in the IR field theory.

The configuration presented above can be argued to be dynamically stable. There are various contributions to the energy of this configuration. As we already mentioned, the Hall droplet prefers to shrink due to its tension and the tension of the physical boundary. Both these contributions are positive and scale linearly with N, so it is preferable for the droplet to simply disappear. However, as soon as the vertex operator (2.29) is excited, the natural tendency of the droplet to shrink due to its tension cannot eliminate this configuration. The final product is a baryon with size that does not scale with N, as we expect.

One can understand qualitatively why the excitation corresponding to the baryon vertex operator (2.29) may stop the droplet from shrinking altogether. In the presence of the baryon vertex operator, there is a force that counteracts the tension of the droplet and its boundary. Qualitatively, the energy of a droplet of size R is (omitting numerical factors)

$$E(R) \simeq TR^2 + T_{\text{bdry}}R + \frac{N}{R}, \tag{2.30}$$

where T is the tension of the droplet and T_{bdry} is the tension of the boundary. The first two terms scale like N and simply prefer to shrink the droplet altogether. But the last term, which is associated with the baryon vertex energy, counteracts the tension forces and may lead to a stable droplet of size (up to numerical factors)

$$R \sim \frac{1}{\Lambda_{\text{QCD}}}. \tag{2.31}$$

This size follows simply from dimensional arguments: Λ_{QCD} is the only dimensional quantity of the theory. Of course, any computation in the effective theory breaks down at the QCD scale, but it is encouraging to see that one can understand qualitatively why the droplet may be stable in the full theory in the presence of the vertex operator.

Interestingly, in addition to $\mathcal{V}_1$, the theory also contains $\mathcal{V}_{1/N} =: e^{i\chi} :$ that carries fractional $1/N$ baryon charge. This is the basic anyon of FQHE and can be identified with the microscopic quark. We can dress the operator (2.29) with these anyonic-quark excitations, which do not change the baryon charge. For instance, we can consider the state corresponding to the vertex operator:

$$: \partial\chi \, e^{iN\chi} : \tag{2.32}$$

This would be an excitation of the baryon, like we have excited one of the quarks that form the baryon, where the energy is greater by $\sim 1/R$ ($\sim \Lambda_{\rm QCD}$) and the spin is one unit higher.

Hall droplet baryons in the $N_f > 1$ case.

Let us now consider the SU(N) gauge theory coupled to N_f light Dirac quarks in the fundamental representation of the gauge group. We take $\theta = 0$ as previously. In this setup, the analog of the conserved current discussed in equation (2.6) becomes

$$J = \mathrm{Tr}(\mathcal{U}^{-1} d\mathcal{U}), \tag{2.33}$$

where $\mathcal{U}$ is a U(N_f)-valued field parameterizing the low-energy degrees of freedom. This current corresponds to a two-form U(1) symmetry, generalizing the Abelian case considered previously. In the confined phase, the theory admits a unique vacuum, realized at $\mathcal{U} = \mathbb{I}_{N_f}$. Nevertheless, the existence of the conserved two-form symmetry implies the presence of codimension-one objects, the sheets, which interpolate between topologically distinct configurations. Specifically, the sheet induces a jump in the phase of $\mathcal{U}$ from $\mathcal{U} = \mathbb{I}_{N_f}$ to $\mathcal{U} = e^{i2\pi}\mathbb{I}_{N_f}$, and must carry nontrivial degrees of freedom to match the anomaly associated with the two-form symmetry.

It can be argued that the infrared theory on the sheet supports an SU$(N)_{-N_f}$ Chern-Simons topological field theory. This follows from anomaly inflow arguments and can be understood as a generalization of the single-flavor case. Recalling the standard level-rank duality,

$$\mathrm{SU}(N)_{-N_f} \longleftrightarrow \mathrm{U}(N_f)_N, \tag{2.34}$$

we can interpret the sheet as hosting a U$(N_f)_N$ theory in dual variables, with a background $u(N_f)$ connection a living on its worldvolume. The baryon number symmetry, as before, couples to the U(1) part of a via the coupling

$$\frac{1}{2\pi}\int_{M_3} \mathrm{Tr}(a \wedge dA_B), \tag{2.35}$$

where A_B is a background gauge field for the global U$(1)_B$ symmetry. This coupling captures the baryon number carried by the edge modes of the Hall droplet.

There are many interesting features and open questions associated with this multi-flavor generalization. While we do not explore them in full detail here, let us highlight a few reasons why this construction is physically significant. One particularly intriguing aspect is its potential connection to the Skyrme model. It is tempting to conjecture that the dynamics of the η' field, the associated Hall droplet, and the chiral edge states provide a useful description for high-spin baryons. In contrast, low-spin baryons may be better captured by the conventional Skyrmion picture. Importantly, the baryon number symmetry is unique and universal; thus, the same background field A_B couples both to the Skyrmion current in the bulk and to the Hall droplet degrees of freedom on the sheet. This suggests that transitions between Skyrmions and Hall droplets should be possible, and understanding such transitions remains an important direction for future work. We will return to these ideas in Chapter 7.

In the real world, with $N = 3$, extrapolations to large N can be subtle and potentially ambiguous. Take, for example, the Δ^{++} or Ω^{-} baryons, which both have spin 3/2. At large N, one can interpret such states in two qualitatively different ways. In one approach, we hold the spin fixed and consider baryons built from multiple quark flavors, maintaining spin 3/2 even as N grows. This perspective aligns well with the Skyrmion description, where the baryon is a topological soliton of the chiral Lagrangian. Alternatively, we can consider baryons composed predominantly of a single quark flavor, such that the total spin scales with N, typically as $J \sim N/2$. This matches the structure of the quantum Hall droplet picture, which naturally accommodates such high-spin states through collective edge excitations. Both extrapolations are valid and may capture complementary aspects of the same physical baryons. Notably, the Hall droplet model appears to reproduce key quantum numbers and structural features of the Δ^{++} and Ω^{-}, suggesting it provides a useful dual perspective, especially in the high-spin, single-flavor regime.

Chapter 3

Holographic QCD

The holographic correspondence provides a robust framework for investigating the non-perturbative dynamics of quantum field theories. A key focus within this approach has been the study of large-N models of QCD in the strongly coupled regime, where traditional methods face significant challenges. Over the years, significant progress has been made in developing holographic models of QCD, leading to the so called *holographic QCD framework* [31, 113, 32, 34, 35, 36, 37]. The original contributions of the present thesis focus on some applications of holography to QCD-like theories, and therefore, in this chapter, we review the foundations of holographic QCD.

This chapter is organized as follows. In section 3.1, we recall the basics of the holographic correspondence. We will focus on how confinement and the breaking of conformality can be achieved in holography. We will also show how flavors can be introduced in the holographic dual of gauge theories. In section 3.2, we present the WSS model, which is the top-down holographic model that better resembles QCD in the planar limit and in the low-energy, strongly coupled regime, while in section 3.3, we discuss the finite-temperature version of the WSS model.

3.1 Basics of the gauge/gravity correspondence

3.1.1 Strings and branes

The basic object of string theory is the string, a one-dimensional object with characteristic size l_s, referred to as string length. The classical description of a relativistic bosonic string is inspired by that of a point-particle with mass m in special relativity, whose action is proportional to the integral of the line element ds along the trajectory in (flat) spacetime $X^\mu(s)$, namely

$$S = -m \int ds = -m \int ds \sqrt{\eta_{\mu\nu} \frac{dX^\mu(s)}{ds} \frac{dX^\nu(s)}{ds}}, \tag{3.1}$$

where s is the affine parameter. From a geometrical point of view, this is just the length of the worldline. A string moving in spacetime describes a surface Σ known as the worldsheet, whose area element is $d\Sigma$. Then, the immediate generalization of

(3.1) for a string is given by the Nambu-Goto action

$$S_{\rm NG} = -T_f \int_\Sigma d\Sigma = -T_f \int_\Sigma d^2 s \sqrt{\det P[g_{ab}]}\,, \tag{3.2}$$

where

$$P[g_{ab}] = g_{\mu\nu} \frac{dX^\mu}{ds^a} \frac{dX^\nu}{ds^b}\,, \tag{3.3}$$

is the pullback of the background curved spacetime metric $g_{\mu\nu}$, and T_f is the tension of the fundamental string, which can be expressed in terms of the string length as

$$T_f = \frac{1}{2\pi l_s^2}. \tag{3.4}$$

There is an equivalent description of the string dynamics, known as the Polyakov action

$$S_{\rm P} = -\frac{T_f}{2} \int_\Sigma d^2 s \sqrt{-h}\, h^{\alpha\beta} g_{\mu\nu} \frac{dX^\mu}{ds^\alpha} \frac{dX^\nu}{ds^\beta}\,. \tag{3.5}$$

The price we pay is the introduction of an auxiliary field h, which is the intrinsic metric on the worldsheet Σ. The action enjoys the Weyl invariance

$$X^\mu(s) \to X'^\mu(s) = X^\mu(s), \tag{3.6}$$

$$h_{\alpha\beta}(s) \to h'_{\alpha\beta}(s) = \Omega^2(s) h_{\alpha\beta}(s), \tag{3.7}$$

for some arbitrary positive function Ω. Weyl invariance can be used, together with the reparameterization invariance, to make the intrinsic metric flat $h = \eta$.

The quantization of the bosonic string in flat spacetime leads to a spectrum which includes tachyons, *i.e* particles with $m^2 < 0$, signalling an instability of the theory. To overcome this problem, the theory must include fermionic coordinates for the string and require the theory to be supersymmetric. This is realized, with $h = \eta$, by

$$S_{\rm P} \to S_{\rm P} - \frac{T_f}{2} \int_\Sigma d^2 s\, \overline{\Psi}^{\,\mu} \gamma_\alpha \partial_\beta \overline{\Psi}^{\,\nu} \eta^{\alpha\beta} \eta_{\mu\nu}\,, \tag{3.8}$$

where γ_α is the two-dimensional gamma matrix and Ψ^μ is a two-dimensional Majorana spinor. Such a theory, called *superstring* theory, is anomalous at the quantum level unless it lives in *ten* spacetime dimensions.

A string can be open or closed. The spectrum of open strings contains massless particles of spin one whose dynamic is effectively described by the action of gauge bosons. The closed string spectrum contains massless spin two particles, which satisfy the Einstein equations. They are therefore identified with the gravitons. Therefore, the spectrum of strings contains the fundamental fields of particle physics (gauge bosons) and gravity (gravitons), living in the same target space, providing an important step towards a unifying theory.

Several string theories can be built out of string quantization. Here, we focus on the so-called type IIA and type IIB string theory, living in ten dimensions, which in the low-energy limit and perturbative regime reduce to type IIA and IIB supergravity theories whose degrees of freedom arise from the massless excitations of the closed string spectrum. The bosonic part of the spectrum is

$$\text{Type IIA:} \qquad \phi, \qquad B_2, \qquad g_{\mu\nu}, \qquad C_1, \qquad C_3, \tag{3.9}$$

$$\text{Type IIB:} \qquad \phi, \qquad B_2, \qquad g_{\mu\nu}, \qquad C_0, \qquad C_2 \qquad C_4, \tag{3.10}$$

where ϕ is a scalar field known as dilaton, B_2 is the Kalb-Ramond two-form, g is the metric, and C_n are the Ramond-Ramond n-forms. The expectation value of the dilaton determines the string coupling constant

$$g_s = e^{\langle \phi \rangle}, \tag{3.11}$$

which controls the perturbative expansion of string theory. In particular, string perturbation theory is organized as a sum over (string) worldsheet topologies: a genus-g worldsheet corresponds to a g-loop contribution, and each additional handle is weighted by a factor of g_s^{2g-2}. Hence, perturbation theory is reliable only in the regime $g_s \ll 1$. Crucially, g_s is not an independent parameter, but is instead determined dynamically by the expectation value of the dilaton field.

The bosonic part of the type IIA and type IIB supergravity actions reads

$$\begin{aligned} S_{\mathrm{IIA}} =& \frac{1}{2\kappa_{10}^2} \int d^{10}x \sqrt{-g} \left[e^{-2\phi} \left(R + 4(\partial\phi)^2 - \frac{1}{2}|H_3|^2 \right) - \frac{1}{2}|F_2|^2 \right. \\ & \left. - \frac{1}{2}|\widetilde{F}_4|^2 \right] - \frac{1}{4\kappa_{10}^2} \int B_2 \wedge F_4 \wedge F_4, \end{aligned} \tag{3.12}$$

$$\begin{aligned} S_{\mathrm{IIB}} =& \frac{1}{2\kappa_{10}^2} \int d^{10}x \sqrt{-g} \left[e^{-2\phi} \left(R + 4(\partial\phi)^2 - \frac{1}{2}|H_3|^2 \right) - \frac{1}{2}|F_1|^2 \right. \\ & \left. - \frac{1}{2}|\widetilde{F}_3|^2 - \frac{1}{2}|\widetilde{F}_5|^2 \right] - \frac{1}{4\kappa_{10}^2} \int C_4 \wedge H_3 \wedge F_3, \end{aligned} \tag{3.13}$$

where

$$2\kappa_{10}^2 = (2\pi)^7 l_s^8. \tag{3.14}$$

The forms appearing in the action are defined as

$$\begin{aligned} &F_p = dC_{p-1}, && H_3 = dB_2, && \widetilde{F}_3 = F_3 - C_0\, F_3, \\ &\widetilde{F}_4 = F_4 - C_1 \wedge F_3, && \widetilde{F}_5 = F_5 - \frac{1}{2}C_2 \wedge H_3 + \frac{1}{2}B_2 \wedge F_3. \end{aligned}$$

We stress that these actions are valid in the low-energy limit and in the perturbative regime

$$\text{energy} \ll l_s^{-1}, \qquad g_s \ll 1. \tag{3.15}$$

The effective actions above are written in the so-called *string frame*, in which the dilaton couples explicitly as an overall factor $e^{-2\phi}$ in front of the Einstein-Hilbert term. In this frame, the metric $g_{\mu\nu}$ corresponds directly to the one seen by the fundamental string. One can alternatively define the *Einstein frame* by performing a Weyl rescaling of the metric, so that the Einstein-Hilbert term takes the canonical form without a dilaton prefactor. Unless otherwise stated, we will work in the string frame.

The equations of motion derived from the above actions admit a particular class of solutions charged under the RR potentials C_{p+1}. These solutions are known as extremal p-branes [114, 115, 116]. Requiring Poincaré symmetry in $(p+1)$-dimensions and rotational symmetry along the $(9-p)$ remaining dimensions, the metric associated with these solutions reads

$$ds^2 = H^{-1/2}(r)\eta_{\alpha\beta}dx^\alpha dx^\beta + H^{1/2}(r)\left(dr^2 + r^2 d\Omega^2_{8-p}\right), \tag{3.16}$$

where $\alpha, \beta = 0, 1, ..., p$, the coordinate r is the radius of the transverse space to the $(p+1)$-dimensional worldvolume, and

$$H(r) = 1 + \left(\frac{R_p}{r}\right)^{7-p}, \quad R_p^{7-p} = \frac{g_s N (2\pi l_s)^{7-p}}{(7-p)V(S^{8-p})}, \quad V(S^n) = \frac{2\pi^{\frac{n+1}{2}}}{\Gamma(\frac{n+1}{2})}. \tag{3.17}$$

In the formulas above, we have defined the warp factor $H(r)$, R_p as the characteristic length of the spacetime, and given their expressions in terms of g_s and N, an integer number which denotes the units of RR flux on the S^{8-p} sphere. The other (bosonic) fields in the extremal p-brane solution are

$$e^{\phi(r)} = g_s |H(r)|^{(3-p)/4}, \qquad C_{p+1} = g_s^{-1}(H^{-1}(r) - 1)dx^0 \wedge \cdots \wedge dx^p. \tag{3.18}$$

The supergravity approximation is consistent if we can neglect the $\mathcal{O}(l_s)$ corrections. Therefore, the solution is reliable only if its curvature is small in string length units, namely $R_p/l_s \gg 1$. In terms of g_s and N:

$$g_s N \gg 1. \tag{3.19}$$

Since the perturbative regime requires that $g_s \ll 1$, the above relation translates to $N \gg 1$. This means that the solution is reliable only in the large-N limit.

The seminal paper of Polchinski [117] shows that these extremal p-brane solutions can be identified with the backreaction of extended objects in string theory placed at $r = 0$, known as Dp-branes. In particular, the flux of the RR form on S^{8-p} is related to the charge of N coincident Dp-branes through the following formula

$$\frac{1}{2\kappa_{10}^2} \int_{S^{8-p}} \star F_{p+2} = N\,\mu_p, \tag{3.20}$$

where μ_p is the Dp-brane charge whose expression is given a few lines below in (3.22).

From a microscopic point of view, Dp-branes are $(p+1)$-dimensional objects in string theory, on which open strings can end. Dp-branes are not just geometrical objects but also have their own dynamics. In particular, since the open string spectrum contains a U(1) gauge field, we can interpret the corresponding field strength as an internal excitation, living on the Dp-brane worldvolume. Moreover, the embedding of the brane in the ambient spacetime can be parametrized by $(9-p)$ coordinates Φ^I $(I = 1, \ldots, 9-p)$ transverse to the brane, which behave as scalar fields. When two branes are separated, the low-energy states in the open strings stretching between them acquire mass proportional to their separation, leading to a Higgs-like mechanism. If the branes coincide, the lightest states are massless gauge vectors, scalars, and their superpartners. Introducing Chan-Paton factors adds global labels to string endpoints, promoting global symmetries on the worldsheet to local gauge symmetries in spacetime. For N Dp-branes, assigning each Chan-Paton index to a different brane yields a $\mathrm{U}(1)^N$ gauge group, enhanced to $\mathrm{U}(k) \times \mathrm{U}(1)^{N-k}$ when k branes coincide. Fields V_{ij} represent strings between branes i and j, with massless states for coinciding branes and massive states for separated ones. Massless vectors A_{ij} transform non-trivially under $SO(1,p)$ on the brane, while scalars Φ_{ij} transform non-trivially under internal $SO(d-p-1)$. Massive vectors W_{ij} and scalars Φ_{ij} arise from symmetry breaking, with the scalar acquiring a vacuum expectation value, restoring the correct degree of freedom count via the Higgs mechanism.

The action for a single Dp-brane is given by the Dirac-Born-Infeld (DBI) action plus a Chern-Simons term for the non-zero Ramond-Ramond forms, which couple to the brane. In the string frame, the action is given by[1]

$$\begin{aligned} S_{\mathrm{D}p} =& - T_p \int d^{p+1}x\, e^{-\phi} \sqrt{-\det(P[g+B]_{ab} + 2\pi\alpha' F)} + \\ &+ \mu_p \int \sum_{q=0}^{p+1} P[C_q e^B] \wedge e^{2\pi\alpha' F}, \end{aligned} \tag{3.21}$$

where $\alpha' = l_s^2$ is the inverse string tension, F is the field strength of the gauge field living on the Dp-brane, and

$$T_p = \frac{1}{(2\pi)^p l_s^{p+1}}, \qquad\qquad \mu_p = g_s\, T_p. \tag{3.22}$$

The quantity T_p is the Dp-brane tension, and is in an extremality relation with the brane charge. The effective tension scales with $1/g_s$ (due to the presence of the dilaton, see equation (3.11)), and it is a manifestation of the non-perturbative nature of the D-branes.

3.1.2 The holographic correspondence

The fundamental ideas behind the holographic correspondence have their roots in what is known as the *holographic principle*, proposed by 't Hooft [22] and Susskind [23]. In a few words, it states that given a quantum gravity theory in a volume V, the information about its spectrum and dynamics are encoded in a non-gravitational theory living on the boundary ∂V. Therefore, the holographic correspondence describes dualities between two theories, one of quantum gravity and the other without dynamical gravity. Here, duality means that the two theories describe the very same physics. One of the most interesting aspects of these dualities is that they are weak/strong dualities, meaning that a computation in the non-perturbative regime of a theory can be mapped into a relatively simple perturbative computation of the other theory.

The first and most famous explicit realization of such a duality was proposed by Juan Maldacena in [24], where he conjectured the duality between the conformal $\mathcal{N} = 4$ $\mathrm{U}(N)$ Super-Yang-Mills (SYM) theory and Type IIB string theory on asymptotically $AdS_5 \times S^5$ spacetime. This example is a realization of the famous *AdS/CFT correspondence*, a well-known realization of the holographic principle

[1] We stress that this action is valid in the limit $g_s \ll 1$.

where a CFT is thought to live on the boundary of an asymptotically AdS spacetime where a quantum gravity theory lives.

In the case of [24], the duality arises from considering two complementary descriptions of a stack of N coincident D3-branes. On the one hand, taking the low-energy limit of open strings ending on the branes, only the massless excitations survive. These degrees of freedom are associated with a four-dimensional $\mathcal{N}=4$ U(N) SYM theory, which is conformal. The gauge group factorizes as $\mathrm{U}(N) \simeq \mathrm{SU}(N) \times \mathrm{U}(1)$, where the U(1) factor corresponds to the center-of-mass motion of the branes and decouples. The resulting $\mathcal{N}=4$ SU(N) SYM theory is a conformal field theory with global SO(4, 2) superconformal symmetry and $\mathrm{SU}(4) \simeq \mathrm{SO}(6)$ R-symmetry.

On the other hand, from the closed string (supergravity) perspective, the stack of N D3-branes is described as an extremal solution of type IIB supergravity given by (3.16), (3.17), and (3.18) with $p=3$. The corresponding metric reads

$$ds^2 = H^{-1/2}(r)\eta_{\alpha\beta}dx^\alpha dx^\beta + H^{1/2}(r)\left(dr^2 + r^2 d\Omega_5^2\right), \tag{3.23}$$

where now $H(r) = 1 + R_3^4/r^4$, $\alpha, \beta = 0, 1, 2, 3$, and R_3 is the characteristic length of the geometry. For $r \gg R_3$, the metric approaches flat ten-dimensional Minkowski space, while in the near-horizon region $r \ll R_3$ one obtains the $AdS_5 \times S^5$ metric

$$ds^2 = R_3^2\left(\frac{1}{z^2}\eta_{\alpha\beta}dx^\alpha dx^\beta + \frac{dz^2}{z^2} + d\Omega_5^2\right), \tag{3.24}$$

where $z = R_3^2/r$ is the so-called holographic coordinate, and R_3 is interpreted as the radius of both the AdS_5 and the S^5 factors. The limit $r \to 0$ is known as *near-horizon limit* of the solution. The isometry group of AdS_5 is SO(4, 2) and that of the five-sphere is SO(6), precisely matching the global symmetries of $\mathcal{N}=4$ SU(N) SYM.

In this case, the dilaton field reads $\exp(2\phi) = g_s^2$, and it is constant in r. This fact is related to the property of conformal invariance of the dual field theory. There is also a non-trivial RR form C_4 with the associated field strength $F_5 = dC_4$. In particular, the flux of F_5 over the five-sphere is non-zero, and it is related to the number of colors N of the dual gauge theory

$$\int_{S^5} F_5 = (2\pi)^4 N. \tag{3.25}$$

An important feature of the holographic setup is the so-called radius/energy relation, or UV/IR correspondence. It can be understood as follows: the time component of the $AdS_5 \times S^5$ metric in the near-horizon region reads

$$ds^2 \supset -\frac{r^2}{R_3^2}\,dt^2, \tag{3.26}$$

so that the proper energy of a bulk excitation located at a radial position r is redshifted with respect to the energy measured at the boundary ($r \to \infty$, or equivalently $z \to 0$). A mode of local energy E_{local} at radius r is seen by a boundary observer with energy

$$E \sim \frac{r}{R_3^2}\,E_{\text{local}}. \tag{3.27}$$

Taking E_{local} to be of order 1, we obtain the identification of the radial coordinate with an energy scale in the boundary field theory:

$$E \sim \frac{r}{R_3^2} \sim \frac{1}{z}. \tag{3.28}$$

Large values of r (small z) correspond to ultraviolet scales in the field theory, while small values of r (large z) correspond to infrared scales. This is the essence of the UV/IR correspondence, which provides a geometric interpretation of the renormalization group scale of the boundary theory in terms of radial motion in the bulk spacetime.

Maldacena's conjecture thus relies on the identification of the two low-energy limits: the open-string description yields the $\mathcal{N}=4$ SU(N) SYM theory, while the closed-string near-horizon geometry corresponds to string theory on $AdS_5 \times S^5$. In the large-N and large-'t Hooft coupling limit $\lambda = g_{\mathrm{YM}}^2 N \gg 1$, the string background reduces to weakly coupled type IIB supergravity on $AdS_5 \times S^5$, establishing a duality between strongly coupled $\mathcal{N}=4$ SU(N) SYM theory and classical supergravity.

Once the duality between two theories is stated, we have to understand how the correspondence works and how it can be used to perform computations. The two sides of the duality talk to each other through the so-called *holographic dictionary* [25, 26]. In particular, every gauge-invariant operator $\mathcal{O}(x)$ in the boundary field theory is associated with a field in the bulk $\phi(x,z)$ that has the same quantum numbers under the symmetries of the theory. On the bulk field ϕ, some boundary conditions have to be imposed, and the restriction $\phi_0 \equiv \phi|_{\mathrm{bdry}}$ of the field to the boundary acts as a source for the dual operator[2]

$$S_{\mathrm{QFT}} \to S_{\mathrm{QFT}} + \int_{\mathrm{bdry}} d^d x\, \phi_0(x)\mathcal{O}(x). \tag{3.29}$$

The bulk theory partition function will depend on the boundary condition $\phi_0 \equiv \phi|_{\mathrm{bdry}}$, which, from the boundary field theory, is interpreted as a deformation of the bare Lagrangian. At the same time, the boundary field theory partition function, since it will depend on the source ϕ_0 - it is a generating functional $\mathcal{Z}_{\mathrm{QFT}}[\phi_0]$. At the same time, the bulk theory partition function will depend on the boundary conditions imposed on the field ϕ. The holographic duality states that the partition functions of the two theories coincide

$$\mathcal{Z}_{\mathrm{QFT}}[\phi_0] = \left\langle \exp\left(i \int \phi_0\, \mathcal{O} \right) \right\rangle_{\mathrm{QFT}} = \mathcal{Z}_{\mathrm{bulk}}[\phi_0]. \tag{3.30}$$

Then, correlation functions of boundary operators $\mathcal{O}$ can be computed by taking functional derivatives of the bulk theory partition function with respect to ϕ_0:

$$\langle \mathcal{O}(x_1) \dots \mathcal{O}(x_n) \rangle_{\mathrm{QFT}} = \frac{1}{i^n} \frac{\delta}{\delta\phi_0(x_1)} \cdots \frac{\delta}{\delta\phi_0(x_n)} \log \mathcal{Z}_{\mathrm{bulk}}[\phi_0]. \tag{3.31}$$

[2] To be more precise, ϕ_0 is the restriction of the field ϕ on the boundary only after extracting a factor of the holographic coordinate to some power. For example, in pure AdS written in Poincarè coordinates, for $z \to 0$ (AdS boundary), $\phi \sim z^{d-\Delta}\phi_0$. For a massive field ϕ, $d \neq \Delta$ and therefore, strictly speaking, ϕ_0 is not the boundary value of ϕ.

In general, $\mathcal{Z}_{\text{bulk}}[\phi_0]$ is a very complicated object, but in the large-N and large-λ limit, we can use the classical supergravity approximation such that

$$\mathcal{Z}_{\text{bulk}}[\phi_0] = \left\langle \exp\left(i \int \phi_0 \, \mathcal{O}\right) \right\rangle_{\text{QFT}} \approx \exp\left(i \, S^{\text{on-shell}}_{\text{class.}}[\phi_0]\right), \tag{3.32}$$

where $S^{\text{on-shell}}_{\text{class.}}[\phi_0]$ is the classical supergravity action computed on a solution of the field equation of motion with appropriate boundary conditions.[3]

In many cases, the right-hand side of (3.32) is relatively tractable from a computational standpoint. The efficacy of the holographic approach is then evident: the computation of correlation functions in the strongly coupled dual gauge theory can be obtained by taking functional derivatives of a classical on-shell action. Nevertheless, the on-shell action generally exhibits divergences, primarily originating from infrared divergences in the bulk gravitational theory. Owing to the holographic correspondence, these IR divergences in the bulk are mapped into UV divergences in the boundary gauge theory. To render the theory finite, one must introduce carefully constructed boundary counterterms to cancel these divergences. This renormalization procedure is known as *holographic renormalization* [118, 119] and can be implemented in a systematic manner.

Another interesting aspect of the correspondence is that by analyzing the near-boundary behavior of fields, one finds that the mass m of a bulk field is dual to the scaling dimension Δ of the dual boundary operator:

$$\text{mass} \quad \leftrightarrow \quad \Delta. \tag{3.33}$$

For instance, in a $(d+1)$-dimensional AdS spacetime with radius L, the relation for a free scalar field ϕ, dual to a boundary operator $\mathcal{O}$, reads

$$\Delta = \frac{d}{2} + \sqrt{\frac{d^2}{4} + m^2 L^2}\,. \tag{3.34}$$

As a consequence,

- if $m^2 > 0$, the $\Delta > d$ and $\mathcal{O}$ is an irrelevant operator,
- if $m^2 = 0$, the $\Delta = d$ and $\mathcal{O}$ is a marginal operator,
- if $m^2 < 0$, the $\Delta < d$ and $\mathcal{O}$ is a relevant operator.

A peculiarity of AdS spacetime is that scalar fields can have negative mass as long as they obey the Breitenlohner-Freedman bound [120, 121]

$$m^2 L^2 \geq -\frac{d^2}{4}. \tag{3.35}$$

While equation (3.32) was initially presented for a specific scalar operator, its validity extends more generally to all single-trace operators[4]. In such cases, the source

[3] Multiple saddle points can be present, and the right-hand side of the holographic expression becomes a sum over all relevant saddle point contributions.

[4] One can also include multi-trace operators with appropriate modification in the identification of the source from the boundary behavior of the field.

term ϕ_0 should be interpreted as the boundary value of the bulk field corresponding to the operator in question. A particularly significant aspect of the holographic dictionary concerns the dual description of conserved currents. When the boundary theory exhibits a global symmetry associated with a conserved current J^μ, the dual bulk theory contains a corresponding vector field A_M. The conservation of the current implies invariance of the bulk action under gauge transformations of A_M, thereby identifying A_M as a gauge field. The associated bulk gauge group corresponds to the continuous extension of the global symmetry group of the boundary theory, now embedded in one higher spacetime dimension.

A paradigmatic example arises from the current associated with translation invariance, namely, the stress-energy tensor $T^{\mu\nu}$. Applying the holographic correspondence to $T^{\mu\nu}$ implies that its dual in the bulk is a spin-2 gauge field whose gauge symmetry consists of diffeomorphisms. In other words, the stress-energy tensor is holographically dual to the bulk metric itself. This leads to a central conclusion of holography: any boundary theory that is invariant under spacetime translations must be dual to a bulk theory that includes a metric field.

3.1.3 Confinement in holography

In the introductory chapter 1, we have seen that one of the crucial aspects of QCD at low energies is the confinement of gluons and quarks within hadrons. Since the formulation of the holographic correspondence, there has been interest in trying to incorporate confinement in this framework. We have seen that the natural object to probe confinement is the Wilson loop. Holography provides a simple prescription to compute it within the holographic description of a quantum field theory [122].

The Wilson loop expectation value can be computed holographically in the low-energy gravity regime as

$$\langle \mathcal{W}(\mathcal{C} = \partial\Sigma) \rangle = \exp\Big(-S_{\mathrm{NG}}^{\text{on-shell}}(\Sigma)\Big), \tag{3.36}$$

where $\mathcal{C}$ is the closed path present in the field theory definition. In the gravitational dual, $\mathcal{C}$ is a curve on the boundary of the bulk spacetime at which a string is attached. The string worldsheet is a surface Σ such that $\partial\Sigma = \mathcal{C}$. The dynamics of the string is given just by the Nambu-Goto action S_{NG}, hence the surface Σ prefers to minimize its area, and therefore $\mathcal{C}$ is the boundary of the minimal area Σ. The on-shell action $S_{\mathrm{NG}}^{\text{on-shell}}(\Sigma)$ in (3.36) is evaluated on the surface Σ that extremizes the action. With such a prescription, we can investigate the confining nature of bulk geometries, dual to field theories.

Let us consider a rectangular Wilson loop with sides T and R, as the one represented in figure 1.1 of chapter 1, in an AdS spacetime with radius L. After the renormalization of the divergences, we get the following result

$$S_{\mathrm{NG}}^{\text{on-shell}}(\Sigma)|_{\text{renormalized}} = T\,V(R) = T\frac{4\pi^2 L^2}{(\Gamma(1/4))^4\alpha'}\frac{1}{R}. \tag{3.37}$$

The behavior $\sim 1/R$ is typical of a Coulomb-like potential due to the absence of an explicit scale in a CFT (dual to a pure AdS solution).

The general paradigm in holography to have a confining background is for the geometry to end at some finite value z_0 of the holographic coordinate (where the metric along the Minkowski time direction $g_{tt} \neq 0$). This value sets the confining scale of the boundary theory. In other words, a key feature of CFT is the existence of excitations at arbitrary low energies, and this corresponds to the fact that the spacetime geometry extends throughout the full range of AdS itself. On the contrary, a mass gap in a quantum field theory corresponds to a geometry that ends at some point in the bulk. In these cases, one can compute holographically the Wilson loop by computing the on-shell Nambu-Goto action, which goes like

$$S_{\mathrm{NG}}^{\text{on-shell}}(\Sigma)|_{\text{renormalized}} \sim T\, R. \tag{3.38}$$

A way to describe the breaking of conformal symmetry in the framework of gauge/gravity duality is to consider an AdS_{d+1} black hole with an event horizon at $z = z_h$. Its metric is given by

$$ds^2 = \frac{L^2}{z^2}\left(-f(z)dt^2 + dx_i dx_i + \frac{dz^2}{f(z)}\right), \tag{3.39}$$

where $i = 1, ..., d$ and the blackening factor is given by

$$f(z) = 1 - \left(\frac{z}{z_h}\right)^d. \tag{3.40}$$

In Euclidean signature, this gravitational theory is dual to an Euclidean QFT at finite temperature T, given by the Bekenstein-Hawking black hole temperature

$$T = \frac{|f'(z_h)|}{4\pi}. \tag{3.41}$$

This is another aspect of the AdS/CFT correspondence: the geometry of an AdS_{d+1} black hole is dual to a quantum theory in d-dimensions at finite temperature T. The finite temperature correlation functions are computed as already explained following the holographic dictionary, but in the black hole metric.

A way to describe a non-conformal confining theory at zero temperature is through the compactification of one spatial coordinate.[5] This way, the inverse length scale arising from the compactification will be interpreted as the dynamically generated energy scale of the non-conformal field theory. In the dual field theory description, this corresponds to the renormalization group IR scale emerging in quantum field theories with a non-vanishing beta-function. One of the most famous examples is the AdS soliton geometry

$$ds^2 = \frac{L^2}{z^2}\left(-dt^2 + dx_i dx_i + f(z)d\tau^2 + \frac{dz^2}{f(z)}\right), \tag{3.42}$$

with $i = 1, ..., d-2$ and $f(z)$ is given in (3.40). This geometry ends smoothly at $z = z_h$ and does not have an event horizon. The compactified coordinate here is referred to as τ.

[5] We mention that, among several approaches to achieve confinement, a successful bottum-up approach is to end the AdS space at some IR cutoff. See [123, 124, 34, 125, 126] for explicit realizations.

This spatial compactification also has the consequence of breaking supersymmetry and follows from the Kaluza-Klein reduction on S^1. Choosing anti-periodic boundary conditions for fermions, one can show that they acquire a mass proportional to z_h^{-1}. This breaks supersymmetry since bosons acquire mass only due to quantum effects. At low energies, we are left with the gauge fields since they remain massless. These observations set the basis for the construction of a top-down holographic model for large-N QCD-like theories, as we will see in 3.2.

3.1.4 Flavors in holography

The formulation of AdS/CFT we discussed so far only involves fields in the adjoint representation of the CFT gauge group. In order to describe holographically QCD-like theories, we have to introduce quark degrees of freedom, which are fermions in the fundamental representation of the gauge group. Let us review how this is done in the gravitational dual of $\mathcal{N} = 4$ SYM.

Open strings attached to the background D3-branes generate degrees of freedom in the adjoint representation of the gauge group. However, if a string has only one end on the D3-branes and the other end on a different brane, it generates matter in the fundamental representation. In this context, the natural candidate[6] for the other brane is a D7-brane [128, 129, 113]. Table 3.1 shows the embedding of the D3/D7 system of branes in the spacetime.

	0	1	2	3	4	5	6	7	8	9
D3	•	•	•	•	◦	◦	◦	◦	◦	◦
D7	•	•	•	•	•	•	•	•	◦	◦

Table 3.1. D3/D7 intersection. A bullet indicates a direction where the branes are extended, and an empty dot indicates a direction where the branes are localized.

We consider a number N_f of D7-branes that *probe* the geometry generated by the D3-branes. The backreaction of the D7-brane on the background geometry can be neglected only if, roughly, their number is small compared to N, the number of D3-branes. From the dual field theory perspective, this limit corresponds to a scenario in which quarks propagate within a fixed gauge background, represented by the geometry. Ignoring the influence of the D7-branes is equivalent to neglecting quark-loop contributions, effectively placing the theory in the quenched approximation. In the supergravity dual, the low-energy degrees of freedom of a single D7-brane are described by the DBI action, and they correspond to open string fluctuations on the probe D7-brane. In the case of multiple, coincident D7-branes, one has to consider the non-Abelian generalization of the DBI action [130].

The D3/D7 brane configuration preserves one-quarter of the total supersymmetry of type IIB string theory, corresponding to eight supercharges. It exhibits an SO(4) $\times$ SO(2) isometry in the directions transverse to the D3-branes. Given

[6]The new stack of branes has to be separated from the background stack of D3-branes. This request excludes D9-branes as probes. It can be shown that D3-branes and D5-brane probes lead to defect field theories, if supersymmetry has to be preserved (see [127] for more details). This leaves D7-brane probes as a candidate for adding flavors to the theory.

X^I, with $I = 0, ...9$, the spacetime coordinates, the SO(4) symmetry acts on the X^4, X^5, X^6, X^7 coordinates, while the SO(2) symmetry rotates the X^8, X^9 plane. Introducing a separation L between the D3 and D7-branes along the X^8-X^9 directions explicitly breaks the SO(2) symmetry. These geometric symmetries are reflected in the global symmetries of the dual field theory.

The presence of the D7-branes leads to a $\mathcal{N} = 2$ supersymmetric U(N) gauge theory which contains N_f hypermultiplets in the fundamental representation associated with the light modes coming from strings stretching from D3-branes and D7-branes. If the D7-branes are separated from the D3-branes in the transverse space (X^8, X^9), then the hypermultiplets acquire a mass $m_q \propto L$, and breaks the SO(2) $\sim$ U(1), where U(1) is a field theory R-symmetry. Note that the hypermultiplets also enjoy a baryonic symmetry $\mathrm{U}(1)_B$, which is a subgroup of the U(N_f) flavor group.

3.2 The Witten-Sakai-Sugimoto model

In this section, we review the Witten-Sakai-Sugimoto model [31, 32, 33], which is the top-down holographic model that better resembles QCD in the planar limit and in the strongly coupled regime. It describes a non-supersymmetric Yang-Mills theory in (3+1) dimensions with gauge group SU(N), interacting with N_f quark flavors as well as with (an infinite tower of) massive Kaluza Klein (KK) modes transforming in the adjoint representation of SU(N). The model emerges in the low-energy limit of a string theory construction based on N D4-branes compactified on a circle $S^1_{x_4}$, where the coordinate x_4 satisfies the periodicity condition

$$x_4 \sim x_4 + 2\pi/M_{KK}, \tag{3.43}$$

with M_{KK}, the inverse radius of $S^1_{x_4}$ being the KK mass scale. In order to break supersymmetry, we choose periodic boundary conditions for the fermionic fields and anti-periodic boundary conditions for bosonic fields. This way, the fermions take a mass $\sim M_{KK}$ at tree level, whereas the traceless components of the bosonic scalar take mass $\sim \lambda M_{KK}$ at one-loop level.

At zero temperature, the large-N strong coupling regime $\lambda \gg 1$ of the unflavored model, where λ is the 't Hooft coupling at the KK mass scale M_{KK}, is holographically described by a type IIA supergravity background sourced by the N D4-branes [31]:

$$ds^2 = \left(\frac{u}{R}\right)^{3/2} (dx^\mu dx_\mu + f(u)dx_4^2) + \left(\frac{R}{u}\right)^{3/2} \frac{du^2}{f(u)} + R^{3/2}u^{1/2}d\Omega_4^2, \tag{3.44}$$
$$f(u) = 1 - \frac{u_0^3}{u^3}, \qquad e^\phi = g_s \left(\frac{u}{R}\right)^{3/2}, \qquad F_4 = \frac{2\pi N}{V_4}\omega_4, \qquad R^3 = \pi g_s l_s^3 N,$$

where x^μ spans the four-dimensional Minkowski directions, $u \in [u_0, +\infty)$ is the radial coordinate holographically related to the renormalization group energy scale of the dual field theory, and ω_4 is the volume form of the unit S^4, with volume $V_4 = 8\pi^2/3$. The field ϕ is the (running) dilaton, and F_4 is the Ramond-Ramond four-form field strength. The above background holographically accounts for confinement and mass gap formation in the dual SU(N) gauge theory. The mass scale of the glueballs is set by M_{KK}, which thus essentially also accounts for the dynamical scale Λ of the dual quantum field theory

$$M_{KK} \leftrightarrow \Lambda. \tag{3.45}$$

To avoid conical singularities in the (u, x_4) subspace, the KK mass scale is related to the background parameters through

$$M_{KK} = \frac{3}{2}\sqrt{\frac{u_0}{R^3}}. \tag{3.46}$$

Moreover, the 't Hooft coupling λ is related to the string theory parameters through

$$\frac{R^3}{l_s^2} = \frac{1}{2}\frac{\lambda}{M_{KK}}. \tag{3.47}$$

The supergravity approximation works as long as the background's curvature is small in string units, namely when the curvature radius is large. The smallest value of the curvature radius is of order $\sim (u_0 R^3)^{1/4}$ and it is reached at $u = u_0$. Therefore

$$\frac{(u_0 R^3)^{1/2}}{l_s^2} \sim \lambda, \tag{3.48}$$

so the supergravity description is reliable as long as $\lambda \gg 1$. However, we should mention that, in this limit, the extra fields that make the Witten theory differ from the YM theory, namely the adjoint scalars and fermions, do not decouple from the dynamics. Their mass is of order $\sim M_{KK}$. As a consequence, there is no asymptotic freedom in the supergravity approximation. Moreover, in the UV limit $u \to \infty$, the dilaton diverges. This reflects the non-renormalizability of the five-dimensional YM theory living on the D4-brane worldvolume. The supergravity description is thus reliable as long as the dilaton does not become too large. We can define a critical value of the holographic coordinate u_{crit} such that $\exp(\phi_{\text{crit}}) = 1$, demanding that $u_{\text{crit}} \gg u_0$:

$$u_{\text{crit}} \gg u_0 \longrightarrow N^{3/2} \gg \lambda. \tag{3.49}$$

We conclude this section by showing that it is possible to introduce the YM θ-term in the holographic dual and to compute the topological susceptibility. The D4-brane dynamics is regulated by its DBI+CS action. Let us consider the following term of the total action

$$S_{\text{D4}} \supset \frac{1}{2(2\pi)^2}\int C_1 \wedge \text{tr}(F \wedge F), \tag{3.50}$$

where we have used the conventions of [32] for the RR forms. Here F is the field strength whose dimensional reduction on $S^1_{x_4}$ yields the gluon field. Assuming that F is along the Minkowski directions and does not depend on x_4, we can reduce the above term to the four-dimensional YM θ-term

$$\frac{\theta}{8\pi^2}\text{tr}(F \wedge F), \tag{3.51}$$

with the identification

$$\int_{S^1_{x_4}} C_1 = \theta + 2\pi k, \tag{3.52}$$

where $k \in \mathbb{Z}$. In order not to change the background, we have to neglect the backreaction of dC_1, meaning that [131]

$$\frac{\lambda}{4\pi^2}\frac{\theta}{N} \ll 1 \qquad \text{for} \qquad k = 0. \tag{3.53}$$

Solving the supergravity equation of motion for C_1, we get the on-shell field strength

$$F_2 = dC_1 = \frac{4\lambda^3 M_{KK}^4 l_s^6}{3^5\pi}\frac{\theta + 2\pi k}{u^4} du \wedge dx_4. \tag{3.54}$$

We can compute the vacuum energy density[7] $\varepsilon(\theta)$, which is given holographically by

$$\varepsilon(\theta) - \varepsilon(0) = \min_{k\in\mathbb{Z}} \frac{1}{2\kappa_0^2}\frac{l_s^2}{2}\int dC_1 \wedge \star dC_1\bigg|_{\text{on-shell}} = \min_{k\in\mathbb{Z}} \frac{\lambda^3 M_{KK}^4}{8(3\pi)^6}(\theta + 2\pi k)^2. \tag{3.55}$$

The associated topological susceptibility reads

$$\chi_g = \frac{d^2\varepsilon(\theta)}{d\theta^2}\bigg|_{\theta=0} = \frac{\lambda^3 M_{KK}^4}{4(3\pi)^6}, \tag{3.56}$$

which is non-zero as expected in a YM-like theory.

3.2.1 Introducing flavors

In [32], flavors were added to the Witten background. These are realized holographically in terms of a stack of N_f D8/$\overline{\text{D8}}$-branes transverse to the $S^1_{x_4}$ circle, treated in the probe approximation. The embedding of the branes in the model is described in the following table.

	0	1	2	3	4	5	6	7	8	9
D4	•	•	•	•	•	◦	◦	◦	◦	◦
D8	•	•	•	•	◦	•	•	•	•	•

Table 3.2. D4/D8 intersection. A bullet indicates a direction where the branes are extended, and an empty dot indicates a direction where the branes are localized.

As explained in [132], the parameter that accounts for the backreaction of the D8-branes on the Witten background is

$$\epsilon_f = \frac{\lambda^2}{12\pi^2}\frac{N_f}{N}, \tag{3.57}$$

which is smaller than 1 as long as N_f is not too big. Throughout this work, we neglect $\mathcal{O}(\epsilon_f)$ corrections to the background so that we can still use (3.44).

According to the holographic dictionary, the gauge group $\text{U}(N_f)_{\text{D8}} \times \text{U}(N_f)_{\overline{\text{D8}}}$ living on the D8/$\overline{\text{D8}}$ worldvolume is dual to the global chiral group rotating the quark degrees of freedom. Thus, the analysis of the low-energy spectrum (which we

[7] We remember that, at zero temperature, the free energy of the dual QFT coincides with its vacuum energy (or generating functional at fixed sources), which in holography is computed by evaluating the renormalized on-shell Euclidean gravitational action.

omit here for brevity) of strings connecting the D4-branes to the D8 ($\overline{\text{D8}}$) branes shows the presence of left (right) quarks, with one color index and one flavor index. Since there is no room for the D8-branes to be separated from the D4-branes, these excitations are necessarily massless. Therefore, the WSS model at low energy reduces to a large-N QCD-like theory with massless chiral quarks.

Now, we are going to show that the embedding of the D8/$\overline{\text{D8}}$-branes with minimal energy is such that the branes join at some value of the holographic coordinate u. This has a very compelling interpretation in terms of the boundary theory: if the branes are separated, the flavor symmetry group is $\mathrm{U}(N_f)_L \times \mathrm{U}(N_f)_R$, however, when they are joined the flavor group is broken to its diagonal part $\mathrm{U}(N_f)$. This is precisely the spontaneous symmetry-breaking pattern of flavor symmetry, which is then realized geometrically by minimizing the energy of the D8-brane configuration.

We start by writing the induced metric on the D8-brane worldvolume in terms of the embedding inverse function $u = u(x_4)$

$$ds^2_{\text{D8}} = \left(\frac{u}{R}\right)^{3/2} dx^\mu dx_\mu + \left(\left(\frac{u}{R}\right)^{3/2} f(u) + \left(\frac{R}{u}\right)^{3/2} \frac{u'(x_4)^2}{f(u)}\right) dx_4^2 + R^{3/2} u^{1/2} d\Omega_4^2, \tag{3.58}$$

where $u'(x_4) = du/dx_4$. The DBI action (with no gauge fields) for the D8-brane reads

$$S^{\text{DBI}}_{\text{D8}} = -T_{\text{D8}} V_{3+1} V_{S^4} \int dx_4\, u^4 \sqrt{f(u) + \left(\frac{R}{u}\right)^{3/2} \frac{u'(x_4)^2}{f(u)}}\,, \tag{3.59}$$

where $T_{\text{D8}} = (2\pi)^{-8} l_s^{-9}$ is the D8-brane tension, V_{3+1} is the volume of the Minkowski space and V_{S^4} the volume of the four-sphere. The action has a first integral

$$u' \frac{\partial \mathcal{L}}{\partial u'} - \mathcal{L} = -\frac{u^4 f(u)}{\sqrt{f(u) + \left(\frac{R}{u}\right)^3 \frac{u'(x_4)^2}{f(u)}}} = \text{constant}, \tag{3.60}$$

with $\mathcal{L}$ proportional to $\mathcal{L}^{\text{DBI}}_{\text{D8}}$, the Lagrangian associated with the action (3.59). The D8-brane profile can be found by imposing the following boundary conditions: $u(x_4 = 0) = u_J$ and $u'(x_4 = 0) = 0$. As a result one gets:

$$x_4^\pm(u) = \pm \int_{u_J}^u du \left(\frac{R}{u}\right)^{3/2} \frac{u_J^4 \sqrt{f(u_J)}}{f(u)\sqrt{u^8 f(u) - u_J^8 f(u_J)}}, \tag{3.61}$$

where the $\pm$ holds for the D8/$\overline{\text{D8}}$-branes. These two solutions coincide at $u = u_J$, meaning that the two stacks of branes join at u_J to form a single component of the D8-branes stack, on which only a single factor of $\mathrm{U}(N_f)$ survives as a gauge symmetry. From the boundary theory point of view, this accounts for the breaking of the chiral group $\mathrm{U}(N_f)_L \times \mathrm{U}(N_f)_R$ to its vector component $\mathrm{U}(N_f)$. Therefore, we interpret this mechanism as the holographic realization of the pattern of spontaneous symmetry breaking of chiral symmetry.

We can now integrate the equation (3.61) to get the asymptotic brane separation L

$$L = \int dx_4 = 2 \int \frac{du}{u'} = J(b) \frac{R^{3/2}}{u_J^{1/2}}, \tag{3.62}$$

where

$$b \equiv \frac{u_0}{u_J}, \tag{3.63}$$

and

$$J(b) = \frac{2}{3}\sqrt{1-b^3}\int_0^1 dv \frac{\sqrt{v}}{(1-b^3\,v)\sqrt{1-b^3\,v-(1-b^3)v^{8/3}}}. \tag{3.64}$$

The case $u_J = u_0$ is known as *antipodal* embedding because the two staks of D8/$\overline{\text{D8}}$-branes are asymptotically placed at antipodal points on $S^1_{x_4}$. In this case, $x'(u) = 0\ \forall u$, which is solved by

$$x_4^{\pm}(u) = \pm\frac{\pi}{2M_{KK}} \qquad \Rightarrow \qquad |\Delta x_4| = \pi M_{KK}. \tag{3.65}$$

For the antipodal embedding, it is useful to introduce new coordinates on the (u, x_4) subspace, known as *cigar* subspace

$$y = r\,\cos(x_4 M_{KK}), \qquad z = r\,\sin(x_4 M_{KK}), \qquad u^3 = u_0^3 + u_0 r^2. \tag{3.66}$$

Then, the metric on the cigar subspace (x_4, u) reads

$$ds^2_{\text{cigar}} = \frac{4}{9}\left(\frac{R}{u}\right)^{3/2}\Big[(1-h(r)z^2)dz^2 + (1-h(r)y^2)dy^2 - 2h(r)yz\,dydz\Big], \tag{3.67}$$

$$h(r) = \frac{1}{r^2}\left(1-\frac{u_0}{u}\right), \tag{3.68}$$

where $u = u_0$ and $u = \infty$ correspond respectively to $z = 0$ and $z = \pm\infty$. The antipodal embedding is realized by setting $y = 0$ so that $u = u(z) = (u_0^3 + u_0 z^2)^{1/3}$ is only a function of z.

The D8-brane theory

Now, we study the effective theory living on the D8-branes worldvolume in the presence of a U(N_f) connection $\mathcal{A}$. We set to zero all the components along the four-sphere since we are interested in the SO(5) singlet states. Moreover, we assume that the other components do not depend on the four-sphere coordinates. It is convenient to decompose the U(N_f) connection in its U(1) part $\hat{A}$, and SU(N_f) part A, as

$$\mathcal{A} = \frac{\hat{A}}{\sqrt{2N_f}}\,\mathbb{I}_{N_f} + A^a T^a, \qquad \text{Tr}\Big(T^a T^b\Big) = \frac{\delta^{ab}}{2}, \tag{3.69}$$

where $a = 1, \ldots, N_f^2 - 1$. The associated field strength is defined as $\mathcal{F} = d\mathcal{A} + i\,d\mathcal{A}\wedge d\mathcal{A}$, and can be decomposed as above.

The total D8-brane action is given by the sum of the DBI term plus the Chern-Simons term for the Ramond-Ramond p-forms C_p (being p an odd number) and the associated kinetic terms:[8]

$$S_{\rm D8} = -\,T_{\rm D8}\int d^9x\,{\rm Str}_{Nf}\left[e^{-\phi}\sqrt{-\det(P[g_{ab}]+2\pi l_s^2\mathcal{F})}\right]+ \tag{3.70}$$
$$\int\sum_{k=1}^{4}C_{9-2k}\wedge\frac{1}{k!(2\pi)^k}\,{\rm Tr}\,\mathcal{F}^k-\frac{1}{4\pi}\sum_{p\ {\rm odd}}(2\pi l_s)^{2(p-4)}\int dC_{p+1}\wedge\star dC_{p+1}\,.$$

Here, we use the notation of [32] for the RR forms. The RR field strengths will also be indicated by $dC_{p+1}=F_{p+2}$ in the following. Moreover, the notation $\mathcal{F}^k$ stands for the wedge product of $\mathcal{F}$ with itself k times. We can work out each term on the Witten background and expand the DBI action to quadratic order in the field strength. The only Wess-Zumino term that survives is the one involving the RR potentials C_3, and C_7. In fact, the Wess-Zumino term with C_1 reads

$$\frac{1}{4!(2\pi)^4}\int C_1\wedge{\rm Tr}\mathcal{F}^4, \tag{3.71}$$

which is zero if we assume, as we did, that the field strength $\mathcal{F}$ has no components along S^4. For the same reason, the term involving C_5 is zero. Moreover, the Wess-Zumino term that involves C_3 is integrated by parts to have F_4 in the action, whose flux is quantized as $\int_{S^4}F_4=2\pi N$.

All in all, we have

$$S_{\rm D8} = -\,\kappa\int d^4x\,dz\left(\frac{1}{2}h(z)\,{\rm Tr}(\mathcal{F}_{\mu\nu}\mathcal{F}^{\mu\nu})+k(z)\,{\rm Tr}(\mathcal{F}_{\mu z}\mathcal{F}^{\mu}{}_{z})\right)+ \tag{3.72}$$
$$\frac{N}{3!(2\pi)^2}\int_{M_5}\omega_5^{{\rm U}(N_f)}(\mathcal{A})-\frac{(2\pi l_s)^6}{4\pi}\int dC_7\wedge\star dC_7+\frac{1}{2\pi}\int C_7\wedge{\rm Tr}\ \mathcal{F}\wedge\omega_1,$$

where

$$\kappa=\frac{N\,M_{KK}}{54\pi^3 l_s^2}=\frac{N\,\lambda\,M_{KK}}{216\pi^3},\qquad k(z)=1+z^2,\quad h(z)=\frac{1}{(1+z^2)^{1/3}}, \tag{3.73}$$
$$\omega_5^{{\rm U}(N_f)}={\rm Tr}\left(\mathcal{A}\wedge\mathcal{F}^2-\frac{i}{2}\mathcal{A}^3\wedge\mathcal{F}-\frac{1}{10}\mathcal{A}^5\right),\qquad d\omega_5^{{\rm U}(N_f)}(\mathcal{A})={\rm Tr}\ \mathcal{F}^3. \tag{3.74}$$

Moreover, ω_1 is a one-form, representing the D8-brane embedding in order to extend the CS integral to the whole spacetime. M_5 is the sub-space spanned by (t,x^1,x^2,x^3,z) where the theory effectively lives.

The first term of (3.72) is the five-dimensional YM action of the D8-branes gauge field, while the second term is the five-dimensional CS term for $\mathcal{A}$. The last two terms of (3.72) involve the Ramond-Ramond potential C_7 and, in particular, the last term indicates that the presence of the D8-branes acts as a source term in the equation of motion for C_7, resulting in a violation of the Bianchi identity for its Hodge dual form. The equation of motion for C_7 is

$$d\star dC_7=\frac{1}{(2\pi l_s)^6}\,{\rm Tr}\ \mathcal{F}\wedge\omega_1. \tag{3.75}$$

[8] Formally, the kinetic terms for the RR form comes form the Type IIA supergravity action and not from the brane action.

However, the presence of flavor branes spoils the gauge invariance of the RR form $F_2 = dC_1$, therefore, an anomaly arises [133]. We can still define the dC_7 Hodge-dual two-form

$$\star\widetilde{F}_2 = (2\pi l_s)^6 dC_7, \tag{3.76}$$

with the notation $\widetilde{F}_2 \neq dC_1$. The equation of motion for C_7 translates into the following Bianchi identity

$$d\widetilde{F}_2 = \mathrm{Tr}\,\mathcal{F}\wedge\omega_1 = \sqrt{\frac{N_f}{2}}\,\hat{F}\wedge\omega_1, \tag{3.77}$$

where we used the decomposition (3.69). One can solve the above equation formally to get

$$\widetilde{F}_2 = dC_1 + \sqrt{\frac{N_f}{2}}\,\hat{A}\wedge\omega_1. \tag{3.78}$$

It has been shown that the C_7 action

$$S_{C_7} = -\frac{(2\pi l_s)^6}{4\pi}\int dC_7\wedge\star dC_7 + \frac{1}{2\pi}\int C_7\wedge\mathrm{Tr}\,\mathcal{F}\wedge\omega_1, \tag{3.79}$$

supported with the equation of motion (3.75) is equivalent to the following action for $\widetilde{F}_2$[9]

$$S_{\widetilde{F}_2} = -\frac{1}{4\pi(2\pi l_s)^6}\int \widetilde{F}_2\wedge\star\widetilde{F}_2, \tag{3.80}$$

and has to be supplemented with the modified Bianchi identity (3.77). We can use the formal solution of the modified Bianchi identity (3.78) and the holographic definition of the θ-angle (3.52), to get

$$S_{\widetilde{F}_2} = -\frac{\chi_g}{2}\int d^4x\left(\theta + \sqrt{\frac{N_f}{2}}\int_{-\infty}^{+\infty} dz\,\hat{A}_z\right)^2. \tag{3.81}$$

Mesons

Mesonic degrees of freedom arise in the WSS model as excitations of the D8-branes gauge field. We will focus on the antipodal embedding for the flavor branes; however, the same results can be obtained for non-antipodal embeddings. The former case describes a dual theory in which chiral symmetry breaking occurs at the same scale as the mass gap of the glue. Since there is chiral symmetry breaking, there should be Nambu-Goldstone bosons at low energy. In the case of $N_f = 1$, this should play the role of the η' meson in QCD. Remember that we are working at large-N where the chiral anomaly is suppressed.

For a single D8-brane, the DBI action expanded at quadratic order reads

$$S_{\mathrm{D8}} = -\frac{\kappa}{2}\int d^4x\,dz\left(\frac{1}{2}h(z)\mathcal{F}_{\mu\nu}\mathcal{F}^{\mu\nu} + k(z)\mathcal{F}_{\mu z}\mathcal{F}^{\mu}{}_{z}\right). \tag{3.82}$$

[9] See Appendix B of [134] for a derivation.

We can expand the gauge field components as

$$\mathcal{A}_\mu(x^\mu, z) = \sum_n B_\mu^{(n)}(x^\mu)\psi_n(z), \qquad \mathcal{A}_z(x^\mu, z) = \sum_n \varphi^{(n)}(x^\mu)\phi_n(z). \tag{3.83}$$

The functions ψ_n $(n > 0)$ are the eigenfunctions satisfying

$$-\frac{1}{h(z)}\partial_z(k(z)\partial_z\psi_n) = \lambda_n\psi_n, \tag{3.84}$$

together with the normalization condition

$$\kappa \int dz\, h(z)\psi_n\psi_m = \delta_{nm}. \tag{3.85}$$

Combining the above relations, we also have

$$\kappa \int dz\, k(z)\partial_z\psi_n\partial_z\psi_m = \lambda_n\delta_{nm}. \tag{3.86}$$

If we set $\varphi^{(n)} = 0$, the action becomes

$$S_{\rm D8} = -\sum_{n=1}^{\infty} \int d^4x \left[\frac{1}{4}\mathcal{F}_{\mu\nu}^{(n)}\mathcal{F}^{\mu\nu\,(n)} + \frac{1}{2}\lambda_n M_{KK}^2 B_\mu^{(n)} B^{\mu\,(n)}\right], \tag{3.87}$$

where $\mathcal{F}_{\mu\nu}^{(n)} = \partial_\mu B_\nu^{(n)} - \partial_\nu B_\mu^{(n)}$. This is the Proca action for the fields $B_\mu^{(n)}$, with masses $m_n^2 = \lambda_n M_{KK}^2$, and these fields are interpreted as the vector mesons of the theory. Now, we include the fields $\varphi^{(n)}$. In order to have a canonically normalized kinetic term for $\varphi^{(n)}$, we impose the orthonormality condition

$$\kappa \int dz\, k(z)\phi_n\phi_m = \delta_{nm}, \tag{3.88}$$

for every n. From (3.86), it is natural to identify

$$\phi_n = \frac{1}{m_n}\partial_z\psi_n, \qquad\qquad n \geq 1. \tag{3.89}$$

There exists only a function ϕ_0 that is orthogonal to ψ_n' for all $n \geq 1$. Imposing ϕ_0 to be normalized to one, the zero mode reads

$$\phi_0 = \frac{1}{\sqrt{\pi\kappa}}\frac{1}{k(z)}. \tag{3.90}$$

We throw away $\psi_0 \propto \arctan(z)$ since it is not normalizable according to our definition (3.85). Then, the μz component of the field strength can be rewritten as

$$\mathcal{F}_{\mu z} = \partial_\mu\varphi^{(0)}\phi_0 + \sum_{n\geq 1}\left(m_n^{-1}\partial_\mu\varphi^{(n)} - B_\mu^{(n)}\right)\partial_z\psi_n. \tag{3.91}$$

The gauge transformation $B_\mu^{(n)} \to B_\mu^{(n)} + m_n^{-1}\partial_\mu\varphi^{(n)}$ can be used to eliminate from the theory the modes $\varphi^{(n)}$ with $n \geq 1$. The zero mode $\varphi^{(0)}$ survives. All in all, we get the following total action

$$S_{\rm D8} = -\int d^4x \left[\frac{1}{2}\partial_\mu\varphi^{(0)}\partial^\mu\varphi^{(0)} + \sum_{n\geq 1}\left(\frac{1}{4}\mathcal{F}_{\mu\nu}^{(n)}\mathcal{F}^{\mu\nu\,(n)} + \frac{1}{2}m_n^2 B_\mu^{(n)}B^{\mu\,(n)}\right)\right]. \tag{3.92}$$

Under a parity transformation $(x^\mu, z) \to (-x^\mu, -z)$, we have $\mathcal{A}_z \to -\mathcal{A}_z$, so since ϕ_0 is an even function of z, $\varphi^{(0)}$ has to be a pseudoscalar field which we interpret as the Nambu-Goldstone boson of the spontaneous chiral symmetry breaking. A similar analysis can be performed to include also the massive scalar mesons, by fluctuating the embedding of the D8-brane in the Witten background.

This analysis can be generalized to the multi-flavored case $N_f > 1$. The pion matrix is identified in the WSS model with the following quantity

$$\mathcal{U}(x^\mu) = \mathcal{P} \exp\left(-i \int dz\, \mathcal{A}_z(x^\mu, z)\right). \tag{3.93}$$

In [32], it was shown that the effective action for pions reduces to the massless Skyrme model in the limit $\lambda \to \infty$, where the constant coefficients are given by the model's parameters. In particular, the pion decay constant is given by

$$f_\pi = 2\sqrt{\frac{\kappa}{\pi}}\,, \tag{3.94}$$

which has the expected behavior in the large-N limit, $f_\pi \sim \sqrt{N}$. Finally, the Skyrme parameter reads

$$e \simeq -\frac{1}{2.5\kappa}. \tag{3.95}$$

Quark masses

The WSS model offers an effective description of a QCD-like theory with massless flavors. These flavors are introduced as codimension-one defects placed at (non-) antipodal points along the $S^1_{x_4}$. As a result, a local Dirac mass term for the quarks is not allowed. The gauge-invariant boundary operator that better resembles the Dirac mass term is an open Wilson line.

The mass term for flavors in the WSS model was originally introduced in [135, 136] as an open string stretching from the D8-brane and the $\overline{\text{D8}}$-brane, representing a vertex that joins the left and right quark degrees of freedom. The worldsheet of long open strings is holographically mapped into an open Wilson line operator, described by the following action

$$S_{\text{mass}} = c \int d^4x\, \mathrm{Tr}\left(M \exp\left(-i \int_{-\infty}^{+\infty} \mathcal{A}_z dz\right) + \text{c.c.}\right), \tag{3.96}$$

where $M = \mathrm{diag}(m_1, \ldots, m_{N_f})$ is the quark mass matrix and c is a constant which reads

$$c = \frac{\lambda^{3/2} M_{KK}^3}{3^{9/2}\pi^3}. \tag{3.97}$$

3.2.2 Holographic baryons

In section 1.3, we discussed how baryons arise as solitonic solutions of the Skyrme model. In this section, we are going to show that baryons have a low-energy description in terms of solitons, also in the WSS model.

The idea that baryons can be holographically described as Dp-branes on a compact manifold was proposed by Witten in [27]. In string theory, a Dp-brane wrapped on a compact cycle can couple to background flux via a Chern–Simons term, sourcing exactly N fundamental strings in an $\mathrm{SU}(N)$ gauge theory. This configuration naturally represents the baryon vertex, since those N strings correspond to the N quarks that form a color-singlet baryon. The WSS model makes no exception, and the baryon vertex is identified with a D4-brane wrapped on the background internal four-cycle. The baryon number is then defined as the charge of the D4-brane as follows. In the presence of a D4-brane, the Ramond-Ramond forms C_3 and C_5 are not related by Hodge duality, so we have to include in the total D8-brane action the Chern-Simons term

$$\frac{1}{8\pi^2}\int_{\mathrm{D8}} C_5 \wedge \mathrm{Tr}\,(\mathcal{F}\wedge\mathcal{F})\,. \tag{3.98}$$

Assuming that $\mathcal{F}$ is the istantonic configuration satisfying

$$\frac{1}{8\pi^2}\int_{M_4} \mathrm{Tr}\,(\mathcal{F}\wedge\mathcal{F}) = n_B \in \mathbb{Z}, \tag{3.99}$$

where M_4 is the sub-space spanned by (x^1, x^2, x^3, z), then

$$\frac{1}{8\pi^2}\int_{\mathrm{D8}} C_5 \wedge \mathrm{Tr}\,\mathcal{F}^2 = n_B \int_{x^0\times S^4} C_5, \tag{3.100}$$

which is precisely the charge term for a D4-brane with charge n_B. Therefore, an instantonic gauge field configuration on the D8-brane is equivalent to a D4-brane wrapped on S^4 charged under C_5. The charge is given by the instanton number of the gauge configuration.

It is useful to briefly review the derivation in the holographic model. We decompose the $\mathrm{U}(N_f)$ gauge field $\mathcal{A}$ into its $\mathrm{SU}(N_f)$ part A and its $\mathrm{U}(1)$ part $\hat{A}$ as in (3.69). The Yang-Mills-Chern-Simons action, up to total derivatives, is then written as

$$\begin{aligned} S_{\mathrm{D8}} = &-\kappa \int d^4x\, dz \left(\frac{1}{2}h(z)\mathrm{Tr}(F_{\mu\nu}F^{\mu\nu} + k(z)\mathrm{Tr}(F_{\mu z}F^{\mu}{}_{z})\right) + \\ &-\frac{\kappa}{2}\int d^4x\, dz \left(\frac{1}{2}h(z)\hat{F}_{\mu\nu}\hat{F}^{\mu\nu} + k(z)\hat{F}_{\mu z}\hat{F}^{\mu}{}_{z}\right) + \\ &+\frac{N}{24\pi^2}\int_{M_5}\left(\omega_5^{\mathrm{SU}(N_f)}(A) + \frac{3}{\sqrt{2N_f}}\hat{A}\,\mathrm{Tr}(F\wedge F) + \frac{1}{2\sqrt{2N_f}}\hat{A}\hat{F}^2\right), \end{aligned}$$

where M_5 is the sub-space spanned by (x^0, x^1, x^2, x^3, z), and $\omega_5^{\mathrm{SU}(N_f)}$ is defined as in (3.74) but now it depends only on the non-Abelian components.

Following [28], we consider the $N_f = 2$ where $\omega_5^{\mathrm{SU}(2)} = 0$. We define

$$a(x^0) = \frac{\hat{A}}{2}, \tag{3.101}$$

and we treat it as a time-dependent perturbation over the instantonic solution with baryon number n_B. The $\int \hat{A}\ \mathrm{Tr}(F\wedge F)$ term in the action becomes

$$\frac{N}{8\pi^2}\int dx^0 a(x^0)\int_{M_4}\mathrm{Tr}(F\wedge F) = n_B\, N\int dx^0 a(x^0). \tag{3.102}$$

This describes a point-like particle with $\mathrm{U}(1)_B$ charge equal to $N\, n_B$: it is precisely the charge of a baryon (a bound state of N quarks) with baryon number n_B. This justifies the interpretation given above.

The classical solution

Let us recall that in the WSS model, the parameter λ is taken to be large. Given that the YM term of the total action (3.72) scales as $\sim \mathcal{O}(\lambda)$ while the CS term scales as $\sim \mathcal{O}(\lambda^0)$, the dominant contribution to the soliton's mass (or energy) is expected to arise from the Yang-Mills action, $S_{\rm YM}$. Therefore, we can initially neglect the Chern-Simons term. Under this approximation, the U(1) component of the gauge field $\hat{A}$ decouples from the SU(2) component, making it consistent to set $\hat{A}=0$. Our focus is then on finding energy-minimizing configurations that carry a unit baryon number, $n_B = 1$.

If the five-dimensional spacetime, effectively probed by the D8-branes after the integration over S^4, were flat with trivial metric functions $h(z)$ and $k(z)$, *i.e.*, $h(z)=k(z)=1$, the solution would correspond to the BPST instanton with arbitrary size ρ and position in the four-dimensional Euclidean space $M_4=(x^1,x^2,x^3,z)$. The explicit form of the BPST instanton can be found in the lectures [137]. However, within the Witten background, the energy-minimizing configuration corresponds to an instanton whose size shrinks to zero, $\rho\to 0$. To make this point clear, we begin by analyzing how the energy depends on the instanton size by substituting the BPST instanton as a trial configuration. We assume that the instanton is placed at the center of the four-dimensional space $(\vec{x},z)=(\vec{0},0)$, and compute the energy of this configuration as a function of the instanton size ρ:

$$
\begin{aligned}
E(\rho) &= \kappa\int d^3x\,dz\left(\frac{1}{2}h(z)\,\mathrm{Tr}(F_{\mu\nu}F^{\mu\nu})+k(z)\,\mathrm{Tr}(F_{\mu z}F^{\mu}{}_{z})\right)=\\
&=3\pi^2\kappa\left[\frac{\sqrt{\pi}\,\Gamma(7/3)}{\Gamma(17/6)}\,{}_2F_1(1/3,1/2,17/6;1-\rho^2)+\frac{4}{3}+\frac{2}{3}\rho^2\right]. \qquad (3.103)
\end{aligned}
$$

The energy $E(\rho)$ increases monotonically with ρ, attaining its minimum value $E(\rho=0)=8\pi^2\kappa$ when $\rho=0$. This represents the absolute energy minimum within the sector of configurations carrying a single instanton number. Such a minimum is achieved exclusively by (anti-)self-dual instantons that are infinitesimally small and localized at $z=0$.

Now, we consider the contribution from the CS term. This term contains a coupling between the instanton density and $\hat{A}_0$, meaning that the instanton induces an electric charge which couples to the Abelian part of the gauge field. Such coupling leads to a contribution to the energy which, in five dimensions, goes like $\sim\rho^{-2}$ for an object of size ρ and hence it stabilizes the instanton radius to a finite size.

We can work out a systematic expansion in $1/\lambda$. Following [28], we rescale the coordinates and the gauge field as

$$
x^M\sim\mathcal{O}(\lambda^{-1/2}),\qquad x^0\sim\mathcal{O}(\lambda^0),\qquad \mathcal{A}_M\sim\mathcal{O}(\lambda^{1/2}),\qquad \mathcal{A}_0\sim\mathcal{O}(\lambda^0), \qquad (3.104)
$$

and as a consequence $\rho\sim\lambda^{-1/2}$.

The equations of motion, up to $\mathcal{O}(\lambda^{-1})$ corrections, are

$$
\begin{aligned}
&D_N F_{NM}=0, \qquad\qquad \partial_N\hat{F}_{NM}=0,\\
&D_M F_{0M}+\frac{N}{64\pi^2}\epsilon_{MNPQ}\hat{F}_{MN}F_{QP}=0,\\
&\partial_M\hat{F}_{0M}+\frac{N}{64\pi^2}\epsilon_{MNPQ}\left[\mathrm{Tr}(F_{MN}F_{PQ})+\frac{1}{2}\hat{F}_{MN}\hat{F}_{PQ}\right]=0.
\end{aligned}
$$

At this order in λ, the BPST instanton is still a solution of the non-Abelian equation of motion. It is consistent to set $\hat{A}_M = A_0 = 0$, while $\hat{A}_0$ is sourced by the instanton density. The regular solution, which vanishes at spatial infinity for this gauge component, is given by

$$\hat{A}_0 = \frac{N}{8\pi^2\kappa}\frac{1}{\xi^2}\left[1 - \frac{\rho^4}{(\xi^2+\rho^2)^2}\right], \tag{3.105}$$

where $\xi = \sqrt{(\vec{x}-\vec{X})^2 + (z-Z)^2}$, and $\vec{X}, Z$ are moduli in the four-dimensional Euclidean space, *i.e.* the position of the instanton.

Then, the on-shell energy of the system, up to $\mathcal{O}(\lambda^{-2})$ is

$$E(\rho, Z) = 8\pi^2\kappa\left[1 + \left(\frac{\rho^2}{6} + \frac{N}{320\pi^4\kappa^2\rho^2} + \frac{Z^2}{3}\right)\right]. \tag{3.106}$$

The instanton moduli ρ, Z appear explicitly in the action and therefore are not genuine moduli, but are rather called *pseudo-moduli*. The minimization of the on-shell energy over these two parameters gives

$$\rho = \frac{N}{8\pi^2\kappa}\sqrt{\frac{6}{5}}, \qquad\qquad Z = 0. \tag{3.107}$$

The instanton is then located at the tip of the cigar geometry and its size scales as $\rho \sim \lambda^{-1/2}$, consistently with the approximation we used. Finally, the energy computed on these minimal values of the moduli gives the classical value of the baryon mass

$$M_{\mathrm{B}} = 8\pi^2\kappa + \mathcal{O}(\lambda^{-2}). \tag{3.108}$$

$N_f = 1$ WSS baryon

In the picture we have presented, nothing forbids taking only one flavor brane, namely $N_f = 1$. From the point of view of the underlying SU(N) QCD-like theory, there is no reason why there will not exist baryonic states as color singlets composed of N quarks. However, as we will see in a moment, the construction of baryons as instantons is not consistent with taking $N_f = 1$. As we discussed in chapter 2, it is not possible to construct a baryonic configuration using the mesonic fields alone in the low-energy one-flavored QCD. This problem arises in the same way in the holographic model because we can construct a baryon vertex with a single flavor and still cannot identify the baryon number in such a theory with the procedure outlined in [28].

The action describing the one-flavored theory takes the following form

$$S_{\mathrm{D8}} = -\frac{\kappa}{2}\int d^4x\, dz\left(\frac{1}{2}h(z)\hat{F}_{\mu\nu}\hat{F}^{\mu\nu} + k(z)\hat{F}_{\mu z}\hat{F}^{\mu}{}_{z}\right) + \frac{N}{24\pi^2}\int_{M_5}\frac{1}{2\sqrt{2}}\hat{A}\hat{F}^2. \tag{3.109}$$

The corresponding equations of motion are

$$-\kappa\left[h(z)\partial_\nu\hat{F}^{\mu\nu} + \partial_z(k(z)\hat{F}^{\mu}{}_{z})\right] + \frac{N}{128\pi^2}\epsilon^{\mu\alpha\beta\gamma\delta}\hat{F}_{\alpha\beta}\hat{F}_{\gamma\delta} = 0, \tag{3.110}$$

$$\kappa\, k(z)\partial_\mu\hat{F}^{z\mu} + \frac{N}{128\pi^2}\epsilon^{z\mu\nu\rho\sigma}\hat{F}_{\mu\nu}\hat{F}_{\rho\sigma} = 0. \tag{3.111}$$

We assume that the U(1) gauge field is static and we analyze the leading behavior in the λ^{-1} expansion under the rescaling (3.104). Then, the equations of motion are

$$\partial_N \hat{F}^{MN} = 0, \tag{3.112}$$

$$\partial_M^2 \hat{A}_0 + \frac{N}{64\pi^2\kappa}\epsilon_{MNPQ}\hat{F}_{MN}\hat{F}_{PQ} = 0. \tag{3.113}$$

Now it is well known that this Abelian theory, without sources, does not admit a non-singular instanton solution, and thus we are not able to identify the baryon in such a theory, as it happens in low-energy QCD.

3.3 The WSS model at finite temperature

The WSS model exhibits a rich phase structure, featuring both a first-order confinement/deconfinement transition and a first-order transition for the restoration of chiral symmetry. These two transitions can take place at distinct critical temperatures, depending on the specific parameters of the model. Notably, within the strongly coupled, planar regime $\lambda, N \to \infty$, these phenomena can be captured and analyzed in a precise manner using the dual holographic description. The confinement/deconfinement phase transition occurs at the critical temperature

$$T_c = \frac{M_{KK}}{2\pi}. \tag{3.114}$$

In the dual gravity picture, it corresponds to a Hawking-Page transition [138] between the solitonic background (3.44), dual to the confining phase, and a black brane solution dual to the deconfined one. If the flavor branes are placed at antipodal points on the compactification circle, *i.e.* when $LM_{KK} = \pi$, chiral symmetry breaking and confinement occur at the same energy scale. In other words, when $T < T_c$ chiral symmetry is broken and the theory confines, while at $T > T_c$ the theory enters a deconfined phase with chiral symmetry restoration being realized by two disconnected stacks of D8/$\overline{\text{D8}}$ branes crossing the black hole horizon. However, for non-antipodal configurations with $LM_{KK} \lesssim 0.97$, an intermediate phase with deconfinement but broken chiral symmetry arises [139]. This is the scenario we will be interested in.

The black brane background corresponding to the deconfined phase of the WSS model is given, in the string frame, as

$$ds^2 = \left(\frac{u}{R}\right)^{3/2}\left[-f_T(u)dt^2 + dx^i dx^i + dx_4^2\right] + \left(\frac{R}{u}\right)^{3/2}\left[\frac{du^2}{f_T(u)} + u^2 d\Omega_4^2\right], \tag{3.115}$$

$$f_T(u) = 1 - \frac{u_T^3}{u^3}, \qquad e^{\phi} = g_s\left(\frac{u}{R}\right)^{3/4}, \qquad F_4 = \frac{2\pi N}{V_4}\omega_4, \qquad R^3 = \pi g_s N l_s^3,$$

where t, x^i $(i = 1, 2, 3)$ and x^4 span the worldvolume of D4-branes, $u \in [u_T, \infty)$ is again the holographic coordinate. The parameter u_T is related to the black brane temperature T (which corresponds to the field theory temperature) through

$$9u_T = 16\pi^2 R^3 T^2. \tag{3.116}$$

The definition of the other fields and parameters is the same as in the solitonic background.

3.3.1 Flavors in the deconfined phase of the WSS model

In this section, we present the flavor D8-brane embedding at finite temperature and we review the holographic first-order phase transition, occurring in the deconfined phase, between the chiral symmetry broken phase (corresponding to the connected configuration) and the chirally symmetric one (corresponding to the disconnected configuration). We consider $N_f = 1$ since it will be the case of interest in following sections.

We start by writing the induced metric on the D8-brane's world volume, in terms of the inverse embedding $u = u(x_4)$

$$ds^2_{\mathrm{D8}} = \left(\frac{u}{R}\right)^{3/2}\left[-f_T(u)dt^2 + dx^i dx^i + \left(1 + \left(\frac{R}{u}\right)^3 \frac{u'(x_4)^2}{f_T(u)}\right)dx_4^2\right] + \left(\frac{R}{u}\right)^{3/2} u^2 d\Omega_4^2\,,$$

where $u'(x_4) = du/dx_4$. The DBI action (with no gauge fields) for the D8-branes reads

$$S^{\mathrm{DBI}}_{\mathrm{D8}} = -T_8 V_{3+1} V_4 \int dx_4\, u^4 \sqrt{f_T(u) + \left(\frac{R}{u}\right)^3 u'(x_4)^2}\,.$$

The action has a first integral

$$\frac{\partial \mathcal{L}}{\partial u'}u' - \mathcal{L} = -\frac{u^4 f_T(u)}{\sqrt{f_T(u) + \left(\frac{R}{u}\right)^3 u'(x_4)^2}} = \text{constant}\,.$$

The U-shaped connected configuration has a tip at $u = u_J$ where $u' = 0$. Thus, we can derive the profile of the D8-brane as

$$x_4^{\pm} = \pm\int du \left(\frac{R}{u}\right)^{3/2} \frac{u_J^4\sqrt{f_T(u_J)}}{\sqrt{f_T(u)}\sqrt{u^8 f_T(u) - u_J^8 f_T(u_J)}}\,. \tag{3.117}$$

We can now integrate the equation (3.117) to get the asymptotic brane separation L, which reads

$$L = \int dx_4 = 2\int \frac{du}{u'} = J_T(\tilde{b})\frac{R^{3/2}}{u_J^{1/2}}\,, \tag{3.118}$$

where

$$\tilde{b} \equiv \frac{u_T}{u_J}\,, \tag{3.119}$$

and

$$J_T(\tilde{b}) = \frac{2}{3}\sqrt{1-\tilde{b}^3}\int_0^1 dy \frac{\sqrt{y}}{\sqrt{\left(1-\tilde{b}^3 y\right)\left(1-\tilde{b}^3 y - \left(1-\tilde{b}^3\right)y^{8/3}\right)}}\,. \tag{3.120}$$

Using (3.116) we see that u_J becomes a non trivial function of T:

$$LT = \frac{3}{4\pi}J_T(\tilde{b})\sqrt{\tilde{b}}\,. \tag{3.121}$$

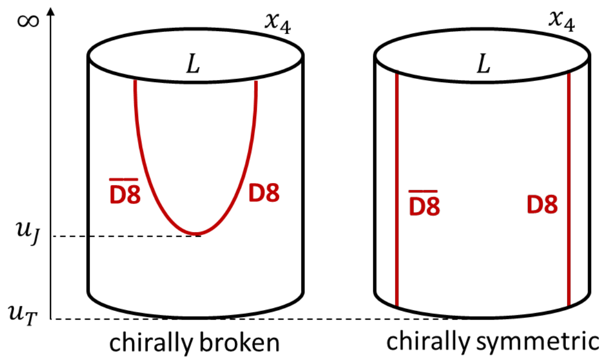

Figure 3.1. Schematic picture of the chirally broken (left) and chirally symmetric (right) phases in the deconfined phase of the Witten-Sakai-Sugimoto model. The x_4-direction is compactified on a circle with radius $1/M_{KK}$, and u is the holographic coordinate with $u = \infty$ being the boundary where the dual field theory lives. If the asymptotic distance L between the flavor branes is sufficiently small, a deconfined, chirally broken phase (left figure) becomes possible. In this phase, the connected flavor branes are embedded non-trivially in the background according to a definite function $x_4(u)$.

The connected configuration is not the only possible solution satisfying the requirement that the asymptotic separation of the flavor brane branches is L. Another solution exists with $u'(x_4) = \pm\infty$, which describes two disconnected branches extended along the radial direction u till the horizon. At

$$T = T_a \simeq \frac{0.154}{L}\,, \tag{3.122}$$

there is a first-order phase transition between the connected solution, holding at $T < T_a$, and the disconnected one. Hence for $T < T_a$ chiral symmetry is broken, while for $T > T_a$ chiral symmetry is restored. See figure 3.1 for a pictorial representation of these two phases in the (x_4, u) subspace.

Non-antipodally embedded D8-branes in the chirally-broken, deconfined phase of WSS describe a dual theory that shares key properties with the theory we are interested in: an SU(N)-like gauge theory coupled to a massless flavor at finite temperature. At low energy, the physics is captured by D8-brane excitations whose zero mode is the pion/axion[10] associated with the pseudo-Goldstone boson of the chiral symmetry breaking [140].

We conclude this section with some useful formulas. We can rewrite the D8-brane induced metric as

$$ds^2_{\mathrm{D8}} = \left(\frac{u}{R}\right)^{3/2}\left[-f_T(u)dt^2 + dx^i dx^i + \left(\frac{R}{u}\right)^3 \frac{du^2}{\gamma_T(u)}\right] + \left(\frac{R}{u}\right)^{3/2} u^2 d\Omega_4^2\,, \tag{3.123}$$

$$\sqrt{-\det g_{\mathrm{D8}}} = \left(\frac{R}{u}\right)^{3/4} u^4 \sqrt{\frac{f_T(u)}{\gamma_T(u)}}\,, \tag{3.124}$$

[10]The distinction between these two terms relies on the interpretation of the theory. We can consider a QCD flavor at finite temperature, and in that case, the Nambu-Goldstone boson will be the pion. However, this scenario can describe an ALP, as discussed in section 1.4. In particular, this is an example of a composite axion model.

where we have introduced the function

$$\gamma_T(u) = \frac{u^8 f_T(u) - u_J^8 f_T(u_J)}{u^8} \,. \tag{3.125}$$

Turning on the gauge field on the worldvolume of the ($N_f = 1$) D8-brane, we get a DBI action which, up to quadratic order in α', can be expanded as

$$\begin{aligned} S_{\rm D8}^{\rm DBI} &= -T_8 \int d^9x\, e^{-\phi}\sqrt{-\det(g_{\rm D8} + (2\pi\alpha')\mathcal{F})} \approx \\ &\approx -\frac{T_8}{4}\frac{V_4}{g_s}(2\pi\alpha')^2 R^{3/2}\int d^4x\, du\, u^{5/2}\sqrt{\frac{f_T(u)}{\gamma_T(u)}}\left[\frac{1}{2}\left(\frac{R}{u}\right)^3 \hat{F}_{ij}^2 - \left(\frac{R}{u}\right)^3 \frac{\hat{F}_{ti}^2}{f_T(u)} + \right. \\ &\quad \left. - \frac{\gamma_T(u)}{f_T(u)}\hat{F}_{tu}^2 + \gamma_T(u)\hat{F}_{iu}^2\right] , \end{aligned} \tag{3.126}$$

where the indices M, N, P, Q run over (t, x^i, u). Upon reduction on the four-sphere, the Chern-Simons part of the action reads

$$\begin{aligned} S_{CS} &= \frac{N}{24\pi^2}\int \mathcal{A}\wedge\mathcal{F}\wedge\mathcal{F} = \frac{N}{48\pi^2\sqrt{2}}\int \hat{A}\wedge\hat{F}\wedge\hat{F} = \\ &= \frac{N}{24\pi^2\sqrt{2}}\epsilon^{tMNPQ}\int d^5x\left(\frac{1}{4}\hat{A}_t\hat{F}_{MN}\hat{F}_{PQ} - \hat{A}_M\hat{F}_{tN}\hat{F}_{PQ}\right) , \end{aligned} \tag{3.127}$$

where the convention for the anti-symmetric tensor is that $\epsilon^{t1234} = 1$.

It is often convenient to work with a dimensionless holographic coordinate z, defined as

$$u(z) = u_J(1+z^2)^{1/3} = u_J k(z)^{1/3} \,, \tag{3.128}$$

where we have used the definition (3.73) of $k(z) = 1 + z^2$. Using this coordinate, the action (3.126) becomes[11]

$$\begin{aligned} S_{\rm D8}^{\rm DBI} = &- \frac{T_8}{4}\frac{V_4}{g_s}(2\pi\alpha')^2 R^{3/2}\int d^4x\, dz\, u^{5/2}\sqrt{\frac{f_T(u)}{\gamma_T(u)}}\left|\frac{\partial u}{\partial z}\right|\left[\frac{1}{2}\left(\frac{R}{u}\right)^3 \hat{F}_{ij}^2 - \left(\frac{R}{u}\right)^3 \frac{\hat{F}_{ti}^2}{f_T(u)} + \right. \\ &\left. - \left|\frac{\partial u}{\partial z}\right|^{-2}\frac{\gamma_T(u)}{f_T(u)}\hat{F}_{tz}^2 + \left|\frac{\partial u}{\partial z}\right|^{-2}\gamma_T(u)\hat{F}_{iz}^2\right] . \end{aligned} \tag{3.129}$$

[11] Even if not specified, every u has to be intended as a function of z.

Part I

Original contributions

Chapter 4

Hall droplet sheets in holographic QCD

In section 2, we discussed in detail the reasons why in the one-flavored QCD, the standard Skyrmion mechanism for baryon construction is not applicable. In this case, baryons may not be particle-like solitons, but rather extended two-dimensional topological defects, termed *Hall droplet sheets*. These configurations are domain walls of the η' field that interpolate between distinct 2π-shifted vacua of the effective potential. Although these vacua are physically equivalent due to the periodicity of η', the non-trivial topological winding across the sheet allows for a non-zero baryon number to reside on its boundary. In this picture, the baryon can be seen as a Hall droplet with gapless chiral edge modes localized on the boundary of the sheet, in analogy with edge currents in fractional quantum Hall systems.

Unfortunately, the dynamical properties of such sheets, including their tension, baryon number density, and interactions with other QCD states, remain challenging to compute directly within the effective field theory framework. The η' potential is generated non-perturbatively via gluon dynamics and is typically non-analytic, making semiclassical treatments subtle.

To address these limitations, we can employ a top-down holographic approach to QCD, in particular, working within the WSS model. As we have seen in 3.2, the WSS model naturally incorporates the η' meson and includes the axial anomaly through Chern–Simons terms, providing a controlled and calculable environment for exploring the physics of Hall droplet sheets.

As a first step towards the construction of baryons as quantum Hall droplets in holography, in this chapter, based on our original results presented in [1], we will provide a concrete realization of the Hall droplet sheet in terms of D6-branes wrapping the internal S^4 of the geometry and extending along two spatial dimensions and time. These D6-branes act as $(2+1)$-dimensional membranes embedded in the bulk geometry, supporting the $\mathrm{U}(1)_N$ CS theory, conjectured in [38]. In this picture, the sheet can be viewed as a wall with a hard (gluonic) D6-brane core, corresponding to the heavy fields associated with the singularity in the chiral Lagrangian, and a soft shell (a mesonic cloud) coming from the non-trivial profile of the η' meson. Indeed, the D6-brane can be viewed as a source for the Maxwell gauge field living on the D8-brane, whose excitations are identified with the meson. The holographic construction makes it transparent that the dynamical gauge field on the sheet is not mesonic; rather, it sources some mesonic profiles through the boundary. See [46, 48, 49] for related discussions.

In this chapter, to simplify our analysis, we will focus on two configurations: the infinite and the semi-infinite sheet with a straight boundary. In the first case, as expected, we find a regular profile for the η'-field both in the massless and the massive quark case. We compute the tension and the thickness of the sheet considering the contributions from the hard core and the mesonic cloud. In the second case, the straight boundary can be viewed as a linear distribution of magnetic charge in the D8-brane five-dimensional Maxwell-Chern-Simons effective theory on a curved background. The corresponding gauge field can be found semi-analytically, through a series expansion, and numerically. From this solution, we extract the effective action for the transverse fluctuations of the boundary and the tension, which scales parametrically as expected from [38]. Then, we can compute the profile of the η' field, which now has two different features depending on the domain. In fact, it is continuous (in analogy with the infinite sheet case) through the D6-brane, while it is discontinuous outside the sheet, enforcing the monodromy of the η' meson around the wall. Finally, we will show that it is possible to turn on, with no energy cost, a chiral component of the gauge field on the boundary of the sheet, possibly connected to the chiral edge mode on the boundary of the Hall droplet.

This chapter is organized as follows. In section 4.1, we describe our proposal for the holographic realization of the sheet in the WSS model. The explicit realization of the infinite Hall droplet sheet, with massless and massive quarks, is presented in section 4.2. The main results of the chapter are contained in section 4.3, where we present the simplest example of a sheet with a boundary, that is, a straight boundary.

4.1 The sheet in the WSS model

We propose that the holographic picture for the $N_f = 1$ baryons considered in [38] is given, in the WSS model, in terms of a D6-brane wrapped on the background S^4. When the D8-branes are antipodally embedded, the D6-brane is localized at $z = 0$, $y = 0$ (*i.e.* $u = u_0$) and can be taken, say, at $x_3 = 0$ in the Witten geometry at zero temperature (3.44); see figure 4.1 for the displacement of the branes in the cigar of the geometry. The following table shows the embedding of the various branes in the model

	0	1	2	3	4	5	6	7	8	9
D4	•	•	•	•	•	◦	◦	◦	◦	◦
D8	•	•	•	•	◦	•	•	•	•	•
D6	•	•	•	◦	◦	◦	•	•	•	•

Table 4.1. D4/D8/D6 intersection. A bullet indicates a direction where the branes are extended, and an empty dot indicates a direction where the branes are localized.

The low-energy theory on the D6-brane world-volume is given by a $\mathrm{U}(1)_N$ CS theory (plus the center of mass degrees of freedom) just because it is wrapped on

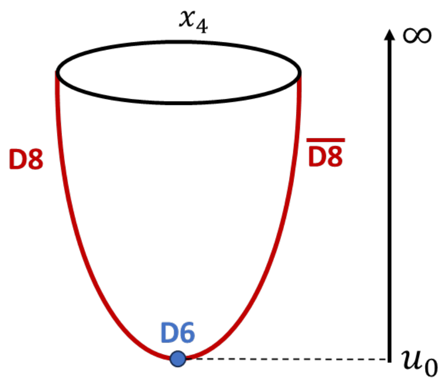

Figure 4.1. The displacement of the D-branes on the cigar of the geometry for antipodally embedded D8-branes.

the S^4 [141], which supports N units of flux of F_4. In particular, from the CS term of the D6-brane, we get

$$\frac{1}{8\pi^2}\int C_3 \wedge f \wedge f = \frac{1}{8\pi^2}\int F_4 \wedge a \wedge f = \frac{N}{4\pi}\int a \wedge f\,, \tag{4.1}$$

where we have used $\int_{S^4} F_4 = 2\pi N$ and $f = da$. Remarkably, the above theory precisely agrees with the expected CS theory proposed in [38] for the theory on the bulk of the sheet.[1]

The DBI action of the D6-brane gives, upon integration on the four-sphere, the effective theory for the Abelian gauge connection a which lives on the D6-brane world-volume. The CS-DBI theory will be extensively discussed in the next chapters, while here we will focus mostly on the effects on the flavor theory of the D6-brane presence.

This picture resembles that of D6-branes as domain walls separating different degenerate vacua in the WSS model at $\theta = \pi$ [142, 141].[2] Across the domain wall, there is a jump of the value of the gluon condensate, while in our case, there is a monodromy of η'. In addition, note that the sheet now does not separate two different vacua since the $\eta' = 0$ and the $\eta' = 2\pi$ ones are the same. The story goes in close analogy with the axion monodromy studied in [143], where interesting comments on the metastability of the D6-brane configuration with a boundary on the D8-brane can be found. In [143], in fact, it is argued that the D6-brane sheet is at best metastable, since it can decay by developing holes with an exponentially suppressed rate $\Gamma \sim e^{-\lambda^2 N}$.

As already mentioned in the introduction of this chapter, the holographic picture of the sheet does not end with the D6-brane. The latter (which in the baryon case is expected to have a finite, disk-like shaped extension) has to be thought of as the hard core of the Hall droplet baryon. On top of this, there will be a soft mesonic

[1]The integration by parts of the D6-brane CS term has to be corrected in the presence of a boundary for the D6-brane. We will come back to this point in chapter 6, since it does not play a role in the present chapter.

[2]The world-volume theory for real QCD has been studied in [105].

cloud due to the non-trivial configuration of the η' field. The latter can be explicitly found considering the whole structure of the D8-brane action in the presence of a D6-brane source.

As we have seen in section 3.2, the flavor gauge field for $N_f = 1$ is just given by the Abelian component $\mathcal{A} = \hat{A}/\sqrt{2}$, so we can drop the hat without ambiguities. The D8-brane action for $N_f = 1$ admits the CS term

$$\frac{1}{2\pi}\int C_7 \wedge \frac{F}{\sqrt{2}}\,. \tag{4.2}$$

Note that, as we will see in the following, the D6-brane source induces a flux

$$\int F_{x_3 z} dx_3 dz = -2\pi\sqrt{2}\,, \tag{4.3}$$

which provides an $\overline{\text{D6}}$-brane charge precisely canceling that of the source. Hence, the total D6-brane charge in the setup is zero. The sheet, in fact, can decay, and thus there cannot be a net D6-brane charge.

The condition (4.3) precisely accounts for a non-trivial profile of the η' field, *i.e.* a non-trivial profile for A_z. The mesonic shell of the sheet can be seen as a non-trivial solution for the Abelian gauge field on the D8-brane satisfying (4.3).

However, this is not enough to get the action for a point-like particle with baryonic $\mathrm{U}(1)_B$ charge on the D8-branes. Following the discussion around (3.101), we can define $a_0(t) = A_0/\sqrt{2}$ and treat it as a time-dependent perturbation. Thus, we can get such a point-particle action only if the other component $F_{x_1 x_2}$ of the field strength is turned on. It is easy to understand this by looking at the five-dimensional CS term in the D8-brane action (3.109)

$$\frac{N}{24\pi^2}\int \frac{1}{2\sqrt{2}} A \wedge F \wedge F = \frac{N}{24\pi^2}\int dt\, a_0(t) \int \frac{F}{\sqrt{2}} \wedge \frac{F}{\sqrt{2}}\,, \tag{4.4}$$

which implies that the baryon solution has to be some kind of "Abelian instanton" with unit instanton number

$$\frac{1}{48\pi^2}\int (F\wedge F)_{x_1 x_2 x_3 z}\, dx_1 dx_2 dx_3 dz = 1. \tag{4.5}$$

As observed in section 3.2.2, there is no such solution in $\mathbb{R}^4$. The conclusion changes if the theory is sourced by some kind of non-trivial extended source or if the theory is defined on a non-trivial manifold. See [144] for a discussion on Abelian instantons. Having in mind the droplet, and therefore a disk geometry, if the overlap between the sheet and the D8-branes in the (x_1, x_2) plane is a disk of radius l, then the above condition has some hope of being satisfied. Analogously to what happens for the standard baryons, due to the five-dimensional CS coupling, the above condition induces an electric field. We expect that the related Coulomb interaction is what stabilizes the sheet to some finite size l_{stable}. We will tackle this problem in the next chapters.

In this chapter, we will focus on infinitely extended sheets, and hence we will not impose the condition (4.5).

4.1.1 Comparison with QCD

In the WSS model, departure from the antipodal D8-brane configuration corresponds to increasing quartic Nambu-Jona-Lasino (NJL) type couplings between the quarks [145]. If this departure is large, *i.e.* the configuration is far from the antipodal one, the effect of large NJL-type couplings is that the critical temperature for chiral symmetry breaking is different (larger) than that for confinement [139]. Thus, this scenario is different from what is expected to happen in QCD. Instead, if the departure from the antipodal configuration is not large, the chiral symmetry breaking and confinement temperatures are still coincident and there is no clear contradiction with QCD expectations.

Thus, the configurations closer to QCD are the antipodal one and the moderately non-antipodal ones. In the antipodal case, the holographic description of the sheet is a D6-brane lying on top of the D8-branes at the tip of the cigar (as in figure 4.1). In flat space, such a configuration is unstable towards the formation of a D8-D6 bound state, where the D6 is melt in the D8 world-volume. This happens because the spectrum of D8-D6 strings contains a scalar. The scalar is tachyonic if the branes are on top of each other (and there are no fluxes turned on). The melting of the D6-brane corresponds to the condensation of this scalar.[3] This corresponds to a complete Higgsing of the U(1) gauge group of the three-dimensional theory living on the world-volume of the sheet (the D6-brane). In this scenario, it should again be possible to describe finite-energy baryons. A very similar situation is found in the case of the domain-wall at $\theta = \pi$ [141].

A small departure from the antipodal configuration is sufficient to give a positive mass to the scalar, avoiding the Higgsing mechanism and so the melting of the D6-brane. Thus, there is a family of moderately non-antipodal configurations whose phase diagram is consistent with the QCD one, and for which the sheet is realized with an actual D6-brane, which is not melted.[4] The D6 melting could also be avoided by introducing sufficiently large masses for the quarks [41, 141].

The condensed scalar scenario is not the one explored in [38]. While it would be of obvious interest to explore the melted-D6 configuration, in this chapter we aim at studying the original proposal in [38], corresponding to an actual D6-brane. In order to simplify the computations, in this chapter, we will consider the antipodal configuration without large quark masses, aiming at revealing some basic features of the sheet. This is obviously an oversimplification, which eventually must be lifted in future studies.

4.2 Infinite sheet

In this section, we study the infinitely extended wall corresponding to a sheet without boundaries, introduced as an example in 2.8. The sheet has a “hard”, gluonic core corresponding to the D6-brane, and a “soft” shell from the η' profile, *i.e.* a meson cloud, as advocated *e.g.* in [41].

[3] It is not immediately evident how to describe the three-dimensional scalar field on the world-volume of the sheet in terms of the elementary fields of the four-dimensional theory.

[4] We thank Ofer Aharony for the exchange of ideas on this issue.

4.2.1 The core

The "hard" gluonic core of the sheet is holographically given by the wrapped D6-brane. Assuming the sheet to be extended along the x_1, x_2 directions, its tension $T_{\rm hard}$ can be extracted from the DBI term of the wrapped D6-brane action

$$S_{\rm D6}^{\rm DBI} = -T_6 \int d^7x\, e^{-\phi}\sqrt{-\det P[g]} \equiv -T_{\rm hard}\int dt dx_1 dx_2\,, \tag{4.6}$$

where $T_6 = (2\pi)^{-6}\, l_s^{-7}$ and

$$T_{\rm hard} = \frac{1}{\pi^3 3^6}\lambda^2 N M_{KK}^3\,. \tag{4.7}$$

As expected, the tension scales as N, but is enhanced by the λ^2 factor, as usual in holographic theories.

Considering the thickness δ of a D-brane sitting at the tip of the background cigar to be given by the effective local string length $l_s^{\rm eff}$, one gets for the thickness of the hard core of the wall (up to a numerical factor)

$$\delta_{\rm hard} \sim l_s^{\rm eff} \sim \frac{1}{\lambda^{1/2} M_{KK}}\,, \tag{4.8}$$

which comes from the scaling of the effective Yang-Mills string tension $\sim (l_s^{\rm eff})^{-2} \sim \lambda M_{KK}^2$ in the model.

4.2.2 The shell

A localized D6-brane is a source for the RR C_7 field. This, in turn, will generate a non-trivial profile for the D8-brane mode corresponding to the η'. The profile of the η', the meson cloud, constitutes the "soft shell" of the sheet.

In order to study the D6-D8 setup we have in mind, we should better consider the total action with the contribution from S_{C_7}. In the presence of an explicit D6-brane, the action for the C_7 form reads

$$S_{C_7} = -\frac{1}{4\pi}(2\pi l_s)^6 \int dC_7 \wedge \star dC_7 + \frac{1}{2\pi}\int C_7 \wedge \frac{F}{\sqrt{2}} \wedge \omega_1 + \int C_7 \wedge \omega_3\,. \tag{4.9}$$

The first two terms are respectively the kinetic term coming from the type IIA supergravity action, and the coupling to the flavor D8-brane, whose embedding, in the antipodal case, is described by a delta-like one form $\omega_1 = \delta(y)dy$. We have discussed these two terms in detail in section 3.2.1. The third term arises from the D6-brane source, whose embedding is described by the three-form $\omega_3 = \delta(z)\delta(y)\delta(x_3)dz \wedge dy \wedge dx_3$, since we have placed the D6-brane at $z = y = x_3 = 0$.

Now, we compute the equation of motion for C_7 as we did in (3.75). This time, there will be an additional source term coming from the presence of the D6-brane. Let us recall that $\star F_8 = (2\pi l_s)^{-6}\widetilde{F}_2$, and we derive

$$d\widetilde{F}_2 = \frac{F}{\sqrt{2}} \wedge \delta(y)dy + 2\pi\delta(z)\delta(y)\delta(x_3)dz \wedge dy \wedge dx_3\,. \tag{4.10}$$

We can formally solve the above equation[5] as

$$\widetilde{F}_2 = \frac{A}{\sqrt{2}} \wedge \delta(y)dy + 2\pi\Theta(x_3)\delta(z)\delta(y)dz \wedge dy\,. \tag{4.11}$$

As we mentioned in 3.2.1, the full action for C_7 turns out to be equivalent to

$$S_{\widetilde{F}_2} = -\frac{1}{4\pi(2\pi l_s)^6}\int \widetilde{F}_2 \wedge \star\widetilde{F}_2\,, \tag{4.12}$$

just as in the case with no explicit D6-brane source. At $\theta = 0$, the above action can be written as

$$S_{\widetilde{F}_2} = -\frac{\chi_g}{2}\int d^4x\left(2\pi\Theta(x_3) + \frac{1}{\sqrt{2}}\int_{-\infty}^{+\infty} dz\, A_z\right)^2, \tag{4.13}$$

where we recall that the topological susceptibility of the unflavored gauge theory, in units of M_{KK}, reads

$$\chi_g = \frac{\lambda^3}{4(3\pi)^6}\,. \tag{4.14}$$

Moreover, we add the mass term as in equation (3.96), which in the one-flavored case becomes

$$S_{\text{mass}} = 2\,c\,m\int d^4x\,\cos\left(\frac{1}{\sqrt{2}}\int_{-\infty}^{+\infty} dz\, A_z\right), \qquad c = \frac{\lambda^{3/2}M_{KK}^3}{3^{9/2}\pi^3}, \tag{4.15}$$

where m is the quark mass.

From the full action, we can obtain an effective four-dimensional Lagrangian for the η' field, after integrating over the four-sphere and the holographic coordinate, using the following ansatz for the flavor gauge field

$$A_z(z, x_3) = -\frac{\sqrt{2}}{\pi\, k(z)}\varphi(x_3)\,, \tag{4.16}$$

where $k(z) = 1 + z^2$, and φ is a function of x_3 alone. Integrating the gauge field over z we get

$$\int A_z dz = -\sqrt{2}\,\varphi \equiv 2\frac{\eta'}{f_\pi}\,, \qquad f_\pi = 2\sqrt{\frac{\kappa}{\pi}}\,, \tag{4.17}$$

where we have written the precise relation between the meson field η' and the bulk field A.

Therefore, the effective Lagrangian reads

$$\mathcal{L} = -\frac{\kappa}{\pi}(\partial_\mu\varphi)(\partial^\mu\varphi) + 2\,c\,m\cos\varphi - \frac{\chi_g}{2}\min_{k\in\mathbb{Z}}\left(\varphi - 2\pi\Theta(x_3) + 2\pi k\right)^2. \tag{4.18}$$

From the above Lagrangian, we can derive the equation of motion for the field $\varphi = \varphi(x_3)$. We are going to search for a configuration interpolating from 0 for $x_3 \to -\infty$ to 2π for $x_3 \to +\infty$ and such that $\varphi(0) = \pi$. In this case, the potential is minimized for $k = 0$, and the equation of motion reads

$$\partial^2\varphi(x_3) - m_{\text{WV}}^2\left(\varphi(x_3) - 2\pi\Theta(x_3)\right) - m_\pi^2\sin(\varphi(x_3)) = 0, \tag{4.19}$$

[5] We set $dC_1 = 0$, which corresponds to treating the theory at zero θ-angle.

where

$$m_{\mathrm{WV}}^2 \equiv \frac{\chi_g \pi}{2\kappa} = \frac{\lambda^2}{27\pi^2 N} \tag{4.20}$$

is the Witten-Veneziano mass, introduced in (1.29). Treating the D8-brane in the probe approximation amounts to taking $m_{\mathrm{WV}} \ll 1$. The other parameter in the equation of motion above is

$$m_\pi^2 = \frac{4cm}{f_\pi^2}, \tag{4.21}$$

which represents the quark mass contribution to the η' mass. As observed in [141], the parameter m_π has to be small, $m_\pi \ll 1$, in order to neglect higher-order corrections to the mass term of the WSS model.

Massless quark

In the massless case $m = 0$ the equation of motion for φ (4.19) has an analytic solution

$$\varphi(x_3) = \pi e^{m_{\mathrm{WV}}\, x_3} - \pi e^{-m_{\mathrm{WV}}\, x_3} \left(e^{m_{\mathrm{WV}}\, x_3} - 1\right)^2 \Theta(x_3)\,, \tag{4.22}$$

where we have imposed the boundary conditions $\varphi(x_3 \to +\infty) = 2\pi$, and $\varphi(x_3 \to -\infty) = 0$. This solution has been derived in the presence of an explicit gluonic source. Similar solutions without explicit sources, with regular or singular potentials, have a very long history, see *e.g.* [41, 42].

The thickness of the "soft" part of the wall (the one given by the η' profile) is clearly linear in $1/m_{\mathrm{WV}}$, as it can be seen from (4.22), so up to a numerical factor,

$$\delta_{\mathrm{soft}} \sim \frac{1}{m_{\mathrm{WV}}} \sim \frac{\sqrt{N}}{\lambda M_{KK}}\,. \tag{4.23}$$

The $\varphi \sim \eta'$ solution (4.22) interpolates between zero (for $x_3 \to -\infty$) and 2π ($x_3 \to \infty$) and it takes the value $\varphi(0) = \pi$ in $x_3 = 0$. See figure 4.2 (left panel).

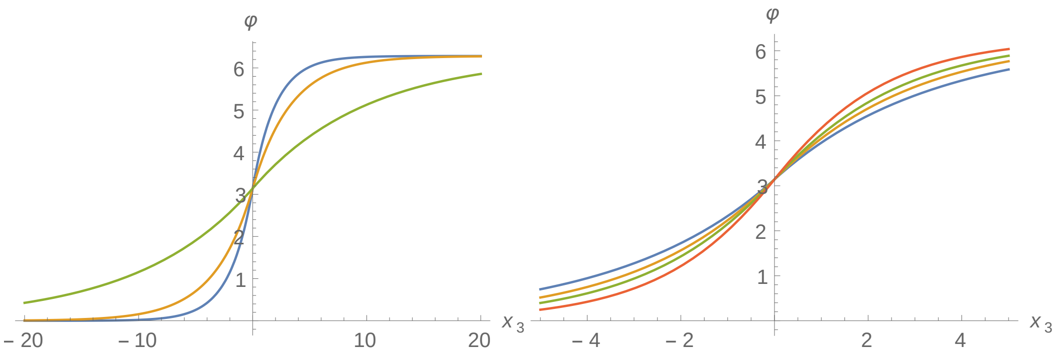

Figure 4.2. Left: the profile of $\varphi = -\sqrt{2}\eta'/f_\pi$ for $m_{\mathrm{WV}}/M_{KK} = 0.1, 0.3, 0.5$ (green, yellow and blue lines). Right: the profile of φ for $m_{\mathrm{WV}}/M_{KK} = 0.3$ and $m_\pi^2/M_{KK}^2 = 0, 0.05, 0.1, 0.2$ (blue, yellow, green and red lines).

Correspondingly, the Abelian field strength on the D8-brane reads

$$F_{x_3 z} = -\frac{\sqrt{2}\, m_{\mathrm{WV}}}{k(z)} \left(e^{m_{\mathrm{WV}}\, x_3} - 2\Theta(x_3) \sinh(m_{\mathrm{WV}}\, x_3)\right)\,, \tag{4.24}$$

where we have reinserted the z-dependent factor. This satisfies

$$\int dx_3\, dz\, F_{x_3 z} = -2\sqrt{2}\pi\,, \tag{4.25}$$

hence, as anticipated in equation (4.3) the η' profile effectively induces a unit of $\overline{\text{D6}}$-brane charge.

Due to the field strength (4.24), the D8-brane has an excess of energy, providing the tension of the soft shell of the sheet. This can be deduced from the on-shell value of the D8-brane DBI action, expanded at the quadratic order in the field strength

$$S_{\text{D8}} = -\frac{\kappa}{2}\int dt\, dx_1\, dx_2 \int dz\, dx_3 (1+z^2) F_{x_3 z}^2\,. \tag{4.26}$$

Inserting the solution (4.24) and performing the integration in z, x_3 we get the tension

$$T_{\text{soft}} = \frac{1}{3^3 2^3 \pi^2}\lambda N m_{\text{WV}} M_{KK}^2 = \frac{1}{3^{9/2} 2^3 \pi^3}\lambda^2 N^{1/2} M_{KK}^3\,. \tag{4.27}$$

Note that considering the expression of f_π in (4.17), one has $T_{\text{soft}} \sim f_\pi^2 m_{\text{WV}}$.

Massive quark

In the massive-quark case, one can integrate numerically the equation (4.19) with $k = 0$. As can be seen from figure 4.2 (right panel), the solution shows a similar behavior to that in the massless case. Also in this case, the solution corresponds to a unit $\overline{\text{D6}}$-brane charge.

The thickness of the soft part of the wall now depends on the quark mass m (and hence on m_π) as well and roughly behaves as (at small φ this comes from (4.18))

$$\delta_{\text{soft}} \sim \frac{1}{\sqrt{m_{\text{WV}}^2 + m_\pi^2}}\,. \tag{4.28}$$

In order to estimate the tension, we have to insert the numerical solution for $F_{x_3 z}$ in formula (4.26), which gives

$$T_{\text{soft}} = \frac{1}{3^3 2^3 \pi^2}\lambda N m_{\text{WV}} \Psi(m_\pi/m_{\text{WV}}) M_{KK}^2\,. \tag{4.29}$$

The result is exactly as in (4.27) but for the substitution

$$m_{\text{WV}} \longrightarrow m_{\text{WV}} \Psi\left(\frac{m_\pi}{m_{\text{WV}}}\right), \tag{4.30}$$

where $\Psi(q)$ is a function reported in figure 4.3, going as $\sqrt{1+q^2}$ at small q.

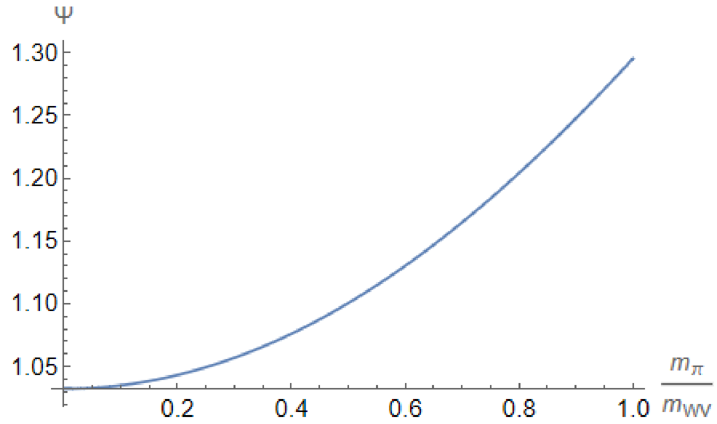

Figure 4.3. The function $\Psi(m_\pi/m_{\rm WV})$ providing the quark-mass dependence of the soft part of the tension of the sheet.

Resume

Table 4.2 contains the parametric dependence of tension and thickness of the core and shell parts of the sheet discussed above.

	Massless quark	Massive quark
Core tension $T_{\rm hard}$	$\lambda^2 N\Lambda^3$	$\lambda^2 N\Lambda^3$
Core thickness $\delta_{\rm hard}$	$\lambda^{-1/2}\Lambda^{-1}$	$\lambda^{-1/2}\Lambda^{-1}$
Shell tension $T_{\rm soft}$	$\lambda N m_{\rm WV}\Lambda^2 \sim \lambda^2 N^{1/2}\Lambda^3$	$\lambda N m_{\rm WV}\Psi(m_\pi/m_{\rm WV})\Lambda^2$
Shell thickness $\delta_{\rm soft}$	$m_{\rm WV}^{-1} \sim \lambda^{-1}N^{1/2}\Lambda^{-1}$	$(m_{\rm WV}^2 + m_\pi^2)^{-1/2}$

Table 4.2. Summary of parametric dependence of tension and thickness of the core and shell parts of the sheet. For the reader's convenience, we used the dynamical scale notation Λ instead of M_{KK}.

4.3 Semi-infinite sheet: the vortex string

In this section, we present the holographic description of the semi-infinite sheet, whose boundary is a straight infinite vortex string.[6] The sheet is dual to a D6-brane, which for convenience is placed at $x_3 = z = y = 0$ and extended along $x_2 \geq 0$. The string is its boundary, which we take at $x_2 = 0$, attached to the D8-brane, see figure 4.4. As it will be clear soon, the boundary is a magnetic source on the D8-brane

[6]The manifold defined by the D6-brane worldvolume has now a boundary. The CS theory for the D6-brane gauge field is now given by (4.1) plus a six-dimensional boundary term. This will be discussed in the next chapter and does not play a role in this discussion since we are interested in the D8-brane's description of the Hall droplet sheet.

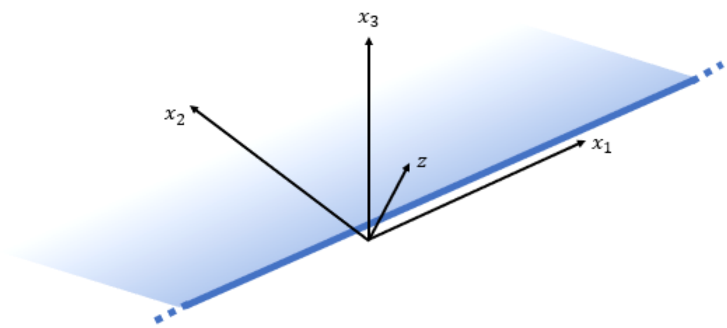

Figure 4.4. D6-brane dual to the semi-infinite sheet. It is taken to be extended along the x_1-axis and along the positive values of the x_2-axis. The directions x_3 and z are orthogonal to the sheet. Every point is also extended in time and along the other four dimensions, which are wrapped on S^4.

worldvolume. In this case the action terms (4.9) take the form

$$\begin{aligned} S_{C_7} = &-\frac{1}{4\pi}(2\pi l_s)^6 \int dC_7 \wedge \star dC_7 \\ &+ \frac{1}{2\pi}\int C_7 \wedge \left[\frac{F}{\sqrt{2}} \wedge \delta(y)dy + 2\pi\Theta(x_2)\delta(x_3)dx_3 \wedge \delta(z)dz \wedge \delta(y)dy\right] , \end{aligned} \tag{4.31}$$

where we used $\omega_3 = \Theta(x_2)\delta(x_3)dx_3 \wedge \delta(z)dz \wedge \delta(y)dy$. The corresponding equation for C_7 can be transformed into the anomalous Bianchi identity for $\widetilde{F}_2$,

$$d\widetilde{F}_2 = \frac{F}{\sqrt{2}} \wedge \delta(y)dy + 2\pi\Theta(x_2)\delta(x_3)dx_3 \wedge \delta(z)dz \wedge \delta(y)dy\,. \tag{4.32}$$

Taking the exterior derivative of the above equation, we have to require that the RHS vanishes. This provides the violation of the Bianchi identity for A due to the presence of a magnetic source, which is the boundary of the D6-brane

$$dF = -2\sqrt{2}\,\pi\,\delta(x_2)\delta(x_3)\delta(z)dx_2 \wedge dx_3 \wedge dz\,. \tag{4.33}$$

Thus, we are led to consider the problem of finding the fields generated by a uniform linear distribution of magnetic charge in five-dimensional electromagnetism with CS and $\widetilde{F}_2$ source terms on the effective curved background

$$ds^2 = k^{2/3}(z)dx^\mu dx_\mu + \frac{dz^2}{k^{2/3}(z)}\,, \tag{4.34}$$

as can be deduced by rewriting the Maxwell action for F in general covariant form. We have not found such type of solution, or part of it, in the literature, so we derive it in this section. The strategy will be the following.

1. We will first find a configuration F^m satisfying the Bianchi equation (4.33) and $d\star F^m = 0$. This corresponds to a kind of magnetic monopole-like solution for a source extended along the x_1 axis.

2. The complete field can be written as

$$F = F^m + dA^c \,, \tag{4.35}$$

being A^c the gauge connection associated to a closed field strength. If we consider a potential A^m for F^m, we have

$$dA^m = F^m + \mathcal{S} \,, \tag{4.36}$$

where $\mathcal{S}$ is the Dirac sheet (a higher-dimensional version of the Dirac string) field strength. A particular gauge choice of the Dirac sheet allows us to solve equation (4.32) as

$$\widetilde{F}_2 = \left(\frac{A^c + A^m}{\sqrt{2}}\right) \wedge \delta(y)dy + 2\pi\Theta(x_3)\delta(z)dz \wedge \delta(y)dy \,. \tag{4.37}$$

Such a gauge choice corresponds to writing

$$\mathcal{S} = -\Theta(-x_2)\delta(x_3)dx_3 \wedge \delta(z)dz, \tag{4.38}$$

meaning that the Dirac sheet is placed at $x_3 = z = 0$ and extended along x_1 and $x_2 < 0$. Following section 4.2, the integral of the field $\widetilde{F}_2$ along the (z, y)-cigar

$$\int_{\text{cigar}} \widetilde{F}_2 = \int \left(\frac{A^c_z + A^m_z}{\sqrt{2}}\right) dz + 2\pi\Theta(x_3) \,, \tag{4.39}$$

enters, through the supergravity term (4.12), the equation for A^c_z. If there are no CS terms (as will be the case), and considering that $d{\star}F^m = 0$, the equation reads schematically

$$d{\star}dA^c_z = \int (A^c_z + A^m_z)\, dz + 2\pi\sqrt{2}\,\Theta(x_3) \,. \tag{4.40}$$

Given that A^m_z is known from step 1, we can solve this equation for A^c_z.

3. We can consider the charged case by switching on the components $A_\pm(x_\pm, x_2, x_3, z)$ of the gauge field, where $x^\pm = (x_1 \pm t)/2$ are the light cone coordinates in the (t, x_1)-space. One can easily realize that $A_\pm$ do not enter the previous equations, but on the contrary, the field $A_z = A^c_z + A^m_z$ generates a CS term for their equations, which schematically read

$$d{\star}dA_\pm = F_{\pm x_2} \wedge F_{x_3 z} + \dots \,. \tag{4.41}$$

The latter can be solved independently after steps 1 and 2 are completed, since the only unknowns are $A_\pm$.

In order to illustrate this procedure, in the next section we consider as a warm-up the flat space case. Then, in section 4.3.2 we will provide the solution on the curved space (4.34). The procedure does not depend on the explicit form of the metric function $k(z)$ and can in principle be applied to a generic metric of the form (4.34).

4.3.1 Solution in flat space

In this section, we consider the case of five-dimensional flat spacetime, *i.e.* $k(z) = 1$. In this case, the configuration has spherical symmetry in the directions x_2, x_3, z transverse to t, x_1 where the line source is placed, so we employ spherical coordinates

$$x_2 = \rho \cos\theta\,, \quad x_3 = \rho \sin\theta \cos\phi\,, \quad z = \rho \sin\theta \sin\phi\,. \tag{4.42}$$

where $\theta \in [0, \pi]$, and $\phi \in [0, 2\pi)$. It is also convenient to parameterize the (t, x_1)-part of spacetime with light-cone coordinates

$$x_\pm = \frac{x_1 \pm t}{2}\,, \tag{4.43}$$

such that the effective five-dimensional spacetime where the Maxwell-Chern-Simons theory lives reduces, in the flat limit, to

$$ds^2 = 4dx_+ dx_- + d\rho^2 + \rho^2 d\Omega_2\,, \tag{4.44}$$

with the two-sphere parameterized by angles θ, ϕ.

We consider an ansatz where:

- all the fields just depend on the radial direction ρ;
- the magnetic charge from equation (4.33) is
$$-2\sqrt{2}\pi\delta(\rho)\rho^2 d\rho \wedge \omega_2\,, \tag{4.45}$$
with $\omega_2 = \sin\theta d\theta \wedge d\phi$ being the two-sphere volume form;
- the field strength has just two components
$$F_{\theta\phi}\omega_2\,, \qquad F_{\pm\rho} dx_\pm \wedge d\rho\,, \tag{4.46}$$
where either A_+ or A_- are turned on. This implies that we have (only) one non-vanishing term in $F \wedge F$, entering the equation for $A_\pm$.

It is readily verified that the ansatz is consistent with the equations of motion and Bianchi identity.

Step 1: monopole-like solution

We start by searching for a solution F^m to the Bianchi equation $dF^m = -2\sqrt{2}\pi\delta(\rho)\rho^2 d\rho\wedge$ ω_2 and the equation of motion (without CS term, as explained above) $d{\star}F^m = 0$.

Considering translation invariance along x_1 and spherical symmetry, the problem is very similar to that of finding the field strength generated by the standard Dirac monopole in four dimensions. Thus, the solution is quite similar

$$F^m = F^m_{\theta\phi}\omega_2 = -\frac{1}{2\rho^2}\rho^2\sqrt{2}\,\omega_2\,, \tag{4.47}$$

where $\omega_2 = \sin\theta d\theta \wedge d\phi$ and we have made explicit the singular behavior at the origin $\rho = 0$. It is straightforward to check that (4.47) solves the equations of motion and that

$$\int_{M_3} dF^m = \int_{M_2} F^m = -2\sqrt{2}\pi\,, \tag{4.48}$$

where M_3, M_2 are three- and two-dimensional closed surfaces containing the point $\rho = 0$, $M_2 = \partial M_3$ being the boundary of M_3.

A standard way of writing a potential A^m for this field is

$$A^m = A^m_\phi d\phi = -\sqrt{2}\frac{(1-\cos\theta)}{2\rho\sin\theta}\rho\sin\theta d\phi\,. \tag{4.49}$$

In this form, we can write a magnetic potential for the monopole solution as

$$dA^m = F^m + \mathcal{S}\,, \tag{4.50}$$

where $\mathcal{S}$ is a Dirac sheet along $\theta = \pi$, *i.e.* extended along x_1 and the negative branch of x_2

$$\mathcal{S} = -2\sqrt{2}\pi\Theta(-x_2)\delta(x_3)\delta(z)dx_3 \wedge dz\,. \tag{4.51}$$

As usual, one could choose the position of the Dirac sheet to be along any other direction, and glue the solutions up to gauge transformations.

The energy associated with the field strength (4.47) is readily checked to be divergent, due to the small-ρ behavior. This can be interpreted as the usual divergence close to the charges (electric or magnetic) in standard electromagnetism, and it is a consequence of having expanded the DBI action at quadratic order. The very same field strength (4.47) with opposite sign represents the solution corresponding to an opposite sign of the charge distribution, $dF^m = 2\sqrt{2}\pi\,\delta^3(\rho)\rho^2 d\rho \wedge \omega_2$. This corresponds to choosing an $\overline{\text{D6}}$-brane instead of a D6-brane in the stringy setup.

Step 2: solution for A^c_z

In flat space, this step is trivial, since there is no (z, y)-cigar over which we can integrate $\widetilde{F}_2$ with a finite result. However, our five-dimensional electromagnetic problem is well-defined without the $\widetilde{F}_2$ source term. Since the CS term does not enter the equations for A_z, A_{x_2}, A_{x_3}, we can just consider (4.47) as a solution of the equations (for those potentials), without the need to turn on further components in directions x_2, x_3, z.

Step 3: solution for $A_\pm$

Even if the equations do not force us to do it, we can switch on the components $A_\pm(x_\pm, \rho)$ of the gauge field. The equations read

$$\frac{1}{g_5^2} d\star F = N F \wedge F\,, \tag{4.52}$$

where the five-dimensional coupling constant is in this case $g_5^2 = 1/(8\pi^2\kappa)$. Considering the solution for $F_{\theta\phi}$ (4.47) in the CS term, the equations of motion for $A_\pm(x_\pm, \rho)$ reduce to

$$\partial_\rho(\rho^2\partial_\rho A_\pm) = \mp g_5^2 N \partial_\rho A_\pm\,, \tag{4.53}$$

with the solutions

$$\partial_\rho A_\pm = c(x_\pm)\frac{e^{\pm\frac{g_5^2 N}{\rho}}}{\rho^2}\,. \tag{4.54}$$

Here we have included a possible arbitrary function $c(x_\pm)$.[7] Since $g_5^2 N \sim 1/(\lambda M_{KK})$, the exponential behavior of the solution, due to the CS term, sets in for radii smaller than $\rho \sim 1/(\lambda M_{KK})$, that is very close to the source (since $\lambda \gg 1$).

Now we can note two interesting facts. First, only one of the two modes, A_-,[8] is normalizable. Second, if we just keep the normalizable mode, *i.e.* as long as we do not switch on both components $F_{\rho -}$ and $F_{\rho +}$ in (4.54), it has zero energy: it is tempting to read this as an indication that the mode $c(x_\pm)$ has zero potential. These properties seem to suggest that the functions $c(x_\pm)$ could be related to the chiral edge modes expected to be present on the boundary of the sheet: they are only left or right moving and have zero Hamiltonian.

4.3.2 Solution on curved space

In this section, we report on the main result of this chapter, that is, the solution for the semi-infinite sheet on the curved background (4.34). For simplicity, we just consider the massless-quark case.

Let us recall that the boundary of the sheet extends along t, x_1, while the sheet itself is placed at $z = x_3 = 0$ and extends along $x_2 \geq 0$ up to the boundary at $x_2 = 0$, see figure 4.4. The configuration without the sheet has translational invariance along x_1 and axial symmetry around the boundary, so we can use polar coordinates

$$x_2 = r\cos\psi\,, \qquad x_3 = r\sin\psi\,, \tag{4.55}$$

where $\psi \in [0, 2\pi)$. In terms of these coordinates, the effective five-dimensional background metric reads

$$ds^2 = k^{2/3}(z)(4dx_+dx_- + dr^2 + r^2 d\psi^2) + \frac{dz^2}{k^{2/3}(z)}\,. \tag{4.56}$$

The ansatz we put forward is such that:

- all the fields are independent on $x_\pm$ (eventually apart from the field $A_\pm$ which can depend on $x_\pm$ through the function $c(x^\pm)$);
- the field strength has the components

$$F_{x_2 z}\,, \quad F_{x_3 z}\,, \quad F_{x_2 x_3}\,, \quad F_{\pm z}\,, \quad F_{\pm x_2}\,, \quad F_{\pm x_3}\,. \tag{4.57}$$

  Thus, the non-vanishing CS terms have components

$$F_{x_2 z}F_{\pm x_3}\,, \quad F_{x_3 z}F_{\pm x_2}\,, \quad F_{x_2 x_3}F_{\pm z}\,, \tag{4.58}$$

  and all of them enter just the equation for $A_\pm$.

The ansatz is consistent with the equations of motion and Bianchi identity (4.33). We proceed to solve them in three steps as explained above.

[7]Note that the component F_{+-} of the gauge field strength would mix the equations among each other, so we are keeping it off.

[8]The fact that A_- is normalizable depends on the sign choice of the magnetic source, *i.e.* on whether we consider a D6 or an $\overline{\text{D6}}$-brane in the string setup.

The vortex string

The goal of this section is to find a solution F^m of the Bianchi equation (4.33) such that $d{\star}F^m = 0$ on the background (4.56). In this section, the only non-zero field strength components will be $F_{x_2z}, F_{x_3z}, F_{x_2x_3}$. The configuration is less symmetric than in flat space, so we are not able to write a compact solution. However, we can expand the fields on an orthonormal basis of eigenfunctions depending only on z, and find the corresponding modes.

We start by writing an ansatz which solves automatically the equation of motion $d{\star}F^m = 0$, which reads

$$F^m_{x_2z} = -\frac{\partial_{x_3}H}{k(z)}\,, \qquad F^m_{x_3z} = \frac{\partial_{x_2}H}{k(z)}\,, \qquad F^m_{x_2x_3} = k^{1/3}(z)\,\partial_z H\,, \tag{4.59}$$

where we recall that $k(z) = 1 + z^2$. Employing the polar symmetry on the plane transverse to the sheet, we can rewrite the monopole field strength as

$$F^m = d\psi \wedge \left[r\,\frac{\partial_r H}{k(z)} dz - k^{1/3}(z)\, r\, \partial_z H dr \right]. \tag{4.60}$$

The function $H = H(x_2, x_3, z)$ is determined by the Bianchi equation (4.33), which, with the ansatz above, reads

$$k^{-1}(z)(\partial^2_{x_2} + \partial^2_{x_3})H + \partial_z(k^{1/3}(z)\,\partial_z H) = -2\sqrt{2}\pi\delta(x_2)\delta(x_3)\delta(z - Z)\,, \tag{4.61}$$

where Z is a (possibly pseudo-) modulus for the position of the string in the z direction. Here we consider just the classical configuration taking $Z = 0$ at the end, but we should remind that, eventually, Z should become a time-dependent operator at the quantum level [28]. Taking inspiration from similar equations in [28], we search for a solution in the form

$$H(x_2, x_3, z) = \sum_{n=0}^{\infty} Y_n(r)\zeta_n(z)\zeta_n(Z)\,, \tag{4.62}$$

where we employed polar symmetry, and we have set to zero, without loss of generality, the modulus R[9] in the argument of the modes $Y_n(r - R)$. Equation (4.61) is equivalent to the infinite set of equations

$$(\partial^2_{x_2} + \partial^2_{x_3} - \lambda_n)Y_n = -2\sqrt{2}\pi\delta(x_2)\delta(x_3)\,, \tag{4.63}$$

$$k(z)\partial_z(k^{1/3}(z)\partial_z\zeta_n) + \lambda_n\zeta_n = 0\,, \tag{4.64}$$

supported by the completeness condition

$$\sum_{n=0}^{\infty} \frac{\zeta_n(z)\zeta_n(Z)}{k(z)} = \delta(z - Z)\,, \tag{4.65}$$

[9]The modulus R is defined as $R = \sqrt{X_2^2 + X_3^2}$, where the moduli X_2 and X_3 together with the pseudo-modulus Z represent the center of mass collective coordinates of the vortex string. We expect X_2 and X_3 to be true moduli of the vortex string, unlike Z, since there is a potential term depending on z due to the warp factor.

satisfied by the functions $\zeta_n(z)$ with orthonormality condition given by

$$\int_{-\infty}^{+\infty} dz \, \frac{\zeta_n(z)\zeta_m(z)}{k(z)} = \delta_{nm} \, . \tag{4.66}$$

As long as $\lambda_n \neq 0$, the first set of equations (4.63) has solutions in terms of the modified Bessel function of order zero of the second kind[10]

$$Y_n(r) = \sqrt{2}\, K_0(\sqrt{\lambda_n}\, r) \, , \qquad n > 0 \, . \tag{4.67}$$

They behave as logarithms at small r, while they fall off exponentially fast at large r. For $\lambda_0 \equiv 0$ the solution of (4.63) is just the logarithm function

$$Y_0(r) = -\sqrt{2} \log{(r)} \, , \qquad n = 0 \, . \tag{4.68}$$

We have chosen to set to zero the constant solution, since the ansatz (4.59) only contains derivatives of H.

We have numerically solved the second set of equations (4.64), determining the eigenvalues λ_n, by requiring that the derivatives of the functions $\zeta_n(z)$ vanish at $z \to \pm\infty$ for $n > 0$, so that they are orthogonal to the even part of the zero-mode, which is just a constant, $\zeta_0 = 1/\sqrt{\pi}$. The masses of the first even modes computed from (4.64) are then

$$\lambda_n = 0, 1.6, 4.6, 9.2, 15.2, 22.8, 31.8, \ldots \tag{4.69}$$

We have checked that the numerical solutions form a complete set according to (4.65).

Notice that since the functions ζ_n have definite parity, so that $\zeta_n(Z = 0) = 0$ for odd parity, classically the function H is even in z. A plot of the resulting solution for H is reported in figure 4.5.

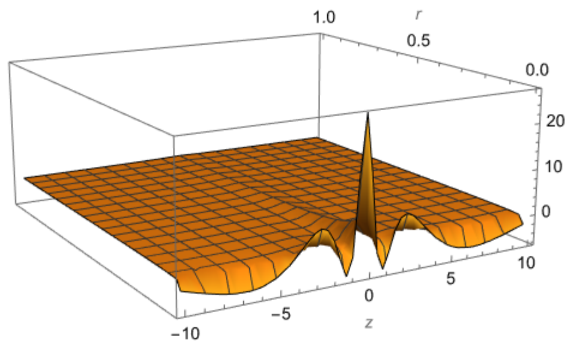

Figure 4.5. The function $H(r, z)$ obtained from the first six (even) modes in (4.62).

It can be checked numerically that with such a solution in (4.60), one has the correct magnetic charge coming from (4.33)

$$\int_{M_3} dF^m = \int_{M_2} F^m = -2\sqrt{2}\pi \, , \tag{4.70}$$

[10]Remember that we are working in units where $M_{KK} = 1$. The correct dimensionalities can be obtained by reinserting the appropriate powers of M_{KK} in these formulas.

where M_3, M_2 are three- and two-dimensional closed surfaces containing the point $r = z = 0$, $M_2 = \partial M_3$ being the boundary of M_3.[11]

We can choose to express the solution in terms of the potentials

$$A_z^m = \psi\, r\, \frac{\partial_r H}{k(z)}\,, \qquad A_r^m = -\psi\, r\, k^{1/3}(z)\partial_z H\,. \tag{4.71}$$

This corresponds to choosing the Dirac sheet $\mathcal{S}$, defined by the equation

$$dA^m = F^m + \mathcal{S}\,, \tag{4.72}$$

to be placed along x_1 and the negative x_2 direction

$$\mathcal{S} = -2\sqrt{2}\pi\Theta(-x_2)\delta(x_3)\delta(z)dx_3 \wedge dz\,. \tag{4.73}$$

We can see explicitly the stringy nature of the solution by plugging formulas (4.60), (4.62) into the quadratic D8-brane action and integrating in z, obtaining the four-dimensional effective action for the vortex string

$$S_{\mathrm{D8}} = -\frac{1}{2}\sum_{n=0}^{\infty}\int d^4x \left[(\partial_r \widetilde{Y}_n(r,\psi))^2 + \lambda_n(\widetilde{Y}_n(r,\psi))^2\right]\,, \tag{4.74}$$

where we defined

$$\widetilde{Y}_n \equiv \sqrt{\kappa}\,\zeta_n(0)Y_n\,. \tag{4.75}$$

As we can see, we have an infinite tower of massive modes depending only on the two coordinates x_2, x_3 transverse to the string (with dynamics only in the radial direction), plus a massless zero-mode.

Putting the Lagrangian density in (4.74) on-shell on the solutions (4.67) and integrating in r, ψ, one can derive the tension of the vortex string (re-inserting the M_{KK} factors)

$$T_{\mathrm{vortex}} = M_{KK}^2 \frac{\lambda N}{108\pi^3}\int_0^{\infty} dr \left\{\frac{1}{r} + \pi r \sum_{n=1}^{\infty}\zeta_n(0)^2\lambda_n\left[K_0^2(\sqrt{\lambda_n}r) + K_1^2(\sqrt{\lambda_n}r)\right]\right\}. \tag{4.76}$$

As expected [41, 42, 44, 38], this scales linearly with N and is divergent at the location $r = 0$ of the string. One has to remember that the solution is derived under the hypothesis that the field strength is small in order to consider only the first term in the expansion of the square root of the DBI action. Thus, the solution we found cannot be trusted close to the source, where the divergence is expected to be avoided in the full DBI setup.

On the other hand, we do know that the core of the string is made by the boundary of the D6-brane on the D8-brane, and that it has the width (4.8)

$$\delta_{\mathrm{vortex,hard}} \sim \frac{1}{\lambda^{1/2}\Lambda}\,. \tag{4.77}$$

This can thus be reasonably used to cut off the integral (4.76) at small r.

[11] Numerically, we used spheres of different radii to perform the check.

There is also a divergence of (4.76) at large distances, due to the zero mode. This divergence is typical of U(1) global strings in the context of topological defects [146], as it will be explained in section 5.1, and it is expected that a natural cutoff exists in the system. This analogy is one of the reasons that motivated the works [1, 5], and they will be discussed in the chapter 5.

Calling R_c the long distance cut-off, one obtains the estimate for the tension of the "soft" shell of the string as

$$T_{\text{vortex,soft}} \sim \Lambda^2 \lambda N \log\left(R_c/\delta_{\text{vortex,hard}}\right) \sim \Lambda^2 \lambda N \log\left(\lambda^{1/2} R_c \Lambda\right), \tag{4.78}$$

while the "hard" core of the strings, coming from the D6-brane, has tension

$$T_{\text{vortex,hard}} \sim \Lambda^2 \lambda^{3/2} N \,. \tag{4.79}$$

This corresponds to considering the boundary of the sheet to have radius $\delta_{\text{vortex,hard}}$ (4.77), which is a reasonable definition in the antipodal D8-brane configuration we are considering.

Finally, the logarithmic behavior of the zero mode means that the soft shell of the string is very spread in space, so that it is not meaningful to identify a thickness different from the above-mentioned large-distance cut-off and

$$\delta_{\text{vortex,soft}} \sim R_c \,. \tag{4.80}$$

The above estimates are summarized in the table 4.3.

Core tension $T_{\text{vortex,hard}}$	$\lambda^{3/2} N \Lambda^2$
Core thickness $\delta_{\text{vortex,hard}}$	$\lambda^{-1/2}\Lambda^{-1}$
Shell tension $T_{\text{vortex,soft}}$	$\lambda \log\left(\lambda^{1/2}\Lambda\, R_c\right) N \Lambda^2$
Shell thickness $\delta_{\text{vortex,soft}}$	R_c

Table 4.3. Summary of parametric dependence of tension and thickness of the core and shell parts of the vortex string. For the reader's convenience, we used the dynamical scale notation Λ instead of M_{KK}. R_c is the large-distance cut-off.

The sheet

In this section, we work out the solution of the equation of motion for the closed part A_z^c of A_z, including the source from $\widetilde{F}_2$.

Let us begin by computing the term in $\widetilde{F}_2$. With the choice of Dirac sheet as in (4.73) we can write

$$\widetilde{F}_2 = \left[\frac{1}{\sqrt{2}}(A^m + A^c) + 2\pi\Theta(x_3)\delta(z)dz\right] \wedge \delta(y)dy \,. \tag{4.81}$$

The integral of $\widetilde{F}_2$ on the cigar gives

$$\int_{\text{cigar}} \widetilde{F}_2 = 2\pi\Theta(x_3) + \frac{1}{\sqrt{2}} \int (A_z^m + A_z^c)dz \,. \tag{4.82}$$

As before, this gives a source term in the equation for A_z^c of the form

$$-\frac{\chi_g}{2}\left[2\pi\Theta(x_3)+\frac{1}{\sqrt{2}}\int(A_z^m+A_z^c)dz\right]^2 . \tag{4.83}$$

Note that we know the explicit form of A_z^m, and so its integral, from (4.71).

The z-dependence of the field A_z^c can be dealt with the ansatz (4.16)

$$A_z^c=-\frac{\sqrt{2}}{\pi\, k(z)}\phi(x_2,x_3)\,. \tag{4.84}$$

Its equation of motion reduces to an equation for $\phi(x_2,x_3)$

$$(\partial_{x_2}^2+\partial_{x_3}^2)\phi-m_{\rm WV}^2\left(\phi-\frac{1}{\sqrt{2}}\int A_z^m dz-2\pi\Theta(x_3)\right)=0\,. \tag{4.85}$$

It is straightforward to integrate numerically this equation. The sum of the solution and the integral of A_z^m gives the profile of the η' field

$$-\frac{\sqrt{2}}{f_\pi}\eta'=\left(\phi(x_2,x_3)-\frac{1}{\sqrt{2}}\int A_z^m dz\right)\,. \tag{4.86}$$

We impose the boundary conditions $\eta'(x_2,-\infty)=0$ (trivial vacuum on one side of the sheet), $\eta'(\infty,x_3)=\eta'_\infty(x_3)$, where $\eta'_\infty(x_3)$ is the profile found in section 4.2.2 for the infinite sheet. We plot this field in figure 4.6. While for $x_2>0$ the profile resembles that of the infinite sheet by construction, for $x_2<0$ it is visible the discontinuity due to the Dirac sheet, enforcing the monodromy of the η' field around the D6-brane wall (whose boundary is at $x_2=x_3=0$ in Minkowski).

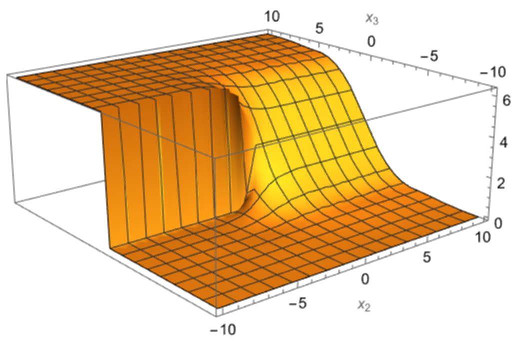

Figure 4.6. The profile of $-\frac{\sqrt{2}}{f_\pi}\eta'$ for $m_{WV}/M_{KK}=0.3$.

As usual, the solution induces a D6-brane charge on the D8-brane, which we can calculate in terms of the flux of F_{x_3z}, obtaining

$$\int dx_3dz\,F_{x_3z}=\int dz\,A_z|_{x_3=-\infty}^{x_3=+\infty}-\int dx_3dz\,\mathcal{S}_{x_3z}=-2\sqrt{2}\pi\,\Theta(x_2)\,, \tag{4.87}$$

where $\mathcal{S}$ is the Dirac sheet in formula (4.73). The result is that there is a unit $\overline{\text{D6}}$-brane charge induced only for $x_2>0$, where the sheet is located. Once again, the condition (4.3) accounting for the cancellation of the total D6-brane charge in the setup is satisfied. The parametric dependence of the tension and thickness of the sheet are the same as in the infinite sheet case, see table 4.2.

The effective action for the system of the vortex string and the sheet can be derived from the total D8-brane action (the Maxwell term plus the $\widetilde{F}_2$ action), considering that the complete field strength reads

$$F_{x_2x_3} = k^{1/3}(z)\,\partial_z H\,, \tag{4.88}$$

$$F_{x_2z} = -k^{-1}(z)\left[\partial_{x_3}H + \frac{\sqrt{2}}{\pi}\partial_{x_2}\phi\right]\,, \tag{4.89}$$

$$F_{x_3z} = k^{-1}(z)\left[\partial_{x_2}H - \frac{\sqrt{2}}{\pi}\partial_{x_3}\phi\right]\,. \tag{4.90}$$

By means of formula (4.62) and integrating in z, the effective action is

$$S_{\text{eff}} = -\frac{1}{2}\int d^4x\Bigg\{\sum_{n=0}^{\infty}\left[(\partial_r\widetilde{Y}_n)^2 + \lambda_n(\widetilde{Y}_n)^2\right] + \left[(\partial_{x_2}\widetilde{\phi})^2 + (\partial_{x_3}\widetilde{\phi})^2\right] + \chi_g\left[\sqrt{\frac{\pi}{2\kappa}}\widetilde{\phi} - \frac{1}{\sqrt{2}}\int A_z^m dz - 2\pi\Theta(x_3)\right]^2\Bigg\}\,, \tag{4.91}$$

where we defined

$$\widetilde{Y}_n \equiv \sqrt{\kappa}\,\zeta_n(0)Y_n\,, \qquad \widetilde{\phi} \equiv \sqrt{\frac{2\kappa}{\pi}}\phi\,. \tag{4.92}$$

The action (4.91) is that for a string configuration (the part in $\widetilde{Y}_n$) and a membrane (the part in ϕ) with a non-trivial potential.

This action must be used with caution. In fact, while it gives the correct equation of motion for $\widetilde{\phi}$, it does not provide the correct equations for the $\widetilde{Y}_n$. This is because of the coupling term between the $\widetilde{Y}_n$ in $\int A_z^m$ and the $\widetilde{\phi}$ in the second line of (4.91), which must be dropped by hand from the equations for the $\widetilde{Y}_n$. Ultimately, the reason for this resides in the fact that the $\widetilde{Y}_n$ and $\widetilde{\phi}$ are both modes of the same gauge field in five dimensions. We chose to solve the equation of motion of the latter by enforcing the extra constraint $d\star F^m = 0$ on the monopole-like part of the solution (which is written in terms of the $\widetilde{Y}_n$). The latter constraint is not included in (4.91) and amounts to dropping the coupling term between the $\widetilde{Y}_n$ and the $\widetilde{\phi}$ in the equations of motion of the $\widetilde{Y}_n$, as stated above.

In any case, we made an extra check that the configuration we found in two steps, first solving for F^m enforcing the constraint $d\star F^m = 0$, and then solving for the rest of F, satisfies the complete equation of motion for the five-dimensional gauge field.

The charged mode

In this section, we solve for the components $A_\pm$ of the D8-brane gauge field. Their equations of motion reduce to

$$\partial_z\left(k(z)\partial_z A_\pm\right)+\frac{1}{k^{1/3}(z)}\left(\partial_{x_3}^2+\partial_{x_2}^2\right)A_\pm\pm\frac{N}{16\pi^2\kappa}\Big[k^{1/3}(z)\partial_z A_\pm\partial_z H+$$
$$+\frac{\partial_{x_2}A_\pm}{k(z)}\left(\partial_{x_2}H-\frac{\sqrt{2}}{\pi}\partial_{x_3}\phi\right)+\frac{\partial_{x_3}A_\pm}{k(z)}\left(\partial_{x_3}H+\frac{\sqrt{2}}{\pi}\partial_{x_2}\phi\right)\Big]=0\,. \tag{4.93}$$

Since the only unknowns in these equations are $A_\pm$, one can find them either numerically or employing the basis $\zeta_n(z)$ to reduce them to a set of equations in just the x_2, x_3 variables. In any case, the solutions can be multiplied by a generic function $c(x_\pm)$, as in the flat space case. The associated energy is zero as long as there is just one of the two components $F_{\pm M}$ turned on ($M = x_\mp, x_2, x_3, z$). Again, this mode could be related to the chiral edge mode expected on the border of the sheet.

In fact, one can argue without solving equation (4.93) that only one of the two modes $A_\pm$ is normalizable. The reason is that the equation simplifies drastically close to the string at $z \sim x_2 \sim x_3 \sim 0$. It can be checked that it reduces to the flat space one (4.53), with the two solutions (4.54), only one of which (A_-) is normalizable at the origin. Thus, there is only a left-moving or a right-moving normalizable mode.

One can derive an explicit numerical solution for this mode given particular boundary conditions. The analysis of the equation in the asymptotic regions of large z, x_2, x_3 shows that one can impose the solution to go to constant values. It is natural to choose a zero constant at large $|z|$. Another boundary condition can be imposed at $z = 0$, where equation (4.93) can be integrated numerically in x_2, x_3. In this case, one can impose that close to the origin the solution is the flat space one (a primitive of equation (4.54) at $z = 0$), and that at large $|x_2|, |x_3|$ it goes to a constant.[12]

With these boundary conditions, one can integrate numerically equation (4.93). Plots representing two slices of the solution at $z = 0$ (the boundary condition) and at a fixed $z > 0$ are reported in figure 4.7.

[12]This condition is the same as in flat space as well. The difference between the flat space case and the curved one (4.93) at $z = 0$ is encoded in the two terms $\partial_{x_2,x_3}\phi$. These are limited and multiplied by derivatives $\partial_{x_2,x_3}A_\pm$, so a constant boundary condition is still the most natural one.

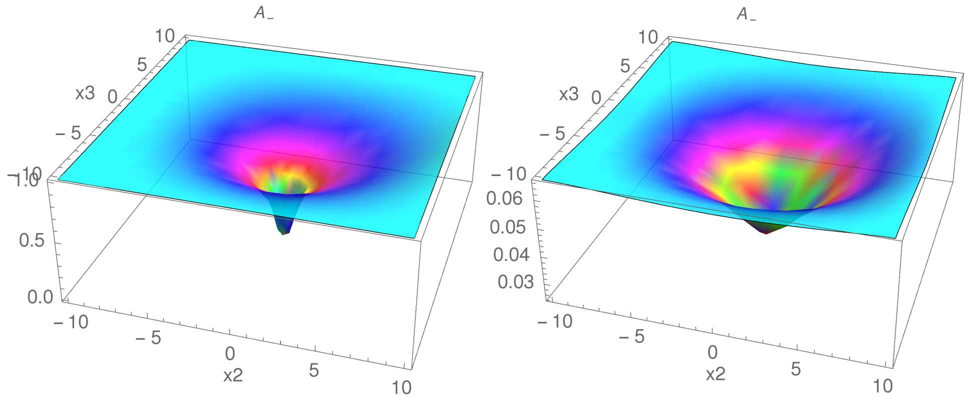

Figure 4.7. Slices of the solution for A_- at $z = 0$ (left) and $z = 5$ (right). For these plots we fixed $N/16\pi^2\kappa = 1$ and $A_-(x_2, x_3, 0) = 1$ at large $|x_2|, |x_3|$. The $z = 0$ slice is almost the same as in flat space. As z increases, the solution reduces in amplitude and eventually goes to zero at large z (as dictated by the boundary conditions).

Chapter 5

Cosmic topological defects from holography

In this chapter, we are going to pause our quest to find the holographic description of the Hall droplet baryon. We will instead show how the brane setup presented in the previous chapter, analyzed here in the deconfined phase of the WSS model (see section 3.3), allows us to describe the so-called *cosmic topological defects*.

Topological defects in gauge theories often arise as remnants of phase transitions in the early Universe [147, 148, 149, 150, 151, 146]. As a playground theory, consider a hidden sector composed of an SU(N) gauge theory coupled with a single massless flavor. At large-N and low energies, this theory can be effectively described by an axion,[1] which is the pseudo-Goldstone boson of the spontaneously broken axial U$(1)_A$ flavor symmetry, as it happens in Kim-Shifman-Vainshtein-Zakharov-like axionic models [95, 96]. This scenario, briefly introduced in section 1.4, and its variants have been widely studied in cosmology due to their rich phenomenological implications. In particular, the cosmological evolution of these theories often leads to the formation of various topological defects, such as cosmic strings and domain walls. A key feature of the model we consider is the presence of a residual vector U$(1)_V$ symmetry, associated with the baryonic charge of the single massless flavor.

In holographic QCD models or their dark sector analogs, these defects typically emerge from the spontaneous breaking of symmetries such as chiral or axial symmetries. In our context, the phase transition responsible for generating topological defects is closely tied to the breaking of chiral symmetry. As the Universe cools below a critical temperature, non-trivial vacuum configurations form, resulting in the creation of the above-mentioned cosmic strings and domain walls.

The WSS model, presented in chapter 3, offers a concrete holographic framework to study such topological defects. To mimic a single flavor SU(N) theory in a cosmological scenario, in this chapter, we study the $N_f = 1$ WSS model at finite temperature, in its deconfined phase (see section 3.3). This phase occurs at high temperatures, analogously to the deconfinement transitions observed in Yang-Mills theories. In this phase, the WSS model can be seen as effectively describing a

[1] This particle could also serve as a QCD axion or an ALP for the Standard Model, as explained in section 1.4. Nevertheless, in our discussion, we do not take into account interactions with the visible sector.

non-supersymmetric SU(N) dark gauge theory coupled with a dark flavor sector, where the gauge fields and flavor degrees of freedom interact in a high-temperature regime. This dark flavor sector plays a crucial role in the study of topological defects, which form when the axial symmetry is spontaneously broken. In this model, the scale of condensation of the extra flavor is set by the strongly coupled version of a non-local quartic Nambu-Jona-Lasinio interaction [145]. Thus, it can have a chiral symmetry-breaking phase in the deconfined regime. See, again, the discussion in section 3.3.

We start from section 5.1, where we will give an overview of the cosmic defects we are interested in: the axionic strings, the vortons, and the domain walls.

In [2], the straight axionic string of the WSS model in the deconfined phase was described as a probe D6-brane wrapped on a four-cycle S^4 of the background geometry. The effective four-dimensional action for this string can be derived from the DBI action of the D8-branes, whose gauge fields are sourced by the D6-brane. This construction provides a physical interpretation for the otherwise problematic short-distance divergence in the effective action of global cosmic strings: the D6-brane, acting as a hard core, regularizes the small-distance behavior of the string. We are going to show how these strings can be described from the D6-brane and the D8-brane perspective.

In a realistic cosmological scenario, axionic strings can break and form string loops. Moreover, when DWs are formed, they can end on cosmic strings. In this chapter, based on [5], these objects are studied in detail as described as probe D6-branes, wrapped on S^4, with a circular boundary on the flavor branes. In particular, it is shown that at fixed temperature, the string loop and the DW solutions are separated by a first-order transition as their size is varied.[2]

Charged string loops with an angular momentum are commonly referred to as *vortons* in the literature. In the scenario we are considering, the conserved charge is associated with the baryon symmetry $\mathrm{U}(1)_V$, and a crucial role is played by the Chern-Simons theory that lives on the world-volume of the wrapped D6-brane, introduced in chapter 4 in formula (4.1). We have already seen that this is effectively a (2+1)-dimensional $\mathrm{U}(1)_N$ CS theory, which is famously the theory that describes the bulk physics of the fractional quantum Hall effect. We postpone to chapter 6 the D6-brane description of these charged objects since it can be done systematically for various D6-brane embeddings.

Section 5.2 is devoted to studying the embeddings of the probe (uncharged) D6-brane representing axionic topological defects. First, we focus on the straight axionic string. Then, we study the string loop and DW embeddings considering a D6-brane with a circular boundary on the flavor branes. We show that these two embeddings, which are both unstable, cannot be realized for every value of the D6-brane boundary radius but are separated by a first-order phase transition. The critical radius for the transition depends on the temperature.

We also provide the effective, low-energy description of straight string, string loops, and vortons, in terms of the degrees of freedom living on the flavor branes, *i.e.* mesonic modes. We provide the four-dimensional effective action for the uncharged

[2] As we will see, these are not equilibrium configurations, so the transition is not the usual first-order phase transition between two equilibrium phases.

straight string and string loop. Then we turn on the electric potential on the flavor branes. In the case of vortons, we study the stability of the defect when charged under the baryon symmetry. The role of the vectorial $U(1)_V$ symmetry, associated with baryonic charge, is essential for the stability properties of these defects. In particular, the baryonic charge could prevent some decay mechanisms that would typically collapse the defects. This will be the content of section 5.3.

5.1 Cosmic topological defects in a nutshell

Phase transitions in the early universe are expected to lead to the spontaneous breaking of fundamental symmetries. The order parameter field responsible for the symmetry breaking (typically a scalar field acquiring a vacuum expectation value) takes values in the vacuum manifold of the theory. According to the Kibble mechanism [147], after the transition, different causally disconnected regions of space randomly settle into different vacuum states. Since the choices in separated regions are uncorrelated, when these domains meet, the order parameter cannot, in general, be smoothly interpolated between the different vacua. This mismatch implies that the field configuration is forced to remain away from the vacuum manifold along certain regions, giving rise to the so-called *topological defects*. The stability of these configurations is guaranteed by the non-trivial topology of the vacuum manifold $M = G/H$, with G the symmetry group and H its unbroken subgroup.
The type of defect depends on the homotopy group $\pi_n(M)$:

$$\begin{aligned}
\pi_0(M) \neq \emptyset \;&\Rightarrow\; \text{domain walls,}\\
\pi_1(M) \neq \emptyset \;&\Rightarrow\; \text{cosmic strings,}\\
\pi_2(M) \neq \emptyset \;&\Rightarrow\; \text{monopoles,}\\
\pi_3(M) \neq \emptyset \;&\Rightarrow\; \text{textures.}
\end{aligned}$$

Of particular importance in cosmology are *axionic strings*, their charged closed loop configurations known as *vortons*, and the *domain walls* which can be attached to strings. These defects arise naturally in theories with an axion or an axion-like particle and are of great interest for cosmology and dark matter phenomenology. In the following, we will focus on the above-mentioned topological defects. The interested reader can find out more about topological defects by looking at [146].

5.1.1 Global strings

Global strings are line-like topological defects that arise when a continuous global U(1) symmetry is spontaneously broken. A prototypical model involves a single complex scalar field ϕ with Lagrangian density

$$\mathcal{L} = \partial_\mu \phi^* \partial^\mu \phi - \frac{\lambda}{4}\Big(|\phi|^2 - \eta^2\Big)^2, \tag{5.1}$$

where η denotes the symmetry-breaking scale. Minimization of the potential shows that the vacuum manifold is given by $|\phi| = \eta$, which is topologically equivalent to S^1. Since $\pi_1(S^1) \simeq \mathbb{Z}$ is non-trivial, one expects the existence of stable string solutions classified by an integer winding number $n \in \mathbb{Z}$.

To construct such a solution, it is convenient to use cylindrical coordinates (r, φ, z) centered on the string axis. A static configuration with winding number n may be written in the form

$$\phi(r, \varphi) = f(r)\, e^{in\varphi}, \tag{5.2}$$

where the real function $f(r)$ represents the radial profile of the scalar condensate. The boundary conditions are determined by regularity and finite energy requirements: the field must vanish at the core, $f(0) = 0$, and approach the vacuum manifold far from the string, $f(r) \to \eta$ as $r \to \infty$. The characteristic size of the core is set by the inverse mass of radial fluctuations, $\delta \sim m_\phi^{-1}$, with $m_\phi = \sqrt{\lambda}\,\eta$.

The energy per unit length μ of the configuration (5.2) can be obtained by integrating the energy density over the transverse plane. Far from the core, the energy density is dominated by gradients of the Goldstone phase $\theta = n\varphi$. In this region one has $|\nabla\theta|^2 = n^2/r^2$, so that

$$\mu \simeq \int_\delta^{R_c} 2\pi r\, dr\, \frac{1}{2}\eta^2 \left(\frac{n}{r}\right)^2 = \pi n^2 \eta^2 \ln\left(\frac{R_c}{\delta}\right), \tag{5.3}$$

where R_c is an infrared cutoff, in cosmology identified with the correlation length or the horizon size.[3] Thus, the tension of a global string diverges logarithmically with system size, in contrast with local (gauge) strings whose energy is confined by gauge fields [146]. This infrared divergence is the manifestation of a long-range Goldstone boson field that mediates interactions between strings. Note that this is the behavior we found for the vortex string tension of the holographic Hall droplet sheet (4.78).

In the early universe, global strings are formed via the Kibble mechanism during the symmetry-breaking transition. Causally disconnected regions choose random values of the vacuum phase, and at their intersections, stable string configurations appear. Numerical simulations indicate that once formed, the string network evolves toward a scaling regime in which the density of long strings per Hubble volume remains approximately constant (see [152] for a recent discussion on this phenomenon). As the network evolves, long uncharged straight strings frequently intersect and reconnect, a process known as *intercommutation*. Each intercommutation event typically leads to the formation of closed loops, which then detach from the long-string network. These loops oscillate under their own tension and gradually lose energy, predominantly by emitting Goldstone bosons in the case of global strings. The continual production and decay of loops is an essential mechanism driving the network toward the scaling regime.

In the specific case of ALP models, these Goldstone quanta are ALPs themselves, and their emission from the string network represents a significant contribution to the cosmic axion population.

Vortons

A particularly interesting class of string configurations arises when charge/currents are trapped on cosmic strings. In theories where additional fermionic or bosonic

[3] Note that the small distance cutoff can only be defined inside the effective field theory (5.1), and it does not know anything about the UV completion of that theory. This limitation is overcome in the holographic model, as we have already seen in chapter 4, since the small distance cutoff is associated with the presence of an "hard core", *i.e.* the D6-brane.

fields couple to the string-forming scalar, massless modes may localize along the string core. These modes can carry conserved charges and currents, endowing the string with additional degrees of freedom. If a closed loop of superconducting string is formed, the presence of such currents can stabilize the loop against collapse, giving rise to non-trivial objects known as *vortons*.

The simplest way to see this is to consider a circular string loop of radius l carrying a conserved charge Q and current I. The energy of the loop receives two competing contributions: on the one hand, the string tension μ tends to contract the loop, producing an energy $\sim \mu\, l$; on the other hand, the momentum of charge carriers trapped on the string generates a centrifugal effect, which resists contraction. The total energy of the loop can be schematically written as

$$E(l) \simeq \mu\, l + \frac{Q^2}{l}. \tag{5.4}$$

The first term decreases with decreasing l, while the second term grows as the loop shrinks. As a consequence, the energy has a minimum at a finite equilibrium radius

$$l_{\text{stable}} \sim \frac{Q}{\sqrt{\mu}}, \tag{5.5}$$

indicating the possibility of a stable configuration. Such an equilibrium loop is what is called a vorton in the literature.

The existence and stability of vortons depend on the microphysics of the underlying theory, and it has been the focus of extensive literature, with renewed interest in recent years (see *e.g.* [151, 153, 154, 155, 156, 157, 158, 159]). These studies argue that charged fermions present on the string can exert pressure to counteract shrinking, potentially leading to stable configurations. Typically, vortons are considered charged under electromagnetic symmetry, and their decay into Standard Model particles often destabilizes them. From a cosmological perspective, the possible survival of a significant vorton population has important implications. A stable population of macroscopic[4] vortons behave like non-relativistic matter and can easily dominate the energy density of the universe if produced abundantly in the early phases of string network evolution. This can lead to stringent cosmological constraints: the absence of vorton observations today excludes large regions of parameter space in models predicting vortons. On the other hand, if vortons are only metastable, their eventual decay provides a potential source of high-energy particles or radiation, which could also be constrained observationally.

5.1.2 Domain walls

Domain walls are sheet-like topological defects that arise when a discrete symmetry is spontaneously broken. Consider a real scalar field ϕ with potential

$$V(\phi) = \frac{\lambda}{4}\left(\phi^2 - \eta^2\right)^2, \tag{5.6}$$

[4]Macroscopic vortons are intended as string loops with a radius which is not parametrically small with respect to the parameters of the theory. However, the vorton stability radius can be set to be very small. In such a case, they behave like point particles, and there is no associated cosmological problem.

which is invariant under $\phi \to -\phi$. The vacuum manifold in this case consists of two disconnected points, $\phi = \pm\eta$. Since the zero$^{\text{th}}$ homotopy group of this manifold is non-trivial, *i.e.* $\pi_0(\{\pm\eta\}) \simeq \mathbb{Z}_2$, stable domain wall solutions exist that interpolate between the two vacua.

The field configuration of a static planar wall, lying for instance in the xy-plane, depends only on the coordinate z transverse to the wall. Solving the Euler–Lagrange equation for $\phi(z)$ yields the kink solution

$$\phi(z) = \eta \tanh\left(\frac{m}{\sqrt{2}}\, z\right), \tag{5.7}$$

where $m = \sqrt{\lambda}\,\eta$ is the scalar mass. This profile smoothly interpolates from $\phi = -\eta$ at $z \to -\infty$ to $\phi = +\eta$ at $z \to +\infty$, with characteristic thickness $\delta \sim m^{-1}$. The surface energy density (or tension) of the wall σ is obtained by integrating the energy density across the profile,

$$\sigma = \int_{-\infty}^{\infty} dz \left[\frac{1}{2}\left(\frac{d\phi}{dz}\right)^2 + V(\phi)\right] = \frac{2\sqrt{2}}{3}\,\lambda^{1/2}\,\eta^3. \tag{5.8}$$

In cosmology, domain walls are produced when a discrete symmetry is broken in the early universe. Different Hubble patches choose different vacuum states, and the boundaries between regions of opposite sign of ϕ become domain walls. Networks of walls are therefore a generic outcome of such transitions. However, domain walls present a serious cosmological problem: their energy density redshifts much more slowly than radiation or matter. A frustrated domain wall network quickly comes to dominate the energy density of the universe, leading to an unacceptable cosmology unless the walls are somehow destabilized or inflated away. This is the well-known "domain wall problem" [160, 161, 148].

In the QCD axion case, the Peccei–Quinn mechanism breaks a global $U(1)_{PQ}$ symmetry, leading initially to axionic strings. At lower temperatures, non-perturbative QCD effects generate a periodic potential for the axion, as we have seen in (1.45),

$$V(a) \approx m_a^2 f_a^2 \left[1 - \cos\left(\frac{a}{f_a}\right)\right], \tag{5.9}$$

which selects discrete vacua $a = 2\pi k f_a / N_{\text{DW}}$, where k is an integer, and N_{DW} is the domain wall number determined by the color anomaly of the PQ symmetry. Each string in the network then becomes attached to N_{DW} domain walls, forming a string-wall system. The cosmological consequences depend crucially on the value of N_{DW}. For $N_{\text{DW}} = 1$, each string is attached to a single wall, and the wall bounded by string quickly collapses and decays, producing axions. For $N_{\text{DW}} > 1$, however, strings are attached to multiple walls, leading to a stable and long-lived network which inevitably dominates the universe, unless explicitly broken by small PQ-violating operators. Thus, viable QCD axion models typically require $N_{\text{DW}} = 1$ or an equivalent mechanism to avoid the domain wall problem.

As we have seen in 1.4, axion-like particles are pseudo-Nambu-Goldstone bosons arising from the breaking of global U(1) symmetries not tied to QCD. Their potential behaves as the QCD one (5.9), and is generated by higher-energy explicit breaking effects. The vacuum structure is then $a = 2\pi k f_a / N_{\text{DW}}$, with N_{DW} determined by the structure of the breaking operator. As for the QCD axion, phenomenological ALP scenarios typically enforce $N_{\mathrm{DW}} = 1$ to remain cosmologically viable.

Domain walls therefore occupy a central role in the cosmology of axions and other theories with discrete symmetry breaking. They not only constrain model building through the requirement of a consistent late-time cosmology, but also act as efficient sources of axion radiation during their decay, contributing significantly to the relic axion abundance.

In our holographic construction, the condition $N_{\mathrm{DW}} = 1$ is automatically realized as it happens in Kim-Shifman-Vainshtein-Zakharov-like ALP models. The extra flavor condenses at a scale f_a much bigger than the confinement scale due to *e.g.* quartic Nambu-Jona-Lasinio-like interactions or some other mechanism preserving $N_{\mathrm{DW}} = 1$.

5.2 D6-brane description of the defects

In this section, we study the various D6-brane embeddings that could holographically describe axionic topological defects, such as the straight axionic string, the axionic string loop, and the axionic DW. In the usual cosmological scenarios, the axionic DWs arise in the confined phase of a QCD-like theory, around the confinement/deconfinement transition, and they are not present at higher temperatures. In our model, DWs can be formed earlier, leading to a novel cosmological feature that can have interesting phenomenological consequences. In particular, DWs charged under the baryon symmetry can form in the early Universe and be (meta)stable, leading to new candidates of dark matter, recently predicted in [2] as *axionic-baryons* (a-baryons).

We will start by presenting the D6-brane embedding associated with the straight axionic string [2]; then, we will study the D6-brane embeddings that describe the axionic string loop and the axionic DW [5]. Surprisingly, these last two embeddings cannot always be realized, but there is a first-order phase transition between the two depending on the radius of the string loop/DW at the tip of the U-shaped D8-branes. As far as we know, this phase transition has not been investigated in the literature.

We have already introduced in chapter 4 the presence of a D6-brane wrapped on the background S^4 of the Witten background. A key feature of this object is the presence of a $\mathrm{U}(1)_N$ Chern-Simons theory on its world-volume. This comes from the CS term of the D6-brane, which does not depend on the specific background metric we are considering

$$\frac{1}{8\pi^2}\int C_3 \wedge da \wedge da = \frac{1}{8\pi^2}\int F_4 \wedge a \wedge da = \frac{N}{4\pi}\int a \wedge da\,, \tag{5.10}$$

where a is the D6-brane gauge field and we have used $\int_{S^4} F_4 = 2\pi N$.[5]

In this section of the chapter, we will turn off the D6-brane gauge field. This will correspond to describing uncharged topological defects. As already said in the introduction to this chapter, the charged version of these topological defects will be studied in detail in chapter 6.

[5]As in the previous chapter, we neglect the boundary term in the integration by parts.

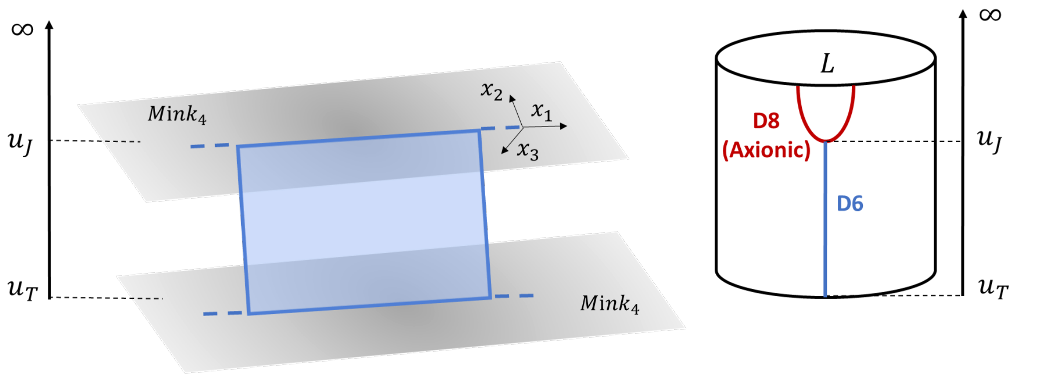

Figure 5.1. The D6-brane embedding for the straight axionic string is presented from the Minkowski space point of view (left) and in the (x_4, u) cylinder sub-space (right). The D6-brane is attached to the D8-brane tip and it ends on the horizon.

5.2.1 Straight axionic string embedding

The straight axionic string can be described holographically by a D6-brane wrapping S^4, attached to the tip of the U-shaped D8-brane, ending on the black-hole horizon. In analogy with the Hall droplet sheet, this represents the "hard core" of the axionic string. The D6-brane is also extended along, say, the x_1-coordinate of Minkowski space. See figure 5.1 for a pictorial representation. The D6-brane, in general, could have a non-trivial profile say in the (x_2, u)-plane[6] and it is described by the embedding function $x_2 = x = x(u)$. The induced metric on the D6-brane reads

$$ds^2_{\text{D6}} = \left(\frac{u}{R}\right)^{3/2}\left[-f_T(u)dt^2 + dx_1^2 + \left(x'(u)^2 + \left(\frac{R}{u}\right)^3 \frac{1}{f_T(u)}\right)du^2\right] + R^{3/2}u^{1/2}d\Omega_4^2\,,$$

where $x'(u) = dx/du$. The DBI action for the D6-brane with the world-volume gauge field switched off is

$$\begin{aligned} S^{\text{DBI}}_{\text{D6}} &= -\frac{T_6 V_4 R^3 V_{x_1}}{g_s}\int dtdu\, u\sqrt{1+\left(\frac{u}{R}\right)^3 f_T(u)x'(u)^2} = V_4 V_{x_1}\int dtdu\,\mathcal{L}\,, \\ \text{where} \quad \mathcal{L} &= -\frac{T_6 R^3}{g_s}u\sqrt{1+\left(\frac{u}{R}\right)^3 f_T(u)x'(u)^2}\,. \end{aligned} \tag{5.11}$$

The Euler-Lagrange equation for the profile $x(u)$ reads

$$x''(u) + \frac{5u^3 - 2u_T^3}{2R^3 u}x'(u)^3 + \frac{4u^3 - u_T^3}{u(u^3 - u_T^3)}x'(u) = 0\,, \tag{5.12}$$

and admits $x' = 0$ as a solution. This is referred to as the straight axionic string configuration (saxs).

The tension of the straight axionic string can be easily computed as

$$S^{\text{DBI}}_{\text{D6}} = T_{\text{saxs}}\int dt\, dx_1,$$

[6] Of course, one could equivalently consider the x_3 direction or both.

In the language of chapter 4, this is the tension of the hard core of the axionic string T_{hard}. Explicitly, it reads

$$T_{\text{saxs}} = \frac{T_6 V_4 R^3}{g_s} \frac{u_J^2 - u_T^2}{2} \simeq \frac{\lambda^2 N}{3 \cdot 2^6 \pi^3} \frac{T_a^4}{M_{KK}^2 c_a^4} \left[1 - \frac{2^8 \pi^4 c_a^4}{3^4} \frac{T^4}{T_a^4} \right], \tag{5.13}$$

where

$$c_a \simeq \frac{0.154}{J_T(\tilde{b})}. \tag{5.14}$$

The tension grows as the temperature T drops towards T_c and it reaches its maximum in the supercooling regime $T \to 0$. The thickness δ_{hard} of this core is provided by the brane thickness, which is roughly the local string length scale and has its largest value at u_T, giving

$$\delta_{\text{hard}} \sim \frac{T_c^{1/2}}{\lambda^{1/2} T^{3/2}}. \tag{5.15}$$

Note that the (inverse) thickness is naturally set by the temperature scale T, rather than the scale of symmetry breaking T_a as commonly assumed in the literature for axionic strings. This is because the transverse size of the D6-brane, as seen by the theory on the boundary (where it represents the axionic string), depends on the holographic direction. Objects localized at u_J have a smaller size than objects localized at u_T. Since the string is really a brane stretched from u_J to u_T (see figure 5.1), its maximal transverse size is set at u_T, giving formula (5.15). Only its portion close to the D8-brane would have size set by u_J, giving a thickness set by the symmetry breaking scale as $\delta \sim T_c^{1/2} \lambda^{-1/2} T_a^{-3/2}$.

5.2.2 Axionic string loop & axionic domain wall embeddings

The axionic string loop and the axionic domain wall configurations correspond to two different profiles of a D6-brane, wrapped on S^4, ending with a circular boundary of radius l (say in the (x_1, x_2) plane) at the tip of the U-shaped D8-brane. The two profiles correspond to two different solutions for the embedding function $\rho = \sqrt{x_1^2 + x_2^2} = \rho(u)$ satisfying the boundary condition $l = \rho(u_J)$. The induced metric on the D6-brane now reads

$$ds_{\text{D6}}^2 = \left(\frac{u}{R}\right)^{3/2} \left[-f_T(u) dt^2 + \rho^2(u) d\psi^2 + \left(\rho'(u)^2 + \left(\frac{R}{u}\right)^3 \frac{1}{f_T(u)} \right) du^2 \right] + R^{3/2} u^{1/2} d\Omega_4^2 ,$$

where $\rho'(u) = d\rho/du$ and the (x_1, x_2) plane has been expressed in terms of polar coordinates (ρ, ψ). The DBI action then reads

$$S_{\text{D6}}^{\text{DBI}} = -C \int dt du\, \rho(u)\, u \sqrt{1 + \frac{u^3}{R^3} f_T(u) \rho'(u)^2} = -C \int dt du\, \rho(u)\, u\, D_0(u) , \tag{5.16}$$

where

$$D_0(u) = \sqrt{1 + \frac{u^3}{R^3} f_T(u) \rho'(u)^2} , \tag{5.17}$$

and

$$C \equiv \frac{T_6}{g_s} R^3 2\pi V_4 = \frac{N}{3(2\pi\alpha')^2} = \frac{1}{3\cdot 2^4\pi^2}\frac{\lambda^2 N}{M_{KK}^2 R^6}\,. \tag{5.18}$$

The Euler-Lagrange equation for $\rho(u)$ derived from the action above

$$\partial_u\left(\frac{u\,\rho(u)}{D_0(u)}\left(\frac{u}{R}\right)^3 f_T(u)\rho'(u)\right) = u\,D_0(u)\,, \tag{5.19}$$

has to be solved numerically and turns out to admit (at least) two solutions: one which describes a D6-brane that extends from $u = u_J$ to the horizon $u = u_T$ (see figure 5.2); another which gives a D6-brane profile going from u_J to some intermediate coordinate $u_E(> u_T)$ at which the configuration shrinks to zero size (see figure 5.3). The first possibility corresponds to an uncharged *axionic string loop* while the second one describes an uncharged *axionic domain wall* ending on a string loop. It is important to notice that, due to the absence of a charge which might counterbalance the tension of these objects, both configurations are, not unexpectedly, *unstable*. In fact, for both of them, it turns out that

$$\rho'(u_J) \neq 0\,, \tag{5.20}$$

which means that the D6-brane does not end orthogonally to the D8, as it would be required by the zero-force condition.[7]

As we will see, at any fixed value of $\tilde{b} = u_T/u_J$ in the chiral symmetry broken phase, the string loop configuration exists only for some $l \geq l_{\rm MIN}$, while the domain wall exists only for $l \leq l_{\rm MAX}$, where $l_{\rm MIN}, l_{\rm MAX}$ are critical values for the D6-brane radii at the tip of the U-shaped D8-brane. This suggests the possible occurrence of a "phase transition" between the two configurations.[8] As we will see, this is the case.

In order to find a numerical solution of (5.19) we adopt dimensionless coordinates, rescaling

$$\rho = L\hat{\rho}\,, \qquad u = u_J\,\hat{u}\,. \tag{5.21}$$

Dropping the hats for simplicity and using (3.118) the action can be rewritten as

$$\begin{gathered} S_{\rm D6}^{\rm DBI} = -C u_J^2 L \int dt du\, \rho(u)\, u\, \hat{D}_0(u)\,, \\ \hat{D}_0(u) \equiv \sqrt{1 + J_T(\tilde{b})^2 f_T(u) u^3 \rho'(u)^2}\,, \qquad f_T(u) = 1 - \frac{\tilde{b}^3}{u^3}\,, \end{gathered} \tag{5.22}$$

and the equation for $\rho(u)$ reads

$$J_T(\tilde{b})^2 \partial_u\left(\frac{u^4\,\rho(u)}{\hat{D}_0(u)} f_T(u)\rho'(u)\right) - u\,\hat{D}_0(u) = 0\,. \tag{5.23}$$

[7]From equation (5.19) it follows that if we impose $\rho'(u_J) = 0$, we get $\rho''(u_J) > 0$ which implies that u_J is a local minimum for the radius $\rho(u)$. This is opposite to the behavior of the unstable solutions shown in figures 5.2 and 5.3.

[8]Here and in the following we will loosely use the term "phase transition" although, properly speaking, this should be referred to transitions between phases that are stable on certain domains at equilibrium, while our uncharged configurations are unstable.

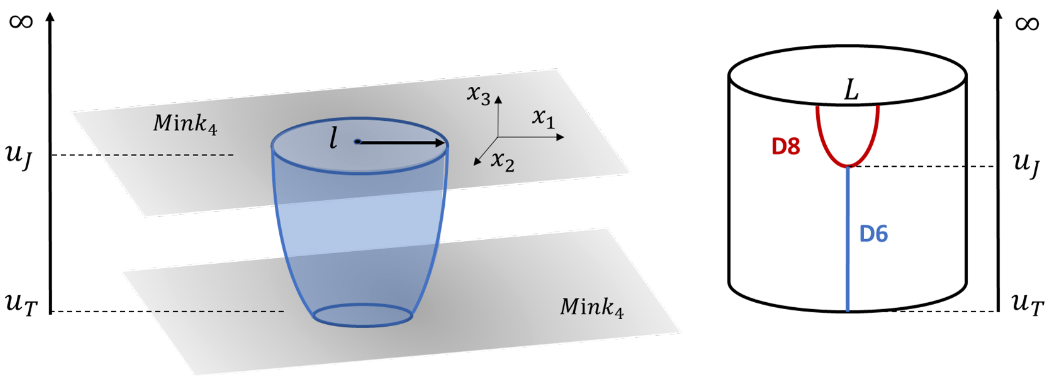

Figure 5.2. Pictorial representation of the D6-brane embedding describing holographically the axionic string loop. The D6-brane has a radius l at $u = u_J$ where it is attached to the D8-brane, while it ends on the horizon with a non-trivial profile.

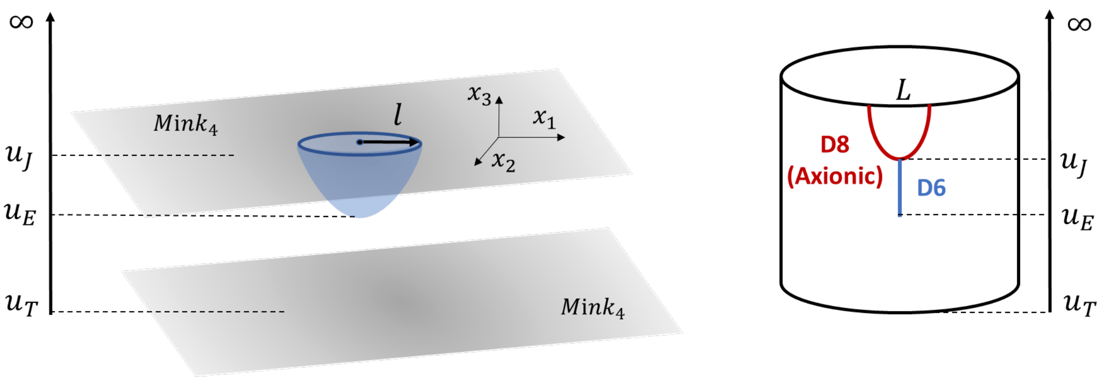

Figure 5.3. Pictorial representation of the D6-brane embedding describing the axionic domain wall ending on a string loop. The domain wall has a radius l at $u = u_J$ where it is attached to the D8-brane, and it shrinks to zero size at $u = u_E$, with $u_T < u_E < u_J$.

The free energy of a D6-brane configuration solving the above equation reads

$$E_{\rm D6} = C u_J^2 L \int_{u^*}^{1} du\, \rho(u)\, u\, \hat{D}_0(u) = \frac{\lambda^2 N}{3\cdot 2^6 \pi^2} \frac{J_T(\tilde{b})^4 T_a^3}{(0.154)^3 M_{KK}^2} \int_{u^*}^{1} du\, \rho(u)\, u\, \tilde{D}_0(u)\,. \tag{5.24}$$

The integral over u runs from $u^* = \tilde{b}$ for the string loop solution and from $u^* = u_E/u_J$ for the domain wall one.

String loop solution

Examining equation (5.23), we can immediately notice that a cylindrical-shaped string loop solution, satisfying $\rho'(u) = 0$ for every u, does not exist. This does not mean that the D6-brane cannot end at the horizon. It does, but with a non-trivial shape that we are going to determine. Since the D6-brane ends at the horizon, we must carefully choose the boundary conditions there. We use a series expansion to give initial values for the solution and its first derivative at the horizon.[9] We insert in equation (5.23) the regular expansion

$$\rho(u) = \sum_{n=0}^{N_b} c_n (u-\tilde{b})^n\,, \tag{5.25}$$

with $N_b = 6$ and we expand it around $u = \tilde{b}$. All the coefficients c_n are determined given c_0, which is the non-zero radius at the horizon. For example, the first coefficients of the expansion are

$$c_1 = \frac{1}{3\tilde{b} J_T(\tilde{b})^2 c_0}\,, \qquad c_2 = -\frac{1 + 18\tilde{b} J_T(\tilde{b})^2 c_0^2}{72\tilde{b}^4 J_T(\tilde{b})^4 c_0^3}\,, \qquad \ldots$$

This series expansion is consistent with the D6-brane entering orthogonally at the horizon. This can be better seen switching to Euclidean space: regularity of the finite temperature WSS background metric (3.115) around $u = u_T$ is immediately realized, after the condition (3.116) is imposed, by introducing the coordinate $v \sim \sqrt{u - u_T}$, which renders the metric in the sub-space (t_E, v) explicitly flat. In terms of this coordinate, the near-horizon equation for the embedding reads

$$(v - \rho(v)\rho'(v))(1 + \rho'(v)^2) = v\rho(v)\rho''(v)\,. \tag{5.26}$$

The orthogonality condition

$$\rho(v = 0) \neq 0\,, \qquad \rho'(v = 0) = 0\,, \tag{5.27}$$

is consistently realized by the series expansion (5.25).

The corresponding solution describes the string loop configuration that ends at the horizon, realizing the axionic string loop in the (3+1)-dimensional Minkowski space. A particular numerical solution with $c_0 = 1$ and $\tilde{b} = 0.1$ is presented in figure 5.4. A numerical study of the solutions leads us to observe that for each value of $\tilde{b}$, we cannot reach an arbitrarily small radius l at u_J. Therefore, the string loop configuration, at fixed $\tilde{b}$, does not exist for arbitrarily small radii l. Another

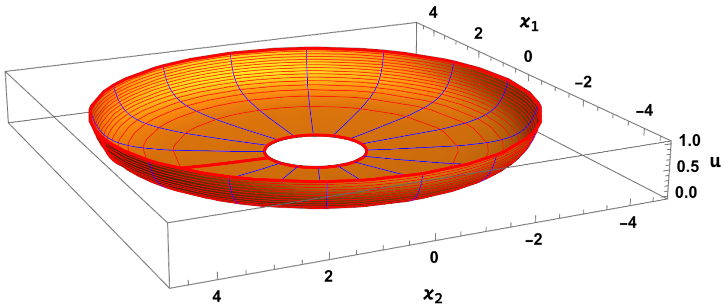

Figure 5.4. Revolution plot around the $\hat{u}$ axis of the non-trivial embedding $\rho(u)$ describing the string loop configuration, for $\tilde{b} = 0.1$ and $c_0 = 1$. The u variable runs from the horizon $\tilde{b} = 0.1$ to the D8-brane tip at $\hat{u} = 1$.

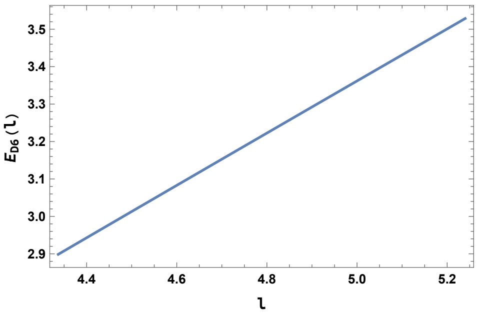

(a) Plot of the D6-brane free energy in the string loop phase for $\tilde{b} = 0.1$.

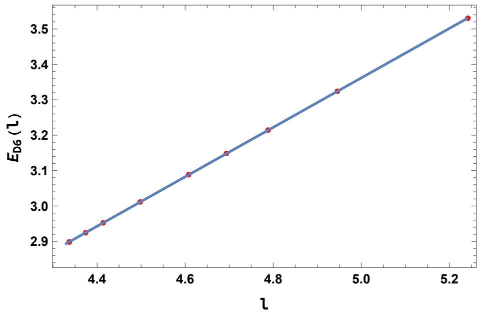

(b) The red points represent values of the D6-brane free energy for $\tilde{b} = 0.1$, while the blue line is a fit with a linear function.

Figure 5.5. Plots of the D6-brane free energy in the string loop phase as a function of l and the fit with a linear function for $\tilde{b} = 0.1$.

observation is that for large values of the radius at the horizon (c_0), the radius l is almost equal to c_0, so we have a quasi-cylinder configuration.

The free energy (5.24) of the string loop configurations at fixed $\tilde{b}$ turns out to be linear in l, as expected by the scaling of their tension with the length. This can be seen, for instance, from the plots in figures 5.5a and 5.5b, where the free energy at $\tilde{b} = 0.1$ is given in units of $Cu_J^2 L$. Figure 5.5b shows the fit of the energy with a linear function of l. Several values of the energy as a function of l (the red dots) are well approximated by the linear function $y(l) = c\, l$ with $c \approx 0.7$ for $\tilde{b} = 0.1$ (the blue line). We have checked that this linear behavior persists also for other values of $\tilde{b}$.

Sandwich defects

Before discussing the DW solution, we mention another possibility for the axionic string and string loop solutions. We have seen that the D6-brane in figures 5.1 and 5.2 has a boundary on the D8-brane and terminates at the horizon. However, the D6-brane can extend from two different flavor branes as in figure 5.6. The second

[9] In our numerics, we employ a cutoff at the horizon of $\epsilon = 10^{-4}$.

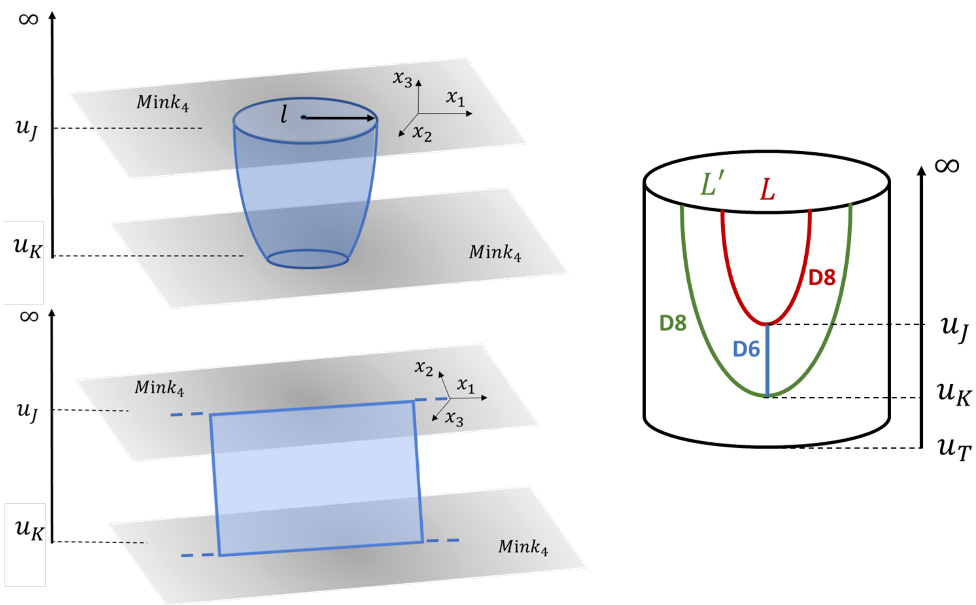

Figure 5.6. Straight axionic string and string loop configurations between two types of D8-branes. The D6-brane does not terminate at the horizon but has two boundaries attached to the two flavor branes.

flavor brane can be thought of as another dark flavor that condenses at a temperature T_a' set by u_K (the radial variable of the tip of the corresponding D8-brane), distinct from T_a. Analogously, if we consider the confined phase of the theory, the second flavor brane can represent a QCD flavor. We have such a possibility because the asymptotic separation between a D8-brane and a $\overline{\text{D8}}$-brane L, of a given flavor, is a free parameter in the model, and hence we can tune L to get the desired T_a at which the chiral symmetry is broken. This "sandwich" structure has been studied in the literature [41, 42, 162, 163], in particular between topological defects composed of the axion and the η' field, realizing composite objects of dark excitations and Standard Model excitations, leading to interactions between the two sectors.

We will come back to these sandwich defects in chapter 6 where their charged (under the baryonic $U(1)$) version will be investigated in detail in both phases of the WSS model.

Domain wall solution

The domain wall configuration is a solution of the equation of motion (5.23) with boundary conditions: $\rho(u_E/u_J) = 0$ and $\rho'(u_E/u_J) = \infty$, *i.e.* the wall closes smoothly at u_E. Notice that the equation depends only on $\tilde{b}$ so, once we have fixed it, by choosing the value of the holographic coordinate u_E, the value of the radius $l = \rho(u_J)$ is determined. A particular solution for $\tilde{b} = 0.1$ is presented in figure 5.7. For a given value of $\tilde{b}$, no matter which value of u_E we pick, the radius l will be limited from above. We cannot get arbitrarily big radii l if we want the configuration not to reach the horizon.

The free energy (5.24) of the domain wall configuration shows the following

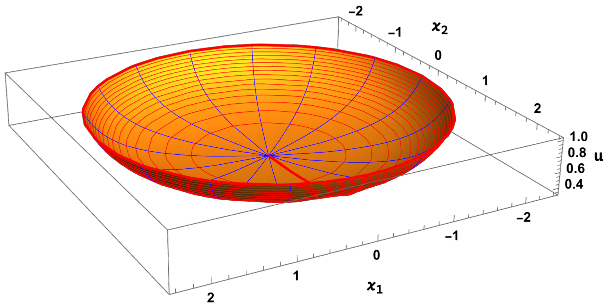

Figure 5.7. Revolution plot around the $\hat{u}$ axis of the non-trivial embedding $\hat{\rho}(\hat{u})$ describing the domain wall configuration for $\tilde{b} = 0.1$. The $\hat{u}$ coordinate runs from $u_E/u_J = 0.35$, where the D6-brane has its tip, to the D8-brane tip at $\hat{u} = 1$.

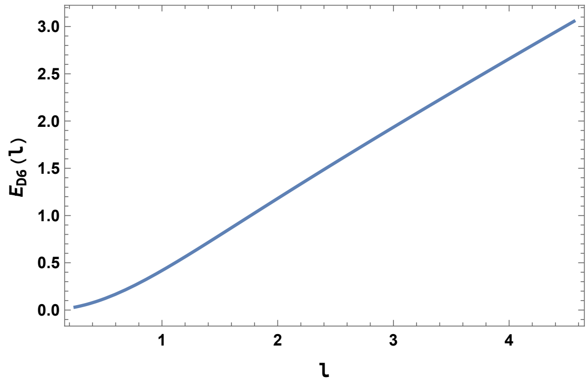

Figure 5.8. The D6-brane free energy of the domain wall configuration as a function of l is plotted for $\tilde{b} = 0.1$.

features. In figure 5.8 we examine it (in units of $Cu_J^2 L$) for $\tilde{b} = 0.1$. For large values of l, the energy scales linearly with l (as the energy of the string loop configuration), while for small l, the energy scales quadratically with l. Figure 5.9a shows the analysis of the D6-brane energy for small radii l. A fit of the energy with a second-degree polynomial is shown in figure 5.9b. We see that a set of values of the energy at a given l (the red dots) are well-approximated by the parabolic curve $p(l) = a\,l^2$ with $a \approx 0.5$ for $\tilde{b} = 0.1$ (blue line).

The reason for this behavior is that at small radii the D6-brane is close to the D8-brane and very flattened, so the energy is coming from a disk shape of almost constant tension. Instead, for large radii the D6-brane has a region where the embedding is almost vertical in the u direction (resembling a string configuration) before turning inside to close near to the horizon, where its tension is small; so its energy is dominated by its string-like portion. In other words, from the holographic QFT dual point of view, the tension of the domain wall is reduced in the region far from the string at its boundary. So at large radii, the string dominates the energy, while at small radii the DW world volume is never far from the string, the tension is never small and the whole world volume contributes to the energy.

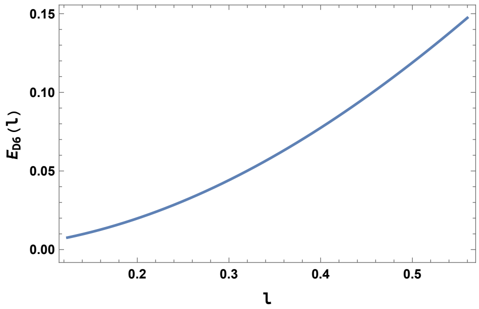

(a) Plot of the D6-brane free energy in the domain wall phase for small l and $\tilde{b} = 0.1$.

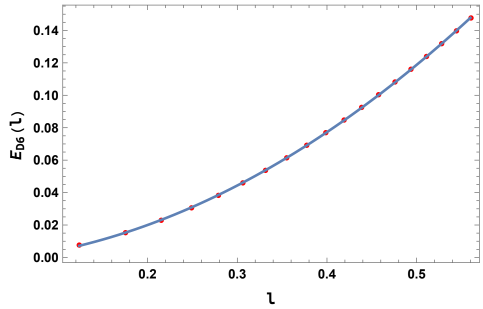

(b) The red points represent values of the D6-brane free energy for $\tilde{b} = 0.1$, while the blue line is a fit with a parabolic function.

Figure 5.9. Plots of the D6-brane free energy in the domain wall phase as a function of l and the fit with a parabolic function for small l and $\tilde{b} = 0.1$.

Analysis of the first-order phase transition

In this section, we analyze the competition between the two configurations studied above. As we said, for the string loop solution, the asymptotic radius l is limited from below, while for the domain wall, l is limited from above. We can therefore compute the minimal allowed radius for the string loop phase and the maximal allowed radius for the domain wall phase as functions of $\tilde{b}$ and compare them. The result is shown in figure 5.10 where the blue line is the minimal allowed radius for the string loop configuration $l_{\rm MIN}$, while the red line is $l_{\rm MAX}$, the maximal radius allowed for the domain wall configuration. At a given value of $\tilde{b}$, for $l < l_{\rm MIN}$ only the DW phase exists, while for $l > l_{\rm MAX}$ only the string loop one is present. Inside the yellow region, $l_{\rm MIN} < l < l_{\rm MAX}$, both phases coexist.

In the small region where the two phases compete, we can compare the free energies of the associated configurations using (5.24). The results are shown in figure 5.11. The plot in figure 5.11a shows the energy of the DW solution (in blue) and the string loop (in red) configurations. For small l the DW phase is less energetic, while for bigger values of l, the string loop phase is less energetic. Despite the difference in energy (see figure 5.11b) being very small, it shows the characteristic behavior of a first-order phase transition, whose occurrence is ubiquitous in holographic scenarios like the one presented in this work. Even if this analysis refers to the model at temperature $\tilde{b} = 0.4$, the results apply to every value of $\tilde{b}$.[10]

All in all, in the *yellow region* of figure 5.10 where both phases are allowed, we find that there is a critical radius $l_{\rm critical}$ such that for $l < l_{\rm critical}$ the DW phase dominates while for $l > l_{\rm critical}$ the string loop phase dominates over the DW one. The value of $l_{\rm critical}$ depends on $\tilde{b}$, and it is the critical value at which the system exhibits a first-order phase transition. We can compute numerically $l_{\rm critical}$ as a function of $\tilde{b}$ and the result is shown in figure 5.12a and in figure 5.12b where the critical radius is plotted together with $l_{\rm MIN}$ and $l_{\rm MAX}$.

[10] The behavior of this energy difference with the temperature is not trivial, but instead grows if $\tilde{b}$ grows.

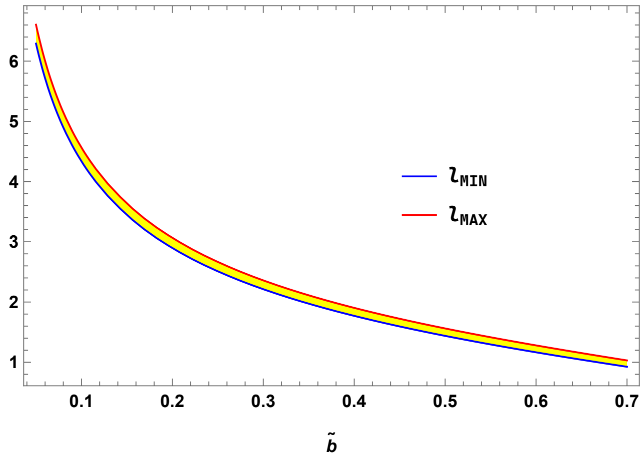

Figure 5.10. The blue line is the minimal allowed radius $l_{\rm MIN}$ for string loop configuration, while the red line is $l_{\rm MAX}$, the maximal radius allowed for the domain wall configuration. Both are functions of $\tilde{b}$. At a given value of $\tilde{b}$, for $l < l_{\rm MIN}$ only the DW phase exists, while for $l > l_{\rm MAX}$ only the string loop one is present. Inside the *yellow region*, $l_{\rm MIN} < l < l_{\rm MAX}$, both phases coexist.

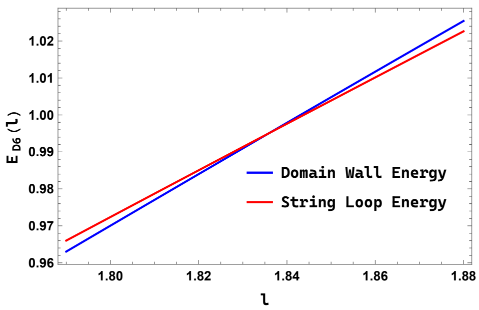

(a) Plot of the free energy of the DW (blue) and string loop (red) configurations in the range of l where both phases coexist. We analyze the model at $\tilde{b} = 0.4$.

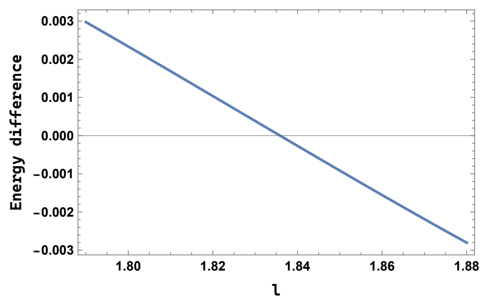

(b) Plot of the difference of free energies, $(E_{\rm D6}^{\rm string\ loop} - E_{\rm D6}^{\rm DW})(l)$ as a function of l, for $\tilde{b} = 0.4$.

Figure 5.11. Analysis and comparison of the free energy balance in the string loop and DW phases for $\tilde{b} = 0.4$.

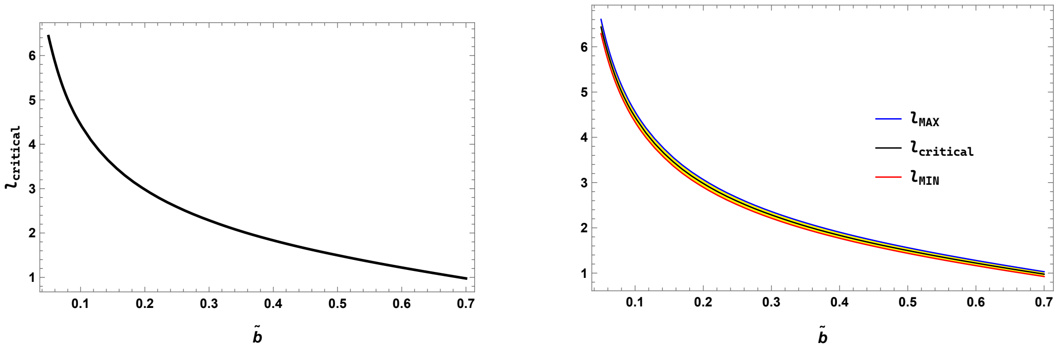

(a) Plot of l_{critical} as a function of $\tilde{b}$ with $\tilde{b} \in (0.05, 0.7)$.

(b) Plot of l_{critical}, l_{MAX} and l_{MIN} as a function of $\tilde{b}$ with $\tilde{b} \in (0.05, 0.7)$.

Figure 5.12. Plot of the critical radius as a function of $\tilde{b}$ with the comparison with l_{MAX} and l_{MIN}.

We can also describe the evolution of the system by varying $\tilde{b}$, or in other words, the temperature of the background. Given an intermediate value of l, looking at figure 5.12b, we can start, for example, at a very high temperature (we are thinking about the thermal evolution of an expanding Universe), corresponding to very high $\tilde{b}$, where only the string loop phase exists. The D6-brane cannot close off, realizing the DW configuration, because the horizon is very close to the D8-brane tip. Then, as the temperature is reduced, we enter the *yellow region*, where the DW configuration exists but the string loop phase still prevails until we reach l_{critical}. A first-order phase transition occurs, and the DW phase starts to dominate because it is energetically favored. Eventually, by lowering the temperature further, we exit the competing region, and only the DW configuration remains from now on. That is, in the thermal history of this theory, string loops produced during the chiral symmetry-breaking phase transition can survive up to the confinement phase transition only if they are very large and do not have the time to decay significantly (a phenomenon which reduces their size); in the other cases, reached a certain temperature they undergo a transition where a DW forms inside the loop.

5.3 D8-brane description of the defects

In this section, we study the charged axionic string and the charged string loop configurations, *i.e.* the vorton, from the point of view of the D8-brane world-volume theory. The latter provides the description of the strings in terms of mesonic degrees of freedom, which are dominated by the (light) axion. Using the vocabulary of the previous chapter, *i.e.* chapter 4, this constitutes the *soft shell* description of these cosmic defects as it was for the vortex string.

The analysis of the D8-D6 setup in the WSS model involves the action (3.126) and (3.127) for the U-shaped D8-branes and the action S_{C_7} for the C_7 RR form in the presence of a localized D6-brane source. We recall that the latter reads

$$S_{C_7} = -\frac{1}{4\pi}(2\pi l_s)^6 \int dC_7 \wedge \star dC_7 + \frac{1}{2\pi} \int C_7 \wedge \frac{F}{\sqrt{2}} \wedge \omega_1 + \int C_7 \wedge \omega_3 \,, \tag{5.28}$$

where F is the U(1) gauge field on the D8-brane and ω_1 and ω_3 are, respectively, the differential forms representing the D8-brane and the D6-brane embeddings in the ten-dimensional spacetime.[11]

As in the previous sections of this chapter, we consider a D6-brane which wraps the internal background S^4 and is extended along the holographic coordinate u and one Minkowski coordinate.

The equation of motion for C_7 deduced from (5.28) leads to a violation of the Bianchi identity for the D8-brane gauge field. The computation of the Bianchi identity reads the same as the one we have seen in section 4.3, so we just give the result depending on the D6-brane embedding we are considering. In particular, if, as in section 5.2.1, the boundary of the D6-brane attached to the tip of the U-shaped D8-brane is a straight line along, say, the x_1 direction, then the non-trivial Bianchi identity reads

$$dF = -2\pi\sqrt{2}\,\delta(x_2)\delta(x_3)\delta(z)dx_2 \wedge dx_3 \wedge dz\,, \tag{5.29}$$

being z the holographic coordinate as defined in the finite temperature WSS background in (3.128). This setup will be investigated in section 5.3.1. First, we will find a full solution for the uncharged axionic string following what has been done for the vortex string in 4.3. Then, we turn on an $\mathrm{U}(1)_V$ charge on the string. This corresponds to turning on an electric potential A_t on the flavor brane. In this case, we will find solutions to the equations of motion for the gauge field A in various regions of the spacetime, and then we glue them together following [165].

If the boundary of the D6-brane is, as in section 5.2.2, a circular loop of radius l in the Minkowski subspace (x_1, x_2), then the Bianchi identity becomes

$$dF = -2\pi\sqrt{2}\,\delta(\rho - l)\delta(x_3)\delta(z)d\rho \wedge dx_3 \wedge dz\,, \tag{5.30}$$

where $\rho = \sqrt{x_1^2 + x_2^2}$. We are going to focus on this setup in sections 5.3.2 and 5.3.3. For this configuration, we will study the solutions of the Maxwell-Bianchi problem for the D8-brane gauge field in various steps. First of all, we will look for a solution near the tip of the D8-brane, where the induced metric, in the subspace transverse to S^4, behaves effectively as a five-dimensional flat metric. This analysis aims to study the system with a non-zero baryon charge and to extract the stability radius l_{stable} due to Coulomb repulsion mediated by the CS term. Then we will move to the asymptotic region where we can solve exactly the equations of motion if the electric potential is turned off; in the presence of the electric potential, we will find linearized solutions following the procedure outlined in [165].

5.3.1 The straight axionic string solution

In this section, we analyze the equations of motion for the D8-brane gauge field on the curved background (3.115). The D6-brane represents a magnetic source

$$dF = -2\pi\sqrt{2}\,\delta(x_2)\delta(x_3)\delta(z)dx_2 \wedge dx_3 \wedge dz\,, \tag{5.31}$$

[11] In the deconfined phase, the contribution from the on-shell action of the C_7 RR form is zero. See [164] for details. In the confined phase, this term is not zero, and the authors considered its contribution in [1] to study a similar D6-D8-brane system.

associated with the presence of a straight axionic string in the dual QFT picture. We start by turning off the electric potential and solving exactly the Maxwell-Bianchi system in the curved background.

The symmetries of the string configuration allow us to turn on only three field strength components: $F_{x_2x_3}$, F_{x_3z}, and F_{x_3z}. The associated action for this field configuration can be easily read from (3.129)

$$S_{\rm D8}^{\rm DBI} = -\frac{3T_8V_4R^{3/2}u_J^{3/2}(2\pi\alpha')^2}{8g_s}\int d^4x\,dz\left\{\frac{k^{3/2}(z)}{|z|}\sqrt{\gamma_T(z)f_T(z)}\left[F_{x_2z}^2+F_{x_3z}^2\right]\right.$$
$$\left.+\frac{4R^3}{9u_J}\frac{|z|}{k^{5/6}(z)}\sqrt{\frac{f_T(z)}{\gamma_T(z)}}\,F_{x_2x_3}^2\right\},$$

where we have used the equation (3.128).

Following the computations of chapter 4, can employ the following ansatz for the field strength components

$$F_{x_2x_3} = \frac{9u_J}{4R^3}\frac{k^{5/6}(z)}{|z|}\sqrt{\frac{\gamma_T(z)}{f_T(z)}}\,\partial_z H_T, \tag{5.32}$$

$$F_{x_3z} = \frac{|z|}{k^{3/2}(z)}\frac{\partial_{x_2}H_T}{\sqrt{f_T(z)\gamma_T(z)}}, \tag{5.33}$$

$$F_{x_2z} = -\frac{|z|}{k^{3/2}(z)}\frac{\partial_{x_3}H_T}{\sqrt{f_T(z)\gamma_T(z)}}. \tag{5.34}$$

This ansatz solves automatically the equation of motion coming from the brane action. The Bianchi identity leads to the following differential equation for H_T

$$-2\pi\sqrt{2}\,\delta(x_2)\delta(x_3)\delta(z) = \partial_{x_2}F_{x_3z}+\partial_zF_{x_2x_3}-\partial_{x_3}F_{x_2z} =$$
$$=\frac{|z|}{k^{3/2}(z)\sqrt{f_T(z)\gamma_T(z)}}\left[\partial_{x_2}^2H_T+\partial_{x_3}^2H_T\right]+\frac{9u_J}{4R^3}\partial_z\left(\frac{k^{5/6}(z)}{|z|}\sqrt{\frac{\gamma_T(z)}{f_T(z)}}\partial_zH_T\right).$$

H_T is an unknown function which we are going to determine by imposing the Bianchi identity (5.31). This is the finite-temperature analog of the function H defined in (4.62). Following the definition (4.62) of H, we look for a solution by series such as

$$H^{(T)}(x_2,x_3,z) = \sum_{n=0}^{\infty}\zeta_n^{(T)}(0)\zeta_n^{(T)}(z)Y_n^{(T)}(x_2,x_3)\,, \tag{5.35}$$

where the center of mass moduli (X_2, X_3, Z) are taken to be zero for simplicity. Then, the Bianchi identity becomes

$$\sum_{n=0}^{\infty}\zeta_n^{(T)}(0)\left[\frac{9u_J}{4R^3}\frac{Y_n^{(T)}}{\rho}\partial_z\left(\frac{k^{5/6}(z)}{|z|}\sqrt{\frac{\gamma_T(z)}{f_T(z)}}\partial_z\zeta_n^{(T)}(z)\right)+\right.$$
$$\left.+\frac{|z|\zeta_n^{(T)}(z)}{k^{3/2}(z)\sqrt{f_T(z)\gamma_T(z)}}\left(\partial_{x_2}^2+\partial_{x_3}^2\right)Y_n^{(T)}\right] = -2\pi\sqrt{2}\,\delta(x_2)\delta(x_3)\delta(z)\,.$$

This is solved by the following infinite set of equations

$$\partial_z \left(\frac{k^{5/6}(z)}{|z|} \sqrt{\frac{\gamma_T(z)}{f_T(z)}} \partial_z \zeta_n^{(T)}(z) \right) + \frac{|z|}{k^{3/2}(z)\sqrt{f_T(z)\gamma_T(z)}} \lambda_n^{(T)} \zeta_n^{(T)}(z) = 0 \,, \tag{5.36}$$

$$\left(\partial_{x_2}^2 + \partial_{x_3}^2\right) Y_n^{(T)} - \frac{9u_J}{4R^3} Y_n^{(T)} = -2\pi\sqrt{2}\,\delta(x_2)\delta(x_3)\,, \tag{5.37}$$

supported by the completeness condition

$$\sum_{n=0}^{\infty} \frac{|z|}{k^{3/2}(z)\sqrt{f_T(z)\gamma_T(z)}} \zeta_n^{(T)}(0)\zeta_n^{(T)}(z) = \delta(z)\,, \tag{5.38}$$

satisfied by the functions ζ_n with orthonormality condition given by

$$\int_{-\infty}^{+\infty} dz \frac{|z|}{k(z)^{3/2}} \frac{\zeta_n^{(T)}(z)\zeta_m^{(T)}(z)}{\sqrt{f_T(z)\gamma_T(z)}} = \delta_{nm}\,. \tag{5.39}$$

We have numerically solved the first set of equations (5.36), determining the eigenvalues $\lambda_n^{(T)}$, by requiring that the derivatives of the functions $\zeta_n^{(T)}$ vanish at $z \to \pm\infty$ for $n > 0$, so that they are orthogonal to the even part of the zero-mode $\zeta_0^{(T)}$, which is just a constant given by

$$\zeta_0^{(T)} = \left(\int_{-\infty}^{+\infty} dz \frac{|z|}{k(z)^{3/2}} \frac{1}{\sqrt{f_T(z)\gamma_T(z)}} \right)^{-1/2}. \tag{5.40}$$

The eigenvalues of the first even modes computed at $\tilde{b} = 0.1$ from (5.36) are

$$\lambda_n^{(T)} = 0,\ 2.11,\ 6.20,\ 12.31,\ 20.43,\ 30.59,\ \ldots \tag{5.41}$$

In general, the eigenvalues $\lambda_n^{(T)}$ and the solutions $\zeta_n^{(T)}$ are the finite-temperature version of λ_n and ζ_n found in the previous chapter for the vortex string. They depend on the temperature, which is encoded in $\tilde{b}$. However, this dependence is very weak and hence the $\lambda_n^{(T)}$'s and the $\zeta_n^{(T)}$'s profile are approximately constant with $\tilde{b}$.

We have checked that the numerical solutions form a complete set according to (5.38). Notice that since the functions $\zeta_n^{(T)}$ have definite parity, so that $\zeta_n^{(T)}(Z = 0) = 0$ for odd parity, the function $H^{(T)}$ is even in z.

The solution for the modes $Y_n^{(T)}$ looks formally identical to the one for the modes Y_n at zero temperature: the differential equation for $Y_n^{(T)}$ (5.37) is the same as the differential equation for Y_n (4.63) with the replacement $\lambda_n \to \lambda_n^{(T)} 9u_J/(4R^3)$. As long as $\lambda_n^{(T)} \neq 0$, the equation (5.37) is solved by

$$Y_n^{(T)}(r) = \sqrt{2}\, K_0 \left(\sqrt{\frac{9u_J}{4R^3} \lambda_n^{(T)}}\, r \right), \qquad n > 0\,, \tag{5.42}$$

where we have introduced the radius $r = \sqrt{x_2^2 + x_3^2}$, as in chapter 4. For $\lambda_0^{(T)} \equiv 0$, the solution is again the logarithm function (4.68), where the constant solution has been set to zero.

We can now write the on-shell D8-brane action

$$
\begin{aligned}
S_{\rm D8}^{\rm DBI} &= -\frac{\kappa_J}{2}\int d^4x\,dz\left\{\frac{k^{3/2}(z)}{|z|}\sqrt{\gamma_T(z)f_T(z)}\left[F_{x_2z}^2+F_{x_3z}^2\right]+\right.\\
&\left.+\frac{4R^3}{9u_J}\frac{|z|}{k^{5/6}(z)}\sqrt{\frac{f_T(z)}{\gamma_T(z)}}F_{x_2x_3}^2\right\}=\\
&=-\frac{\kappa_J}{2}\sum_{n=0}^{\infty}\sum_{m=0}^{\infty}\zeta_n^{(T)}(0)\zeta_m^{(T)}(0)\int d^4x\,dz\left\{\frac{|z|}{k^{3/2}(z)}\frac{\zeta_n^{(T)}(z)\zeta_m^{(T)}(z)}{\sqrt{\gamma_T(z)f_T(z)}}\left(\partial_r Y_n^{(T)}\right)^2+\right.\\
&\left.+\frac{9u_J}{4R^3}\sqrt{\frac{\gamma_T(z)}{f_T(z)}}\frac{k^{5/6}(z)}{|z|}\partial_z\zeta_n^{(T)}(z)\partial_z\zeta_m^{(T)}(z)Y_n^{(T)}Y_m^{(T)}\right\}=\\
&=-\frac{\kappa_J}{2}\sum_{n=0}^{\infty}\left(\zeta_n^{(T)}(0)\right)^2\int d^4x\left\{\left(\partial_r Y_n^{(T)}\right)^2+\frac{9u_J}{4R^3}\lambda_n^{(T)}\left(Y_n^{(T)}\right)^2\right\},
\end{aligned}
$$

where we have introduced the constant

$$
\kappa_J=\frac{\lambda N}{2^6\pi^3 M_{KK}}\left(\frac{u_J}{R^3}\right)^{3/2}. \tag{5.43}
$$

We define

$$
\widetilde{Y}_n^{(T)}(r)=\sqrt{\kappa_J}\,\zeta_n^{(T)}(0)Y_n^{(T)}(r)\,, \tag{5.44}
$$

and we get the canonically normalized action

$$
S_{\rm D8}^{\rm DBI}=-\frac{1}{2}\sum_{n=0}^{\infty}\int d^4x\left\{\left(\partial_r\widetilde{Y}_n^{(T)}\right)^2+\frac{9u_J}{4R^3}\lambda_n^{(T)}\left(\widetilde{Y}_n^{(T)}\right)^2\right\}.
$$

Note that this global string effective action is rigorously derived from the fundamental theory; it is not postulated. It can be seen as the global string analog of the chiral Lagrangian coupled to an infinite tower of massive mesonic modes.

We can extract the tension of the soft part of the axionic string from the action evaluated on-shell on the solution

$$
\begin{aligned}
T_{\rm soft} \;=\; & \frac{\lambda N}{2^6\pi^3 M_{KK}}\left(\frac{u_J}{R^3}\right)^{3/2}\int_0^\infty dr\left\{\left(\zeta_0^{(T)}(0)\right)^2\frac{1}{r}+\right. \\
&\left.+r\frac{9u_J}{4R^3}\sum_{n=1}^{\infty}\left(\zeta_n^{(T)}(0)\right)^2\lambda_n^{(T)}\left[K_0^2\left(\sqrt{\frac{9u_J}{4R^3}\lambda_n}\,r\right)+K_1^2\left(\sqrt{\frac{9u_J}{4R^3}\lambda_n}\,r\right)\right]\right\}.
\end{aligned} \tag{5.45}
$$

The divergence of the tension at the location of the string ($r=0$) should be cut off by the hard core scale $\delta_{\rm hard}$ in (5.15). In fact, the quadratic effective theory on the world-volume of the D8-brane is not suitable to describe the string core. For example, the field strength diverges in that region, so that the employed approximation breaks down. However, the brane construction gives a precise description of the string core: it is the boundary of the D6-brane. It has a gluonic nature and has a thickness given in (5.15), which is thus the natural cut-off in the effective "soft" description. This is the very same behavior of the vortex string studied in chapter 4. However, in this context, it is associated with a cosmic string in a cosmological scenario described by the deconfined phase of the WSS model.

The large distance divergence is the usual one of cosmic global strings discussed in section 5.1.1. Omitting unimportant numerical factors, we get

$$T_{\text{soft}} \sim \lambda N M_{KK}^2 \log\left(R_c/\delta_{\text{hard}}\right), \tag{5.46}$$

where R_c is the large distance cut-off associated with the horizon size, while δ_{hard} is given in equation (5.15).

The charged mode

The straight axionic string can have a $\mathrm{U}(1)_V$ charged mode, described again by the D8-brane gauge field. As we already observed in chapter 4, this topological configuration for the D6-brane boundary does not allow for an Abelian instanton configuration. See discussion around formula (4.5). It is however instructive to derive an approximate solution for the gauge field components A_t (associated with the $\mathrm{U}(1)_V$ charge, *i.e.* the baryon number) and A_{x_1} that does not change the monopole-like solution found in the previous section, following the same kind of approximation employed for the baryons in [136]. First, we find a solution very close to the source, where we can neglect the curvature of the spacetime. In this region, we are able to solve the full equations of motion derived from the five-dimensional Maxwell-Chern-Simons action. As we will show, the solution is localized around the string position in the large λ-limit. As we move away from the string, we can neglect the Chern-Simons term since it is sub-leading in the $1/\lambda$ expansion. The solution in this intermediate (again flat) region matches with the expansion of the full flat-space solution far from the source. Finally, we connect the solution to the large-z region of five-dimensional space-time, where we study the linearized equations of motion.

In the flat space limit we employ the ansatz $A_t(\varrho), A_{x_1}(\varrho)$, where

$$\varrho = \sqrt{x_2^2 + x_3^2 + \omega^2}, \tag{5.47}$$

is the radius of the two-sphere around the axionic string, and the coordinate ω is related to the holographic coordinate z through the rescaling

$$\omega(z) = \sqrt{\frac{4R^3}{3u_J}} \frac{z}{\sqrt{5 - 8\tilde{b}^3}}\,. \tag{5.48}$$

Then, the induced flat metric reads

$$ds^2 = \left(\frac{u_J}{R^3}\right)^{3/2} \left(-\left(1-\tilde{b}\right)^3 dt^2 + dx_1^2 + d\varrho^2 + \varrho^2 d\Omega_2^2\right) + R^{3/2} u_J^{1/2} d\Omega_4^2, \tag{5.49}$$

where $d\Omega_2^2$ is the line element of a two-sphere. Then, we can compute the equations of motion for A_t, and A_{x_1} from the total D8-brane action, which now has a non-zero CS term (3.127)

$$\partial_\varrho(\varrho^2 \partial_\varrho A_t) - \sigma\sqrt{1-\tilde{b}^3}\,\partial_\varrho A_{x_1} = 0\,, \tag{5.50}$$

$$\partial_\varrho(\varrho^2 \partial_\varrho A_{x_1}) - \frac{\sigma}{\sqrt{1-\tilde{b}^3}} \partial_\varrho A_t = 0\,, \tag{5.51}$$

where

$$\sigma \equiv \frac{3\pi\, M_{KK}}{\sqrt{2}\,\lambda}\frac{R^3}{u_J}. \tag{5.52}$$

They can be integrated analytically, neglecting the divergent solution in $\varrho = 0$ and a constant term, to get

$$A_t(\varrho) = c\sqrt{1-\tilde{b}^3}\, e^{-\sigma/\varrho}\,, \tag{5.53}$$

$$A_{x_1}(\varrho) = c\, e^{-\sigma/\varrho}\,, \tag{5.54}$$

with an arbitrary constant c. Note that $\sigma \sim 1/\lambda \ll 1$, and therefore the maximum of the corresponding field strength is much greater than one, and it occurs very close to $\varrho = 0$.

We can employ a $1/\lambda$ expansion and look for a solution in this limit, called the scaling limit. Since, as we have just seen, the solution is very localized around $\varrho = 0$, in the (still flat) intermediate region $1/\lambda \ll \varrho \ll 1$, the Chern-Simons term is sub-leading and does not enter the equations of motion for A_t, and A_{x_1}, which have solutions in terms of the flat three-dimensional Green function

$$A_{t,x_1}(\varrho) \sim \frac{1}{\varrho}, \tag{5.55}$$

with different proportionality constants for the two modes. These solutions can be interpreted as the exponential ones (5.53), (5.54) for $\varrho \gg \sigma$, up to a constant.

Now we look at the system at large distances from the flat region $z = 0$, in order to find the solution in the curved background. In this region, the ansatz is slightly modified to $A_t(r,z)$, $A_{x_1}(r,z)$, where r is again given by $r = \sqrt{x_2^2 + x_3^2}$, since the curvature of the background breaks the spherical symmetry around the string. As it is clear from formula (5.55) in the flat space limit, the solutions become smaller as one moves away from the source. Thus, it makes sense to linearize the equations of motion at large distances (considering also the suppression with λ of the CS term). A-posteriori, one can check that indeed the solutions at large distances are actually small. The linearized equations read

$$\frac{|z|}{k^{5/6}(z)}\frac{1}{\sqrt{f_T(z)\gamma_T(z)}}(\partial_{x_2}^2+\partial_{x_3}^2)A_t + \frac{9u_J}{4R^3}\partial_z\left(\frac{k^{3/2}(z)}{|z|}\sqrt{\frac{\gamma_T(z)}{f_T(z)}}\partial_z A_t\right) = 0,$$

$$\frac{|z|}{k^{5/6}(z)}\sqrt{\frac{f_T(z)}{\gamma_T(z)}}(\partial_{x_2}^2+\partial_{x_3}^2)A_{x_1} + \frac{9u_J}{4R^3}\partial_z\left(\frac{k^{3/2}(z)}{|z|}\sqrt{f_T(z)\gamma_T(z)}\partial_z A_{x_1}\right) = 0.$$

The solutions can be written in terms of a series expansion

$$A_t(r,z) = \sum_{n=1}^{\infty}\alpha_n(0)\alpha_n(z)Y_n^{(T)}(r), \tag{5.56}$$

$$A_{x_1}(r,z) = \sum_{n=1}^{\infty}\beta_n(0)\beta_n(z)Y_n^{(T)}(r). \tag{5.57}$$

The functions α_n and β_n are solutions of the eigenvalue equations

$$\partial_z\left(\frac{k^{3/2}(z)}{|z|}\sqrt{\frac{\gamma_T(z)}{f_T(z)}}\,\partial_z\alpha_n(z)\right)+\frac{|z|}{k^{5/6}(z)}\frac{1}{\sqrt{f_T(z)\gamma_T(z)}}a_n\alpha_n(z)=0\,, \tag{5.58}$$

$$\partial_z\left(\frac{k^{3/2}(z)}{|z|}\sqrt{f_T(z)\gamma_T(z)}\,\partial_z\beta_n(z)\right)+\frac{|z|}{k^{5/6}(z)}\sqrt{\frac{f_T(z)}{\gamma_T(z)}}b_n\beta_n(z)=0\,, \tag{5.59}$$

supported by the completeness conditions

$$\sum_{n=1}\frac{|z|}{k^{5/6}(z)}\frac{\alpha_n(0)\alpha_n(z)}{\sqrt{f_T(z)\gamma_T(z)}}=\delta(z)\,, \tag{5.60}$$

$$\sum_{n=1}\frac{|z|}{k^{5/6}(z)}\sqrt{\frac{f_T(z)}{\gamma_T(z)}}\beta_n(0)\beta_n(z)=\delta(z)\,, \tag{5.61}$$

and the orthonormality conditions given by

$$\int_{-\infty}^{+\infty}dz\frac{|z|}{k^{5/6}(z)}\frac{\alpha_n(z)\alpha_m(z)}{\sqrt{f_T(z)\gamma_T(z)}}=\delta_{nm}\,, \tag{5.62}$$

$$\int_{-\infty}^{+\infty}dz\frac{|z|}{k^{5/6}(z)}\sqrt{\frac{f_T(z)}{\gamma_T(z)}}\beta_n(z)\beta_m(z)=\delta_{nm}\,. \tag{5.63}$$

We have numerically solved the equations (5.58) and (5.59), determining the eigenvalues a_n and b_n, by requiring that the functions α_n and β_n vanish at $z\to\pm\infty$. The first even eigenvalues a_n and b_n are:

$$a_n = 0.92,\ 1.96,\ 3.74,\ 5.84,\ 8.59,\ 11.79,\ 15.58,\ ... \tag{5.64}$$

$$b_n = 0.92,\ 1.96,\ 3.74,\ 5.84,\ 8.59,\ 11.79,\ 15.59,\ ... \tag{5.65}$$

The two sets of eigenvalues appear equal only because we truncated their values to two significant digits. In reality, they differ, albeit slightly. Notice that the eigenvalue equations (5.58) and (5.59) do not admit a normalizable zero mode.

The functions $Y_n^{(T)}$ are again the Bessel functions K_0 (5.42) with the eigenvalue replacement

$$A_t\ :\ \lambda_n^{(T)}\to a_n, \qquad\qquad A_{x_1}\ :\ \lambda_n^{(T)}\to b_n. \tag{5.66}$$

They are exponentially small at large r. The equations of motion are homogeneous, so the solutions are defined up to an overall constant. Thus, the charge and current densities in the dual theory at the boundary are arbitrary parameters in the straight string configuration.

5.3.2 Vorton solution near the D8-brane tip

In this section, we focus on the string loop configuration. Let us start by considering the D8-D6 setup in the region close to the tip of the U-shaped D8-brane. This is where the circular boundary of the D6-brane, acting as a monopole source for the magnetic field on the D8-brane according to (5.30), lies. The near-tip region is thus close to the source and it is expected to capture the main contribution to the full solution. As it will be clear in a moment, the DBI action for the D8-brane in this region effectively reduces to that of a D4-brane in a flat five-dimensional spacetime. In this effective description, the wrapped D6-brane source can be seen as a D2-brane with the same circular boundary. Hence the whole setup, in this limit, resembles that examined in [166] in the context of the supersymmetric supertubes, with the crucial difference being the occurrence, in our case, of a CS term in the five-dimensional effective action.

The induced metric (3.123) on the U-shaped D8-brane near the tip $u = u_J$, hence using (3.128) near $z = 0$, reads

$$
\begin{aligned}
ds^2 &= \left(\frac{u_J}{R}\right)^{3/2}\left(-\left(1-\tilde{b}^3\right)dt^2 + d\rho^2 + \rho^2 d\psi^2 + dx_3^2 + \frac{4R^3}{3u_J}\frac{1}{(8-5\tilde{b}^3)}dz^2\right) \\
&\quad + R^{3/2}u_J^{1/2}d\Omega_4^2 = \\
&= \left(\frac{u_J}{R}\right)^{3/2}\left(-\left(1-\tilde{b}^3\right)dt^2 + d\rho^2 + \rho^2 d\psi^2 + dr^2 + r^2 d\theta^2\right) + R^{3/2}u_J^{1/2}d\Omega_4^2\,,
\end{aligned}
\tag{5.67}
$$

where we have introduced the polar coordinates ρ, ψ in the (x_1, x_2) plane, where the circular source lies, and the polar coordinates r, θ in the orthogonal plane (x_3, ω) with[12]

$$
x_3 = r\cos\theta\,, \qquad \omega = r\sin\theta\,, \tag{5.68}
$$

where ω is given by (5.48).

Let us now assume that the gauge field on the D8-brane only depends on the two radial directions r and ρ. The non-zero field strength components can be chosen to be $F_{t\rho}$, F_{tr}, $F_{\rho\psi}$, $F_{\rho\theta}$, $F_{r\psi}$ and $F_{r\theta}$. Hence, the low-energy D8-brane DBI action (3.126) in the near-tip region reduces to

$$
\begin{aligned}
S_{\rm D8}^{\rm DBI} = -\frac{\lambda N}{M_{KK}}\frac{u_J\sqrt{1-\tilde{b}^3}}{3\cdot 2^6\pi^3 R^3} & \int dt\,\rho\,d\rho\,d\psi\,r\,dr\,d\theta\left[-\frac{\left(F_{t\rho}^2 + F_{tr}^2\right)}{1-\tilde{b}^3} + \frac{F_{\rho\psi}^2}{\rho^2} + \right. \\
&\left. + \frac{F_{\psi r}^2}{\rho^2} + \frac{F_{\rho\theta}^2}{r^2} + \frac{F_{r\theta}^2}{r^2}\right].
\end{aligned}
\tag{5.69}
$$

The CS part of the D8-brane action reads as in (3.127)

$$
S_{CS} = \frac{N}{24\pi^2\sqrt{2}}\epsilon^{tMNPQ}\int d^5x\left(\frac{1}{4}A_t F_{MN}F_{PQ} - A_M F_{tN}F_{PQ}\right), \tag{5.70}
$$

with $M, N = t, \rho, \psi, r, \theta$. If the gauge field is not time-dependent as in our ansatz, then we can integrate by parts the second term in the above integral to get

$$
S_{CS} = \frac{N}{32\pi^2\sqrt{2}}\epsilon^{tMNPQ}\int d^5x\,A_t F_{MN}F_{PQ}\,. \tag{5.71}
$$

[12]The letters used for the radii ρ, and r are used for other radius definitions. The meaning should be clear from the context, and there is no ambiguity within a single section.

The equations of motion for the gauge field A resulting from the sum of the above DBI and CS action terms read

$$\rho\partial_r\left(rF_{rt}\right)+r\partial_\rho\left(\rho F_{\rho t}\right)-\tau\left(F_{\rho\psi}F_{r\theta}-F_{r\psi}F_{\rho\theta}\right)=0\,, \tag{5.72}$$

$$r\partial_\rho\left(\frac{1}{\rho}F_{\rho\psi}\right)+\frac{1}{\rho}\partial_r\left(rF_{r\psi}\right)+\frac{\tau}{1-\tilde{b}^3}\left(F_{t\rho}F_{r\theta}-F_{tr}F_{\rho\theta}\right)=0\,, \tag{5.73}$$

$$\frac{1}{r}\partial_\rho\left(\rho F_{\rho\theta}\right)+\rho\partial_r\left(\frac{1}{r}F_{r\theta}\right)+\frac{\tau}{1-\tilde{b}^3}\left(F_{tr}F_{\rho\psi}-F_{t\rho}F_{r\psi}\right)=0\,, \tag{5.74}$$

where

$$\tau\equiv\frac{24\pi M_{KK}\sqrt{1-\tilde{b}^3}}{\lambda\sqrt{2}}\frac{R^3}{u_J}\,. \tag{5.75}$$

These equations have to be supplemented by the modified Bianchi identity (5.30), with the magnetically charged loop of radius l acting as a source. In polar coordinates it reads

$$dF=-2\pi\sqrt{2}\,\delta(\rho-l)\frac{\delta(r)}{2\pi r}d\rho\wedge dr\wedge rd\theta\,. \tag{5.76}$$

A similar system of equations dealing with five-dimensional CS terms has been studied in the literature, see for example [167, 168, 169, 170].

We have not found an analytic solution to the above set of differential equations. To simplify the problem, we consider the parametric dependence on λ of the gauge field. As we discussed in chapter 4, in analogy with the standard Hata-Sakai-Sugimoto-Yamato baryon [28], we want to get an action for a particle with baryonic charge on the D8-branes. This corresponds to the charge of a D4-brane wrapped on S^4. We will see in detail in the next chapter that this D4-brane charge can be carried by the D6-brane with a non-trivial magnetic flux. Now, defining $a_t(t)=A_t/\sqrt{2}$ and treating it as a time-dependent perturbation, the CS action (5.70) reduces to

$$\frac{N}{12\pi^2}\int dt\,a_t(t)\int d^4x\left(F_{\rho\psi}F_{r\theta}-F_{r\psi}F_{\rho\theta}\right), \tag{5.77}$$

from which we realize that a baryonic solution, as anticipated in section 4.1, has to be some kind of "Abelian instanton" with baryon number n_B equal to the instanton number

$$n_B=\frac{1}{12\pi^2}\int d^4x\left(F_{\rho\psi}F_{r\theta}-F_{r\psi}F_{\rho\theta}\right)=\frac{1}{3}\int dr\,d\rho\,I(r,\rho;l)\,, \tag{5.78}$$

where

$$I(r,\rho;l)=F_{\rho\psi}F_{r\theta}-F_{r\psi}F_{\rho\theta}\,. \tag{5.79}$$

We are looking for a solution with a baryon number of order λ^0 supported by the Abelian instanton density $I(r,\rho;l)$, so the magnetic components of the gauge field do not have to scale with λ at leading order:

$$F_{r\theta},\;\;F_{\rho\theta},\;\;F_{r\psi},\;\;F_{\rho\psi}\;\sim\;\mathcal{O}\left(\lambda^0\right). \tag{5.80}$$

With this observation in mind, let us look at the equation of motion (5.72) for the electric potential A_t, taking into account that τ as defined in (5.75) scales like

λ^{-1}. This equation tells us that the electric potential should scale as λ^{-1} at leading order.[13] As a consequence, the CS term in the equations of motion for the magnetic components of the field strength is negligible due to the $1/\lambda$ suppression. Therefore, the equations of motion for the gauge field A in the flat limit can be approximated as

$$\frac{1}{r}\,\partial_\rho\left(\rho\,F_{\rho\theta}\right)+\rho\,\partial_r\left(\frac{F_{r\theta}}{r}\right)+\mathcal{O}\left(\lambda^{-2}\right)=0\,, \tag{5.81}$$

$$\frac{1}{\rho}\,\partial_r\left(r\,F_{r\psi}\right)+r\,\partial_\rho\left(\frac{F_{\rho\psi}}{\rho}\right)+\mathcal{O}\left(\lambda^{-2}\right)=0\,, \tag{5.82}$$

$$\rho\,\partial_r\left(r\,F_{tr}\right)+r\,\partial_\rho\left(\rho\,F_{t\rho}\right)+\tau(F_{\rho\psi}F_{r\theta}-F_{r\psi}F_{\rho\theta})+\mathcal{O}\left(\lambda^{-3}\right)=0\,, \tag{5.83}$$

ignoring $\mathcal{O}\left(\lambda^{-2}\right)$ and further subleading terms. It can be checked that a correction to the solution from these terms gives a correction of the same order to the action. As a matter of fact, at leading order, the CS term enters only in the equation of motion for A_t. The Bianchi identity (5.76) is topological and it contains only the magnetic components of the field strength so there is no $1/\lambda$ expansion to perform.

The equation (5.81) is automatically solved by the ansatz

$$F_{r\theta}=\frac{r}{\rho}\partial_\rho H_{\rm loop}\,,\qquad F_{\rho\theta}=-\frac{r}{\rho}\partial_r H_{\rm loop}\,, \tag{5.84}$$

where $H_{\rm loop}=H_{\rm loop}(r,\rho;l)$ is a function that has to be determined by solving the Bianchi identity (5.76), which becomes

$$\frac{1}{\rho}\,\frac{1}{r}\,\partial_r(r\,\partial_r H_{\rm loop})+\partial_\rho\left(\frac{1}{\rho}\,\partial_\rho H_{\rm loop}\right)=-2\pi\sqrt{2}\,\delta(\rho-l)\frac{\delta(r)}{2\pi r}\,. \tag{5.85}$$

To solve the differential equation for $H_{\rm loop}$ we use the machinery of the two-dimensional Fourier transform in polar coordinates. Let us define the Fourier transform of $H_{\rm loop}$, namely $\widetilde{H}_{\rm loop}$, as

$$H_{\rm loop}(r,\rho;l)=\frac{1}{2\pi}\int_0^\infty k\,dk\,\widetilde{H}_{\rm loop}(k,\rho;l)J_0(kr), \tag{5.86}$$

$$\widetilde{H}_{\rm loop}(k,\rho;l)=2\pi\int_0^\infty r\,dr\,H_{\rm loop}(r,\rho;l)J_0(kr)\,, \tag{5.87}$$

where we have used the radial symmetry of the problem. J_0 is the 0^{th} order Bessel function. The equation (5.85) can be Fourier transformed to get

$$\partial_\rho\left(\frac{1}{\rho}\,\partial_\rho\widetilde{H}_{\rm loop}\right)-k^2\,\frac{\widetilde{H}_{\rm loop}}{\rho}=-2\pi\sqrt{2}\,\delta(\rho-l)\,. \tag{5.88}$$

This differential equation can be solved with the Green function method and the solution reads[14]

$$\widetilde{H}_{\rm loop}(k,\rho;l)=\begin{cases}2\pi\sqrt{2}\,l\rho\,I_1\left(lk\right)K_1\left(\rho k\right) & \rho>l\,,\\ 2\pi\sqrt{2}\,l\,\rho\,K_1\left(lk\right)I_1\left(\rho k\right) & \rho<l\,.\end{cases} \tag{5.89}$$

[13] As we will see, also the zero mode of the equation of motion will scale as λ^{-1}, and this observation is consistent with a solution with angular momentum of order λ^0. In particular, we will look for a solution with baryon number $n_B=1$ and angular momentum $J=N/2$.

[14] We have to impose the continuity of $\widetilde{H}_{\rm loop}$ at $\rho=l$ and the discontinuity, coming from the δ source, of the ρ-derivative $\partial_\rho\widetilde{H}_{\rm loop}$ at $\rho=l$.

Using the results from [171], we can perform the Hankel transform to get

$$H_{\text{loop}}(r,\rho;l) = \pi\sqrt{2}\left[\frac{\rho^2+l^2+r^2}{\sqrt{(l^2+\rho^2+r^2)^2-4\rho^2l^2}}-1\right]. \tag{5.90}$$

The corresponding field strength components, from (5.84), are thus

$$F_{r\theta} = \frac{4\pi\sqrt{2}\,l^2r\,(l^2-\rho^2+r^2)}{\left((l^2+\rho^2+r^2)^2-4\rho^2l^2\right)^{3/2}}, \tag{5.91}$$

$$F_{\rho\theta} = \frac{8\pi\sqrt{2}\,l^2r^2\rho}{\left((l^2+\rho^2+r^2)^2-4\rho^2l^2\right)^{3/2}}. \tag{5.92}$$

Now we have to solve the equation of motion (5.82) for A_ψ. This equation is homogeneous in A_ψ, and this field does not enter the Bianchi identity; therefore, the solution will be defined up to a constant pre-factor. Remember that the full equation of motion for A_ψ (5.73) has a source term due to the CS contribution, but this is suppressed in the large λ expansion we are considering. To leading order, one can, however, argue that A_ψ is sourced by a current $j_\psi \sim \delta(\rho-l)\delta(r)$, flowing along the circular loop, which is (proportional to) the spatial four-dimensional Hodge dual of the three-form magnetic current entering the modified Bianchi identity (5.76). In the supersymmetric supertubes context [166], the proportionality constant is fixed since the magnetic gauge field is taken to be self-dual w.r.t. the four-dimensional Hodge transform. In our non-supersymmetric setup with CS terms, we will stay agnostic and leave the proportionality constant undetermined. The equation of motion with such a source term looks like (5.85), the differential equation for H_{loop}, hence the solution reads

$$A_\psi = \mathcal{N}\left(\frac{\rho^2+l^2+r^2}{\sqrt{(l^2+\rho^2+r^2)^2-4\rho^2l^2}}-1\right), \tag{5.93}$$

where $\mathcal{N}$ is a constant. The corresponding field strength components are

$$F_{\rho\psi} = 4\mathcal{N}\,\frac{l^2\rho\,(l^2-\rho^2+r^2)}{\left((l^2+\rho^2+r^2)^2-4\rho^2l^2\right)^{3/2}}, \tag{5.94}$$

$$F_{r\psi} = -8\mathcal{N}\,\frac{l^2r\rho^2}{\left((l^2+\rho^2+r^2)^2-4\rho^2l^2\right)^{3/2}}. \tag{5.95}$$

The overall factor $\mathcal{N}$ can be fixed by requiring that the above configuration supports baryon number $n_B=1$. However, it is easy to realize, using the above solutions, that the integral of $I(r,\rho;l)$ in (5.78), giving n_B, diverges close to the circular source, and hence it has to be regularized. We can parametrize the divergence by introducing a small-distance cutoff ϵ along the r integration.

Before going on, let us mention that up to this point, we have overlooked another crucial ingredient that is necessary for the D8-brane description to fully capture the attached D6-brane setup. It is well-known that magnetic charges on a D(p+2)-brane correspond to the endpoints of a Dp-brane [172, 173, 174, 175, 176], and the D8-D6 system studied in this thesis is just a particular example within this class. Given this correspondence, we should be able to read off the D6-brane energy from the energy of the monopole configuration on the D8-branes by turning on a scalar field fluctuation which pulls the D8-branes towards the horizon. Let us thus consider a scalar field $X = \pi\alpha'\,\Phi$, representing the fluctuation along the u direction transverse to the brane at $z \sim 0$. The factor $\pi\alpha'$ is the required normalization for the scalar field to be of the same order as the gauge field A. Within the quadratic low-energy approximation of the DBI action we are considering in this section,[15] the action for the scalar field near the D8-brane tip reads

$$S_X = -\frac{\lambda N}{M_{KK}}\frac{u_J}{R^3}\frac{1}{3\cdot 2^7\pi^3\sqrt{1-\tilde{b}^3}}\int dt\,\rho\,d\rho\,d\psi\,r\,dr\,d\theta\Big[(\partial_r\Phi)^2+(\partial_\rho\Phi)^2\Big]. \tag{5.96}$$

The equation of motion for Φ, sourced by the charge distribution corresponding to the local density of strings ending on the circle of radius l [166] at the tip of the D8-branes is

$$\frac{1}{r}\,\partial_r\left(r\,\partial_r\Phi\right)+\frac{1}{\rho}\,\partial_\rho\left(\rho\,\partial_\rho\Phi\right)\sim\delta(\rho-l)\frac{\delta(r)}{2\pi r}\,. \tag{5.97}$$

The solution reads

$$\Phi = \frac{l\,c}{\sqrt{\left(l^2+\rho^2+r^2\right)^2-4\rho^2 l^2}}\,, \tag{5.98}$$

where we leave the constant c unfixed. In the supersymmetric case of the supertube, the proportionality constant is given in terms of the total charge of the fundamental strings ending on the loop, which in our case would be N. This is because our brane is constructed to support baryon number 1, and therefore, as for the standard WSS baryon, it can be thought of as made out of $N\cdot 1$ fundamental strings. As it will be clear in the following, the scalar field given in (5.98) is proportional to the zero mode of the electric potential A_t (*i.e.* to the solution of the related equation of motion obtained neglecting the CS term contribution), as pointed out in [166]. We will return to this point in a moment.

Let us observe that if we go close to the source, $\rho = l$ and $r=\epsilon$ with $\epsilon\to 0$, the scalar field behaves as the usual transverse field representing a magnetic source on a D(p+2)-brane [172] where now ϵ is the distance from the source

$$X = \pi\alpha'\Phi = \frac{\pi\alpha' c}{2}\frac{1}{\epsilon}+\mathcal{O}(\epsilon). \tag{5.99}$$

In the quadratic approximation of the DBI action, the action for the scalar field sums to the Maxwell action for the monopole gauge field A. Therefore, the total

[15] As stated in [172] in the non-BPS case, the quadratic limit of the DBI action necessarily leads to quantitatively incorrect results and we should make use of the full non-linear action. However, we will use it to study qualitatively the D8-brane embedding around the tip.

energy of the D8-D6 brane system from the D8-brane perspective is

$$
\begin{aligned}
E_{\mathrm{D8}} = E_{\text{monopole}} + E_{\text{scalar}} &= \frac{\lambda N}{M_{KK}} \frac{u_J}{R^3} \frac{\sqrt{1-b^3}}{3 \cdot 2^4 \pi} \int dr\, d\rho \left\{ \frac{r}{\rho} \left[(\partial_\rho H)^2 + (\partial_r H)^2 \right] + \right. \\
&\left. + \frac{r\,\rho}{2(1-\tilde{b}^3)} \left[(\partial_\rho \Phi)^2 + (\partial_r \Phi)^2 \right] \right\} = \\
&= \frac{\lambda\, N}{M_{KK}} \frac{u_J}{R^3} \frac{\pi\sqrt{1-b^3}}{96\,(\chi+\chi^3)} \left\{ \left(1 + \frac{c^2}{16\pi^2(1-\tilde{b}^3)} \right) \cdot \right. \\
&\cdot \left(\pi\chi^2 + 2\left(\chi^2+1\right) \operatorname{arccot}\left(\frac{2\chi}{1-\chi^2} \right) + \pi \right) - 4\chi \left. \left(1 - \frac{c^2}{16\pi^2(1-\tilde{b}^3)} \right) \right\} = \\
&= \frac{\lambda\, N}{M_{KK}} \frac{u_J}{R^3} \frac{g(c,\tilde{b},\chi)}{3 \cdot 2^4}\,,
\end{aligned} \tag{5.100}
$$

where we have introduced the dimensionless quantity $\chi = \epsilon/l$ and we have defined the function

$$
\begin{aligned}
g(c,\tilde{b},\chi) =& \left\{ \left(1 + \frac{c^2}{16\pi^2(1-\tilde{b}^3)} \right) \left(\pi\chi^2 + 2\left(\chi^2+1\right) \operatorname{arccot}\left(\frac{2\chi}{1-\chi^2} \right) + \pi \right) + \right. \\
&\left. - 4\chi \left(1 - \frac{c^2}{16\pi^2(1-\tilde{b}^3)} \right) \right\} \frac{\pi\sqrt{1-b^3}}{2\,(\chi+\chi^3)}\,.
\end{aligned} \tag{5.101}
$$

In the limit $\chi = \epsilon/l \to 0$ with $\epsilon \to 0$, we can expand the energy to get

$$
E_{\mathrm{D8}} = \frac{\lambda N}{M_{KK}} \frac{u_J}{R^3} \frac{\pi^2\sqrt{1-\tilde{b}^3}}{48} \left(1 + \frac{c^2}{16\pi^2\left(1-\tilde{b}^3\right)} \right) \frac{l}{\epsilon} + \ldots \tag{5.102}
$$

From this expansion, we can retrieve the usual formula for the energy for the D(p+2)-Dp system of branes [172], using the expansion of the transverse scalar close to the source

$$
E_{\mathrm{D8}} \sim \frac{\lambda^2 N}{M_{KK}^2} \frac{u_J}{R^6} \frac{\pi\sqrt{1-\tilde{b}^3}}{48c} \left(1 + \frac{c^2}{16\pi^2\left(1-\tilde{b}^3\right)} \right) l\, X(\epsilon)\big|_{\text{div.}}\,, \tag{5.103}
$$

$$
\text{with} \quad X(\epsilon)\big|_{\text{div.}} = \frac{\pi\alpha' c}{2} \frac{1}{\epsilon}\,, \tag{5.104}
$$

where the prefactor reproduces the tension, in a flat spacetime, of a D6-brane with radius l extending from the D8-brane's tip along the u direction. We stress that this result becomes increasingly reliable as the D6-brane extends further along the u direction. In other words, it is the limiting scenario of a BIon in flat space which is infinitely extended along the transverse direction to the D(p+2)-brane. We also remember that when $\epsilon \to 0$, higher-order terms in the full DBI Lagrangian that we dropped become important, and one has to replace the Maxwell action with the Born-Infeld action. We will not investigate these corrections in this thesis.

Now we are going to compute the baryon number, the angular momentum, and the energy of our system giving the results as functions of the parameter χ and

$\tilde{b}$. Then we will analyze them carefully from various perspectives to extract the parametric dependence of the stability radius of the string loop.

We start by performing the integration of the Abelian instanton density to get the baryon charge (5.78). The result reads

$$n_B = \frac{1}{3}\int dr\, d\rho\, I(r,\rho;l) = \frac{\mathcal{N}\,\pi\left(\pi\chi^2 + 2\left(\chi^2+1\right)\operatorname{arccot}\left(\frac{2\chi}{1-\chi^2}\right) - 4\chi + \pi\right)}{6\sqrt{2}\left(\chi^3+\chi\right)}\,.$$

Hence, if we want to focus on solutions with baryon number $n_B = 1$, the normalization of the gauge field component A_ψ has to be fixed as

$$\mathcal{N} = \frac{6\sqrt{2}\left(\chi^3+\chi\right)}{\pi\left(\pi\chi^2 + 2\left(\chi^2+1\right)\operatorname{arccot}\left(\frac{2\chi}{1-\chi^2}\right) - 4\chi + \pi\right)}\,. \tag{5.105}$$

The equation of motion (5.83) for the electric potential A_t can be solved since we know explicitly the source term (see appendix B), and the solution is

$$A_t = \frac{d}{\sqrt{\left(l^2+\rho^2+r^2\right)^2 - 4\rho^2 l^2}} + \frac{2\sqrt{2}\,\pi\mathcal{N}\,\tau\left(\rho^2+r^2\right)}{\left(l^2+\rho^2+r^2\right)^2 - 4\rho^2 l^2}\,, \tag{5.106}$$

where the first term is the zero mode of the differential operator applied to A_t and,[16] as anticipated, it is proportional to the scalar field Φ as given in (5.98). This relation is to be expected from the supersymmetric configuration first studied in [172] and then in [166] in the context of supertubes. In this picture, the presence of A_t accounts for the fundamental strings as constituents of the D6-brane, which sources the D8-brane gauge field. This interpretation will be clearer when, in chapter 6, we will investigate in detail the charged D6-brane, which can be thought of as made out of a D4-brane baryon vertex and a bunch of fundamental strings. More precisely, the charge density sourcing the scalar field equation of motion, which has support on the loop, corresponds to the local density of strings ending on the loop. Note that, in our system, the presence of the CS term prevents a direct identification of the scalar field with A_t. In the supersymmetric case, the constant d would be fixed in terms of c.

The coefficient d in our case can be fixed by requiring that our solution with baryon number $n_B = 1$ has angular momentum

$$J = \frac{\lambda N}{M_{KK}}\frac{u_J}{R^3}\frac{1}{3\cdot 2^5\pi^3\sqrt{1-\tilde{b}^3}}\int \rho\, d\rho\, d\psi\, r\, dr\, d\theta\left[F_{t\rho}F_{\rho\psi} + F_{tr}F_{r\psi}\right]\,, \tag{5.107}$$

equal to $N/2$. In chapter 2, we have seen that this is the only possibility for the one-flavored $n_B = 1$ baryon (ground state) due to the antisymmetry of the wavefunction.

[16] As shown in appendix B, the Laplacian operator in duo-polar coordinates has two zero modes. We set one of them to zero because it leads to unphysical solutions.

The above request fixes the coefficient d to be

$$d = -\frac{8\sqrt{2}\,R^3 M_{KK}\sqrt{1-\tilde{b}^3}}{\lambda\, u_J}\Bigg[-8\pi^2\left(\chi^3+\chi\right)+\pi^3\left(\chi^2+1\right)^2+96\left(\chi^2+1\right)^2+ \\ +16\pi\chi^2+4\pi\left(\chi^2+1\right)\operatorname{arccot}\left(\frac{2\chi}{1-\chi^2}\right)\left(\pi\chi^2+\left(\chi^2+1\right)\operatorname{arccot}\left(\frac{2\chi}{1-\chi^2}\right)+ \\ -4\chi+\pi\right)\Bigg]\left[\left(\chi^2+1\right)\left(\pi\chi^2+2\left(\chi^2+1\right)\operatorname{arccot}\left(\frac{2\chi}{1-\chi^2}\right)-4\chi+\pi\right)^2\right]^{-1}. \tag{5.108}$$

Using these results, we can verify that the solution we have found has the desired scaling with λ that we assumed at the beginning of this section.

Now that we have found the solution that solves the leading-order equations of motion for the gauge field, we can compute the total free energy of the configuration, defined as $S_{\text{TOT}} = -\int dt\, E_{\text{TOT}}$. It can be written as

$$E_{\text{TOT}} = E_{\text{magn.}} + E_{\text{scalar}} + E_{\text{el.}}\,,$$

where $E_{\text{mag.}}$ and E_{scalar} are of order λ while $E_{\text{el.}}$ scales as λ^{-1} and they are associated respectively with the magnetic, scalar, and electric energy of the configuration. They read

$$E_{\text{magn.}} = \frac{\lambda N}{M_{KK}}\frac{u_J\sqrt{1-\tilde{b}^3}}{3\cdot 2^6\pi^3 R^3}\int \rho\, d\rho\, d\psi\, r\, dr\, d\theta\left[\frac{F_{\rho\psi}^2}{\rho^2}+\frac{F_{\psi r}^2}{\rho^2}+\frac{F_{\rho\theta}^2}{r^2}+\frac{F_{r\theta}^2}{r^2}\right], \tag{5.109}$$

$$E_{\text{scalar}} = \frac{\lambda N}{M_{KK}}\frac{u_J}{3\cdot 2^7\pi^3 R^3\sqrt{1-\tilde{b}^3}}\int \rho\, d\rho\, d\psi\, r\, dr\, d\theta\left[(\partial_\rho\Phi)^2+(\partial_r\Phi)^2\right], \tag{5.110}$$

$$E_{\text{el.}} = -\frac{\lambda N}{M_{KK}}\frac{u_J}{3\cdot 2^6\pi^3 R^3\sqrt{1-\tilde{b}^3}}\int \rho\, d\rho\, d\psi\, r\, dr\, d\theta\,\left[F_{t\rho}^2+F_{tr}^2\right] \\ -\frac{N}{4\pi^2\sqrt{2}}\int d^5x\, A_t\left[F_{\rho\psi}F_{r\theta}-F_{\rho\theta}F_{r\psi}\right]. \tag{5.111}$$

Using the solutions to the equations of motion, we find

$$E_{\text{magn.}} = \frac{\lambda N}{M_{KK}}\frac{u_J}{R^3}\, m(\tilde{b},\chi)\,,$$

where

$$m(\tilde{b},\chi) = \frac{\sqrt{1-\tilde{b}^3}}{48\pi}\Bigg[\frac{\pi^3}{2\chi}-\frac{2\pi^2}{\chi^2+1}+\frac{\pi^2\operatorname{arccot}\left(\frac{2\chi}{1-\chi^2}\right)}{\chi}+ \\ +\frac{18\left(\chi^3+\chi\right)}{\pi^2\left(\pi\chi^2+2\left(\chi^2+1\right)\operatorname{arccot}\left(\frac{2\chi}{1-\chi^2}\right)-4\chi+\pi\right)}\Bigg], \tag{5.112}$$

is a function of $\tilde{b}$ and χ. The plot of the function $m(\tilde{b},\chi)$ is shown in figure 5.13a. It encodes the dependence of the magnetic energy on $\tilde{b}$ and χ.

Then, the contribution coming from the transverse scalar field is

$$E_{\text{scalar}} = \frac{\lambda N}{M_{KK}}\frac{u_J}{R^3}\, c^2\, n(\tilde{b},\chi)\,,$$

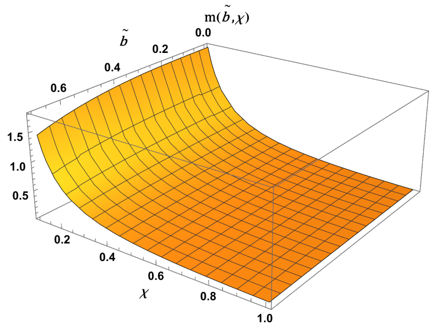

(a) Plot of $m(\tilde{b}, \chi)$.

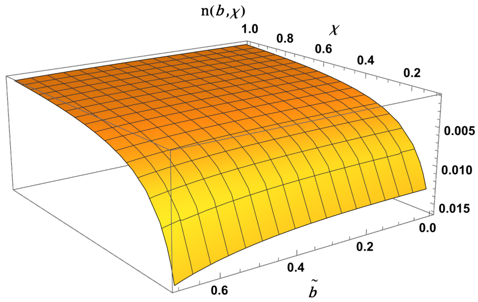

(b) Plot of $n(\tilde{b}, \chi)$.

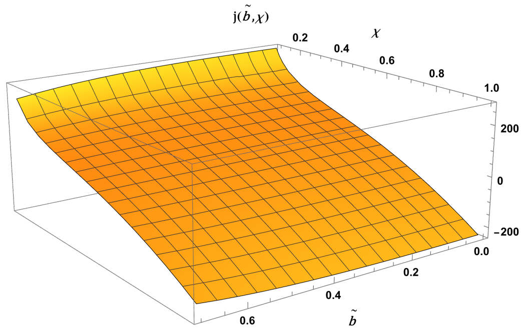

(c) Plot of $j(\tilde{b}, \chi)$.

Figure 5.13. Plots of the energy contributions as functions of $\tilde{b}$ and χ. $\tilde{b}$ spans the whole range of values for which chiral symmetry is broken, while the variable χ spans the range from 0.1 to 1.

where

$$n(\tilde{b}, \chi) = \frac{1}{1536\pi\,(\chi + \chi^3)\,\sqrt{1 - \tilde{b}^3}} \left(\pi\chi^2 - 2\left(\chi^2 + 1\right) \operatorname{arccot}\left(\frac{2\chi}{\chi^2 - 1}\right) + 4\chi + \pi\right), \tag{5.113}$$

is a function of $\tilde{b}$ and χ whose plot is shown in figure 5.13b.

Finally, the electric contribution to the energy $E_{\text{el.}}$ reads

$$E_{\text{el.}} = \frac{N\,M_{KK} R^3}{\lambda\,u_J} \frac{j(\tilde{b}, \chi)}{l^2},$$

with

$$\begin{aligned} j(\tilde{b}, \chi) = \Big\{ &- 2\left(\chi^2 + 1\right)^3 \operatorname{arccot}\left(\frac{2\chi}{1 - \chi^2}\right)\left(\hat{d}^{\,2}\chi^2 + 1152\pi^4\left(1 - \tilde{b}^3\right)\mathcal{N}^{\,2}\left(\chi^2 + 1\right)\right) \\ &- 256\pi^2 \hat{d}\mathcal{N}\,\chi\sqrt{1 - \tilde{b}^3}\,\left(3\chi^6 + 6\chi^4 + 5\chi^2 + 2\right) - 384\pi^4\mathcal{N}^{\,2}\left(1 - \tilde{b}^3\right)\Big(3\pi\left(\chi^2 + 1\right)^4 + \\ &+ 4\chi\left(9x^6 + 9\chi^4 + 11\chi^2 + 3\right)\Big) - \hat{d}^{\,2}\chi^2\left(\pi\chi^2 + 4\chi + \pi\right)\left(\chi^2 + 1\right)^2\Big\} \cdot \\ &\cdot \left[768\,\pi\sqrt{1 - \tilde{b}^3}\left(\chi^3 + \chi\right)^3\right]^{-1}, \end{aligned}$$

a function of $\tilde{b}$ and χ. We remember that $\mathcal{N}$ is also a function of χ and here we have defined $\hat{d} = d\, R^3 M_{KK}/u_J$ which is again a function of $\tilde{b}$ and χ. See figure 5.13c for a plot of $j(\tilde{b}, \chi)$.

At this point, we can analyze the total energy in the limit of a very long spike, which is $\chi = \epsilon/l \to 0$ with $\epsilon \to 0$. The total energy expanded at leading order reads

$$E^{\text{on-shell}}_{\text{TOT}} = \frac{\lambda\, N}{M_{KK} R^3} \frac{\sqrt{1-\tilde{b}^3}}{\pi c} X(\epsilon)\big|_{\text{div.}} \left\{ \frac{\lambda}{M_{KK}} \frac{u_J}{R^3} \frac{\pi}{48} \left(1 + \frac{c^2}{16\pi^2 \left(1-\tilde{b}^3\right)} \right) l + \right. \\ \left. + \frac{M_{KK}}{\lambda} \frac{R^3}{u_J} \frac{1728 - \pi^2(162 - 48\pi + \pi^4)}{3\pi^2} \frac{1}{l} \right\} + ... \tag{5.114}$$

The dependence on the transverse scalar field factorizes and hence we can minimize the action over the free parameter l, representing the loop size. The minimization gives

$$l_{\text{stable}} = \frac{M_{KK}}{\lambda} \frac{u_J}{R^3} \frac{16}{\pi} \sqrt{\frac{\left(1-\tilde{b}^3\right)\left(1728 - \pi^2(162 - 48\pi + \pi^4)\right)}{c^2 + 16\pi^2 \left(1-\tilde{b}^3\right)}} \,. \tag{5.115}$$

From the above result, we can deduce that the stability radius scales like λ^{-1}. Hence the string loop radius in the flat region is suppressed similarly to the instanton size of the standard baryon in the WSS model but with a different power of λ.

It is useful to give the result for the stability radius also in terms of the chiral symmetry breaking critical temperature T_a

$$l_{\text{stable}} = \frac{M_{KK}}{\lambda\, T_a^2} \frac{16(0.154)^2}{\pi\, J_T^2(\tilde{b})} \sqrt{\frac{\left(1-\tilde{b}^3\right)\left(1728 - \pi^2(162 - 48\pi + \pi^4)\right)}{c^2 + 16\pi^2 \left(1-\tilde{b}^3\right)}}. \tag{5.116}$$

It is also interesting to write the stability radius in terms of the more common phenomenological quantity f_a, the axion decay constant. Remembering the relation between f_a and T_a (see *e.g.* [140])

$$f_a^2 = \frac{N\lambda}{16\pi^3} \frac{J_T^3(\tilde{b})}{(0.154)^3\, I_T(\tilde{b})} \frac{T_a^3}{M_{KK}} \,, \tag{5.117}$$

where

$$I_T(\tilde{b}) = \int_0^1 dy \frac{\sqrt{1-\tilde{b}^3 y}}{\sqrt{y\left(1-\tilde{b}^3 y - \left(1-\tilde{b}^3\right) y^{8/3}\right)}} \,, \tag{5.118}$$

we get

$$l_{\text{stable}} = \frac{N\, T_a}{f_a^2} \frac{J_T(\tilde{b})}{0.154\, \pi^4 I_T(\tilde{b})} \sqrt{\frac{\left(1-\tilde{b}^3\right)\left(1728 - \pi^2(162 - 48\pi + \pi^4)\right)}{c^2 + 16\pi^2 \left(1-\tilde{b}^3\right)}} \,. \tag{5.119}$$

The analysis can be repeated by considering an object with baryon number n_B (of order λ^0). This leads to the following redefinition of the integration constants $\mathcal{N}$ and d as

$$\mathcal{N} \to n_B \mathcal{N} \,, \quad d \to n_B\, d \,. \tag{5.120}$$

This propagates to the energy, leading to the following result for its minimization with respect to l:

$$l_{\text{stable}} = n_B \, l^{n_B=1}_{\text{stable}} \,, \tag{5.121}$$

where $l^{n_B=1}_{\text{stable}}$ is the result written in equation (5.115) or equivalently in (5.119). As we will see in section 6.3, the D8-brane analysis in flat space is consistent with the charged D6-brane result for the stability radius

$$l_{\text{stable}} \sim \frac{n_B}{\lambda} \,. \tag{5.122}$$

This confirms that the flat limit gives the correct result for the stability radius scaling, even if it is not able to capture whether the solution exists in the full spacetime. We will come back to this comparison in section 6.3.

Let us make some observations about the cutoff ϵ. The result $l_{\text{stable}} \sim \lambda^{-1}$ leads to observe that in order to have $n_B \sim \lambda^0$ and the scaling (5.80) for the magnetic fields, it follows that $\epsilon \sim \lambda^{-1}$. Therefore, the ratio $\chi = \epsilon/l$ does not scale with λ. This statement is expected to be true also from other perspectives. Going back to the transverse scalar, this represents the extension of the D6-brane along u, and we know from the D6-brane perspective that this length is of order $(\alpha')^0$ in the vorton case. This is because the D6-brane, even if it is charged, is extended from u_J to the horizon radius u_T, and $u_J - u_T \sim (\alpha')^0$. Since $X = \pi\alpha'\Phi \sim \pi\alpha' c/(2\epsilon)$ has to go like $(\alpha')^0$, we get $\epsilon \sim \alpha' \sim \lambda^{-1}$. This identification can be written qualitatively as

$$\epsilon = y(\tilde{b}, c) \, \frac{R^3}{u_J} \frac{M_{KK}}{\lambda} \,, \tag{5.123}$$

where $y(\tilde{b}, c)$ is some function of $\tilde{b}$ and c which cannot be fixed at this level.

Another argument that leads to the same qualitative result comes from equating the energy of the transverse scalar plus the energy of the monopole with the energy of the D6-brane. According to our results in section 5.2.2, the energy of the D6-brane that describes the uncharged string loop can be written as

$$E_{\text{D6}} = \frac{\lambda^2 N}{3 \cdot 2^4 \pi^2} \frac{J_T^5(\tilde{b}) T_a^4}{(0.15)^4 M_{KK}^2} \alpha(\tilde{b}) l \,, \tag{5.124}$$

where $\alpha(\tilde{b})$ is the slope of the linear dependence of the energy with l, which can be found numerically as a function of $\tilde{b}$ and it is shown in figure 5.14.

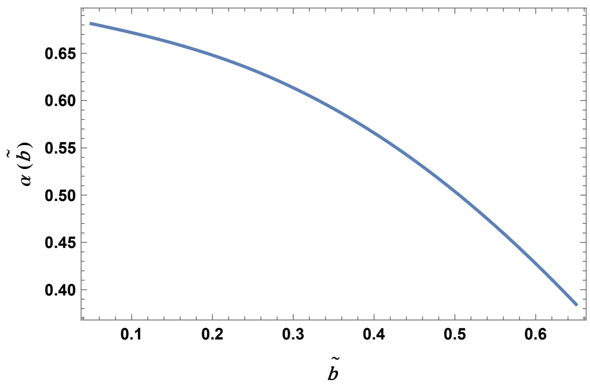

Figure 5.14. Plot of the slope $\alpha(\tilde{b})$ of the D6-brane energy for the string loop configuration as a function of l.

Then, an estimate for the cutoff is obtained by equating the two energies (5.124) and (5.100):

$$\epsilon = y(c,\tilde{b},\chi)\frac{R^3}{u_J}\frac{M_{KK}}{\lambda}\,, \tag{5.125}$$

where

$$y(c,\tilde{b},\chi) \sim \frac{\pi^2}{J_T(\tilde{b})\alpha(\tilde{b})}\,\chi\, g(c,\tilde{b},\chi)\,. \tag{5.126}$$

Once again assuming that the quantity χ does not scale with λ, we get $\epsilon \sim \lambda^{-1}$. The coefficient $y(c,\tilde{b},\chi)$ is a function of $\tilde{b}$ and χ, and its exact value cannot be fixed within our approximations since we cannot compare the flat D8-brane result with the D6-brane result valid in the whole spacetime. This function is more involved than the one defined in (5.123) but since we are not able to fix either of them we will keep generically the cutoff ϵ depending on a function y. The important result relies on the parametric dependence of ϵ with λ.

We are going to show that also in this case we will obtain the same qualitative result for the stability radius. We can express l in terms of χ, using the expression (5.125) for ϵ,

$$l = \frac{M_{KK}}{\lambda}\frac{R^3}{u_J}\frac{y(c,\tilde{b},\chi)}{\chi}\,. \tag{5.127}$$

We can substitute the above relation in the electric contribution to the energy $E_{\text{el.}}$ to give

$$E_{\text{el.}} = \frac{\lambda N}{M_{KK}}\frac{u_J}{R^3}\frac{\chi^2}{y^2(c,\tilde{b},\chi)}\,j(\tilde{b},\chi). \tag{5.128}$$

Remarkably, this term becomes of the same order in the parameters as $E_{\text{magn.}}$ and E_{scalar}. Eventually, the total energy depends only on χ, which has not yet been fixed, and all the dimensionful parameters, together with λ and N, factorize

$$E^{\text{on-shell}}_{\text{TOT}} = \frac{\lambda N}{M_{KK}}\frac{u_J}{R^3}\left(m(\tilde{b},\chi) + c^2\,n(\tilde{b},\chi) + \frac{\chi^2}{y^2(c,\tilde{b},\chi)}\,j(\tilde{b},\chi)\right). \tag{5.129}$$

We have to minimize the above action with respect to χ. This procedure will return a function for $\chi_{\text{stable}}(\tilde{b},c)$ that does not scale with λ. The result of the minimization

$$\partial_\chi m(\tilde{b},\chi) + c^2\,\partial_\chi n(\tilde{b},\chi) + \partial_\chi\left(\frac{\chi^2\,j(\tilde{b},\chi)}{y^2(c,\tilde{b},\chi)}\right) = 0\,, \tag{5.130}$$

depends on c and on the explicit expression for $y(c,\tilde{b},\chi)$ and it is in general a function of the temperature $\tilde{b}$.

We can conclude, from the relation (5.127), that l_{stable} scales like λ^{-1}. More precisely

$$\begin{aligned} l_{\text{stable}} &= \frac{M_{KK}}{\lambda T_a^2}\frac{(0.154)^2 e(c,\tilde{b},\chi_{\text{stable}})}{J_T^2(\tilde{b})\chi_{\text{stable}}(\tilde{b},c)} = p(\tilde{b},c,\chi_{\text{stable}})\,\frac{M_{KK}}{\lambda T_a^2} = \\ &= \frac{p(\tilde{b},c,\chi_{\text{stable}})\,J_T^3(\tilde{b})}{16\pi^3(0.15)^3 I_T(\tilde{b})}\frac{N\,T_a}{f_a^2}\,, \end{aligned} \tag{5.131}$$

where

$$p(\tilde{b}, c, \chi_{\text{stable}}) = \frac{(0.154)^2 y(c, \tilde{b}, \chi_{\text{stable}})}{J_T^2(\tilde{b})\chi_{\text{stable}}(\tilde{b}, c)}\,. \tag{5.132}$$

As we are going to show in section 6.3, the local D8-brane analysis around the tip at $u = u_J$, provides a result on the stability radius which is perfectly consistent with what can be found from the D6-brane perspective. In that case, in fact, any (meta)stable vorton solution would have a radius l scaling as $n_B\lambda^{-1}$. However, we will see that the actual existence of such a solution can be eventually confirmed only by a global analysis of the full equations of motion. In particular, we will show that if $n_B \sim \lambda^0$, as in the case considered in the present section, no (meta)stable vorton solution actually exists. In order for the same conclusion to be drawn from the D8-brane perspective, we should go far beyond the near tip limit and consider the full equations of motion of the D8 on the whole curved background, something which, for the moment, we are not able to do. In other words, the flat limit in the D8-brane perspective captures only the local result near $u = u_J$ of the complementary D6-brane description.

5.3.3 Analysis of the vorton solution in the asymptotic region

In this section, we analyze the equations of motion for the D8-brane gauge field on the curved background (3.115), sourced by the string loop configuration. First, we switch off the electric potential and we solve exactly the Maxwell-Bianchi system in the curved background. Then, we solve the linearized equations of motion with non-zero A_t and A_ψ, following [165]. Such solutions are written in terms of the curved metric Green functions that can be smoothly connected with the flat space solutions. Finally, we compute the one-point function of flavor currents in the deconfined phase of the WSS and we use the result to compute the baryon number of the solution to the linearized equations of motion.

The D6-brane-monopole source for the D8-brane gauge field leads to the modified Bianchi identity (5.30), which complements the equations of motion for the D8-branes gauge field. Turning off for a moment the potentials A_t and A_ψ, the only field strength components that we need to consider are $F_{\rho x_3}$, $F_{\rho z}$ and $F_{x_3 z}$. With this gauge choice, there is no contribution from the five-dimensional CS term of flavor brane.

The action (3.129) in the present case reduces to

$$\begin{aligned} S_{\text{D8}}^{\text{DBI}} = -\,\frac{3T_8 V_4 R^{3/2} u_J^{3/2}(2\pi\alpha')^2}{8g_s} \int d^4x\, dz \left\{ \frac{k^{3/2}(z)}{|z|}\sqrt{\gamma_T(z) f_T(z)}\left[F_{\rho z}^2 + F_{x_3 z}^2\right] \right. \\ \left. + \frac{4R^3}{9u_J}\frac{|z|}{k^{5/6}(z)}\sqrt{\frac{f_T(z)}{\gamma_T(z)}}\,F_{\rho x_3}^2 \right\}, \end{aligned}$$

where, again, $\rho = \sqrt{x_1^2 + x_2^2}$ and we have used the equation (3.128). Moreover,

$d^4x = dt\rho d\rho d\psi dx_3$. The resulting equations of motion

$$\partial_\rho\left(\rho F_{\rho z}\right) + \rho\,\partial_{x_3}F_{x_3 z} = 0\,, \tag{5.133}$$

$$\frac{4R^3}{9u_J}\frac{|z|}{k(z)^{5/6}}\sqrt{\frac{f_T(z)}{\gamma_T(z)}}\,\partial_{x_3}F_{\rho x_3} + \partial_z\left(\frac{k^{3/2}(z)}{|z|}\sqrt{\gamma_T(z)f_T(z)}\,F_{\rho z}\right) = 0\,, \tag{5.134}$$

$$\frac{4R^3}{9u_J}\frac{|z|}{k^{5/6}(z)}\sqrt{\frac{f_T(z)}{\gamma_T(z)}}\,\partial_\rho\left(\rho F_{\rho x_3}\right) - \rho\,\partial_z\left(\frac{k^{3/2}(z)}{|z|}\sqrt{\gamma_T(z)f_T(z)}\,F_{x_3 z}\right) = 0\,, \tag{5.135}$$

can be solved by the following ansatz

$$F_{\rho x_3} = \frac{9u_J}{4R^3}\frac{k^{5/6}(z)}{|z|}\sqrt{\frac{\gamma_T(z)}{f_T(z)}}\frac{\partial_z H^{(C)}_{\text{loop}}}{\rho}\,, \tag{5.136}$$

$$F_{x_3 z} = \frac{|z|}{k^{3/2}(z)}\frac{\partial_\rho H^{(C)}_{\text{loop}}}{\rho\sqrt{f_T(z)\gamma_T(z)}}\,, \tag{5.137}$$

$$F_{\rho z} = -\frac{|z|}{k^{3/2}(z)}\frac{\partial_{x_3} H^{(C)}_{\text{loop}}}{\rho\sqrt{f_T(z)\gamma_T(z)}}\,, \tag{5.138}$$

where $H^{(C)}_{\text{loop}}$ is an unknown function that has to be determined by requiring that the above components of the field strength satisfy the Bianchi identity (5.30),

$$\begin{aligned}
&-2\pi\sqrt{2}\,\delta(\rho-l)\delta(x_3)\delta(z) = \partial_\rho F_{x_3 z} + \partial_z F_{\rho x_3} - \partial_{x_3}F_{\rho z} = \\
&= \frac{|z|}{k^{3/2}(z)\sqrt{f_T(z)\gamma_T(z)}}\left[\partial_\rho\left(\frac{\partial_\rho H^{(C)}_{\text{loop}}}{\rho}\right) + \frac{\partial^2_{x_3}H^{(C)}_{\text{loop}}}{\rho}\right] + \\
&\quad + \frac{9u_J}{4R^3}\frac{1}{\rho}\partial_z\left(\frac{k^{5/6}(z)}{|z|}\sqrt{\frac{\gamma_T(z)}{f_T(z)}}\partial_z H^{(C)}_{\text{loop}}\right).
\end{aligned}$$

The function $H^{(C)}_{\text{loop}}$ is the curved space generalization of the function H_{loop} introduced in the formula (5.90). We look for a solution by series, such as

$$H^{(C)}_{\text{loop}}(\rho, x_3, z; l) = \sum_{n=0}^{\infty}\zeta^{(T)}_n(0)\zeta^{(T)}_n(z)J_n\left(\rho, x_3; l\right), \tag{5.139}$$

where the center of mass moduli (X_3, Z) are taken to be zero for simplicity. The Bianchi identity becomes

$$\begin{aligned}
&\sum_{n=0}^{\infty}\zeta^{(T)}_n(0)\Big[\frac{9u_J}{4R^3}\frac{J_n}{\rho}\partial_z\left(\frac{k^{5/6}(z)}{|z|}\sqrt{\frac{\gamma_T(z)}{f_T(z)}}\partial_z\zeta^{(T)}_n(z)\right) + \\
&+ \frac{|z|\zeta^{(T)}_n(z)}{k^{3/2}(z)\sqrt{f_T(z)\gamma_T(z)}}\left(\partial_\rho\left(\frac{\partial_\rho J_n}{r}\right) + \frac{\partial^2_{x_3}J_n}{\rho}\right)\Big] = -2\pi\sqrt{2}\,\delta(\rho-l)\delta(x_3)\delta(z)\,.
\end{aligned}$$

The eigenfunctions $\zeta^{(T)}_n$ are the same defined for the straight axionic string in formulas (5.36)

$$\partial_z\left(\frac{k^{5/6}(z)}{|z|}\sqrt{\frac{\gamma_T(z)}{f_T(z)}}\partial_z\zeta_n(z)\right) + \frac{|z|}{k^{3/2}(z)\sqrt{f_T(z)\gamma_T(z)}}\,\lambda_n\,\zeta_n(z) = 0\,, \tag{5.140}$$

with the associated completeness and orthonormality conditions.

Then, the Bianchi identity is solved if the modes J_n satisfy the following equation

$$\partial_\rho\left(\frac{\partial_\rho J_n}{\rho}\right)+\frac{\partial^2_{x_3}J_n}{\rho}-\frac{9u_J}{4R^3}\lambda_n^{(T)}\frac{J_n}{\rho}=-2\pi\sqrt{2}\,\delta(\rho-l)\delta(x_3)\,. \tag{5.141}$$

The solution to (5.141) can be found by performing the Fourier transform along the coordinate x_3

$$J_n(\rho,x_3;l)=\int\frac{dk}{2\pi}e^{ikx_3}\hat{J}_n(\rho,k;l)\,, \tag{5.142}$$

and then by solving the following equation for $\hat{J}_n$ through the Green function method

$$\partial_\rho\left(\frac{\partial_\rho\hat{J}_n(\rho,k;l)}{\rho}\right)-\left(k^2+\frac{9u_J}{4R^3}\lambda_n^{(T)}\right)\frac{\hat{J}_n(\rho,k;l)}{\rho}=-2\pi\sqrt{2}\,\delta(\rho-l)\,. \tag{5.143}$$

Using the Green's theorem, we can write the solutions as

$$\hat{J}_n(\rho,k;l)=\begin{cases}2\pi\sqrt{2}\,lI_1\left(l\sqrt{k^2+\frac{9u_J}{4R^3}\lambda_n^{(T)}}\right)\rho K_1\left(\rho\sqrt{k^2+\frac{9u_J}{4R^3}\lambda_n^{(T)}}\right) & \rho>l\,,\\ 2\pi\sqrt{2}\,lK_1\left(l\sqrt{k^2+\frac{9u_J}{4R^3}\lambda_n^{(T)}}\right)\rho I_1\left(\rho\sqrt{k^2+\frac{9u_J}{4R^3}\lambda_n^{(T)}}\right) & \rho<l\,.\end{cases} \tag{5.144}$$

In order to obtain the solutions $J_n(\rho,x_3;l)$ we have to perform the Fourier transform (5.142) numerically. The first modes J_0, J_2, J_4 and J_6 are shown in figure 5.15, for $l=1$, $9u_J/(4R^3)=1$ and $\tilde{b}=0.1$.

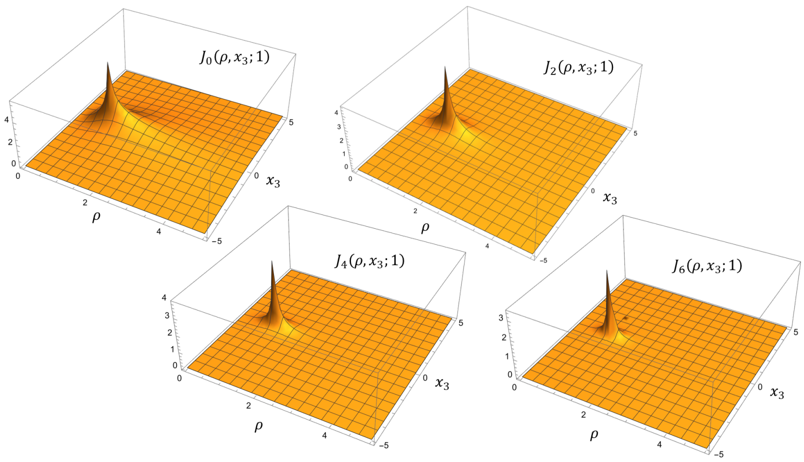

Figure 5.15. The first modes of $J_n(\rho,x_3;l)$ for $l=1$, $9u_J/(4R^3)=1$ and $\tilde{b}=0.1$.

We can now evaluate the on-shell D8-branes action,

$$
\begin{aligned}
S_{\mathrm{D8}}^{\mathrm{DBI}} &= -\frac{\kappa_J}{2}\int d^4x\,dz\left\{\frac{k^{3/2}(z)}{|z|}\sqrt{\gamma_T(z)f_T(z)}\left[F_{\rho z}^2+F_{x_3 z}^2\right]\right.\\
&\quad\left.+\frac{4R^3}{9u_J}\frac{|z|}{k^{5/6}(z)}\sqrt{\frac{f_T(z)}{\gamma_T(z)}}\,F_{\rho x_3}^2\right\}=\\
&=-\frac{\kappa_J}{2}\sum_{n=0}^{\infty}\sum_{m=0}^{\infty}\zeta_n^{(T)}(0)\zeta_m^{(T)}(0)\int\frac{d^4x}{\rho^2}\,dz\left\{\frac{|z|}{k^{3/2}(z)}\frac{\zeta_n^{(T)}(z)\zeta_m^{(T)}(z)}{\sqrt{\gamma_T(z)f_T(z)}}\cdot+\right.\\
&\quad\left.\cdot\left[(\partial_\rho J_n)^2+(\partial_{x_3}J_n)^2\right]+\frac{9u_J}{4R^3}\sqrt{\frac{\gamma_T(z)}{f_T(z)}}\frac{k^{5/6}(z)}{|z|}\partial_z\zeta_n^{(T)}(z)\partial_z\zeta_m^{(T)}(z)J_nJ_m\right\}=\\
&=-\frac{\kappa_J}{2}\sum_{n=0}^{\infty}\left(\zeta_n^{(T)}(0)\right)^2\int\frac{d^4x}{\rho^2}\left\{(\partial_\rho J_n)^2+(\partial_{x_3}J_n)^2+\frac{9u_J}{4R^3}\lambda_n^{(T)}J_n^2\right\},
\end{aligned}
$$

where κ_J is defined in (5.43). We define

$$
\phi_n(\rho,x_3;l)=\sqrt{\kappa_J}\,\zeta_n^{(T)}(0)\frac{J_n(\rho,x_3;l)}{\rho}\,, \tag{5.145}
$$

to get the canonically normalized action

$$
S_{\mathrm{D8}}^{\mathrm{DBI}}=-\frac{1}{2}\sum_{n=0}^{\infty}\int d^4x\left\{(\partial_\rho\phi_n)^2+(\partial_{x_3}\phi_n)^2+\frac{\phi_n^2}{\rho^2}+2\frac{\phi_n}{\rho}\partial_\rho\phi_n+\frac{9u_J}{4R^3}\lambda_n^{(T)}\phi_n^2\right\}.
$$

The interaction term $\phi\partial\phi$ can be eliminated by integrating by parts so that finally we get

$$
S_{\mathrm{D8}}^{\mathrm{DBI}}=-\frac{1}{2}\sum_{n=0}^{\infty}\int d^4x\left\{(\partial_\rho\phi_n)^2+(\partial_{x_3}\phi_n)^2+\left(\frac{1}{\rho^2}+\frac{9u_J}{4R^3}\lambda_n^{(T)}\right)\phi_n^2\right\}. \tag{5.146}
$$

Upon extending the derivatives to the four coordinates and adding the source term

$$
S_{\mathrm{source}}=\int d^4x\,2\pi\sqrt{2}\,\delta(\rho-l)\delta(x_3)\frac{\rho}{\sqrt{\kappa_J}\,\zeta_n^{(T)}(0)}\phi_n\,, \tag{5.147}
$$

this can be read as the four-dimensional effective action for the uncharged string loop, with the eigenvalues $\lambda_n^{(T)}$ being related to mass parameters. The fields in this action come from the mesonic modes at finite temperature, the lightest one being the axion (the zero-mode with $\lambda_0^{(T)}=0$). More precisely, the fields ϕ_n come from the D8 gauge field modes "transverse" to the circular source, *i.e.* A_z (including the axion) and A_ρ, A_{x_3} (two components of the (tower of) vector mesons), with a specific identification, coming from the five-dimensional equations of motion, reducing to the single tower ϕ_n the number of independent fields.

The free energy of the string loop, defined as $S_{\mathrm{D8}}^{\mathrm{DBI}}=-\int dt\,E_{\mathrm{loop}}$, scales linearly with N. The energy is divergent at the location $x_3=0$, $\rho=l$ of the string while it does not diverge at large distances, *i.e.* for $x_3\to\pm\infty$ and $\rho\to\infty$, as expected from the literature [147, 148]. One must remember that the solution is derived under the hypothesis that the field strength is small (compared to l_s^{-1}) so to consider the quadratic expansion of the DBI action. Thus, the solution we found cannot be trusted close to the source, where the divergence is expected to be resolved in the full DBI analysis.

The charged mode

If we turn on the gauge field components A_t and A_ψ we also have contributions from the CS term in the action. The equations of motion, in this case, are[17]

- $$\kappa_J \rho \left\{ \frac{4R^3}{9u_J} \frac{|z|}{k^{5/6}(z)} \sqrt{\frac{f_T(z)}{\gamma_T(z)}}\, \partial_{x_3} F_{\rho x_3} + \partial_z \left(\frac{k^{3/2}(z)}{|z|} \sqrt{\gamma_T(z) f_T(z)}\, F_{\rho z} \right) \right\} + \\ + \frac{N\sqrt{2}}{68\pi^2} \epsilon^{\rho MNPQ} F_{MN} F_{PQ} = 0 \,. \tag{5.148}$$

- $$-\kappa_J \left\{ \frac{4R^3}{9u_J} \frac{|z|}{k^{5/6}(z)} \sqrt{\frac{f_T(z)}{\gamma_T(z)}}\, \partial_\rho \left(\rho F_{\rho x_3}\right) - \rho\, \partial_z \left(\frac{k^{3/2}(z)}{|z|} \sqrt{\gamma_T(z) f_T(z)}\, F_{x_3 z} \right) \right\} + \\ + \frac{N\sqrt{2}}{68\pi^2} \epsilon^{3MNPQ} F_{MN} F_{PQ} = 0 \,. \tag{5.149}$$

- $$-\kappa_J \frac{k^{3/2}(z)}{|z|} \sqrt{\gamma_T(z) f_T(z)} \left\{ \partial_\rho \left(\rho F_{\rho z}\right) + \rho\, \partial_{x_3} F_{x_3 z} \right\} + \frac{N\sqrt{2}}{68\pi^2} \epsilon^{zMNPQ} F_{MN} F_{PQ} = 0 \,. \tag{5.150}$$

- $$-\kappa_J \left\{ \frac{4R^3}{9u_J} \frac{|z|}{k^{5/6}(z)} \sqrt{\frac{1}{f_T(z)\gamma_T(z)}} \left[\partial_\rho \left(\rho F_{t\rho}\right) + \rho\, \partial_{x_3} F_{t x_3} \right] + \\ + \rho\, \partial_z \left(\frac{k^{3/2}(z)}{|z|} \sqrt{\frac{\gamma_T(z)}{f_T(z)}}\, F_{tz} \right) \right\} + \frac{N\sqrt{2}}{68\pi^2} \epsilon^{tMNPQ} F_{MN} F_{PQ} = 0 \,. \tag{5.151}$$

- $$-\kappa_J \left\{ \frac{4R^3}{9u_J} \frac{|z|}{k^{5/6}(z)} \sqrt{\frac{f_T(z)}{\gamma_T(z)}} \left[\partial_\rho \left(\frac{1}{\rho} F_{\rho\psi} \right) - \frac{1}{\rho} \partial_{x_3} F_{\psi x_3} \right] + \\ - \frac{1}{\rho}\, \partial_z \left(\frac{k^{3/2}(z)}{|z|} \sqrt{\gamma_T(z) f_T(z)}\, F_{\psi z} \right) \right\} + \frac{N\sqrt{2}}{68\pi^2} \epsilon^{\psi MNPQ} F_{MN} F_{PQ} = 0 \,. \tag{5.152}$$

This system of equations is very hard to solve in general. Following [165], and what we have done for the straight string configuration, we can linearize the equations of motion, neglecting the non-linear terms since they are small for large λ and because we look for solutions in the large-z region. In this regime, the monopole solution found in the previous section is not spoiled. We can thus study the linearized equations of motion for A_t and A_ψ (5.151), (5.152), searching for curved space Green

[17] Under the reasonable assumption that the gauge field still depends only on (ρ, x_3, z) and the parameter l.

functions sourced by a circular loop distribution

$$\frac{4R^3}{9u_J}\frac{|z|}{k^{5/6}(z)}\sqrt{\frac{1}{f_T(z)\gamma_T(z)}}\left[\partial_\rho\left(\rho\,\partial_\rho A_t\right)+\rho\,\partial_{x_3}^2 A_t\right]+ \rho\,\partial_z\left(\frac{k^{3/2}(z)}{|z|}\sqrt{\frac{\gamma_T(z)}{f_T(z)}}\,\partial_z A_t\right)\sim\delta(x_3)\delta(\rho-l)\delta(z)\,, \tag{5.153}$$

$$\frac{4R^3}{9u_J}\frac{|z|}{k^{5/6}(z)}\sqrt{\frac{f_T(z)}{\gamma_T(z)}}\left[\partial_\rho\left(\frac{1}{\rho}\partial_\rho A_\psi\right)+\frac{1}{\rho}\partial_{x_3}^2 A_\psi\right]+ \frac{1}{\rho}\,\partial_z\left(\frac{k^{3/2}(z)}{|z|}\sqrt{\gamma_T(z)f_T(z)}\,\partial_z A_\psi\right)\sim\delta(x_3)\delta(\rho-l)\delta(z)\,. \tag{5.154}$$

To solve these equations we define A_t and A_ψ as Green's functions in curved space,[18]

$$A_t(\rho,x_3,z;l)\sim\sum_{n=1}^{\infty}\alpha_n(0)\alpha_n(z)E_n(\rho,x_3;l)\,, \tag{5.155}$$

$$A_\psi(\rho,x_3,z;l)\sim\sum_{n=1}^{\infty}\beta_n(0)\beta_n(z)F_n(\rho,x_3;l)\,, \tag{5.156}$$

where functions α_n and β_n are defined in (5.58), (5.59), and the formulas below them.

The modes E_n and F_n are the solutions of the infinite set of equations

$$\frac{1}{\rho}\partial_\rho\left(\rho\,\partial_\rho E_n(\rho,x_3;l)\right)+\partial_{x_3}^2 E_n(\rho,x_3;l)-\frac{9u_J}{4R^3}a_n E_n(\rho,x_3;l)=\delta(\rho-l)\delta(x_3)\,, \tag{5.157}$$

$$\rho\,\partial_\rho\left(\frac{1}{\rho}\partial_\rho F_n(\rho,x_3;l)\right)+\partial_{x_3}^2 F_n(\rho,x_3;l)-\frac{9u_J}{4R^3}b_n F_n(\rho,x_3;l)=\delta(\rho-l)\delta(x_3)\,. \tag{5.158}$$

In order to solve these equations we have to perform the Fourier transform and use the Green theorem

$$E_n(\rho,x_3;l)=\int_{-\infty}^{+\infty}\frac{dk}{2\pi}e^{ikx_3}\hat{E}_n(\rho,k;l)\,, \tag{5.159}$$

$$F_n(\rho,x_3;l)=\int_{-\infty}^{+\infty}\frac{dk}{2\pi}e^{ikx_3}\hat{F}_n(\rho,k;l)\,. \tag{5.160}$$

Following the same computations we have done for the monopole solution we get

$$\frac{1}{\rho}\partial_\rho\left(\rho\,\partial_\rho\hat{E}_n\right)-\left(k^2+\frac{9u_J}{4R^3}a_n\right)\hat{E}_n=\delta(\rho-l)\,, \tag{5.161}$$

$$\rho\,\partial_\rho\left(\frac{1}{\rho}\partial_\rho\hat{F}_n\right)-\left(k^2+\frac{9u_J}{4R^3}b_n\right)\hat{F}_n=\delta(\rho-l)\,, \tag{5.162}$$

[18] We set to zero the center of mass moduli (X_3, Z), as we did previously in this chapter.

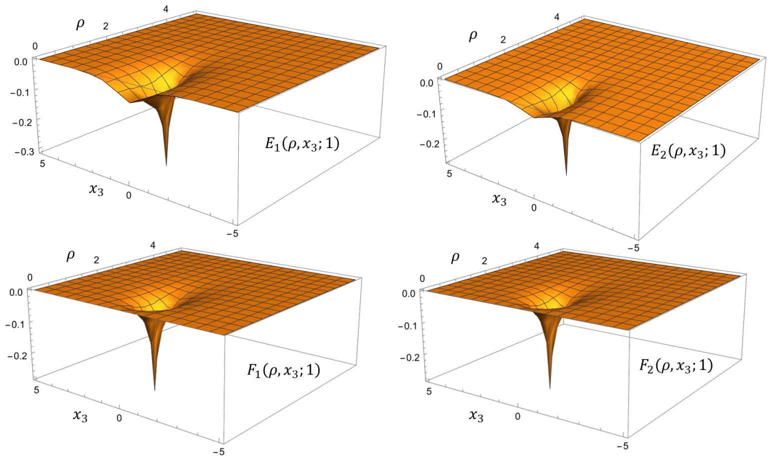

Figure 5.16. The first modes of $E_n(\rho, x_3; l)$ and $F_n(\rho, x_3; l)$ for $l = 1$, $9u_J/(4R^3) = 1$ and $\tilde{b} = 0.1$.

whose solutions are

$$\hat{E}_n(\rho, k, l) = \begin{cases} -I_0\left(l\sqrt{k^2 + \frac{9u_J}{4R^3}a_n}\right) K_0\left(\rho\sqrt{k^2 + \frac{9u_J}{4R^3}a_n}\right) & \rho > l\,, \\ -K_0\left(l\sqrt{k^2 + \frac{9u_J}{4R^3}a_n}\right) I_0\left(\rho\sqrt{k^2 + \frac{9u_J}{4R^3}a_n}\right) & \rho < l\,. \end{cases} \tag{5.163}$$

$$\hat{F}_n(\rho, k, l) = \begin{cases} -l\rho I_1\left(l\sqrt{k^2 + \frac{9u_J}{4R^3}b_n}\right) K_1\left(\rho\sqrt{k^2 + \frac{9u_J}{4R^3}b_n}\right) & \rho > l\,, \\ -l\rho K_1\left(l\sqrt{k^2 + \frac{9u_J}{4R^3}b_n}\right) I_1\left(\rho\sqrt{k^2 + \frac{9u_J}{4R^3}b_n}\right) & \rho < l\,. \end{cases} \tag{5.164}$$

Figure 5.16 shows the plots of the first modes E_n and F_n for $l = 1$, $9u_J/(4R^3) = 1$ and $\tilde{b} = 0.1$. They are obtained by numerically performing the Fourier transforms (5.159) and (5.160). Physically, they are the excitation modes of the t and ψ components of the field theory vector mesons, whose non-trivial profiles encompass the charge of the string loop.

We conclude this section by writing the effective action arising from the on-shell

Maxwellian DBI action. For A_t we have

$$
\begin{aligned}
S^{\mathrm{DBI}}_{A_t} &\sim \frac{\lambda N}{9\cdot 2^5\pi^3 M_{KK}}\sqrt{\frac{u_J}{R^3}}\int d^4x\,dz\bigg\{\frac{|z|}{k^{5/6}(z)\sqrt{\gamma_T(z)f_T(z)}}[F^2_{tx_3}+F^2_{t\rho}]+\\
&\quad+\frac{9u_J}{4R^3}\frac{k^{3/2}(z)}{|z|}\sqrt{\frac{\gamma_T(z)}{f_T(z)}}\,F^2_{tz}\bigg\} =\\
&=\frac{\lambda N}{9\cdot 2^5\pi^3 M_{KK}}\sqrt{\frac{u_J}{R^3}}\sum_{n=1}^{\infty}\sum_{m=1}^{\infty}\alpha_n(0)\alpha_m(0)\int d^4x\,dz\bigg\{\frac{|z|\,\alpha_n(z)\alpha_m(z)}{k^{5/6}(z)\sqrt{\gamma_T(z)f_T(z)}}\cdot\\
&\quad\cdot[(\partial_{x_3}E_n)^2+(\partial_\rho E_n)^2]+\frac{9u_J}{4R^3}\frac{k^{3/2}(z)}{|z|}\sqrt{\frac{\gamma_T(z)}{f_T(z)}}\,\partial_z\alpha_n(z)\partial_z\alpha_m(z)E_nE_m\bigg\} =\\
&=\frac{\lambda N}{9\cdot 2^5\pi^3 M_{KK}}\sqrt{\frac{u_J}{R^3}}\sum_{n=1}^{\infty}\alpha_n^2(0)\int d^4x\bigg\{(\partial_{x_3}E_n)^2+(\partial_\rho E_n)^2+\frac{9u_J}{4R^3}a_nE_n^2\bigg\}.
\end{aligned}
\tag{5.165}
$$

We can define

$$
\varepsilon_n(\rho,x_3;l)=\sqrt{\frac{\lambda N}{9\cdot 2^4\pi^3 M_{KK}}\sqrt{\frac{u_J}{R^3}}}\,\alpha_n(0)E_n(\rho,x_3;l), \tag{5.166}
$$

to get

$$
S^{\mathrm{DBI}}_{A_t}\sim\frac{1}{2}\sum_{n=1}^{\infty}\int d^4x\bigg\{(\partial_{x_3}\varepsilon_n)^2+(\partial_\rho\varepsilon_n)^2+\frac{9u_J}{4R^3}a_n\varepsilon_n^2\bigg\}. \tag{5.167}
$$

We can do the same thing for A_ψ:

$$
\begin{aligned}
S^{\mathrm{DBI}}_{A_\psi} &\sim -\frac{\lambda N}{9\cdot 2^5\pi^3 M_{KK}}\sqrt{\frac{u_J}{R^3}}\int\frac{d^4x}{\rho^2}\,dz\bigg\{\frac{|z|}{k^{5/6}(z)}\sqrt{\frac{f_T(z)}{\gamma_T(z)}}[F^2_{\psi x_3}+F^2_{\psi\rho}]+\\
&\quad+\frac{9u_J}{4R^3}\frac{k^{3/2}(z)}{|z|}\sqrt{\gamma_T(z)f_T(z)}\,F^2_{\psi z}\bigg\} =\\
&=-\frac{\lambda N}{9\cdot 2^5\pi^3 M_{KK}}\sqrt{\frac{u_J}{R^3}}\sum_{n=1}^{\infty}\sum_{m=1}^{\infty}\alpha_n(0)\alpha_m(0)\cdot\\
&\quad\cdot\int\frac{d^4x}{\rho^2}\,dz\bigg\{\frac{|z|}{k^{5/6}(z)}\sqrt{\frac{f_T(z)}{\gamma_T(z)}}\,\beta_n(z)\beta_m(z)[(\partial_{x_3}F_n)^2+(\partial_\rho F_n)^2]+\\
&\quad+\frac{9u_J}{4R^3}\frac{k^{3/2}(z)}{|z|}\sqrt{\gamma_T(z)f_T(z)}\,\partial_z\beta_n(z)\partial_z\beta_m(z)F_nF_m\bigg\} =\\
&=-\frac{\lambda N}{9\cdot 2^5\pi^3 M_{KK}}\sqrt{\frac{u_J}{R^3}}\sum_{n=1}^{\infty}\beta_n^2(0)\int\frac{d^4x}{\rho^2}\bigg\{(\partial_{x_3}F_n)^2+(\partial_\rho F_n)^2+\frac{9u_J}{4R^3}b_nF_n^2\bigg\},
\end{aligned}
\tag{5.168}
$$

and define

$$
\varsigma_n(\rho,x_3;l)=\sqrt{\frac{\lambda N}{9\cdot 2^4\pi^3 M_{KK}}\sqrt{\frac{u_J}{R^3}}}\,\beta_n(0)\frac{F_n(\rho,x_3;l)}{\rho}, \tag{5.169}
$$

so that we can write

$$S^{\mathrm{DBI}}_{A_\psi} \sim -\frac{1}{2}\sum_{n=1}^{\infty}\int d^4x\left\{(\partial_{x_3}\varsigma_n)^2+(\partial_\rho\varsigma_n)^2+\left(\frac{1}{\rho^2}+\frac{9u_J}{4R^3}b_n\right)\varsigma_n^2\right\}. \tag{5.170}$$

Promoting the derivatives to the four coordinates, the actions (5.167), (5.170) represent the four-dimensional effective actions for the charged modes of the vortons. They are nothing else than the reduced actions, in cylindrical coordinates, for the D8 gauge field components "longitudinal" to the circular source, *i.e.* A_t and A_ψ, corresponding to two components of the (tower of) vector mesons.[19]

Currents in the deconfined phase of the WSS model

In this section, we compute the currents associated with the WSS flavor symmetry in the deconfined phase. The procedure is analogous to the computation of the chiral currents in the confined phase of the WSS model [165]. In order to study the flavor currents, it is useful to introduce external gauge fields $\mathcal{A}_{L\,\mu}$, $\mathcal{A}_{R\,\mu}$, associated to the chiral symmetry $\mathrm{U}(N_f)_L\times\mathrm{U}(N_f)_R$ in Minkowski space. The chiral currents $\mathcal{J}^\mu_L$, $\mathcal{J}^\mu_R$ can be read off from the action term that is linear in the external gauge fields:

$$S_{\mathrm{eff}}[\mathcal{A}_L,\mathcal{A}_R] = -2\int d^4x\,\mathrm{tr}\,(\mathcal{A}_{L\,\mu}\mathcal{J}^\mu_L+\mathcal{A}_{R\,\mu}\mathcal{J}^\mu_R)\,. \tag{5.171}$$

We can trade the left and right components for the vectorial and axial components of the current

$$S_{\mathrm{eff}}[\mathcal{A}_L,\mathcal{A}_R] = -2\int d^4x\,\mathrm{tr}\left(\mathcal{V}^{(+)}_\mu\mathcal{J}^\mu_V+\mathcal{V}^{(-)}_\mu\mathcal{J}^\mu_A\right), \tag{5.172}$$

where

$$\mathcal{J}^\mu_V=\mathcal{J}^\mu_L+\mathcal{J}^\mu_R\,,\qquad \mathcal{J}^\mu_A=\mathcal{J}^\mu_L-\mathcal{J}^\mu_R\,,\qquad \mathcal{V}^{(\pm)}_\mu=\frac{\mathcal{A}_{\mu,L}\pm\mathcal{A}_{\mu,R}}{2}\,. \tag{5.173}$$

In the WSS model the chiral symmetry is identified with the constant gauge transformation at $z=\pm\infty$, and the external gauge fields $\mathcal{A}_{L\,\mu}$, $\mathcal{A}_{R\,\mu}$ can be introduced by the following boundary conditions for the five-dimensional fields

$$\mathcal{A}_\mu(x^\mu,z\to+\infty)=\mathcal{A}_{\mu,L}(x^\mu)\,,\qquad \mathcal{A}_\mu(x^\mu,z\to-\infty)=\mathcal{A}_{\mu,R}(x^\mu)\,. \tag{5.174}$$

In order to write down an expression for the current, we need to compute the first variation of the action. Let us consider the connection

$$\mathcal{A}_M(x^\mu,z)=\mathcal{A}^{\mathrm{cl}}_M(x^\mu,z)+\delta\mathcal{A}_M(x^\mu,z)\,, \tag{5.175}$$

such that $\mathcal{A}^{\mathrm{cl}}_M(x^\mu,z)$ is a classical solution to the equations of motion with boundary conditions $\mathcal{A}^{\mathrm{cl}}_M(x^\mu,z\to\pm\infty)=0$ while $\delta\mathcal{A}_M(x^\mu,z)$ is a small deviation from the classical solution such that

$$\delta\mathcal{A}_\mu(x^\mu,z\to+\infty)=\mathcal{A}_{L\,\mu}(x^\mu),\qquad \delta\mathcal{A}_\mu(x^\mu,z\to-\infty)=\mathcal{A}_{R\,\mu}(x^\mu)\,. \tag{5.176}$$

[19] The masses appearing in the four-dimensional effective actions are different for the various components due to the breaking of Lorentz invariance by the temperature and the choice of cylindrical coordinates.

Remember that for the one-flavored case $\mathcal{A} = A/\sqrt{2}$, with A the U(1) gauge field.

The background metric in the deconfined phase breaks the covariance in the Minkowski space but it is straightforward to find the currents as in the confined background. The DBI action for the D8-brane expanded at quadratic order is

$$S_{\rm D8}^{\rm DBI} = -\frac{T_8 V_4 R^{3/2}(2\pi\alpha')^2}{4g_s}\int d^4x\,dz\,u^{5/2}\sqrt{\frac{f_T(u)}{\gamma_T(u)}}\left|\frac{\partial u}{\partial z}\right|\left[\frac{1}{2}\left(\frac{R}{u}\right)^3 F_{ij}^2 + \right.$$
$$\left. -\left(\frac{R}{u}\right)^3\frac{F_{ti}^2}{f_T(u)}\left|\frac{\partial u}{\partial z}\right|^{-2}\frac{\gamma_T(u)}{f_T(u)}F_{tz}^2 + \left|\frac{\partial u}{\partial z}\right|^{-2}\gamma_T(u)F_{iz}^2\right].$$

The CS term leads to a vanishing boundary term (at $z \to \pm\infty$) and hence it does not contribute to the current computation. This is why we will not consider the CS term in this section even if it does contribute to the bulk action and hence to the equations of motion for the gauge field.

We consider a small deviation δA_M from the classical solution to the equation of motion obeying the boundary conditions (5.176). The field strength components can be written as

$$\begin{aligned}
F_{ij}^2 &= \left(F_{ij}^{\rm cl}\right)^2 + 2\eta^{ik}\eta^{jl}F_{kl}^{\rm cl}\left(\partial_i\delta A_j - \partial_j\delta A_i\right),\\
F_{ti}^2 &= \left(F_{ti}^{\rm cl}\right)^2 + 2F_{ti}^{\rm cl}\left(\partial_t\delta A_i - \partial_i\delta A_t\right),\\
F_{tz}^2 &= \left(F_{tz}^{\rm cl}\right)^2 + 2F_{tz}^{\rm cl}\left(\partial_t\delta A_z - \partial_z\delta A_t\right),\\
F_{iz}^2 &= \left(F_{iz}^{\rm cl}\right)^2 + 2F_{iz}^{\rm cl}\left(\partial_i\delta A_z - \partial_z\delta A_i\right),
\end{aligned}$$

where the coefficients η_{MN} $(M, N = t, x_1, x_2, x_3, z)$ refer to the five-dimensional flat metric.

In order to read off the flavor currents we look at the terms with derivatives w.r.t. the holographic direction z since they give the boundary terms of the action:

$$\begin{aligned}
S_{\rm bdry} &= \frac{T_8 V_4 R^{3/2}(2\pi\alpha')^2}{2g_s}\int d^4x\,dz\,\partial_z\left[u^{5/2}\left|\frac{\partial u}{\partial z}\right|^{-1}\left(\sqrt{\frac{\gamma_T(u)}{f_T(u)}}\,\eta^{tt}F_{tz}^{cl}\delta A_t + \right.\right.\\
&\left.\left. + \sqrt{\gamma_T(u)f_T(u)}\,\eta^{ij}F_{iz}^{cl}\delta A_j\right)\right] =\\
&= \frac{T_8 V_4 R^{3/2}(2\pi\alpha')^2}{2g_s}\int d^4x\left[u^{5/2}\left|\frac{\partial u}{\partial z}\right|^{-1}\left(\sqrt{\frac{\gamma_T(u)}{f_T(u)}}\,\eta^{tt}F_{tz}^{cl}\delta A_t + \right.\right.\\
&\left.\left. + \sqrt{\gamma_T(u)f_T(u)}\,\eta^{ij}F_{iz}^{cl}\delta A_j\right)\right]\Bigg|_{z=-\infty}^{z=+\infty}.
\end{aligned}$$

Following the prescription (5.171), the chiral currents can be written as

$$J_L^t = -\kappa_J \left[\frac{k(z)^{3/2}}{|z|} \sqrt{\frac{\gamma_T(z)}{f_T(z)}}\, \eta^{tt} F_{tz}^{\mathrm{cl}} \right]\Big|_{z=+\infty} , \tag{5.177}$$

$$J_R^t = \kappa_J \left[\frac{k(z)^{3/2}}{|z|} \sqrt{\frac{\gamma_T(z)}{f_T(z)}}\, \eta^{tt} F_{tz}^{\mathrm{cl}} \right]\Big|_{z=-\infty} , \tag{5.178}$$

$$J_L^i = -\kappa_J \left[\frac{k(z)^{3/2}}{|z|} \sqrt{\gamma_T(z) f_T(z)}\, \eta^{ij} F_{jz}^{\mathrm{cl}} \right]\Big|_{z=+\infty} , \tag{5.179}$$

$$J_R^i = \kappa_J \left[\frac{k(z)^{3/2}}{|z|} \sqrt{\gamma_T(z) f_T(z)}\, \eta^{ij} F_{jz}^{\mathrm{cl}} \right]\Big|_{z=-\infty} , \tag{5.180}$$

where κ_J has been defined in (5.43).

From these expressions, we can extract the vectorial and axial components of the currents:

$$J_V^t = -\kappa_J \left[\frac{k(z)^{3/2}}{|z|} \sqrt{\frac{\gamma_T(z)}{f_T(z)}}\, \eta^{tt} F_{tz}^{\mathrm{cl}} \right]\Big|_{z=-\infty}^{z=+\infty} , \tag{5.181}$$

$$J_A^t = -\kappa_J \left[\frac{\psi_0(z) k(z)^{3/2}}{|z|} \sqrt{\frac{\gamma_T(z)}{f_T(z)}}\, \eta^{tt} F_{tz}^{\mathrm{cl}} \right]\Big|_{z=-\infty}^{z=+\infty} , \tag{5.182}$$

$$J_V^i = -\kappa_J \left[\frac{k(z)^{3/2}}{|z|} \sqrt{\gamma_T(z) f_T(z)}\, \eta^{ij} F_{jz}^{\mathrm{cl}} \right]\Big|_{z=-\infty}^{z=+\infty} , \tag{5.183}$$

$$J_A^i = -\kappa_J \left[\frac{\psi_0(z) k(z)^{3/2}}{|z|} \sqrt{\gamma_T(z) f_T(z)}\, \eta^{ij} F_{jz}^{\mathrm{cl}} \right]\Big|_{z=-\infty}^{z=+\infty} , \tag{5.184}$$

where $\psi_0(z) = \frac{2}{\pi}\arctan(z)$. We will drop the apex "cl." from now on.

We can use these results to compute the baryon number current (and in general all the other components of the currents J_R and J_L) associated with the electric potential A_t. This fixes the proportionality constant in front of the solution (5.155) for A_t to $K = -(3^2 2^3 \pi^3 R^{3/2})/(u_J^{1/2} M_{KK}\lambda)$:

$$\begin{aligned} J_B^t &= \frac{2}{N} J_V^t = -\frac{2}{N}\kappa_J \left[\frac{k^{3/2}(z)}{|z|} \sqrt{\frac{\gamma_T(z)}{f_T(z)}} \eta^{tt} F_{tz} \right] \Big|_{z=-\infty}^{z=+\infty} \\ &= K\kappa_J \sum_{n=1}^{\infty} \alpha_n(0) E_n(\rho, x_3; l) \left[\frac{k^{3/2}(z)}{|z|} \sqrt{\frac{\gamma_T(z)}{f_T(z)}} \partial_z \alpha_n(z) \right] \Big|_{z=-\infty}^{z=+\infty} = \\ &= K\kappa_J \sum_{n=1}^{\infty} g^{\alpha}_{V^n} \alpha_{2n-1}(0) E_{2n-1}(\rho, x_3; l)\,, \end{aligned} \tag{5.185}$$

where we have defined the decay constants associated with the eigenfunctions $\alpha_n(z)$ as

$$g^{\alpha}_{V^n} = a_{2n-1} \int dz\, \frac{|z|}{k^{5/6}(z)} \frac{\alpha_{2n-1}(z)}{\sqrt{\gamma_T(z) f_T(z)}}\,, \qquad g^{\alpha}_{A^n} = a_{2n} \int dz\, \frac{|z|}{k^{5/6}(z)} \frac{\alpha_{2n}(z)\psi_0(z)}{\sqrt{\gamma_T(z) f_T(z)}}\,.$$

A direct application of this formula is to compute the baryon number charge

$$\begin{aligned}
n_B &= \int_{-\infty}^{+\infty} dx_3 \int_0^{\infty} \rho \, d\psi \, d\rho \, \langle J_B^t \rangle = 2\pi \int_{-\infty}^{+\infty} dx_3 \int_0^{\infty} \rho \, d\rho \, \langle J_B^t \rangle \\
&= 2\pi \frac{9u_J}{4R^3} \sum_{n=1}^{\infty} g_{V^n}^{\alpha} \langle \alpha_{2n-1}(0) \rangle \int_{-\infty}^{+\infty} dx_3 \int_0^{\infty} \rho \, d\rho \, E_{2n-1}(\rho, x_3; l) = \\
&= \sum_{n=1}^{\infty} \frac{g_{V^n}^{\alpha}}{a_{2n-1}} \langle \alpha_{2n-1}(0) \rangle = 1 \,,
\end{aligned} \tag{5.186}$$

where we used the properties of the Fourier transform and the addition sum rule of Bessel functions. Note that this definition of baryon number is equivalent to the one given in terms of the CS term in equation (5.78) (plus total derivatives) by using the equations of motion.

Chapter 6

Holographic baryons as quantum Hall droplets

In this chapter, we finally provide a first-principle construction of baryons as quantum Hall droplets in a QCD-like theory admitting a holographic dual. We observed at the beginning of chapter 2 that in QCD-like theories with gauge group $\mathrm{SU}(N)$ and a single massless flavor ($N_f = 1$), the low-energy description of baryons as solitonic Skyrmions is not available. This puzzle can be overcome by following the ideas of [40, 41, 42, 43, 44], and recently carried on by Komargodski in [38]. In the planar limit of these theories, baryons at low energy should correspond to some kind of "brane-like" objects related to the singular locus of the low-energy η' potential defined by $\eta' = \pi$. Moreover, on the worldvolume of these objects, there should live a (2+1)-dimensional $\mathrm{U}(1)_N$ Chern-Simons theory [38]. In this respect, the baryons would be analogous to the quantum Hall droplets of the fractional Hall system.

Several expected properties of the baryons have been derived from these premises, yet precise quantitative statements are, as usual, difficult to achieve from purely effective descriptions [40, 41, 42, 43, 44, 38, 45, 46, 47, 48, 49, 50, 51, 52].

In this chapter, based on [6], we adopt the WSS model as a playground theory to construct the one-flavored baryon. We will focus on its D6-brane description, corresponding to the gluonic core of the baryons. In the language introduced in chapter 4, we do not consider here its mesonic description given in terms of the flavor brane gauge field. We also construct related configurations, such as vortons, "sandwich vortons" and domain walls with holes, study their stability, and (some of) their possible decay channels.

In section 6.1, which constitutes the core of this chapter, we set up the study of various configurations, including the baryons, as D6-branes ending on the flavor D8-brane with a circular boundary, in both confined and deconfined phases. Indeed, as we have seen in the previous chapters, the D6-brane is the object realizing the correct monodromy of the field dual to the η' [1], and after reduction on the four-sphere of the background, it naturally hosts on its worldvolume the $\mathrm{U}(1)_N$ CS theory advocated in [38]. In order to describe a (meta)stable baryon as a quantum Hall droplet, as well as other baryonic configurations, it is necessary to consider charged configurations under the baryonic symmetry. This corresponds to switching on an electromagnetic field on the D6-branes.

We thus describe in detail the equations of motion, variational principle, boundary conditions, and the relations between the baryon charge n_B, the quark charge q_s, and the spin J associated with the D6-brane. In particular, we study configurations such that $J = n_B^2 N/2$ (as in the standard Fractional Quantum Hall Effect) - this reduces to the expected relation $J = N/2$ for the elementary $n_B = 1$ baryon made by N quarks with aligned spins. By analyzing the topology of the configuration, we are able to identify the solitonic mode living on the boundary of the droplet and carrying integer baryonic charge, in close analogy to the description of the electron in the FQHE. Perhaps not surprisingly, the solitonic mode is a would-be gauge mode of the gauge connection on the D6-brane worldvolume.

Section 6.2 is devoted to the presentation of the (numerical) solution corresponding to the baryon, *i.e.* the embedding profile and the electromagnetic field of the D6-brane. The solution allows to compute precisely, from first principles, the baryon properties, such as its mass and radius. As envisaged in [38], while the mass scales linearly with the number of colors N, as customary for baryons in the planar limit [16], the radius is N-independent. Instead, both these observables depend on the 't Hooft coupling λ, the chiral symmetry breaking scale $f_{(T),\eta'}$, and the temperature (in the deconfined phase). In particular, it turns out that these baryons are small particles in the holographic regime, with size suppressed by the large value of λ, as in the case of the standard $N_f \geq 2$ baryons in the WSS model [28, 165] (but with a different power law suppression).

The charged string loops, *i.e.* the vortons, are studied in detail in section 6.3. As we have seen in the previous chapter, they correspond to a D6-brane extended from the flavor brane tip, where it has a circular boundary, to the horizon of the finite temperature WSS background. We will find that stable vortons with baryon number $n_B \sim \lambda^0$ do not exist. The only way to find metastable vortons is if they carry a very large charge $n_B \sim \lambda$. Then, we will connect these findings with the results coming from the D8-brane analysis presented in section 5.3.

In section 6.4, we study two different but related configurations: a domain wall with a hole and a "sandwich vorton", briefly introduced in section 5.2. Both correspond to a D6-brane with a circular boundary at the D8-brane tip (as the baryon). The former is expected to play a role in the decay of infinite domain walls, which develop holes that eventually eat up all their worldvolume. We concentrate on metastable configurations with baryonic charge, but analogous metastable uncharged solutions and unstable solutions exist as well.

The "sandwich vorton" is a charged string loop whose structure depends on two different fields. A prototype example is the "axionic-η' string" (or the "axionic-pionic" string) [41]. In the holographic model, it corresponds to a cylindrical D6-brane terminating on two D8-branes whose tips are at different holographic radial positions. In the WSS model, it can carry baryonic charge, which makes it (meta)stable.

Section 6.5 discusses possible decay channels between various configurations: baryons, "sandwich vortons", ordinary vortons, quarks (in the deconfined phase). The discussion is based on energy and charge considerations. The results are non-trivial "phase diagrams" highlighting the most stable configurations depending on the theory parameters (*e.g.* $f_{\eta',a}$, temperature, λ).

Finally, Appendix C provides more details on the topology of the solutions, while appendix D describes the numerical integration procedure followed to solve the equations in the main body of this chapter.

6.1 The D6-brane system

In this section, we present a detailed analysis of the Euler-Lagrange equations and the related variational problem for a D6-brane wrapped on the background S^4, extended along the holographic coordinate u with a circular boundary at the tip of a U-shaped D8-brane. We find a zoo of solutions associated with different D6-brane profiles. We present the analysis in both the confined and deconfined phases of the WSS model.[1]

The worldvolume action for the D6-brane is composed of two parts: the Dirac-Born-Infeld action and the Chern-Simons one. We remind the reader that this reads

$$S_{\text{D6}}^{\text{DBI}} = -T_6 \int d^7x\, e^{-\phi} \sqrt{-\det\left(g + (2\pi l_s^2)\, f + B\right)}\,, \tag{6.1}$$

where $T_6 = (2\pi)^{-6} l_s^{-7}$ is the D6-brane tension and f is the field strength associated to the U(1) gauge connection a living on the D6-brane worldvolume. Locally, we can write $f = da$. The Kalb-Ramond field B appearing in the DBI action will be set to zero, as always in this thesis. Integrating out the four-sphere, the above action reduces effectively to the DBI action of a membrane with a three-dimensional worldvolume M_3. The worldvolume coordinates of the manifold M_3 are identified with t, ψ, u, where ψ is the polar angular variable of a circle in Minkowski, whose radius $\rho(u)$ (which we take to be (t,ψ)-independent) has to be determined by solving the Euler-Lagrange equation. The manifold M_3 has a boundary ∂M_3, which has in general a non-trivial topology. It has one connected circular component in u_J, and depending on the nature of the solution for $\rho(u)$, it might have a second connected component at the position where the D6-brane ends, which we denote by u_*. In the following, we use the convention $\epsilon^{t\psi u} = +1$ which is equivalent to $dt \wedge d\psi \wedge du = dt\, d\psi\, du$. Note that this induces an orientation on ∂M_3, spanned by ψ, t.

The Chern-Simons action for the D6-brane is given by

$$\begin{aligned} S_{\text{D6}}^{\text{CS}} &= \frac{1}{8\pi^2} \int C_3 \wedge f \wedge f = \\ &= \frac{N}{4\pi} \int_{M_3} a \wedge f - \frac{1}{8\pi^2} \int_{\partial \text{D6}} C_3 \wedge a \wedge f\,, \end{aligned} \tag{6.2}$$

where in the last equality, we have integrated by parts and used $\int_{S^4} F_4 = 2\pi N$. We have also used that $d^2 a = 0$, and we denoted with ∂D6 the boundary of the seven-dimensional D6-brane worldvolume. The effective theory on the D6-brane is thus described by a three-dimensional DBI-CS action with $\text{U}(1)_N$ CS term [179, 141]. In the case of a D6-brane with a boundary $\partial\text{D6} = \partial M_3 \times S^4$, there is also a six-dimensional boundary term. Since in the previous sections we were not interested in the charged D6-brane, we always forgot about such a boundary term.

[1] Let us remind that the physics of fractional quantum Hall effects has been studied widely in the literature. See, for example [177, 178] and related works.

Let us comment on this result. The authors of [32], following the results presented in the seminal paper [133], observe that the standard Wess-Zumino term, involving a RR form C, for a wrapped brane in the presence of a non-trivial flux on the compact manifold, has to be traded (integrating by parts) with the term involving the field strength of C. This is the case whenever C is not single-valued. Looking at (6.2), the first line has to be traded with the first term of the second line. However, our configuration is more complicated than the one described in [133, 32], since we have a physical boundary. This leads to the presence of a boundary term in the second line of (6.2), involving explicitly C_3, which could be problematic as well. Anyway, we are going to impose that the gauge connection vanishes at the boundary of the D6-brane worldvolume ∂D6:[2]

$$f \underset{\partial \mathrm{D6}}{=} 0\,. \tag{6.3}$$

This way, the CS theory on the D6-brane worldvolume reduces effectively to three-dimensional $\mathrm{U}(1)_N$ CS theory, ubiquitous in this thesis.

Let us comment now on the gauge invariance of the theory. Consider the first line of (6.2), since the action depends only on the gauge curvature f, it is manifestly gauge invariant. However, after the integration by parts, performed in the second line of (6.2), the two terms are not independently gauge invariant. In particular, the $\mathrm{U}(1)_N$ CS theory alone is not gauge invariant if the manifold M_3 has a boundary (see *e.g.* [180]). We study this issue by allowing for a general variation of the gauge connection $a \to a + \delta a$, and then by specializing this variation to a gauge transformation. The corresponding variation of the CS action to first order in the fluctuations reads

$$\delta S_{CS} = \frac{N}{4\pi} \int_{M_3} d(\delta a \wedge a) + 2\delta a \wedge da\,. \tag{6.4}$$

In the specific case of a pure gauge transformation, we have $\delta a = -ig^{-1}dg = d\varphi$, where $g = e^{i\varphi}$ is an element of $\mathrm{U}(1)$. With these definitions, the phase φ is a periodic scalar field with period 2π. We can use Stokes's theorem to rewrite (6.4) for pure gauge transformations:

$$\delta S_{CS} = \frac{N}{4\pi} \int_{M_3} d\varphi \wedge f = \frac{N}{4\pi} \int_{\partial M_3} \varphi\, f\,. \tag{6.5}$$

Therefore, the condition for gauge invariance is that the curvature of the connection a identically vanishes at the boundary:

$$f \underset{\partial M_3}{=} 0\,. \tag{6.6}$$

One can realize that this condition is nothing but the reduction on M_3, of the condition (6.3) that we imposed to get rid of the six-dimensional boundary term in the Wess-Zumino action. Note that we are considering a gauge connection a which does not depend on the four-sphere coordinates, and with null components along S^4. Therefore, imposing (6.3), we get for free the gauge invariance of the effective theory after the integration by parts.

[2] This condition preserves the gauge invariance of the RR form C_3 in the seven-dimensional D6-brane worldvolume with a boundary. This is not the only choice that preserves this gauge invariance.

A simple way to guarantee that (6.6) vanishes is to make an ansatz for the gauge connection corresponding to time-independent axisymmetric solutions, *i.e.* such that its components depend on the holographic coordinate u alone.[3] In addition, to simplify our study, in the following we will work in the radial gauge $a_u = 0$. Therefore, our gauge connection configuration will be given by

$$a_t(u)\,, \quad a_\psi(u)\,. \tag{6.7}$$

Let us now derive the equations of motion both in the confined and deconfined phases for the D6-brane embedding and its gauge connection. We do this assuming to have a well-posed variational problem, and then we will discuss how, imposing particular boundary conditions, this analysis is consistent.

Confining phase

We start with the Witten confining background (3.44). The induced metric on the D6-brane is

$$ds^2_{\rm D6} = \left(\frac{u}{R}\right)^{3/2}\left(-dt^2 + \rho^2(u)d\psi^2 + \left(\rho'(u)^2 + \left(\frac{R}{u}\right)^3 \frac{1}{f(u)}\right)du^2\right) + R^{3/2}u^{1/2}d\Omega_4^2\,. \tag{6.8}$$

After some algebra, the full action can be written as

$$S_{\rm D6} = -N\int dt \int_{u_*}^{u_J} du \left\{\frac{(a_t\,\partial_u a_\psi - a_\psi\,\partial_u a_t)}{2} + \frac{u\,\rho(u) D(u)}{3(2\pi l_s^2)^2}\right\}, \tag{6.9}$$

where we have introduced the function

$$D(u) = \sqrt{\rho'(u)^2\left(\frac{u}{R}\right)^3 + \frac{1}{f(u)} + (2\pi l_s^2)^2\left(\frac{(\partial_u a_\psi)^2}{\rho^2} - (\partial_u a_t)^2\right)}\,. \tag{6.10}$$

Let us now write the Euler-Lagrange equations for $\rho(u)$, $a_t(u)$, and $a_\psi(u)$, defining a Lagrangian density $\mathcal{L}_{\rm D6}$ from the action by

$$S = \int dt\, d\psi\, du\, \mathcal{L}_{\rm D6}. \tag{6.11}$$

The equations of motion read:

- Equation of motion for $\rho(u)$

$$\partial_u\left(\frac{u^4\rho'(u)\rho(u)}{D(u)}\right) = \frac{R^3 u}{D(u)}\left(\rho'(u)^2\left(\frac{u}{R}\right)^3 + \frac{1}{f(u)} - (2\pi l_s^2)^2(\partial_u a_t)^2\right). \tag{6.12}$$

- Equation of motion for $a_t(u)$

$$3\,\partial_u a_\psi + \partial_u\left(\frac{u\,\rho(u)\partial_u a_t}{D(u)}\right) = 0\,. \tag{6.13}$$

[3] Note that, with our choice of coordinates and orientation, the equation (6.6) can be written in components and reads $f_{t\psi} \underset{\partial M_3}{=} 0$. By choosing a time-independent axisymmetric configuration, this is automatically satisfied.

- Equation of motion for $a_\psi(u)$

$$3\,\partial_u a_t + \partial_u \left(\frac{u\,\partial_u a_\psi}{\rho(u) D(u)} \right) = 0\,. \tag{6.14}$$

We can rescale the gauge connection by a factor $(2\pi l_s^2)$ in such a way that there is no more explicit dependence on l_s in the equations:

$$\bar{a} = (2\pi l_s^2) a\,. \tag{6.15}$$

The equations of motion (6.13) and (6.14) for the gauge connection components are total derivatives, so from them we get

$$\frac{u\,\rho(u)}{D(u)} \partial_u \bar{a}_t + 3\bar{a}_\psi = \bar{\mathbf{k}}_t\,, \tag{6.16}$$

$$\frac{u}{\rho(u) D(u)} \partial_u \bar{a}_\psi + 3\bar{a}_t = \bar{\mathbf{k}}_\psi\,, \tag{6.17}$$

where $\bar{\mathbf{k}}_t$ and $\bar{\mathbf{k}}_\psi$ are two constants of motion to be fixed. As for the gauge connection, the barred constants are related to unbarred ones through $\bar{\mathbf{k}}_{t,\psi} \equiv 2\pi l_s^2\, \mathbf{k}_{t,\psi}$. Defining

$$\tilde{a}_\psi = \bar{a}_\psi - \frac{\bar{\mathbf{k}}_t}{3}\,, \qquad\qquad \tilde{a}_t = \bar{a}_t - \frac{\bar{\mathbf{k}}_\psi}{3}\,, \tag{6.18}$$

the equations of motion can be rewritten as

$$\begin{aligned} \frac{\partial}{\partial u}\left(\frac{u^4 \rho'(u) \rho(u)}{D(u)} \right) - R^3 u\, D(u) \left(1 - \frac{9}{u^2} \tilde{a}_t^2 \right) = 0\,, \\ \partial_u \tilde{a}_\psi + \frac{3}{u} \rho(u) D(u)\, \tilde{a}_t = 0\,, \\ \partial_u \tilde{a}_t + \frac{3}{u} \frac{D(u)}{\rho(u)}\, \tilde{a}_\psi = 0\,. \end{aligned} \tag{6.19}$$

Using the latter we can write $D(u)$ as

$$D(u) = \sqrt{ \frac{ \rho'(u)^2 \left(\dfrac{u}{R}\right)^3 + \dfrac{1}{f(u)} }{ 1 + \dfrac{9}{u^2} \left(\dfrac{\tilde{a}_\psi^2}{\rho^2(u)} - \tilde{a}_t^2 \right) } }\,. \tag{6.20}$$

This on-shell expression for $D(u)$ will be helpful in the numerical resolution of the differential equations.

Deconfined phase

In the deconfined phase, where the background metric is given by (3.115), a similar approach can be followed. The D6-brane induced metric reads

$$\begin{aligned} ds^2_{T,\,\mathrm{D6}} = \left(\frac{u}{R}\right)^{3/2} \left(-f_T(u) dt^2 + \rho^2(u) d\psi^2 + \left(\rho'(u)^2 + \left(\frac{R}{u}\right)^3 \frac{1}{f_T(u)} \right) du^2 \right) + \\ + R^{3/2} u^{1/2} d\Omega_4^2\,. \end{aligned} \tag{6.21}$$

The full D6-brane action is

$$S_{\rm D6} = -N \int dt \int_{u_*}^{u_J} du \left\{ \frac{(a_t\, \partial_u a_\psi - a_\psi\, \partial_u a_t)}{2} + \frac{u\, \rho(u) D_T(u)}{3(2\pi l_s^2)^2} \right\}, \tag{6.22}$$

where we have defined $D_T(u)$ as

$$D_T(u) = \sqrt{1 + \rho'(u)^2 \left(\frac{u}{R}\right)^3 f_T(u) + (2\pi l_s^2)^2 \left(\frac{f_T(u)(\partial_u a_\psi)^2}{\rho^2(u)} - (\partial_u a_t)^2 \right)}\,. \tag{6.23}$$

Using the rescaling (6.15) the equations of motion read

$$\partial_u \left(\frac{u\, \rho(u)}{D_T(u)} \left(\frac{u}{R}\right)^3 f_T(u) \rho'(u) \right) - u\, D_T(u) + \frac{u\, f_T(u)}{D_T(u)} \frac{(\partial_u \bar{a}_\psi)^2}{\rho^2(u)} = 0\,, \tag{6.24}$$

$$\frac{u\, \rho(u)}{D_T(u)} \partial_u \bar{a}_t + 3\bar{a}_\psi = \bar{\mathbf{k}}_t\,, \tag{6.25}$$

$$\frac{u}{D_T(u)} \frac{f_T(u)}{\rho(u)} \partial_u \bar{a}_\psi + 3\bar{a}_t = \bar{\mathbf{k}}_\psi\,, \tag{6.26}$$

where $\bar{\mathbf{k}}_t$ and $\bar{\mathbf{k}}_\psi$ are two constants of motion which, despite we adopt the same notations, are *a priori* different from their counterparts in the confined phase.

Using the analogous redefinition as in (6.18), the complete set of equations of motion in the deconfined phase can be written as

$$\begin{aligned} \partial_u \left(\frac{u^4 \rho'(u) \rho(u) f_T(u)}{D_T(u)} \right) - R^3 u\, D_T(u) \left(1 - \frac{9\tilde{a}_t^2}{u^2 f_T(u)} \right) = 0\,, \\ \partial_u \tilde{a}_\psi + \frac{3}{u\, f_T(u)} \rho(u)\, D_T(u)\, \tilde{a}_t = 0\,, \\ \partial_u \tilde{a}_t + \frac{3}{u} \frac{D_T(u)}{\rho(u)}\, \tilde{a}_\psi = 0\,. \end{aligned} \tag{6.27}$$

Using the latter we can rewrite $D_T(u)$ as

$$D_T(u) = \sqrt{\frac{1 + \rho'(u)^2 \left(\frac{u}{R}\right)^3 f_T(u)}{1 + \frac{9}{u^2} \left(\frac{\tilde{a}_\psi^2}{\rho^2(u)} - \frac{\tilde{a}_t^2}{f_T(u)} \right)}}\,. \tag{6.28}$$

In both phases, we verified that imposing the gauge $a_u = 0$ does not impose a constraint on the non-zero fields. This can be done, as usual, by deriving the equations of motion with $a_u \neq 0$ for all the fields (also a_u) and then setting $a_u = 0$. The equation of motion of a_u could, in principle, give rise to a constraint. This is not the case for our system since it leads to a trivial identity.

Baryon number, fundamental string charge and angular momentum

In the WSS model, the baryon vertex is associated with a D4-brane wrapped on the background four-sphere S^4. The presence of n_B D4-branes sources the C_5 Ramond-Ramond field through the Wess-Zumino term

$$n_B \int_{S^4 \times \mathbb{R}_t} C_5\,. \tag{6.29}$$

If the gauge connection on the wrapped D6-brane is turned on, the D6-brane can carry a wrapped (on S^4) D4-brane charge, hence a baryon charge n_B. The D6-brane can also carry a fundamental string charge, which corresponds in the field theory picture to the number of quarks building up the baryonic configuration. These features recall those of a charged cylindrical D2-brane (eventually ending on a D4-brane) in flat spacetime, known as *supertube*, which supports both fundamental string charge and D0-brane charge [181, 166].

The induced baryon charge can be read from the D6-brane CS coupling. Let us write the D6-brane worldvolume as $M_3 \times S^4 = \mathbb{R}_t \times \Sigma \times S^4$, where Σ is a surface extended along ψ and $\rho(u)$, or equivalently along ψ and u with $u \in [u_*, u_J]$. Therefore, the D6-brane CS term reads

$$\frac{1}{2\pi}\int_{\mathrm{D6}} C_5 \wedge f = \frac{1}{2\pi}\int_{\Sigma} f \cdot \int_{S^4\times\mathbb{R}_t} C_5\,, \tag{6.30}$$

so that

$$n_B = \frac{1}{2\pi}\int_{\Sigma} f = -\frac{1}{2\pi}\int_{\Sigma} du\, d\psi\, \partial_u a_\psi = a_\psi(u_*) - a_\psi(u_J)\,, \tag{6.31}$$

where in the last equality, we used the axisymmetry of the gauge connection. Notably, n_B appears as an integrated magnetic flux for the U(1) gauge connection on the D6-brane, and it is related to the boundary values of the connection. We will return to the topological interpretation of the baryon number in section 6.1.3. If we define the shifted gauge connection as

$$\hat{a}_\psi = a_\psi - \frac{\mathbf{k}_t}{3}, \qquad\qquad \hat{a}_t = a_t - \frac{\mathbf{k}_\psi}{3}, \tag{6.32}$$

we can rewrite (6.31) as

$$n_B = \hat{a}_\psi(u_*) - \hat{a}_\psi(u_J)\,. \tag{6.33}$$

Fixing the baryon number thus gives a boundary condition on a or, equivalently, on $\hat{a}$. As we will see shortly, the solutions to the equations of motion have to satisfy appropriate boundary conditions to describe metastable objects with baryon number.

The induced fundamental string charge on the D6-brane can be computed by doing the variation of the total action with respect to f[4]

$$q_s = \frac{\partial}{\partial(\partial_u a_t)}\int d\psi\, \mathcal{L}_{\mathrm{D6}} = N\,\frac{\mathbf{k}_t}{3}\,, \tag{6.34}$$

where in the last identity, we used the equations of motion. We stress that the above formula holds both in the confined and in the deconfined phases since the equation of motion for a_t has the same expression in both phases (up to replacing D by D_T).

[4]The identification of the string charge q_s with the variation with respect to f comes from considering that the latter appears in the fundamental string action as

$$S_{\text{f-string}} \supset -\frac{q_s}{2\pi l_s^2}\int \left(B + 2\pi l_s^2 f\right)\,.$$

Then, we can write

$$q_s = -2\pi l_s^2 \frac{\delta S_{\text{f-string}}}{\delta B} = -\frac{\delta S_{\text{f-string}}}{\delta f}\,.$$

As we have already shown in equation (6.2), on the D6-brane worldvolume, there is also the term

$$\frac{N}{4\pi}\int_{M_3} a\wedge f\,, \tag{6.35}$$

which in the presence of the non-trivial magnetic flux in (6.31) becomes

$$N\,n_B\int_{\mathbb{R}_t} a_t(t)dt \quad\Rightarrow\quad q_s = Nn_B\,, \tag{6.36}$$

where $a_t(t)$ is now a gauge connection fluctuation.[5] The result $q_s = N\,n_B$ comes from the identification of the D6-brane CS Lagrangian (6.36) with the fundamental string Lagrangian; and it is physically expected to hold in the presence of baryonic objects.[6] From this result and the definition (6.32), it also follows that

$$\hat{a}_\psi = a_\psi - n_B\,. \tag{6.37}$$

Because of the matching condition we enforced gave $q_s = N\,\mathbf{k}_t/3 = Nn_B$, we have to impose $\mathbf{k}_t/3 = n_B$ when we solve the equations of motion for the gauge connection.

Another property of the charged D6-brane configurations we are focusing on is that they carry angular momentum [5, 6]. Following Noether's theorem, the angular momentum along the u axis is

$$J = \int_{\Sigma\times S^4} d^6x\,\sqrt{-g}\,g_{\psi\psi}\,T^{t\psi}. \tag{6.38}$$

The Chern-Simons term is topological, and hence its contribution to the stress-energy tensor vanishes. We are thus left with the stress-energy tensor contribution from the DBI action

$$T_{MN} = -\frac{2}{\sqrt{-g}}\frac{\delta\mathcal{L}_{\rm D6}}{\delta g^{MN}} = T_6\,e^{-\phi}\Bigg(-g_{MN}\sqrt{1+\frac{1}{2}g^{AB}g^{CD}\bar{f}_{AC}\bar{f}_{BD}}+ \\ +\frac{g^{AB}\,\bar{f}_{MA}\bar{f}_{NB}}{\sqrt{1+\frac{1}{2}g^{AB}g^{CD}\bar{f}_{AC}\bar{f}_{BD}}}\Bigg)\,, \tag{6.39}$$

where g is the induced D6-brane metric and the indices M, N, A, B, C, D run over the D6-brane worldvolume coordinates. In particular

$$T^{t\psi} = \frac{T_6\,e^{-\phi}}{\sqrt{-g_{tt}g_{\psi\psi}g_{uu}}}\frac{\partial_u\bar{a}_t\partial_u\bar{a}_\psi}{\sqrt{-[g_{tt}(g_{\psi\psi}g_{uu}+(\partial_u\bar{a}_\psi)^2)+g_{\psi\psi}(\partial_u\bar{a}_t)^2]}}\,. \tag{6.40}$$

Using the above expression and the equations of motion, we get, from (6.38)

$$J = \frac{N}{2}\int du\,\partial_u\left[\left(a_\psi - \frac{\mathbf{k}_t}{3}\right)^2\right]. \tag{6.41}$$

[5] It can be shown that our time-independent axisymmetric gauge connection can be gauge transformed into this new gauge configuration. This can be done by performing a gauge transformation $a_\mu \to a_\mu + \partial_\mu\Lambda$ with the gauge parameter $\Lambda = -a_t(u)t + \int^t a_t(t')dt'$. The field strength f is trivially gauge invariant, so equation (6.36) is not spoiled. We have to mention that, this way we exit the radial gauge since the component a_u is turned on.

[6] This relation holds only for confined baryonic objects, and it has to be modified in the presence of free quarks.

This formula holds for every D6-brane embedding and in both the confined and the deconfined phases. We can integrate it in u between the generic endpoint in u_* and u_J to get

$$
\begin{aligned}
J &= \frac{N}{2}\left[\left(a_\psi(u_J) - \frac{\mathbf{k}_t}{3}\right)^2 - \left(a_\psi(u_*) - \frac{\mathbf{k}_t}{3}\right)^2\right] = \\
&= \frac{N}{2}\left[(\hat{a}_\psi(u_J))^2 - (\hat{a}_\psi(u_*))^2\right] = -\frac{N}{2}\left(\hat{a}_\psi(u_*) + \hat{a}_\psi(u_J)\right) n_B . \qquad (6.42)
\end{aligned}
$$

6.1.1 Zoology of (meta)stable solutions

For a given value of $\mathbf{k}_t$ and $\mathbf{k}_\psi$, the space of solutions of the system of differential equations derived in (6.19) and (6.27) is a four-parameter space whose general structure is challenging to determine.

We focus on the zoology of time-independent axisymmetric solutions, which can be interpreted from the field theory point of view:

- **Baryons**. They correspond to D6-brane configurations that shrink to zero size at some value of the holographic coordinate $u_* = u_E$ so that $\rho(u_E) = 0$. See figure 6.1.

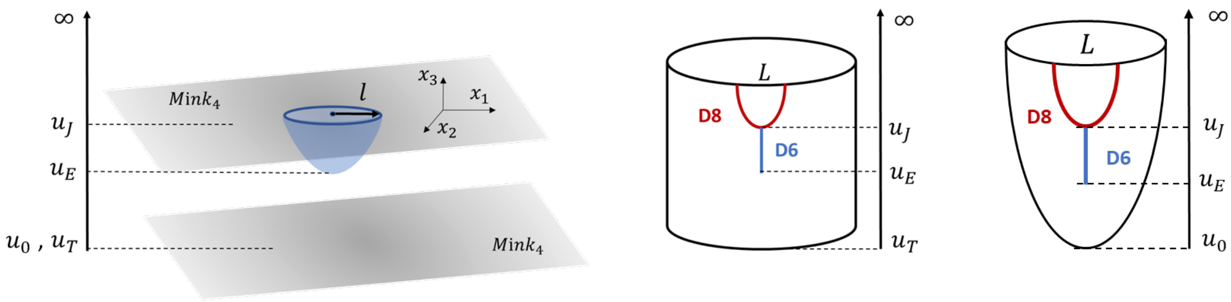

Figure 6.1. Pictorial representation of the D6-brane embedding describing holographically the Hall droplet baryon. The D6-brane has a radius l at $u = u_J$ where it is attached to the D8-brane, and it shrinks to zero size at $u = u_E$. We present the embedding both in the deconfined (cylinder) phase and the confined (cigar) phase of the WSS model.

- **Vortons**. They are solutions in the deconfined phase for which $\rho(u) \neq 0$ for all u, and they extend from u_J to the horizon $u_* = u_T$ (see the discussion in section 5.2). See figure 6.2.

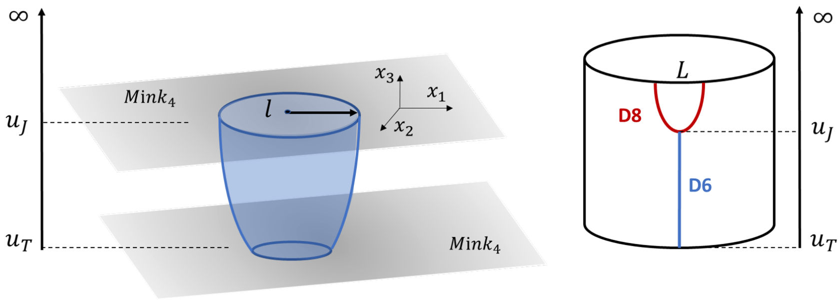

Figure 6.2. Pictorial representation of the D6-brane embedding describing holographically the vorton. The D6-brane has a radius l at $u = u_J$ where it is attached to the D8-brane, while it ends on the horizon with a non-trivial profile.

- ***Sandwich* vortons**. These are solutions such that $\rho(u) \neq 0$ for all u, and they extend from u_J to $u_* = u_K$, which corresponds to the tip of another U-shaped flavor D8-brane.[7] These topological defects can be interpreted as excitations of two different flavors leading to a "sandwich" structure. We will return to the interpretation of these objects in section 6.4. [8]. See figure 6.3.

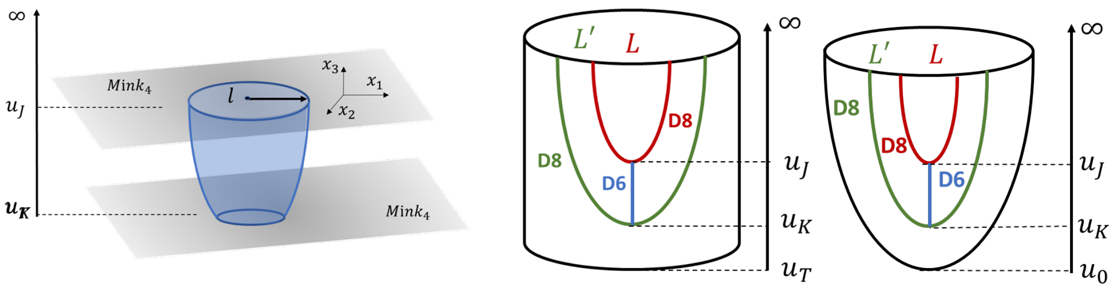

Figure 6.3. Pictorial representation of the D6-brane embedding describing holographically the *sandwich* vorton. The D6-brane has a radius l at $u = u_J$ where it is attached to the first D8-brane, while it ends on a second D8-brane at $u = u_K$. The embedding is presented in the deconfined (cylinder) and the confined (cigar) phase of the WSS model.

- **Punctured domain walls**. They are domain wall solutions attached to a circle of radius l at u_J that extend to $\rho \to \infty$ at some $u_* \geqslant u_0$ in the confined phase and $u_* \geqslant u_T$ in the deconfined phase. See figure 6.4.

[7] Thus, since $u_K \neq u_J$, the two flavors condense at different scales.

[8] We can also think of *sandwich* defects with a straight boundary on the two D8-branes. In this case, the composite objects are straight global strings associated with two different flavors. See figure 5.6

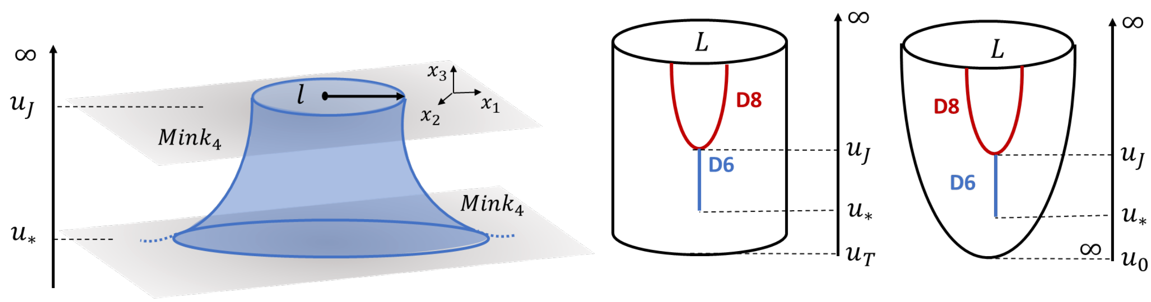

Figure 6.4. Pictorial representation of the D6-brane embedding describing holographically the punctured domain wall. The D6-brane has a radius l at $u = u_J$ where it is attached to the first D8-brane. It extends to $\rho \to \infty$ for a finite $u = u_*$. The embedding is presented in the deconfined (cylinder) phase and the confined (cigar) phase of the WSS model.

These configurations are not necessarily metastable. Time-independent stable or metastable solutions are generally a very restricted subclass of solutions for which we need to impose other constraints.

The first necessary criterion for (meta)stability comes from a no-force condition for intersecting branes, which is achieved when the intersection is orthogonal. This, in our case, will result in a first boundary condition

$$\rho'(u_J) = 0\,. \tag{6.43}$$

For D6-brane embeddings associated with baryon solutions, we also have to require that the embedding is a smooth manifold. For example, a conical shape at u_* will result in tension, causing the brane to shrink. As a result, in the baryon case, we must have

$$\rho'(u_E) \to \infty\,, \tag{6.44}$$

where $u_* = u_E$ is the value of the holographic coordinate such that $\rho(u_E) = 0$.

For vortons in the deconfined phase, together with $\rho'(u_J) = 0$, the orthogonality requirement at the horizon is discussed in section 5.2. Expanding the metric in the near-horizon region, it is possible to show that orthogonality is guaranteed if and only if the embedding $\rho(u)$ admits a (regular) Taylor expansion in u_T.

The *sandwich* vortons have to be supported also with the orthogonality condition at u_K

$$\rho'(u_K) = 0\,. \tag{6.45}$$

6.1.2 Variational principle for a DBI-CS action

In this section, we address the variational problem for a DBI-CS action in the presence of a boundary. Let us recall that $M_3 = \Sigma \times \mathbb{R}_t$ (and $\partial M_3 = \partial\Sigma \times \mathbb{R}_t$) with $\mathbb{R}_t$ the time axis and Σ a surface extended along $\psi, \rho(u)$, or equivalently along ψ, u, with $u \in [u_*, u_J]$ and with some profile $\rho(u)$.

In our setup, both the DBI action and CS action produce a boundary variation under $a \to a + \delta a$, and therefore, it has to be taken into account. As a consequence of the presence of the DBI action, unlike in the pure CS case [180], the variables

δa_t and δa_ψ are not conjugate to each other, and we can safely choose Dirichlet boundary conditions for both of them to work out the variational problem. See *e.g.* [182] for a recent discussion on this topic. Therefore, we set[9]

$$\delta a_t\Big|_{u_*}^{u_J} = 0, \qquad\qquad \delta a_\psi\Big|_{u_*}^{u_J} = 0, \tag{6.46}$$

and the variational problem is automatically well-posed.

Boundary conditions for the gauge connection

We are now ready to discuss the boundary conditions, consistent with the variational principle, that we will impose to solve the equations of motion. In the baryon setup, and in both phases, assuming that the electric field is finite at the tip of the D6-brane, the equation of motion for a_t implies that, at the tip where $\rho(u_E) = 0$ and $\rho'(u_E) \to \infty$, we have $a_\psi(u_E) = n_B$. This, together with the baryon number definition $n_B = a_\psi(u_E) - a_\psi(u_J)$, implies $a_\psi(u_J) = 0$ for the baryon.

In both phases and for all the other solutions with baryon number n_B, we will impose the same conditions, $a_\psi(u_J) = 0$ and $a_\psi(u_*) = n_B$. As a consequence for all solutions we have $\hat{a}_\psi(u_*) = 0$ and $\hat{a}_\psi(u_J) = -n_B$ using (6.37). Let us summarize the boundary conditions of each configuration presented in section 6.1.1 separately:

Baryons:	$a_\psi(u_E) = n_B$	$a_t(u_E) = 0$	$a_\psi(u_J) = 0\,.$	(6.47)
Vortons:	$a_\psi(u_T) = n_B$	$a_t(u_T) = 0$	$a_\psi(u_J) = 0\,.$	(6.48)
Sandwich vortons:	$a_\psi(u_K) = n_B$	$a_t(u_K) = 0$	$a_\psi(u_J) = 0\,.$	(6.49)
Punctured domain walls:	$a_\psi(u_*) = n_B$	$a_t(u_*) = 0$	$a_\psi(u_J) = 0\,.$	(6.50)

Imposing the above conditions and recalling equation (6.42), we find

$$J = \frac{N}{2} n_B^2\,, \tag{6.51}$$

for every configuration. We insist that in the baryon case this is derived, while it is a consequence of our choice of boundary conditions for the other solutions. This quadratic dependence of the angular momentum on the charge is a typical feature of anyonic systems, and it is consistent with the observation that the charged D6-brane configurations we are focusing on are excitations of a topological phase of a $\mathrm{U}(1)_N$ CS theory.[10]

6.1.3 Topological interpretation of the baryon number

In this section, we classify the principal U(1)-bundles that can be defined on the D6-brane worldvolume. We show that these bundles are precisely classified by the baryon number. We identify the topological data at the intersection of the D6-brane

[9] Let us recall that $u = u_J$, and $u = u_*$ represent the location of the boundary.

[10] The state with opposite spin $J = -(N/2)n_B^2$ can be obtained by considering a $\overline{\text{D6}}$-brane for which the CS term changes sign.

and the D8-brane, we connect this boundary data to the baryon number, and show the similarities with the well-known Yang-Mills instanton description of baryons. Then, we provide a physical interpretation of the shifted gauge connection $\hat{a}$, which, as we shall see, describes in the baryon case a vortex living on the D6-brane. Finally, we outline some similarities and differences between the well-known Nielsen-Olesen vortex [183] and the one we study throughout this chapter, which we will refer to as *DBI-CS vortex.*

Topological properties of the D6-brane

In this section, we do not consider the S^4 on which the D6-brane and the D8-brane are wrapped. Moreover, for our purpose, the time axis will be neglected; therefore, the manifold of interest is the above-defined Σ. All the D6-brane configurations considered in this chapter (and the previous chapters) have an intersection with the D8-brane in $u = u_J$, which has the topology of a circle S^1. This circle is a connected component of $\partial\Sigma$. For baryon solutions, it is *a priori* the only one, but the other solutions may have other connected components. Hence, we discuss separately the solutions for which $\rho(u) \neq 0$ for all u and the baryon.

In the $\rho(u) \neq 0$ case, which corresponds to the *sandwich* vorton, the vorton and the punctured domain wall cases presented in section 6.1.1, the boundary has two circular connected components. One is the circle in u_J, and the other is in u_*. This last circle is either the intersection with another U-shaped D8-brane (for *sandwich* vortons), the intersection with the horizon (for vortons), or a circle at infinity (for the punctured domain walls). In all these cases, Σ has the global topology of a cylinder between two circles, which we will denote $S^1_{J,*}$.

In the baryon case, Σ has a priori the topology of a disk. However, as we have seen in equation (6.47), a has a *vortex-like* singularity in u_E. We will interpret this $a_\psi(u_E) \neq 0$ as a topological defect at the tip of the D6-brane. A common workaround procedure to study these defects is to consider instead the manifold Σ with a small neighborhood of the defect excised. This has multiple topological and physical consequences. Firstly, it adds another circular boundary component in $u_* = u_E$, which allows for a non-trivial value of the gauge connection at the tip without a singularity. Moreover, this implies that the discussion of baryons and the other D6-brane configurations can be conducted simultaneously, as both can be treated by considering a cylinder between two circles.

Classification of the principal $\mathrm{U}(1)$-bundles

We now want to work out a classification of the principal $\mathrm{U}(1)$-bundles defined on the manifold Σ, which, as we have shown, can be reduced to the study of a cylinder. Note that, because of (6.6), the curvature f has to vanish on both bounding circles of the cylinder. Therefore, f restricts to a map on the one-point compactification of $\Sigma \setminus \partial\Sigma$. This corresponds to identifying the entire boundary $\partial\Sigma$ as a single point. Doing so, we obtain a *pinched* torus, noted $\mathbb{PT}$, illustrated in figure 6.5.

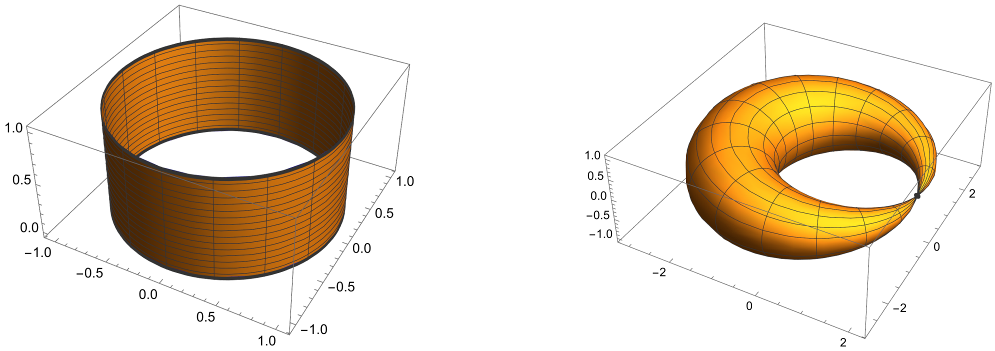

(a) **(b)**

Figure 6.5. Cylinder configuration (a) and its one-point compactification $\mathbb{PT}$ (b). The boundary is indicated in blue.

It has been shown that U(1)-principal bundles are classified up to gauge transformations by the second cohomology group of this manifold, with integer coefficients (see appendix C for a more detailed explanation of this statement). This is a crucial difference with the baryons constructed usually with more flavors, which rely on non-trivial SU(N_f)-principal bundles, classified by the fourth cohomology group. The cohomology of the pinched torus is

$$H^*(\mathbb{PT};\mathbb{Z}) = (H^0(\mathbb{PT};\mathbb{Z}), H^1(\mathbb{PT};\mathbb{Z}), H^2(\mathbb{PT};\mathbb{Z}), 0\dots) = (\mathbb{Z},\mathbb{Z},\mathbb{Z},0\dots), \tag{6.52}$$

and all the higher cohomology groups vanish because of $\dim(\mathbb{PT}) = 2$. $H^0 = \mathbb{Z}$ is a direct consequence of the connectedness of $\mathbb{PT}$. The coefficient of H^1 describes a winding number.[11] The last integer classifies U(1)-principal bundles up to gauge transformations. It can be extracted by computing the first Chern number over the pinched torus:

$$\frac{1}{2\pi}\int_{\mathbb{PT}} f \in \mathbb{Z}\,. \tag{6.53}$$

This quantity is a quantized magnetic flux over $\mathbb{PT}$. The compactification we used mapped Σ to $\mathbb{PT}$ and therefore the above integral is exactly the baryon number previously defined on Σ in equation (6.31). Therefore, the baryon number classifies the U(1)-principal bundles on M_3 up to gauge transformations.

It is useful to consider the link between this construction and $SU(2)$ instantons in four-dimensional Euclidean space, which share many similarities. The mathematical objects we used and the analogous ones appearing in the instanton study are reported in table 6.1.

	Manifold	Boundary	Compactification	Group	Classification
Baryon	$S^1 \times [u_*, u_J]$	$S^1_* \cup S^1_J$	$\mathbb{PT}$	U(1)	$H^2(\mathbb{PT};\mathbb{Z})$
Instanton	$\mathbb{R}^4$	S^3_∞	S^4	SU(2)	$H^4(S^4;\mathbb{Z})$

Table 6.1. Relevant groups and manifolds to the topology of the baryon and instanton case.

[11] Though in this case it comes from the "gluing" operation we performed and is not physical.

Though there are many similarities between these constructions, there is an additional element in our setup. The structure of the large gauge transformations on Σ is non-trivial. The entire cylinder has a non-trivial first cohomology group, equal to $\mathbb{Z}$. Moreover, as is well known [180], the allowed holonomies around circles for an Abelian Chern-Simons theory at level N like the one we consider are given in units of $1/N$. Therefore, for every integer (divided by N), we can define a unique large gauge transformation[12] over the manifold. We denote the fraction associated with such a transformation as n_G. As an example, in the particular case of an integer $n_G = n_B$, we can define a scalar χ as

$$\chi = \frac{\mathbf{k}_\psi}{3}\, t + \frac{\mathbf{k}_t}{3}\, \psi = \frac{\mathbf{k}_\psi}{3}\, t + n_B\, \psi\,, \tag{6.54}$$

where we used the result $\mathbf{k}_t = 3n_B$ coming from (6.36), such that we can send a to the shifted gauge connection $\hat{a}$ through the following large gauge transformation

$$a = \hat{a} + d\chi\,. \tag{6.55}$$

Importantly, after this transformation, $\hat{a}$ is always a regular field, *i.e.* $\hat{a}(u_E) = 0$ in the baryon case. This was already known from the boundary conditions (6.47), though in the baryon case, connecting them by a large gauge transformation was only possible because of this excision of the defect.

We will now connect the bulk data (the baryon number) to the topological data of the boundary. As we have seen, the latter consists of two disconnected circles on which $f = 0$, therefore, locally $a = d\varphi$ but not globally, as a can wind around circles. This winding is classified by $\pi_1(\mathrm{U}(1)) = \mathbb{Z}$. The possible pure gauge configurations are therefore split into topological sectors, labeled by their holonomies. We define two fractional topological numbers from the holonomy of $\hat{a}$ (the regularized gauge connection) over the bounding circle. The orientation we chose for M_3, $dt \wedge d\psi \wedge du = +dt\, d\psi\, du$, induces an orientation on the bounding circles, which results in an opposite sign for the u_J circle and the u_* one:[13]

$$n_J = -\frac{1}{2\pi}\int_{S^1_J} \hat{a}(u_J)\,, \qquad n_* = \frac{1}{2\pi}\int_{S^1_*} \hat{a}(u_*)\,. \tag{6.56}$$

Recall that for baryon configurations $u_* = u_E$ and therefore $n_* = n_E = 0$, while for sandwich solutions $u_* = u_K$ and hence $n_* = n_K$. These numbers are connected to the winding numbers $n^{(W)}_{J,*}$ by the following relations:

$$n^{(W)}_J \equiv -\frac{N}{2\pi}\int_{S^1_J} \hat{a}(u_J) = N n_J\,, \qquad n^{(W)}_* \equiv \frac{N}{2\pi}\int_{S^1_*} \hat{a}(u_*) = N n_*\,. \tag{6.57}$$

The gauge connection $\hat{a}$ can then be interpreted as a topological soliton interpolating between two topological sectors, one at $u = u_J$ characterized by n_J and the

[12] A large gauge transformation is a gauge transformation that is not homotopic to the identity. As we will see, it acts non-trivially on the boundary and has to be viewed as a global symmetry of the theory. The argued uniqueness is assuming it does not spoil the axisymmetry and time invariance of our ansatz.

[13] Subtleties might arise when $u_* = u_T$ is the event horizon of the spacetime.

other $u = u_*$ by n_*. Using Stokes' theorem, we can then rewrite the baryon number n_B as

$$n_B = n_* + n_J \,, \tag{6.58}$$

where we stress that, even though n_* and n_J are fractional, their sum has to be an integer in virtue of (6.52). Importantly, these two fractional numbers are not invariant under a global action n_G, which can, for the same reason, take fractional values $n_G = n_G^{(W)}/N$, with $n_G^{(W)} \in \mathbb{Z}$. One can check that the large gauge transformation n_G transforms $n_J \to n_J - n_G$ and $n_* \to n_* + n_G$, which confirms that even though these numbers are not invariant, their sum n_B is. Moreover, equation (6.58) implies that for a D6-brane solution to have a non-zero baryon number, it has to have at least one non-trivial winding over one of the circles at the boundary. With the choice of conventions that we made, the winding number on an intersection with a U-shaped flavor D8-brane counts exactly the net number of fundamental strings coming out from the aforementioned flavor brane. This number corresponds in the field theory to the number of quarks associated with the corresponding flavor.

We can rewrite the formula for the angular momentum (6.42) in terms of the holonomies of a (6.56)

$$J = \frac{N}{2}(n_J^2 - n_*^2) = \frac{N\, n_B}{2}(n_J - n_*). \tag{6.59}$$

Then we can change the topological sectors defined by the two holonomies by $n_J \to n_J - n_G$ and $n_* \to n_* + n_G$. As we have seen before, this transformation associated with n_G does not change the baryon number n_B, however, it affects the total spin of the D6-brane:

$$J \to J - N\, n_B\, n_G = J - n_B\, n_G^{(W)}. \tag{6.60}$$

Therefore, the spin is shifted by an integer number $-n_B\, n_G^{(W)}$.[14]

It is instructive to visualize the gauge connection component a_ψ for a baryon solution to illustrate the singularity we discussed. We have not yet illustrated the strategy to solve the equations of motion, but for the purposes of this section, we can present directly the result for the gauge connection component a_ψ, and its shifted version $\hat{a}_\psi$. Figure 6.6 shows the revolution plot around u of $a_\psi(u)$ (left panel) and $\hat{a}_\psi(u)$ (right panel) projected into a plane of fixed u. The solid circumference corresponds to the value of the field at $u = u_J$, while the center corresponds to $u = u_E$. The color represents the strength of the field, going from 0 in blue to $|n_B|$ in yellow. As explained previously, the gauge connection a_ψ is singular at the D6-brane tip while it is zero in $u = u_J$, as imposed by the boundary conditions discussed in the previous section. The shifted gauge connection $\hat{a}_\psi$ is regularized, but becomes nonzero at the boundary $u = u_J$ due to the action of the large gauge transformation.

[14] We want to outline a connection between formulas (6.33), (6.42) or equivalently (6.58), (6.59) and the results presented in [184] where they study an Abelian Chern-Simons theory coupled with a charged scalar field in (2+1)-dimensions. They find the very same formula for the magnetic flux, and the anyonic-like angular momentum for solitons in this theory. See also [185] for more recent investigation of Chern-Simons solitons.

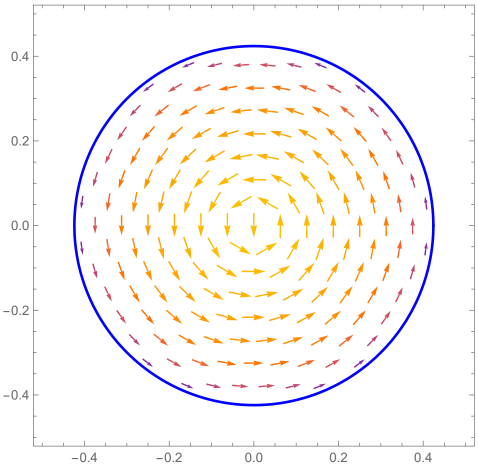

(a) Singular connection a_ψ.

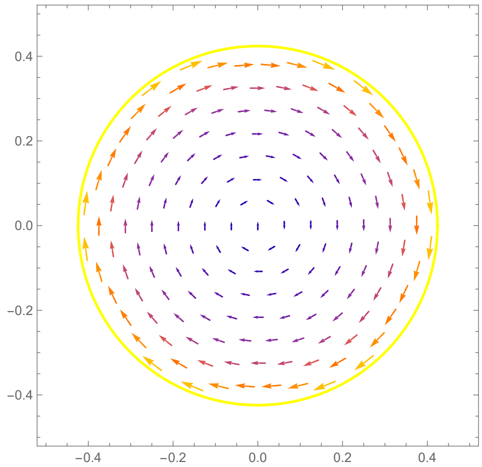

(b) Regular connection $\hat{a}_\psi$.

Figure 6.6. Projection of the revolution plot of a_ψ (left panel) and $\hat{a}_\psi$ (right panel). This solution is computed for $\lambda = 100$ and $b = 0.4$ in the confined phase.

Summarizing the discussion of this section, in all the cases under study, we can define a global baryon number, which is shown to be given by the first Chern number, and classifies the possible U(1)-principal bundles up to gauge transformations. Up to removing (in the baryon case) from the manifold a small circle around the point where the defect is located, one can define a global topological number n_G around the D6-brane profile. χ, a large gauge transformation connecting a and $\hat{a}$, has a non-trivial $n_G = n_B$. For the baryon, $\hat{a}$ appears as a regularized connection, in the sense that the singularity is removed from the tip of the D6-brane in u_E. This regular field is then used to define two boundary holonomies, n_* and n_J, that are directly related to the baryon number, counting the number of field theory quarks (divided by N) that form the baryonic state.

The DBI-CS vortex

We shall now point out an interesting interpretation of $\hat{a}$ in the baryon case, which has a single non-zero integer holonomy in u_J. The baryon solution we are studying shares many similarities with the Nielsen-Olesen vortex [183] (see also [186] for a review). Most importantly, both of them arise from a similar topological construction: as we discussed, the shifted gauge connection $\hat{a}$ is regular in u_E, so that the non-trivial topological number is given just by n_J (since $n_E = 0$, this is an integer), which is associated with the homotopy group

$$\pi_1(\mathrm{U}(1)) = \mathbb{Z}\,, \tag{6.61}$$

as for the Nielsen-Olesen vortex. Additionally, both configurations carry a magnetic flux, quantized for topological reasons. However, there are two significant differences with respect to the Nielsen-Olesen case. Nielsen-Olesen vortex solutions are constructed by starting with a non-trivial singular solution with non-zero winding at the boundary at infinity, and then allowing it to depend on a radial coordinate to regularize it at the origin. Instead, we first obtained the gauge connection a, which did not have winding around the boundary u_J, and it was singular in u_E (see left panel of figure 6.6). Then, the singularity is resolved by applying a non-trivial gauge transformation χ, which gives it a winding at the boundary in u_J.

The second difference is that Nielsen-Olesen vortices are often introduced for theories with another scalar field charged under the U(1), typically a Higgs field, which is absent here. In these Maxwell-Higgs models, the scalar vacuum expectation value connects a_t and $\partial_u a_\psi$ as well as a_ψ and $\partial_u a_t$, see [187]. In our system, by looking at the equations of motion in the confined and the deconfined phase (6.19) and (6.27), we observe that the quantity that connects them comes from the DBI Lagrangian and it is mediated by the quantity $D_{(T)}(u)$. We can interpret this observation as if the role of the scalar field is played by geometrical degrees of freedom in our system.

Comments on the interpretation of baryons as quantum Hall droplets

The D6-brane configurations presented in this work correspond to non-trivial excitations of a topological phase of matter given by the $\mathrm{U}(1)_N$ CS theory living on their worldvolume (after the reduction on the four-sphere). Such excitations are also commonly studied from the boundary point of view, after adding a dynamical term living on the boundary for phenomenological reasons. For comprehensive reviews on the topic, see *e.g.* [188, 189, 190]. This famously known edge dynamics is then described by the Floreanini-Jackiw action [112], and is the one governing the boundary physics of quantum Hall states. In our setup, we do not have access to the standard Floreanini-Jackiw action, since there is no explicit boundary term in the effective three-dimensional theory. However, we can identify the solitonic mode of the gauge configuration a with χ, being $a = d\chi$.

With this observation in mind, we can discuss the topological sectors of the edge theory, which on the field theory side allow us to define the "electron operators" of integer charge in the FQHE. They are used to define the baryon charge and the corresponding charged operator. See, for example, [38]. In our holographic model, such an operator can be formulated as

$$\mathcal{O}_B = e^{iN\chi}\,. \tag{6.62}$$

This is the minimal local operator that carries a baryon charge. See the discussion in section 2.4 of chapter 2, and the appendix A.

For the field χ, it is easy to verify that

$$n_B = \frac{1}{2\pi}\int_{u_J} d\chi\,. \tag{6.63}$$

Therefore, as in the standard FQHE, the solitonic part of the edge mode gives the charge of the droplet configuration.

6.1.4 Analysis of the D6-brane energy

In this section, we derive the formula for the energy of the D6-brane configuration. The total D6-brane energy can also be derived from Noether's theorem by means of the stress-energy tensor (6.39)[15]

$$E = -\int du\, d\psi\, d\Omega_4 \sqrt{-g}\; T_t^{\ t}\,, \tag{6.64}$$

with

$$T_t^{\ t} = g^{tt} T_{tt} = -\left(\frac{R}{u}\right)^{3/4} \frac{1}{g_s (2\pi)^6 l_s^7} \left(u^{7/4} R^{9/4} \rho(u) D(u) + \frac{u^{7/4} R^{9/4} \rho(u) (\partial_u \tilde{a}_t)^2}{D(u)} \right). \tag{6.65}$$

After some algebra, we get

$$E = \frac{N}{3(2\pi l_s^2)^2} \int_{u_*}^{u_J} du\, u\, \rho(u) \left(D(u) + \frac{(\partial_u \tilde{a}_t)^2}{D(u)} \right). \tag{6.66}$$

Using the equations of motion for $\tilde{a}_\psi$ in (6.19) and the definitions in (6.18) we get

$$\begin{aligned} E &= \frac{N}{3(2\pi l_s^2)^2} \int_{u_*}^{u_J} du \left(u\, \rho(u) D(u) - 3 \tilde{a}_\psi \partial_u \tilde{a}_t \right) \\ &= \frac{N}{3(2\pi l_s^2)^2} \int_{u_*}^{u_J} du \left(u\, \rho(u) D(u) - 3 \bar{a}_\psi \partial_u \bar{a}_t \right) + N\, n_B\, \mu\,, \end{aligned} \tag{6.67}$$

where we have introduced a would-be chemical potential μ conjugate to n_B

$$\mu \equiv \int_{u_*}^{u_J} du\, \partial_u a_t = a_t(u_J). \tag{6.68}$$

In the deconfined phase, the result looks formally the same

$$E = \frac{N}{3(2\pi l_s^2)^2} \int_{u_*}^{u_J} du \left(u\, \rho(u) D_T(u) - 3 \bar{a}_\psi \partial_u \bar{a}_t \right) + N\, n_B\, \mu\,. \tag{6.69}$$

Let us observe that the final form of the energy is the non-supersymmetric version of the BPS result present in [181, 191, 192, 166] where the sum of the charges (with appropriate coefficients) gives the energy. In fact, in our case, the energy can be rewritten as a free-energy bulk term

$$F_{\text{bulk}} = N \int_{u_*}^{u_J} du \left\{ \frac{(a_t\, \partial_u a_\psi - a_\psi\, \partial_u a_t)}{2} + \frac{u\, \rho(u) D(u)}{3(2\pi l_s^2)^2} \right\}, \tag{6.70}$$

where we have defined the free energy associated with a generic action as

$$S = -\int dt\, F, \tag{6.71}$$

plus the sum of charges:

$$E = F_{\text{bulk}} + \mu\, \frac{q_s + N\, n_B}{2}\,, \tag{6.72}$$

with $q_s = N n_B$. The F_{bulk} term (as well as the presence of a chemical potential factor) makes the difference with respect to the BPS case.

[15] Just as the CS term, the boundary action does not contribute to the stress-energy tensor.

The energy of the D6-brane configurations we are focusing on, is bounded from below by a *Bogomol'nyi bound* that arises because of the topological nature of the solutions we are considering. The derivation of the bound is very similar in both phases, though the result differs. We show the derivation in the confined phase, and we indicate the result in the deconfined phase at the end. Let us start from the total energy of the configuration

$$E = \frac{N}{3(2\pi l_s^2)^2} \int_{u_E}^{u_J} du \, \frac{u\,\rho(u)}{D(u)} \left(\frac{1}{f(u)} + \rho'(u)^2 \left(\frac{u}{R}\right)^3 + \frac{(\partial_u \tilde{a}_\psi)^2}{\rho^2(u)} \right). \tag{6.73}$$

The first two terms can be combined to give the Lagrangian in the uncharged ($a = 0$) case, and we can use the usual Bogomol'nyi trick of completing the square to get

$$\begin{aligned} E =& \frac{N}{3(2\pi l_s^2)^2} \int_{u_E}^{u_J} \left\{ du \frac{u\,\rho(u)}{D(u)} \left(\sqrt{\frac{1}{f(u)} + \rho'(u)^2 \left(\frac{u}{R}\right)^3} + \frac{\partial_u \tilde{a}_\psi}{\rho(u)} \right)^2 \right. \\ & \left. - 2\partial_u \tilde{a}_\psi \sqrt{u^2 + 9\left(\frac{\tilde{a}_\psi^2}{\rho^2(u)} - \tilde{a}_t^2\right)} \right\}. \end{aligned} \tag{6.74}$$

Now, we can easily derive the Bogomol'nyi bound

$$E \geqslant E_B^{\text{conf.}} \equiv -\frac{2N}{3(2\pi l_s^2)^2} \int_{u_E}^{u_J} du \, u \, \partial_u \tilde{a}_\psi \sqrt{1 + \frac{9}{u^2}\left(\frac{\tilde{a}_\psi^2}{\rho^2(u)} - \tilde{a}_t^2\right)}\,, \tag{6.75}$$

with the associated Bogomol'nyi equation

$$\partial_u \tilde{a}_\psi = -\rho(u) \sqrt{\rho'(u)^2 \left(\frac{u}{R}\right)^3 + \frac{1}{f(u)}}\,, \tag{6.76}$$

which has to hold if the bound is saturated.

In the deconfined phase, the Bogomol'nyi bound reads

$$E \geqslant E_B^{\text{deconf.}} \equiv -\frac{2N}{3(2\pi l_s^2)^2} \int_{u_*}^{u_J} du \, u \, \partial_u \tilde{a}_\psi \sqrt{f_T(u)} \sqrt{1 + \frac{9}{u^2}\left(\frac{\tilde{a}_\psi^2}{\rho^2(u)} - \frac{\tilde{a}_t^2}{f_T(u)}\right)}\,, \tag{6.77}$$

and the associated Bogomol'nyi equation

$$\partial_u \tilde{a}_\psi = -\rho(u) \sqrt{\rho'(u)^2 \left(\frac{u}{R}\right)^3 + \frac{1}{f_T(u)}}\,, \tag{6.78}$$

We do not expect a solution to the full problem satisfying (6.78) or (6.76) to exist. However, if it were possible to saturate the bound, we would get an energy formally given by the same expression in the two phases

$$E = E_B^{\text{deconf.}} = E_B^{\text{conf.}} = -\frac{2N}{3(2\pi l_s^2)^2} \int_{u_*}^{u_J} du \, \tilde{a}_t \partial_u \tilde{a}_\psi \geqslant C_{\lambda,b} |n_B|, \tag{6.79}$$

where $C_{\lambda,b}$ is a strictly positive constant, depending on the value of λ and b.

6.2 The Hall droplet baryon

In this section, with the aim of providing a D6-brane realization, within the WSS model, of the Hall droplet baryon discussed in [38], we present the numerical solutions of the Euler-Lagrange equations for the baryon configuration. We remind that the baryon solution corresponds to a charged D6-brane configuration, which is attached at the D8-branes' tip at $u = u_J$, and it smoothly shrinks to zero size at $u = u_E < u_J$. The details on the numerical methods used to solve the equations of motion can be found in the appendix D. We will present the results separately for the confined and deconfined phases of the WSS model. For both phases, we have checked analytically that the boundary conditions for the fields $\rho(u)$, $\tilde{a}_t(u)$, and $\tilde{a}_\psi(u)$ are consistent with the equations of motion by employing a series expansion around u_E and u_J.

6.2.1 Excursus: rigid rotor estimates

Before we present the numerical results, we approximate the D6-brane as a disk-like rigid rotor in order to extract analytic estimates for the stability radius and the energy. We will then compare these estimates with the numerical results and show that the rigid rotor is a good approximation for the baryonic D6-brane's size.

For a rigid rotor with mass M, moment of inertia I, spinning with angular momentum of modulus J, the total energy in the non-relativistic limit can be approximated as

$$E = M + \frac{J^2}{2I}\,. \tag{6.80}$$

For a disk-like rigid rotor of radius l, $I = \frac{1}{2}M\,l^2$. Approximating the D6-brane baryon with such an object is justified since, as we will show, the extension of the D6-brane along the holographic coordinate u, compared to its radius on the D8-brane, is found to be parametrically small in λ. This means that the D6-brane is squeezed at $u = u_J$ for which $l = \rho(u_J) \sim$ constant, making the disk approximation consistent.

Let us consider solutions that satisfy the relation $J = N\,n_B^2/2$. The mass M can be estimated from the D6-brane DBI action by setting the gauge connection a to zero. Let us proceed in the confining phase for which M, defined as $S_{\mathrm{D6}} = -\int dt\,M$, reads

$$M = \frac{N}{3(2\pi l_s^2)^2}\int du\,u\,\rho(u)D(u)_{a=0}\,. \tag{6.81}$$

In the disk approximation, the first derivative of the embedding, $\rho'(u)$, tends to infinity throughout the D6-brane extension, and hence D (defined in equation (6.10)) at $a = 0$ can be approximated as

$$D(u)_{a=0} = \sqrt{\left(\frac{u}{R}\right)^3\rho'(u)^2 + \frac{1}{f(u)}} = \left(\frac{u}{R}\right)^{3/2}\rho'(u) + \ldots \tag{6.82}$$

Therefore, after some algebra, the mass M can be written as

$$M = \frac{2N\lambda^2}{3^6\pi^2\,b^{5/2}}\,M_{KK}^3\,l^2\,. \tag{6.83}$$

We can replace this value of M in the equation for the total energy (6.80) and minimize it as a function of $l = \rho(u_J)$. As a result, we get an analytical, approximate estimate of the corresponding stability radius l_{stable}, given by

$$l_{\text{stable}}\, M_{KK} = \frac{3^2 \pi^{2/3}\, b^{5/6}}{\sqrt{2}} \left(\frac{n_B}{\lambda}\right)^{2/3} . \tag{6.84}$$

Therefore, the stability radius in the confined phase scales with the dimensional parameter $M_{KK} \leftrightarrow \Lambda$ as $l_{\text{stable}} \sim \Lambda^{-1}$, and is independent of N, in agreement with field theory expectations [38]. Moreover, $l_{\text{stable}} \sim (n_B/\lambda)^{2/3}$ and therefore if $n_B = 1$ we find $l_{\text{stable}} \sim \lambda^{-2/3}$. We can introduce the parameter

$$\xi = \frac{n_B}{\lambda}, \tag{6.85}$$

to write the stability radius as

$$l_{\text{stable}}\, M_{KK} = \frac{3^2 \pi^{2/3}\, b^{5/6}}{\sqrt{2}}\, \xi^{2/3} . \tag{6.86}$$

The parameter ξ is parametrically small whenever we consider a baryon with $n_B \sim \mathcal{O}(\lambda^0)$ while it becomes of order one when $n_B \sim \lambda$. We can also derive an analytical estimate for the on-shell energy of the stable configuration as

$$E = \frac{N\, n_B^{4/3} \lambda^{2/3}}{6\pi^{2/3} b^{5/6}}\, M_{KK} = \frac{N\, \lambda^2}{6\pi^{2/3} b^{5/6}}\, \xi^{4/3} M_{KK} . \tag{6.87}$$

Therefore, if we consider a solution with baryon number $n_B \sim \mathcal{O}(\lambda^0)$, the energy scales with λ as $E \sim \lambda^{2/3}$.

In the deconfined phase, similar formulas can be worked out, starting from the $a = 0$ limit of eqns. (6.22) and (6.23). The mass of the rigid rotor now reads

$$M = \frac{2N\lambda_T^2}{3^6 \pi^2\, \tilde{b}^{5/2}} \left(1 - \tilde{b}^3\right) \left(\frac{T}{T_c}\right)^3 M_{KK}^3\, l^2 , \tag{6.88}$$

where we have defined the temperature-dependent 't Hooft coupling

$$\lambda_T = \frac{T}{T_c}\, \lambda , \tag{6.89}$$

with T_c being the critical temperature for deconfinement (3.114). The stability radius and the corresponding energy now read

$$l_{\text{stable}}\, M_{KK} = \frac{3^2 \pi^{2/3}\, \tilde{b}^{5/6}}{\left(1 - \tilde{b}^3\right)^{1/3} \sqrt{2}} \frac{T_c}{T} \left(\frac{n_B}{\lambda_T}\right)^{2/3} = \frac{3^2 \pi^{2/3}\, \tilde{b}^{5/6}}{\left(1 - \tilde{b}^3\right)^{1/3} \sqrt{2}} \frac{T_c}{T}\, \xi_T^{2/3}, \tag{6.90}$$

$$E = \frac{N\, n_B^{4/3} \lambda_T^{2/3}}{6\pi^{2/3} \tilde{b}^{5/6}} \left(1 - \tilde{b}^3\right)^{1/3} \frac{T}{T_c} M_{KK} = \frac{N\, \lambda_T^2}{6\pi^{2/3} \tilde{b}^{5/6}} \left(1 - \tilde{b}^3\right)^{1/3} \xi_T^{4/3}\, \frac{T}{T_c} M_{KK} , \tag{6.91}$$

where

$$\xi_T = \frac{n_B}{\lambda_T} . \tag{6.92}$$

In the following, we will present the actual numerical results for the D6-brane baryon solutions in both the confined and the deconfined phases and compare them with the above analytical estimates. We will see that the rigid rotor approximation correctly captures the behavior of the stability radius as a function of b (or $\tilde{b}$) and λ (or λ_T) while the energy fails to be reproduced by this approximation.

6.2.2 Confined phase

We present the baryon solution with $n_B = 1$ in the confined phase in figures 6.7 and 6.8 for $\lambda = 100$ and $b = 0.1$. The integration of the differential equations stops when $\rho'(u) \to \infty$, and this happens at $u = u_E$, which for the present solution is numerically found to be $u_E \approx 0.92\, u_J$. The details of the numerical methods used to solve the set of differential equations can be found in appendix D; let us simply mention that to simplify the numerics, we performed the following coordinate and field redefinitions

$$u \to u_J\, \hat{u}, \qquad \rho \to L\, \check{\rho}, \qquad a_\psi \to L\, u_J\, \check{a}_\psi, \qquad a_t \to u_J\, \check{a}_t\,. \tag{6.93}$$

We will specify whenever we are dealing with rescaled fields in the following. The plots of the solutions to the equations of motion are shown as a function of the rescaled coordinate $\hat{u}$.

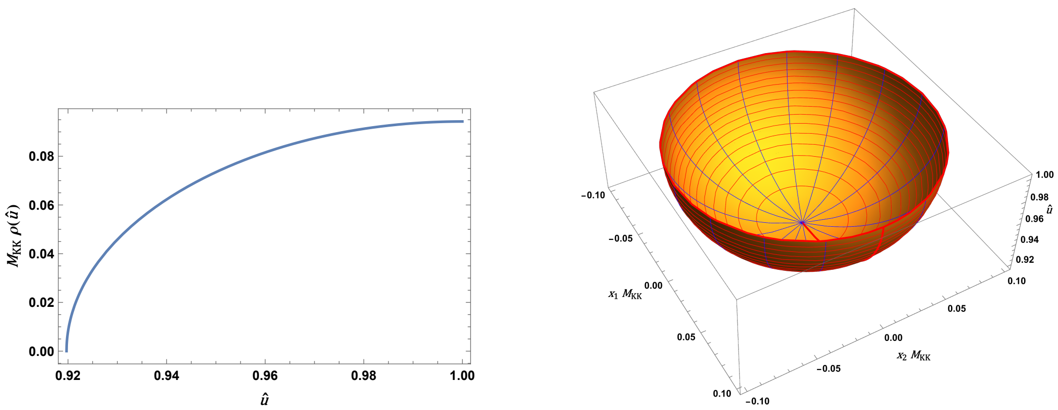

Figure 6.7. Numerical solution of ρ (times M_{KK}) for $b = 0.1$ and $\lambda = 100$ as a function of the rescaled holographic coordinate $\hat{u} = u/u_J \in [0.92, 1]$, describing a stable baryon with baryon number $n_B = 1$. The profile's derivative at $\hat{u} = 1$ is zero, indicating the (meta)stability of this embedding, while it goes to ∞ at $\hat{u} = u_E/u_J$, enforcing the smoothness of the manifold.

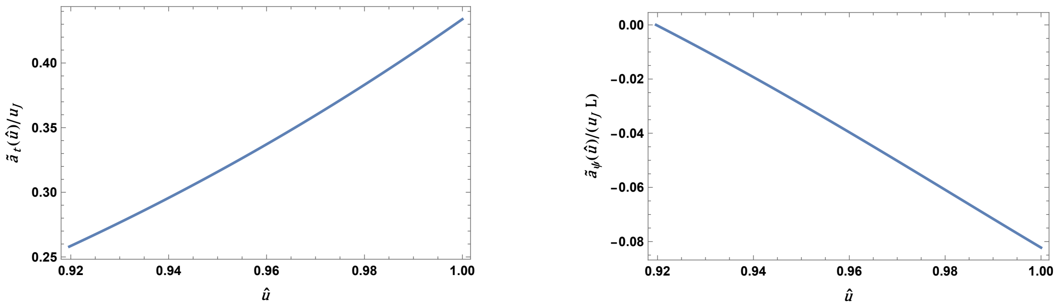

Figure 6.8. Numerical solutions for $u_J^{-1}\tilde{a}_t$ (left panel) $(u_J L)^{-1}\tilde{a}_\psi$ (right panel) as a function of the rescaled holographic coordinate $\hat{u}$ for $b = 0.1$ and $\lambda = 100$.

We can compute the extension along u of the D6-brane embedding with baryon number $n_B = 1$. This is shown in figure 6.9. The left panel shows the behavior of the relative extension $(u_J - u_E)/(u_J - u_0)$ for fixed $\lambda = 100$ as a function of b. The right one shows $(u_J - u_E)/(u_J - u_0)$ for fixed $b = 0.1$ as a function of λ. Moreover, in red, we present a fit for a fixed $b = 0.1$ (The result does not depend on the specific value of b), for which we have

$$\left.\frac{u_J - u_E}{u_J - u_0}\right|_{b\,\text{fixed}} \sim \lambda^{-\gamma} \qquad \text{with} \qquad \gamma \approx 0.8\,. \tag{6.94}$$

Since $\lambda \gg 1$ for the reliability of the holographic model at hand, the extension of the D6-brane along u is parametrically small in λ for every value of b.

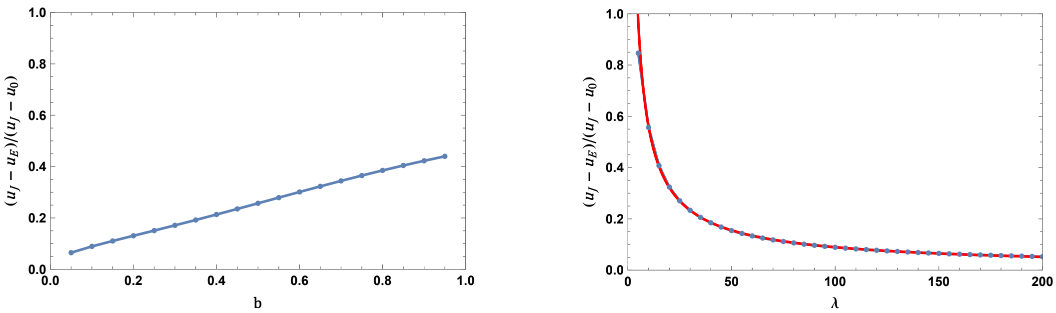

Figure 6.9. In these plots, we show the behavior of the extension of the D6-brane along the u coordinate $(u_J - u_E)/(u_J - u_0)$. In the left panel, we fix $\lambda = 100$ and we show the dependence on b. In the right panel, we fix $b = 0.1$ and we show the behavior of $(u_J - u_E)/(u_J - u_0)$ as a function of λ.

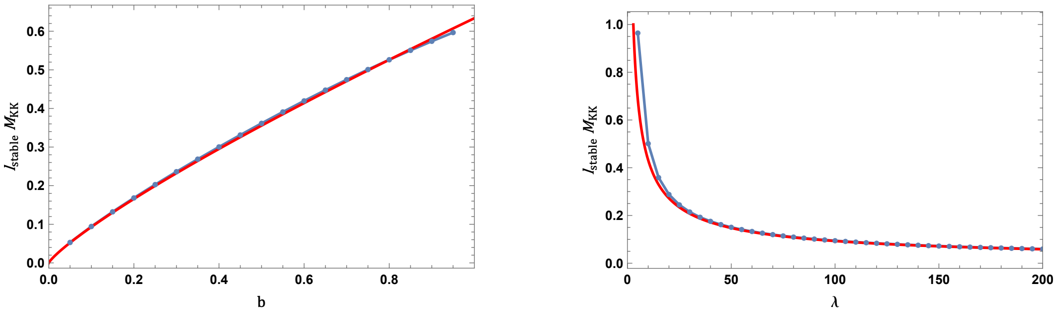

Figure 6.10. The plot of $l_{\rm stable}M_{KK}$ is shown (in blue) for fixed $\lambda = 100$ as a function of b (left panel) and for fixed $b = 0.1$ as a function of λ (right panel). The red lines are the analytical estimates coming from the rigid rotor.

The rigid rotor approximation perfectly fits the behavior of the stability radius $l_{\rm stable}$, computed as the on-shell value of $\rho(u_J)$, as a function of (large) λ. In the left panel of figure 6.10, the plot of $l_{\rm stable}$ as a function of b for fixed $\lambda = 100$ is shown in blue, together with the analytical result in red coming from the rigid rotor (6.84). The right panel shows the plot of $l_{\rm stable}$ for $b = 0.1$ as a function of λ (in blue) together with the analytic prediction at fixed $b = 0.1$ coming from the rigid rotor (in red). The analytic prediction is very reliable for large λ, while it starts to fail at very small λ, where in any case the holographic approximation is not expected to be reliable.

We can observe that the approximation of the D6-brane as a rotating disk seems reasonable since the extension along u of the D6-brane ($\sim \lambda^{-0.8}$) is parametrically smaller than the radius of the D6-brane ($\sim \lambda^{-2/3}$).

Then, we can compute the energy numerically from the following formula (see equation (6.66))

$$E = \frac{N\,\lambda^2}{2\cdot 3^4\pi^2}\frac{J(b)}{b^{3/2}}\,M_{KK}\int_{u_E/u_J}^{1} d\hat{u}\,\hat{u}\,\rho(\hat{u})\left(D(\hat{u}) + \frac{(\partial_u\tilde{a}_t)^2}{D(\hat{u})}\right), \qquad (6.95)$$

where $\rho(\hat{u})$, and $D(\hat{u})$ are computed for the rescaled fields. In figure 6.11 we plot the on-shell energy for a fixed value of $b = 0.1$ as a function of λ and show that for this observable, the rigid rotor approximation (6.87) is not reliable. We suspect that dropping the gauge connection in the mass term of the rigid rotor energy might be too drastic, and it spoils the λ-dependence of the energy.

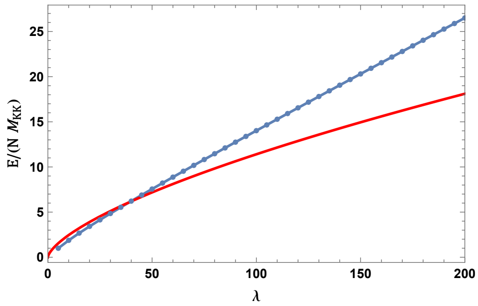

Figure 6.11. The plot shows the energy of the baryon solution with $n_B = 1$ in blue for $b = 0.1$ as a function of $\lambda \in [5, 200]$. The red curve is the corresponding analytical prediction from the rigid rotor.

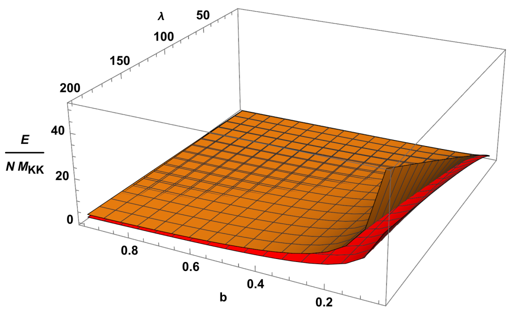

Figure 6.12. The figure shows the plot the energy for a D6-brane solution with $n_B = 1$ in orange as a function of b and $\lambda \in [5, 200]$. We plot it together with the associated Bogomol'nyi bound (6.79) in red.

In figure 6.12, we plot the energy of a D6-brane solution with $n_B = 1$ in orange as a function of b and λ. We plot it together with the associated Bogomol'nyi bound (6.79) in red.

It is also interesting to shed light on the picture of the D6-brane as composed of a D4-brane vertex and a bunch of fundamental strings. This interpretation has been made precise in the supersymmetric case [192] also at the level of the energy. We would like to see the emergence of this structure even in our non-supersymmetric case. Therefore, we can compare the energy of the D6-brane baryon solution with the energy of a wrapped D4-brane placed at u_E plus the energy of N fundamental strings hanging from u_J to u_E giving

$$E_{\text{D4+f-strings}} = \frac{N}{6\pi l_s^2} u_E + \frac{N}{2\pi l_s^2}(u_J - u_E). \tag{6.96}$$

As it can be seen from figure 6.13, the actual energy of the D6-brane baryon solution (in violet) and that given in equation (6.96) (in orange) are, remarkably, almost equal, especially in the large-λ limit, reinforcing the reliability of the above-mentioned picture.

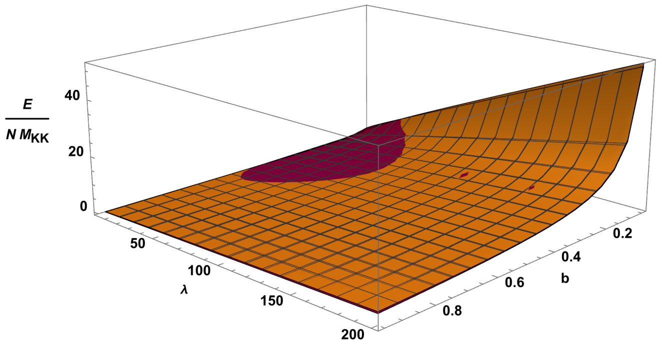

Figure 6.13. The plot shows the energy of the D6-brane baryon solution in violet and the energy of the D4-brane vertex plus the energy of N fundamental strings in orange. The range of parameters is $\lambda \in [5, 200]$ and $b \in [0, 1]$.

We remind that the equations of motion together with the associated boundary conditions depend on the ratio $\xi = n_B/\lambda$ and not on λ alone. We also observe that if $n_B \sim \lambda^0$, the large-λ limit corresponds to the $\xi \to 0$ limit. Moreover, we can have ξ of order one in the large-λ limit if $n_B \sim \lambda$.[16] In the confined phase, baryons are found for every value of b in the regime where ξ is less than some critical value $\xi_{\text{cr.}}$. In the regime where ξ is close to $\xi_{\text{cr.}}$, the solutions are typically parametrically larger, and tend to occupy a larger fraction of the space between u_0 and u_J until they become almost space-filling, and eventually, we do not find any solution.

6.2.3 Deconfined phase

In this section, we present the baryon solution with $n_B = 1$ in the deconfined phase for $\lambda_T = 100$ and $\tilde{b} = 0.1$, in figures 6.14 and 6.15. For these values of the parameters, the integration stops at $u_E \approx 0.92$. The plots show functions of the rescaled holographic coordinate $\hat{u} = u/u_J$.

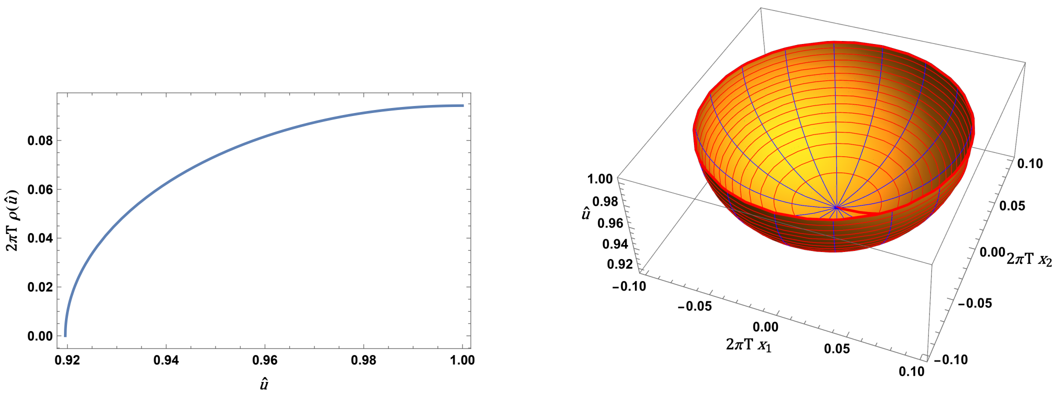

Figure 6.14. Numerical solution of ρ (times $2\pi T$) for $\tilde{b} = 0.1$ and $\lambda_T = 100$ as a function of the rescaled holographic coordinate $\hat{u} = u/u_J \in [0.92, 1]$, describing a (meta)stable baryon with baryon number $n_B = 1$. The profile's derivative at $\hat{u} = 1$ is zero, indicating the (meta)stability of this embedding, while it goes to ∞ at $\hat{u} = u_E/u_J$.

[16] Note that ξ can be of order one also if $n_B \sim \lambda^0$ and $\lambda \sim \mathcal{O}(1)$, but in this case the holographic model is not reliable.

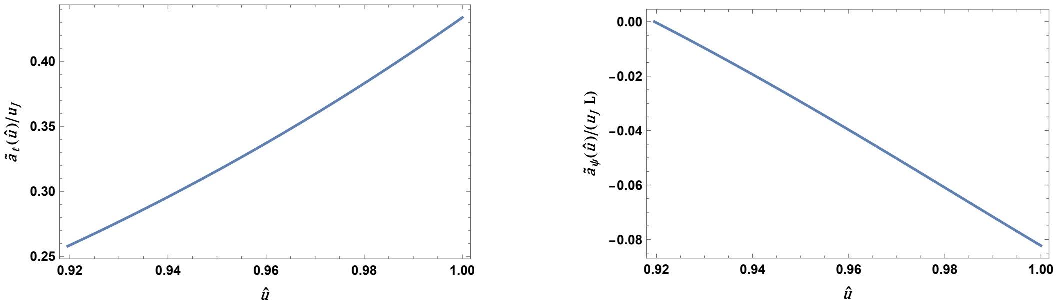

Figure 6.15. Numerical solutions for $u_J^{-1}\tilde{a}_t$ (left panel) and $(u_J L)^{-1}\tilde{a}_\psi$ (right panel) as a function of the rescaled holographic coordinate $\hat{u}$ for $\tilde{b} = 0.1$ and $\lambda_T = 100$.

We can compute the extension along u of the D6-brane embedding with baryon number $n_B = 1$ also in this case. The left panel of figure 6.16 shows the plot of $(u_J - u_E)/(u_J - u_T)$ as a function of $\tilde{b}$ for fixed $\lambda_T = 100$. In the right panel of figure 6.16, we show the plot of the same quantity for fixed $\tilde{b} = 0.1$ as a function of λ_T (in blue). We also show a fit (in red) with a power function of λ_T

$$\left.\frac{u_J - u_E}{u_J - u_T}\right|_{\tilde{b}\,\text{fixed}} \sim \lambda_T^{-\gamma} \qquad \text{with} \qquad \gamma \approx 0.8\,. \tag{6.97}$$

In all the plots for the deconfined phase, we remind that $\tilde{b} \simeq 0.75$ is the value for which we have chiral symmetry restoration, after which the D6-brane configurations do not make sense anymore. Therefore, we stop all the deconfined phase plots at $\tilde{b} = 0.7$.

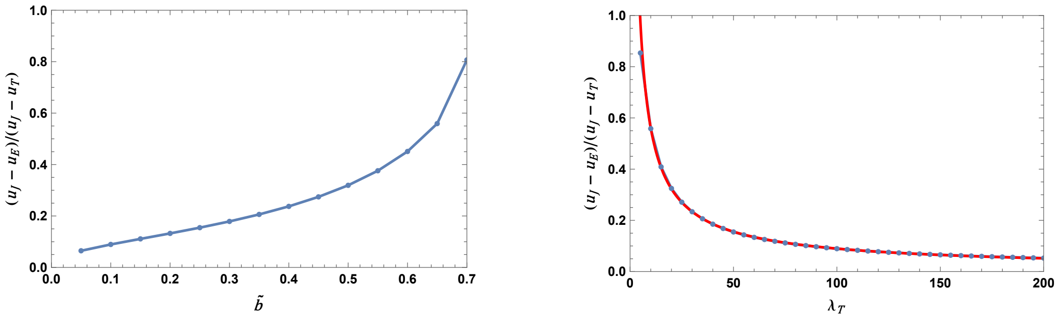

Figure 6.16. In these plots, we show the behavior of the extension of the D6-brane along the u coordinate $(u_J - u_E)/(u_J - u_T)$. In the left panel, we fix $\lambda_T = 100$ and we show the behavior as a function of $\tilde{b}$. In the right panel, we fix $\tilde{b} = 0.1$ and we show the behavior of $(u_J - u_E)/(u_J - u_T)$ as a function of λ_T. A fit with a function of λ_T is indicated in red and goes like $\sim \lambda_T^{-0.8}$.

Also in the deconfined phase, the rigid rotor approximation perfectly fits the behavior of the stability radius l_{stable} as a function of λ. In the left panel of figure 6.17, it is shown the plot of l_{stable} as a function of $\tilde{b}$ for fixed $\lambda_T = 100$ in blue, together with the analytical result in red coming from the rigid rotor approximation (6.90). In the right panel of figure 6.17, it is shown the plot of l_{stable} for $\tilde{b} = 0.1$ as a function of λ_T (in blue) together with the analytic prediction at fixed $\tilde{b} = 0.1$ coming from the rigid rotor. The analytic prediction is very reliable for large λ_T, while it starts to fail at very small λ_T where, anyway, the holographic results are not reliable.

Therefore, also in the deconfined phase, the approximation of the D6-brane as a rotating disk looks reasonable since the extension along u of the D6-brane ($\sim \lambda^{-0.8}$) is parametrically smaller than the radius of the D6-brane ($\sim \lambda^{-2/3}$).

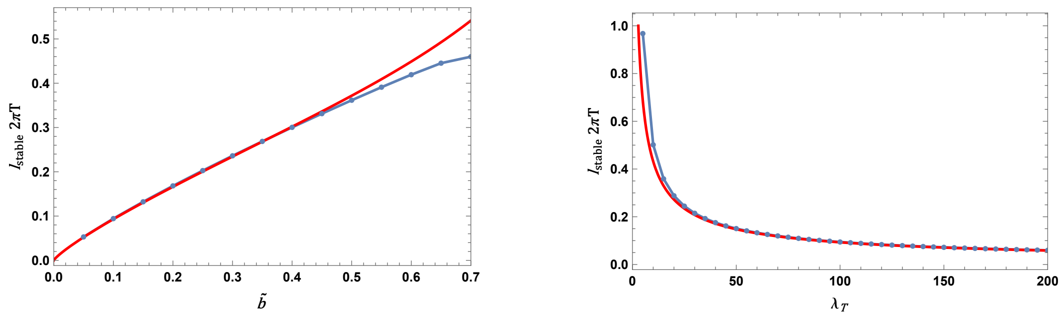

Figure 6.17. The plot of $l_{\text{stable}} 2\pi T$ is shown (in blue) for fixed $\lambda_T = 100$ as a function of $\tilde{b}$ (left panel) and for fixed $\tilde{b} = 0.1$ as a function of λ_T (right panel). The red lines are the analytical estimates coming from the rigid rotor.

The energy of the solution in the deconfined phase can be computed numerically starting from the following formula (see also equation (6.73))

$$E = N\,\lambda^2 \frac{2^2\pi\, J_T(\tilde{b})}{3^4\, \tilde{b}^{3/2}} \frac{T^3}{M_{KK}^2} \int_{u_E/u_J}^{1} d\hat{u}\, \hat{u}\, \rho(\hat{u}) \left(D_T(\hat{u}) + \frac{(\partial_u \tilde{a}_t)^2}{D_T(\hat{u})} \right), \tag{6.98}$$

where $\rho(\hat{u})$ and $D_T(\hat{u})$ are computed for the rescaled fields. In figure 6.18 we plot the energy for $\tilde{b} = 0.1$ as a function of λ_T and show that for this observable, the rigid rotor approximation (6.91) is not reliable. Again, we suspect that dropping the gauge connection in the mass term of the rigid rotor energy might be too drastic, and it spoils the λ_T-dependence of the energy.

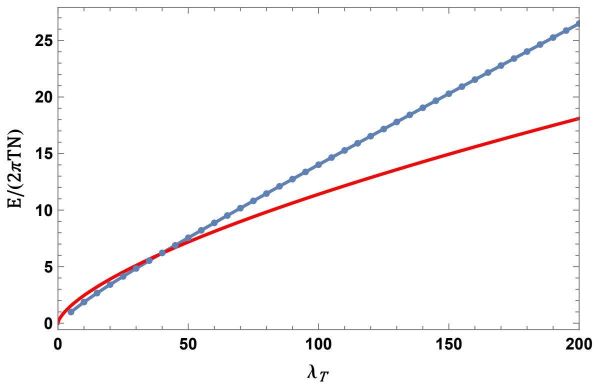

Figure 6.18. The plot shows the energy of the baryon solution with $n_B = 1$ in blue for $\tilde{b} = 0.1$ as a function of $\lambda_T \in [5, 200]$. The red curve is the corresponding analytical prediction from the rigid rotor.

In figure 6.19, we plot the energy for a D6-brane solution with $n_B = 1$ in orange as a function of $\tilde{b}$ and λ_T. We plot it together with the associated Bogomol'nyi bound (6.79) in red.

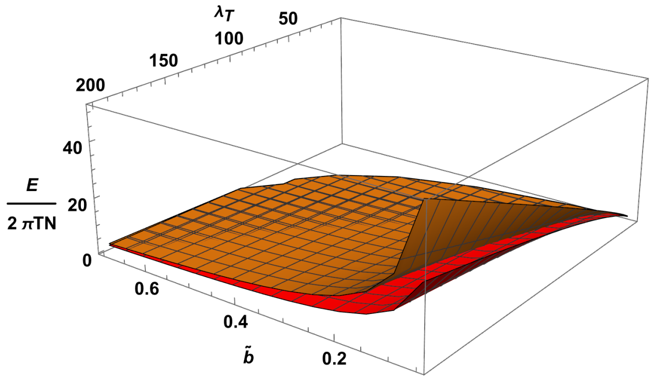

Figure 6.19. The figure shows the plot the energy for a D6-brane solution with $n_B = 1$ in orange as a function of $\tilde{b}$ and $\lambda_T \in [5, 200]$. We plot it together with the associated Bogomol'nyi bound (6.79) in red.

We conclude by noting that for small enough $\xi_T (\lesssim 0.01)$, we find baryon solutions in the deconfined phase for every value of $\tilde{b}$. However, for small ξ_T such that the holographic model is still reliable in the $n_B \sim \lambda^0$ case, baryon solutions exist only for $\tilde{b}$ less than a critical value $\tilde{b}(\xi_T)$, which decreases as a function of ξ_T. This means that for sufficiently large temperatures, the baryons cease to exist, since they melt in the plasma. The existence region of baryons in parameter space is shown in figure 6.20.

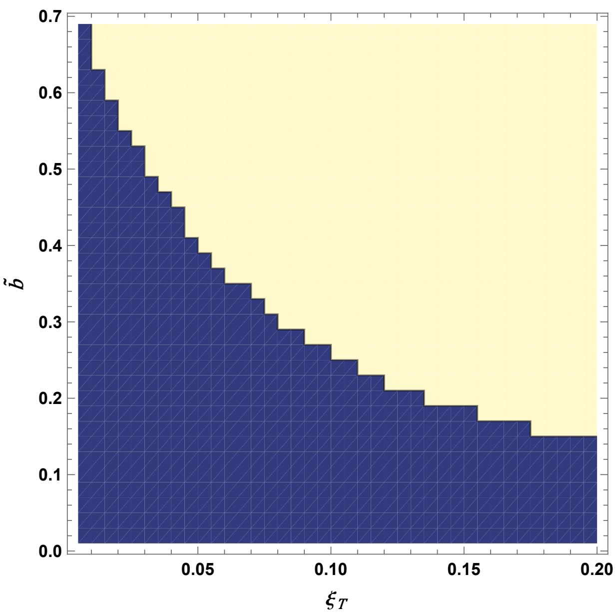

Figure 6.20. In blue the region, in the parameter space $0 < \tilde{b} < 0.7$ and $\xi_T \in [0.005, 0.2]$, where D6 baryons exist in the deconfined phase.

6.2.4 Summary of the baryon's properties

We conclude the analysis of the D6-brane baryon solution by collecting the results about its physical properties, namely its mass (*i.e.* the on-shell energy E) and its radius. We list them for both the confined and the deconfined phases. In table 6.2, they are shown as functions of the string theory parameters (neglecting multiplicative constants) while in table 6.3 we give their full expressions in terms of "phenomenological" parameters, like the η' decay constant $f_{\eta'}$. The definition of the latter in the confined phase, for generic non-antipodal branes, reads

$$f_{\eta'}^2 = \frac{N\,\lambda}{54\pi^3}\frac{M_{KK}^2}{I(b)b^{3/2}} \quad \text{with} \quad I(b) = \int_0^1 dy \frac{y^{-1/2}}{\sqrt{1-b^3 y-(1-b^3)y^{8/3}}}\,. \tag{6.99}$$

The decay constant at finite temperature is[17]

$$f_{T,\eta'}^2 = \frac{N\,\lambda_T(2\pi T)^2}{54\pi^3 I_T(\tilde{b})\tilde{b}^{3/2}} \quad \text{with} \quad I_T(\tilde{b}) = \int_0^1 dy \frac{y^{-1/2}\sqrt{1-\tilde{b}^3 y}}{\sqrt{1-\tilde{b}^3 y-(1-\tilde{b}^3)y^{8/3}}}\,. \tag{6.100}$$

See *e.g.* [140] for a review on the derivation of the above expressions. Note that they have a non-trivial N-dependence. In the following, we will use the approximations $I(b) \approx I(0) = I = 2.48$, and $I_T(\tilde{b}) \approx I_T(0) = I = 2.48$.[18].

The results are given in the large-λ limit for a baryon with $n_B = 1$:

	Confined phase	Deconfined phase
Radius	$l_{\text{stable}} \sim \lambda^{-2/3}\Lambda^{-1}b^{5/6}$	$l_{\text{stable}} \sim \lambda_T^{-2/3}T^{-1}\tilde{b}^{5/6}(1-\tilde{b}^3)^{-1/3}$
Mass	$E \sim N\lambda\Lambda b^{-1}$	$E \sim N\lambda_T T\tilde{b}^{-1}$

Table 6.2. Summary of parametric scaling properties of the baryon solution's radius and mass. For the reader's convenience, we used the dynamical scale notation Λ instead of M_{KK}.

	Confined phase	Deconfined phase
Radius	$l_{\text{stable}} \approx C_l\,N^{5/9}(\Lambda/\lambda)^{1/9}f_{\eta'}^{-10/9}$	$l_{\text{stable}} \approx C_l\,N^{5/9}(\Lambda/\lambda)^{1/9}f_{T,\eta'}^{-10/9}$
Mass	$E \approx C_E\,N^{1/3}(\lambda/\Lambda)^{1/3}f_{\eta'}^{4/3}$	$E \approx C_E\,N^{1/3}(\lambda/\Lambda)^{1/3}f_{T,\eta'}^{4/3}$

Table 6.3. Summary of the main properties of the baryon.

To obtain the radius estimation, we can use the rigid rotor values, which give

$$C_l = 2^{-19/18}3^{1/3}\pi^{-1}I^{-5/9} \approx 0.221\,. \tag{6.101}$$

[17]The expression for $f_{T,\eta'}$ reads the same as the one for f_a introduced in chapter 5 in equation (5.117).

[18]This is a fairly good approximation since $I(b)$ and $I(\tilde{b})$ are monotonic functions, with $I(b = 1) = \pi$, $I(\tilde{b} = 1) = 2$

For the mass estimation, we use a power law fit for b and λ. C_E is a constant obtained by a fit of the energy scaling law obtained numerically. Notably, the same value is obtained in both phases

$$C_E \approx 0.129\, I^{2/3} \approx 0.236\,. \tag{6.102}$$

6.3 Vortons

In section 5.2.2, we studied the uncharged axionic loop by analyzing the D6-brane embedding with no gauge field. The fact that the embedding does not end orthogonally at the D8-brane tip is a signal that the D6-brane is going to shrink in size due to its tension. In fact, both the string loops and the (uncharged) DWs can decay at least by emitting mesons (mostly axions) on the D8-brane. In this section, we consider the charged version of the D6-brane representing the string loop, *i.e.* the vorton, and we discuss its stability.

The main difference between the vorton embedding and the baryon one is that for the vorton, the extension along the u-coordinate does not scale with λ (or equivalently α'), $u_J - u_T \sim \lambda^0$, while for the baryon we have seen that $u_J - u_E \sim \lambda^{0.8}$. This leads to important consequences for the vorton stability. Let us analyze the λ-dependence of the fields in the vorton case. Since in this case the integration domain in (6.31) is of order zero in λ, we need to have $a_\psi \sim n_B \lambda^0$. Moreover, in order for the angular momentum J not to scale with λ, the fields ρ and a_t have to scale as

$$\rho \sim \lambda^{-\upsilon}\,, \qquad\qquad a_t \sim \lambda^{\upsilon}\,, \tag{6.103}$$

for some $\upsilon \geq 0$. We rule out immediately the case $\upsilon > 1$ because it leads to an imaginary action.[19] Moreover, for $\upsilon \in [0,1)$, in the large-λ limit, the equations of motion do not admit solutions.

Actually, from the equations of motion (6.27) for the fields, the condition $\rho'(u_J) = 0$, the relations $\alpha' \sim \lambda^{-1}$ and $\mathbf{k}_t/3 = n_B$, and the above observation concerning the scaling of a_ψ, it follows that $a_t'(u_J) \sim \lambda$ and

$$l \equiv \rho(u_J) \sim \frac{n_B}{\lambda}\,. \tag{6.104}$$

Thus, if a (meta)stable vorton solution exists, the vorton radius l is expected to scale as above. Note that this result, as anticipated, is consistent with the findings of section 5.3.2 where the vorton stability radius has been computed from the D8-brane perspective in the flat approximation.

It is interesting to notice that the above result also agrees with the following estimates. Let us approximate the vorton as a rigid non-relativistic cylindrical rotor of radius l, with mass M, moment of inertia $I = Ml^2$, and angular momentum $J = N\, n_B^2/2$. We will do the same thing for the sandwich vortons in the next section. The total energy is given by

$$E = M + \frac{J^2}{2I}. \tag{6.105}$$

[19] Remember that we are working in the large-λ limit.

We approximate $\rho(u)$ to a constant $\rho(u) \approx l$ throughout the whole u-range and therefore $\rho'(u) = 0$. Setting $a = 0$ in the action (6.22), the mass of the rigid rotor reads

$$M = \frac{N\,\lambda_T^2}{3^5 2\pi^2 \tilde{b}^2}\left(\frac{T}{T_c}\right)^2\left(1 - \frac{2^8\pi^4}{3^4 c_a^2}\frac{T^2}{T_a^2}\right). \tag{6.106}$$

Then, we can minimize the total energy with respect to l, and extract the stability radius, which reads

$$M_{KK}\, l_{\text{stable}} = \frac{3^{11/4}\,\pi\,\tilde{b}}{2^{3/4}}\left(1 - \frac{2^8\pi^4}{3^4 c_a^2}\frac{T^2}{T_a^2}\right)^{-1/2}\left(\frac{T_c}{T}\right)\xi_T. \tag{6.107}$$

Since $\xi_T = n_B/\lambda_T$, the minimization over l gives $l_{\text{stable}} \sim n_B/\lambda$ consistently with eq. (6.104).

It is easy to realize that if $n_B = \mathcal{O}(\lambda^0)$, the equations of motion for the embedding and the gauge field on the D6-brane do not admit (meta)stable vorton solutions. In fact, in this case, we would need to have $\rho(u) \sim \lambda^{-1}$ for any u: in the large-λ limit, this would lead to a solution to the equations of motion with a constant radius that is inconsistent with the other equations of motion.

Actually, if $n_B = \mathcal{O}(\lambda^0)$, it turns out that the gauge field is subleading w.r.t. the profile $\rho(u)$, and as such it can be treated in a probe approximation. But such an approximation does not change the embedding solution found in section 5.2.2 and thus, in particular, the charged string loop remains unstable: it is not possible to find a solution with $\rho'(u_J) = 0$, which is the condition for stability at the tip of the D8-branes.

The instability of the charged string loop solution with order-one baryon charge is easily seen also by looking at the free energy in the probe approximation. The expansion up to quadratic order in the gauge field of the free energy reads

$$\begin{aligned} E_{\text{D6}} &\approx N\lambda^2\widetilde{C}\int dt\,du\,\rho(u)\,u\,D_0(u) + \frac{N}{2}\int dt\,du\,\frac{\rho(u)\,u}{D_0(u)}\left[-(\partial_u a_t)^2 + \frac{f_T(u)}{\rho(u)^2}(\partial_u a_\psi)^2\right] \\ &\quad - \frac{N}{2}\int dt\,du\,(a_\psi\partial_u a_t - a_t\partial_u a_\psi)\,, \end{aligned} \tag{6.108}$$

where $D_0(u)$ is given in equation (5.17), and

$$\widetilde{C} \equiv \frac{1}{3\cdot 2^4\pi^2 R^6 M_{KK}^2}\,. \tag{6.109}$$

From the above expression of the free energy, we can deduce that no stability radius l can exist with scaling λ^0. The Maxwell-Chern-Simons free energy is of order λ^0 if $l \sim \lambda^0$, so it cannot counter-balance the energy due to the tension from the first term (which scales as λ^2), and no (meta)stable solution can be found. In order to be stable, the vorton radius should be suppressed with a power of λ, which is not possible as we have seen when we studied the string loop embedding in section 5.2.2 (the minimal radius of the string loop was of order λ^0). Thus, if a string loop of radius of order λ^0 has an order-one baryon charge, it is still unstable. It will evolve in a smaller configuration with the same charge by emitting axions, eventually decaying completely (for example in a charged DW) before its size can become parametrically small in λ. Phenomenologically, this defect is expected to decay producing axions and gravitational waves (if one adds gravitational interactions to the story).

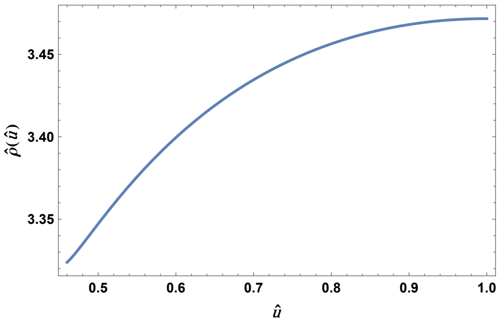

(a) Plot of the solution $\hat{\rho}$ for $\tilde{b} = 0.45$.

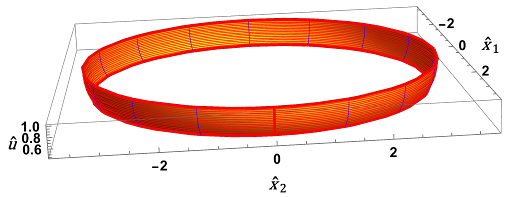

(b) Revolution plot around the $\hat{u}$ axis of the embedding $\hat{\rho}$ for $\tilde{b} = 0.45$.

Figure 6.21. Numerical solution of $\hat{\rho}$ for $\tilde{b} = 0.45$ as function of the holographic coordinate $\hat{u}$, describing the metastable vorton configuration with large charge. The profile derivative at $\hat{u} = 1$ is zero, indicating the (meta)stability of this embedding. The $\hat{u}$ variable runs from the horizon $\tilde{b} = 0.45$ to the D8-brane tip.

6.3.1 Vortons with large baryon charge

The conclusions about the instability of the vorton come from the requirement that such a solution should have baryon number and angular momentum of order λ^0. As a consequence, the gauge field can be treated in the probe approximation, and the vorton cannot be stabilized by the D6-brane spin or the Coulomb repulsion due to the electric field.

However, there is the case where the vorton solution can be at least metastable if we allow it to carry a large baryon charge of order λ. It can be shown, by a parametric analysis, that this is the only possible choice. Let us then consider

$$n_B = -\int_{u_T}^{u_J} du\, \partial_u a_\psi \sim \lambda\,, \tag{6.110}$$

which, according to (6.104), would correspond to a vorton radius l of order λ^0. In this case, $a_\psi \sim n_B \sim \lambda$. Then, if we want a vorton with $\rho \sim \lambda^0$ we must also have $a_t \sim \lambda$. These scalings for the fields completely factorize the λ dependence out of the action. The equations of motion for the fields are formally identical to the ones we derived in (6.27). However, in the present case, the gauge field a is not the barred one $\bar{a}$, since the λ-dependence has factorized out. With this in mind, we solved the equations of motion numerically, following again the procedure outlined in appendix D.

Examples of the related numerical solutions for the intermediate temperature corresponding to $\tilde{b} = 0.45$ are shown in figures 6.21, 6.22. Remember that these plots refer to the hatted fields, as indicated in the plots' labels. The plot of the profile $\rho(u)$ and its revolution plot around the u axis of the profile are shown in figures 6.21a and 6.21b respectively. Figure 6.22a shows the plot of $a_t(u)$, which goes to zero at the horizon consistently with regularity. The plot of the gauge field component $a_\psi(u)$ is shown in figure 6.22b. In a sentence, these big vortons are stabilized by their huge charge, which balances their tension.

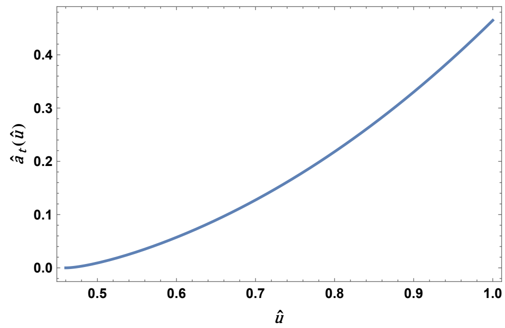

(a) Numerical solution for $\hat{a}_t$ for $\tilde{b} = 0.45$. The gauge field component $\hat{a}_t$ goes to zero to enforce regularity at the horizon.

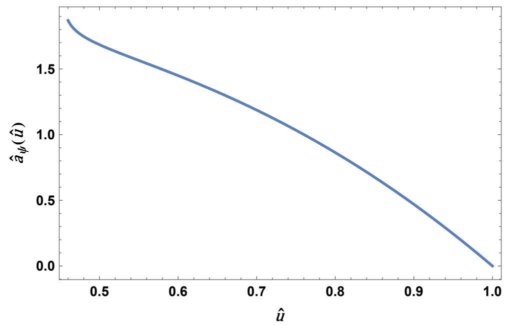

(b) Numerical solution for $\hat{a}_\psi$ for $\tilde{b} = 0.45$. This solution has the right boundary conditions to give baryon number λ.

Figure 6.22. Numerical solutions for $\hat{a}_t$ and $\hat{a}_\psi$ for $\tilde{b} = 0.45$ as function of the holographic coordinate $\hat{u}$.

6.4 Punctured domain walls and *sandwich* defects

In this section, we present more exotic solutions to the D6-brane equations of motion, which are not baryons but have non-zero baryon number: sandwich defects (see figure 6.3) and punctured domain walls (see figure 6.4). Before we present the associated numerical solutions of the equations of motion, let us describe in more detail the dual interpretation of these D6-brane configurations.

Punctured domain walls are infinitely extended domain walls with a hole inside. They could form either from the chiral symmetry breaking phase transition, or by tunneling transitions which open up a hole in an infinite DW. The latter is actually a standard decay channel of infinite DWs (see *e.g.* [42]): holes can form on the worldvolume, then they start to expand, and eventually eat up all of the defect; collisions of the hole boundaries, *i.e.* global strings, can produce gravitational waves [193].

An amusing feature of these configurations is that the D6-brane can end orthogonally to the D8-brane, signaling a force balance, even in the uncharged case. Indeed, there is a specific value of the radius $\rho(u_J)$ for which we get the necessary metastability condition $\rho'(u_J) = 0$. We can interpret this behavior by commenting on what happens if we vary the hole radius. If we increase the radius of the hole, the energy of the DW is reduced, as we are decreasing its worldvolume.[20] At the same time, the energy of the bounding string is increased, since its length increases.[21] Thus, there can be a critical radius for which the two opposite forces are exactly balanced.

In this chapter, we can also consider their charged version under the baryonic symmetry. Holographically, these are charged D6-brane solutions. The charge just adds a force component to the picture described above, with the only result that the critical radius of the hole for which there is orthogonality is different w.r.t. the uncharged case. In the following, we are going to show only the results for the

[20]Note that this behavior is opposite w.r.t. all the other configurations we consider in this chapter.

[21]Holographically, this is seen as an increase of the area of the "vertical portion" (in u) of the D6-brane.

charged critical (orthogonal) case.

Sandwich defects are even more exotic objects. We introduced them in section 5.2.2 in the deconfined phase of the WSS model. From the holographic point of view, these are described by D6-branes ending on two different flavor branes. These objects can be studied in the confined and deconfined phases. The two flavor branes can be interpreted as both dark (for the Standard Model interactions) flavors in the dual QFT, or one of the two flavor branes (the one that condenses at a lower scale), or both, can be associated with QCD flavors. We have such a possibility because the asymptotic separation between a D8-brane and a $\overline{\text{D8}}$-brane L, of a given flavor, is a free parameter in the model and hence we can tune L to get the desired T_a (see equation (3.122)) at which the chiral symmetry is broken. In the framework of SU(N) Yang-Mills theories with flavors, the interplay between a dark and the η' meson (or any other dark meson) leads to the formation of rich topological structures. These arise due to a sequence of symmetry-breaking patterns, each introducing different types of defects, which can ultimately combine into composite structures carrying both axion (for example) and η' excitations (see *e.g.* [41, 42]). The formation of these defects is a natural consequence of the non-trivial vacuum structure of the theory, and their evolution depends on the dynamics of spontaneous and explicit symmetry breaking. The presence of both η' and dark topological defects (or two dark topological defects) in the same system means that, in certain regions, these structures can overlap or interact. This is where the idea of *sandwich* structures emerges: a layered configuration where the presence of one field influences the stability and interactions of the other. We can think of these objects both at zero and at finite temperature. In a realistic cosmological scenario at finite temperature, the evolution of these defects depends on their stability and interactions with the surrounding plasma.

Sandwich solutions, if not charged, are not stable and will decay. They can be stabilized, like the other kinds of configurations, by turning on the gauge connection on the D6-brane worldvolume. In this case, these objects will have a baryon number given by (see equation (6.31))

$$n_B = -\int_{u_K}^{u_J} du\, \partial_u a_\psi = n_J + n_K, \tag{6.111}$$

where u_K and u_J (with $u_K < u_J$ without loss of generality) are the positions of the tip, respectively, of the less and more energetic flavor branes. Importantly, in the deconfined phase, the value of u_K (as the value of u_J) is bounded from below by the quantity $\sim 0.75\, u_T$, to ensure that also the second set of branes is in the chirally broken phase. As discussed in section 6.1, n_J and n_K are physically associated with two different flavor degrees of freedom, counting the number of quarks of each flavor (divided by N). These sandwiches are therefore prototypes of multi-flavored configurations that support a baryon number, and we expect them to be enclosed in a more general theory that describes $N_f \geq 2$ Hall droplet baryons.[22]

In the following, we will present the numerical solution for the punctured domain walls and for the sandwich defects with non-zero baryon number n_B and angular momentum $J = N\, n_B^2/2$, obtained from $n_K = 0$ and $n_J = 1$. We first check if the

[22]Let us mention that these sandwich configurations resemble the construction presented in [194].

expansion around $u = u_K$ allows for $\tilde{a}_\psi(u_K) = 0$ and regularity ($\rho'(u_K) = 0$). We demand that the fields have a regular expansion around u_K

$$\rho(u) = \sum_{n=0}^{\infty} c_n (u - u_K)^n, \quad \tilde{a}_t(u) = \sum_{n=0}^{\infty} b_n (u - u_K)^n, \quad \tilde{a}_\psi(u) = \sum_{n=0}^{\infty} d_n (u - u_K)^n, \tag{6.112}$$

and we impose $c_1 = 0$ for orthogonality and $d_0 = 0$ to enforce the relation between the angular momentum and the baryon number. We checked that both in the confined and the deconfined phase we get a consistent series expansion in terms of $c_0 = \rho(u_K)$ and b_0. An analogous consistency check for the boundary condition with the equations of motion has been done for the punctured domain wall configuration.

Rotor estimates

We end this introduction by giving a numerical estimate of the stability radius and the energy of the sandwich solution, which can be approximated by a rotating cylinder, as for the vorton (see section 6.3). As we have seen previously, for a rotating cylinder with mass M, radius l, and angular momentum J, the total energy in the non-relativistic limit can be approximated by

$$E = M + \frac{J^2}{2I}\,, \tag{6.113}$$

where $I = Ml^2$ is the moment of inertia, and $J = N\, n_B^2/2$. For this type of solution, we can approximate $\rho(u)$ as a constant $\rho(u) \approx l$ throughout the whole u-range and therefore $\rho'(u) = 0$. Let us start from the confined phase. The mass M of the rotating circle is obtained, with the above assumption, from the DBI action in (6.9), setting the gauge field $a = 0$

$$M = \frac{N\,\lambda^2}{3^5\pi^2 b^2}\alpha\, M_{KK}^2\, l\,, \tag{6.114}$$

with

$$\begin{aligned}\alpha =& \frac{1}{2}\left(\sqrt{\frac{u_K}{u_J}}\sqrt{\frac{u_K^3}{u_J^3} - b^3}\left({}_2F_1\left(\frac{2}{3}, 1; \frac{7}{6}; \frac{u_K^3}{u_J^3\, b^3}\right) - 1\right) + \right.\\ &\left. - \sqrt{1 - b^3}\left({}_2F_1\left(\frac{2}{3}, 1; \frac{7}{6}; \frac{1}{b^3}\right) - 1\right)\right).\end{aligned} \tag{6.115}$$

Analogously, in the deconfined phase, setting $a = 0$ in (6.22), the mass of the rotating cylinder is approximated by

$$M = \frac{N\,\lambda_T^2}{3^5\pi^2\,\tilde{b}^2}\,\alpha_T\left(\frac{T}{T_c}\right)^2 M_{KK}^2\, l\,, \qquad \text{with} \qquad \alpha_T = \frac{1}{2}\left(1 - \frac{u_K^2}{u_J^2}\right). \tag{6.116}$$

Minimizing the total energy of the rotor w.r.t. the radius, we find the following results:

- Confined phase:[23]

$$M_{KK}\, l_{\text{stable}} = \frac{3^{11/4}\pi\, b}{2^{3/4}\alpha^{1/2}}\,\xi\,, \tag{6.117}$$
$$E = \frac{2^{5/4}N\,\lambda^2}{3^{13/4}\pi\ b}\,\alpha^{1/2}M_{KK}\,\xi\,. \tag{6.118}$$

- Deconfined phase:

$$M_{KK}\, l_{\text{stable}} = \frac{3^{11/4}\,\pi\,\tilde{b}}{2^{3/4}\,\alpha_T^{1/2}}\left(\frac{T_c}{T}\right)\xi_T\,, \tag{6.119}$$
$$E = \frac{2^{5/4}N\,\lambda_T^2}{3^{13/4}\pi\ \tilde{b}}\,\alpha_T^{1/2}\left(\frac{T}{T_c}\right)M_{KK}\,\xi_T\,. \tag{6.120}$$

In both phases, the stability radius and the on-shell energy scale linearly with $\xi_{(T)}$.

We checked that these analytical estimates correctly reproduce the sandwich stability radius and energy in the large-λ limit, up to numerical factors.[24]

6.4.1 Confined phase

We start by presenting the punctured domain wall solutions. These are infinitely energetic configurations with non-zero baryon number. We are free to choose the value of the holographic coordinate u_* at which the D6-brane profile has infinite radius. This value fixes the stability radius of the hole. In figures 6.23 and 6.24 we show the solutions to the equations of motion for $n_B = 1$, $b = 0.1$, $\lambda = 100$, and for which we have chosen $u_*/u_J = 0.6$.

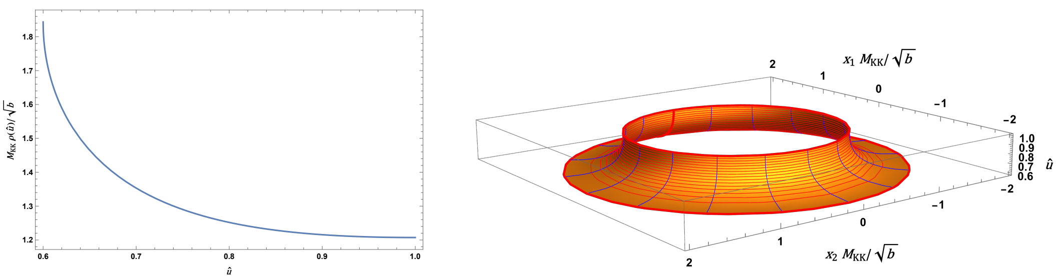

Figure 6.23. Numerical solution of ρ (times $M_{KK}/\sqrt{b}$) for $b = 0.1$ and $\lambda = 100$ as a function of the rescaled holographic coordinate $\hat{u} = u/u_J \in [0.6, 1]$, describing a stable punctured domain wall with baryon number $n_B = 1$. The profile's derivative at $\hat{u} = 1$ is zero, indicating the (meta)stability of this embedding. At $\hat{u} = u_*/u_J$, the profile's radius goes to infinity while in the plot we cut it for clarity at some finite value.

[23] Remember that $\xi_{(T)} = \frac{n_B}{\lambda_{(T)}}$.

[24] This marks a difference with the baryon case, where the energy scaling with $\lambda_{(T)}$ is not well reconstructed. This can be attributed to the less stringent approximation that we did in the rigid rotor analysis for the sandwiches, for which the integration region stays finite.

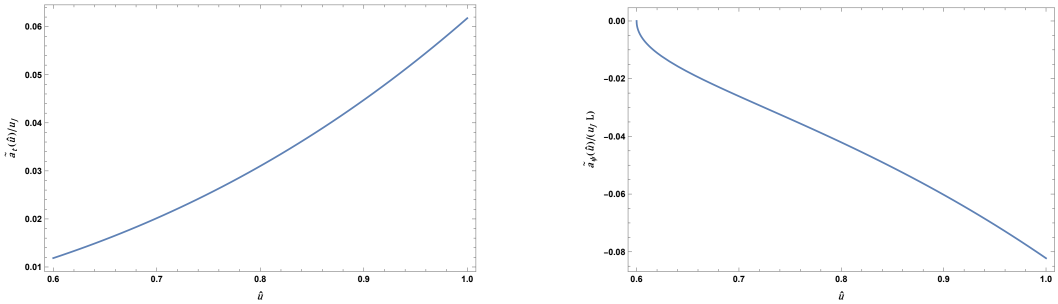

Figure 6.24. Numerical solutions for $u_J^{-1}\tilde{a}_t$ (left panel) and $(u_J L)^{-1}\tilde{a}_\psi$ (right panel) as a function of the rescaled holographic coordinate $\hat{u}$ for $b = 0.1$ and $\lambda = 100$.

Then, we present the sandwich solution for $\lambda = 20$ and $b = 0.1$ associated with the choice of holonomies $n_K = 0$ and $n_J = 1$. We are *a priori* free to set the position of the tip of the second (set of) D8-brane(s), which we will fix to $u_K/u_J = 0.6$ in the plots. The profile ρ of the sandwich, as a function of the rescaled holographic coordinate $\hat{u}$, is shown in figure 6.25, while the associated gauge connection is shown in figure 6.26.

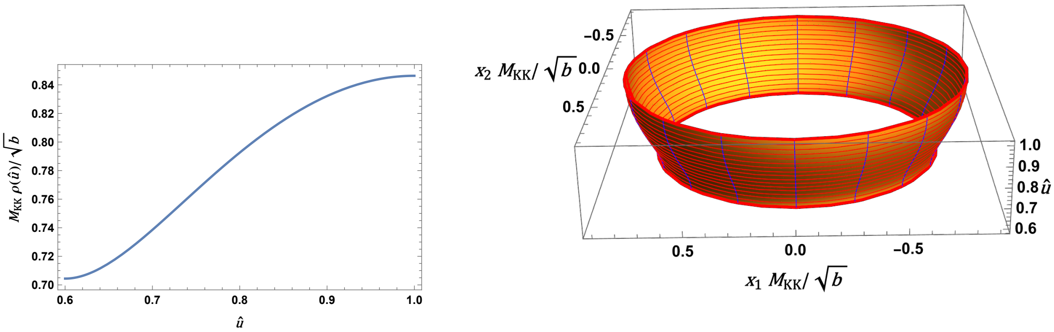

Figure 6.25. Numerical solution of ρ (times $M_{KK}/\sqrt{b}$) for $\lambda = 20$, $b = 0.1$ and $\hat{u}_K = u_K/u_J = 0.6$, as a function of the rescaled holographic coordinate $\hat{u} = u/u_J \in [0.6, 1]$, describing a stable sandwich defect with baryon number $n_B = 1$. The profile's derivative at both $\hat{u}_K$ and $\hat{u} = 1$ is zero, indicating the (meta)stability of this embedding.

The sandwich defect solutions exist only if the two D8-branes are close enough to each other. That is, for every b and λ, there is a minimum value of u, denoted as $\hat{u}_{\min}(b, \lambda)$, such that the sandwich solutions are found for every $\hat{u}_{\min}(b, \lambda) < \hat{u}_K < 1$. As in the baryon case, these solutions are more and more extended along u and larger in ρ as we consider smaller values of λ. We find numerically that $\hat{u}_{\min}$ is a monotonously increasing function of b and λ.

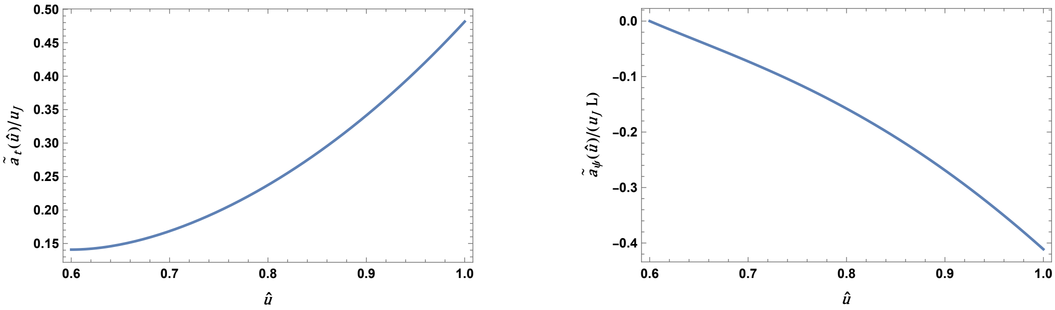

Figure 6.26. Numerical solutions for $u_J^{-1}\tilde{a}_t$ (left panel) and $(u_J L)^{-1}\tilde{a}_\psi$ (right panel) as a function of the rescaled holographic coordinate $\hat{u}$ for $\lambda = 20$, $b = 0.1$ and $\hat{u}_K = 0.6$.

We conclude by mentioning that we can find a sandwich solution with n_K and n_J interchanged, that is, $n_K = 1$ and $n_J = 0$. This solution shows the opposite behavior for the profile $\rho(u)$, meaning that for all u, $\rho'(u) < 0$.

6.4.2 Deconfined phase

Let us now present the punctured domain wall solutions in the deconfined phase. In figures 6.27 and 6.28 we show the solutions to the equations of motion for $\tilde{b} = 0.1$, $\lambda_T = 100$, and for which we have chosen to end the integration at $u_*/u_J = 0.6$.

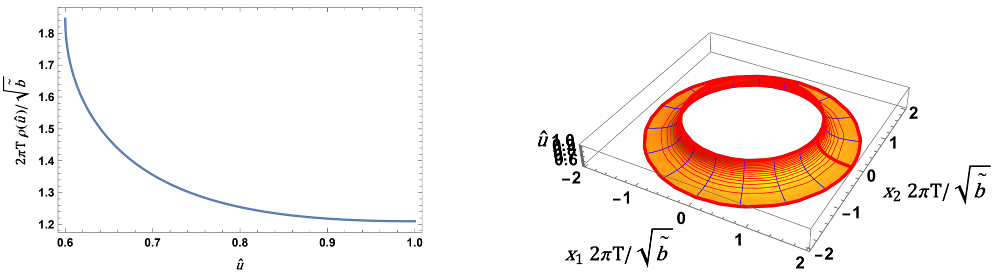

Figure 6.27. Numerical solution of ρ (times $2\pi T/\sqrt{\tilde{b}}$) for $\lambda_T = 20$, $\tilde{b} = 0.1$ and $\hat{u}_* = 0.6$, as a function of the rescaled holographic coordinate $\hat{u} = u/u_J \in [0.6, 1]$, describing a stable punctured domain wall with baryon number $n_B = 1$. The profile's derivative $\hat{u} = 1$ is zero, indicating the (meta)stability of this embedding. At $\hat{u}_* = u_*/u_J = 0.6$ the profile's radius goes to infinity while in the plot we cut it for clarity at some finite value.

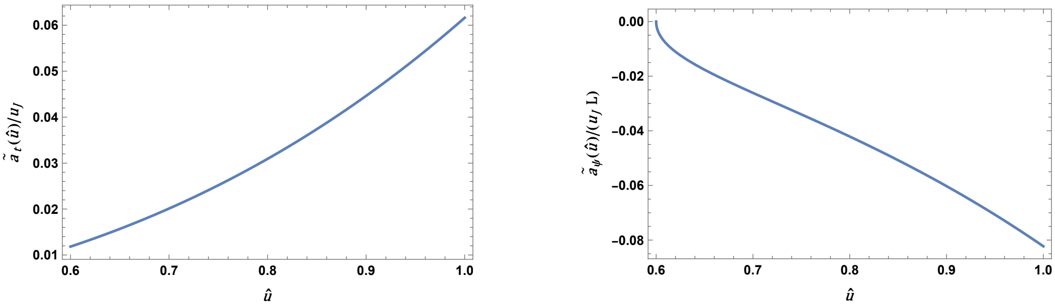

Figure 6.28. Numerical solutions for $u_J^{-1}\tilde{a}_t$ (left panel) and $(u_J L)^{-1}\tilde{a}_\psi$ (right panel) as a function of the rescaled holographic coordinate $\hat{u}$ for $\tilde{b} = 0.1$ and $\lambda = 100$, with the singularity in $\hat{u}_* = 0.6$.

In figures 6.29 and 6.30, we present sandwich solutions in the deconfined phase.

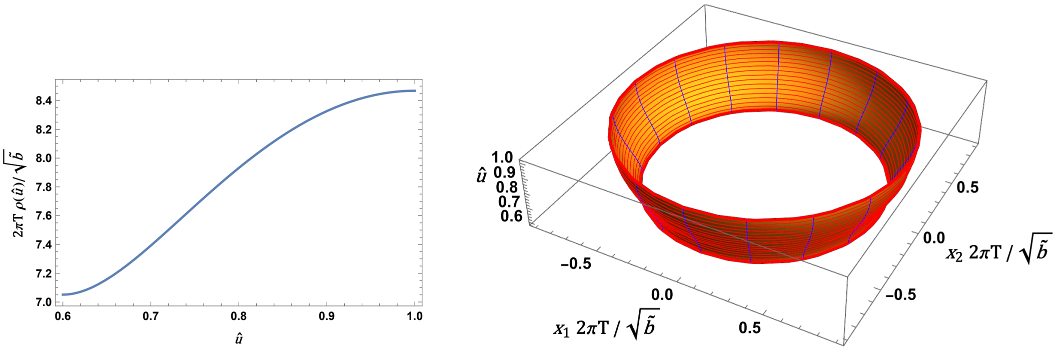

Figure 6.29. Numerical solution of ρ (times $2\pi T/\sqrt{\tilde{b}}$) for $\tilde{b} = 0.1$ and $\lambda_T = 100$ as a function of the rescaled holographic coordinate $\hat{u} = u/u_J \in [0.6, 1]$, describing a stable baryon with baryon number $n_B = 1$. The profile's derivative at both $\hat{u}_K$ and $\hat{u} = 1$ is zero, indicating the (meta)stability of this embedding. At $\hat{u} = u_*/u_J$, the profile's radius goes to infinity while in the plot we cut it for clarity at some finite value.

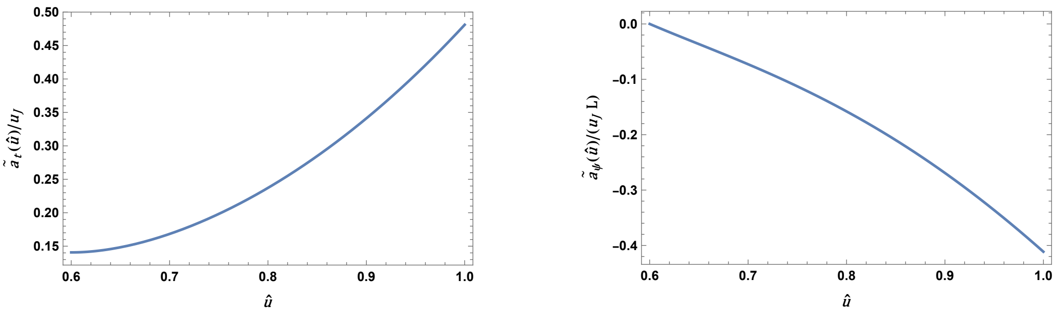

Figure 6.30. Numerical solutions for $u_J^{-1}\tilde{a}_t$ (left panel) and $(u_J L)^{-1}\tilde{a}_\psi$ (right panel) as a function of the rescaled holographic coordinate $\hat{u}$ for $\tilde{b} = 0.1$ and $\lambda_T = 100$.

Much like in the confined phase, we obtain these solutions for every value of $\hat{u}_K$ above a minimal value $\hat{u}_{\min}$. This function is once again an increasing function of both $\tilde{b}$ and λ_T. As mentioned previously, both $\tilde{b} = u_T/u_J$ and $\tilde{b}_K = u_T/u_K$ are bounded from above by a fixed value (~ 0.75) if we want the D8-branes to be in the

U-shaped configuration corresponding to the chirally broken phase. The region of existence of physical sandwich domain walls with $n_B = 1$ for $\tilde{b} = 0.2$ is shown in red in figure 6.31.

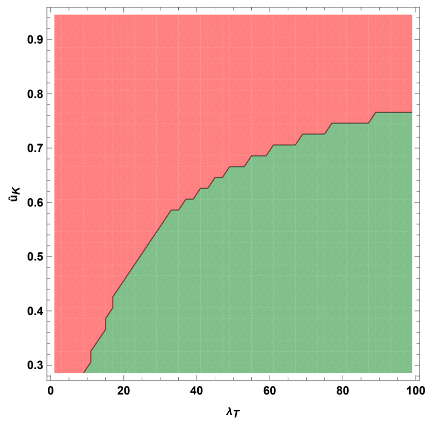

Figure 6.31. Region of existence (red) of sandwich domain walls solution in the deconfined phase between $\hat{u}_K = 0.27$ and $\hat{u}_K = 1$, for values of $\lambda_T \in [1, 100]$.

Also in the deconfined phase, we can find sandwich solutions with $n_K = 1$ and $n_J = 0$ with an associated profile $\rho(u)$ for which for all u, $\rho'(u) < 0$.

We conclude by mentioning a connection of the sandwich solutions with the simple vortons studied in section 6.3. Let us ignore for a moment the chiral symmetry restoration mechanism and consider the family of sandwich solutions as it could be defined in a larger interval of values of u. Then, if we take the limit $u_K \to u_T$ at fixed value of $\tilde{b}$ and λ_T, that is, if the tip of the lower D8-brane approaches the horizon, we observe that the limiting solution is precisely the vorton solution at the same $\tilde{b}$ and λ_T and with the same baryon number as the sandwich. This family of sandwich solutions transitioning to the limiting vorton solution is shown in figure 6.32.

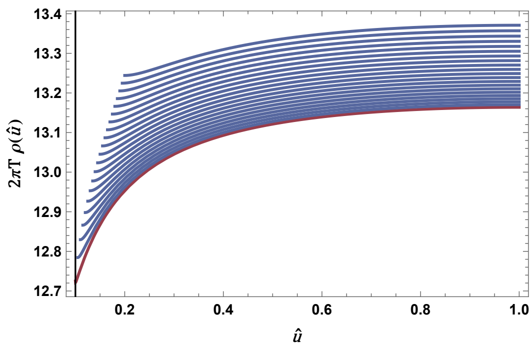

Figure 6.32. Family of sandwich domain walls for $u_K \to u_T$ in the deconfined phase (blue) and vorton solution (red). The black vertical line shows the position of the horizon.

6.5 Instabilities and decay channels

In this section, we will examine in detail the energy balance of all the solutions presented in this chapter. All the solutions are either stable (for the baryon in the confined phase) or metastable, meaning that they can decay into less energetic configurations. Let us mention that at finite temperature, the possible instabilities of the D6-brane configuration can be thought of as driven by changing the value of the temperature, mimicking what happens in a cosmological scenario.

In both phases, we will focus on the fate of the baryon solution, considering all the other solutions as possible decay channels that conserve the baryon number.

6.5.1 Confined phase

In the confined phase, it is interesting to analyze whether the baryon solution is unstable, meaning in this context that it is more energetic than another configuration with the same baryon number.

In the case of a single flavor, the $n_B = 1$ baryon is completely stable in the confined phase, being the lightest charged particle. An interesting instability can arise if the model features at least two non-coincident U-shaped D8-branes, when considering sandwich solutions in the confined phase. These objects, as discussed in section 6.4, have to be interpreted from the dual field theory point of view as composite objects of two global strings charged under different (flavor) U(1)s living on two separated flavor branes. We can therefore think of a decay of these sandwiches in two different channels corresponding to the two different baryon solutions associated with the two flavors. Our theory only features flavor-conserving interactions, so the flavor numbers must be conserved quantities in these decays. The flavor numbers associated with D6-brane sandwich configurations are directly given by $n_K^{(W)}$ and $n_J^{(W)}$ and they count the net number of fundamental strings coming out of the flavor brane, *i.e.* the quarks. In addition to this, we associated with every actual fundamental string coming out from a D8-brane a charge contributing $1/N$ to n_K or n_J, depending on the flavor brane. Let us also recall that the baryon number is given by the first Chern class n_B associated with the manifold we are considering, and is also conserved. We start from a sandwich solution with baryon number n_B.

We consider the possibility of a decay of this sandwich vorton into two charged D6-brane configurations, one attached at u_J and the other at u_K. These decay products have respectively baryon numbers $n_B^{(J)}$ and $n_B^{(K)}$

$$n_B^{(J)} = n_J + p\,, \qquad\qquad n_B^{(K)} = n_K - p\,, \tag{6.121}$$

compatible with the total baryon number conservation. Here p is an integer divided by N, which will be determined by the total angular momentum conservation and flavor conservation.[25]

These decay products are associated in the holographic model with the splitting of the D6-brane sandwich solution into baryon-like solutions anchored respectively at u_J and u_K. In general, they have to be complemented by fundamental strings

[25] Recall that a non-zero p corresponds to shifting the flavor number by a global holonomy $p = -n_G$.

linking the two sets of D8-branes to conserve flavor number. We first enforce the total angular momentum conservation. We study decays starting from sandwich domain walls that satisfy the anyonic relation $J = n_B^2 N/2$, this choice is restrictive and enforces $n_K = 0$.[26] From this, it follows

$$n_J^2 = p^2 + (n_J + p)^2 \qquad \Rightarrow \qquad p^2 + p\, n_J = 0\,, \tag{6.122}$$

which is solved by $p = \{0, -n_J\}$. There are then two possibilities:

- $p = 0$. In this case, we have

$$n_B^{(J)} = n_J\,, \qquad\qquad n_B^{(K)} = 0\,, \tag{6.123}$$

  which means that in u_J there is a D6-brane baryon solution with baryon number n_B while in u_K the D6-brane has zero baryon number and thus it is unstable under mesonic radiation. Therefore, this competing solution consists of a baryon on the D8-brane with tip in u_J, plus some mesonic radiation due to the decay of the unstable decay product.

- $p = -n_J$. In this case, we have

$$n_B^{(J)} = 0, \qquad\qquad n_B^{(K)} = n_J. \tag{6.124}$$

  As before, we can think of this as the decay of the same sandwich solution into a baryon, now hanging from u_K, Nn_J fundamental strings linking the two sets of D8-branes oriented from u_J to u_K, plus some mesonic radiation due to the decay of the uncharged decay product at u_J.

We thus conclude that the baryon number on one of the two U-shaped D8-branes is zero, leaving only two interesting competing solutions. We also showed that, as a consequence of flavor number conservation, the allowed solutions must have a number $N|p|$ of strings, corresponding to multi-flavored mesons, stretched between the two flavor branes. Considering the example that we studied in section 6.4 of a sandwich with $n_K = 0$ and $n_J = 1$, the possible decays are therefore to a baryon in u_J with no extra strings linking the D8 branes, or to a baryon in u_K, with N strings going from u_J to u_K, *i.e.* N multi-flavored mesons. Therefore, we are interested in comparing the energies of these decay products in the large-λ limit. Their free energies are given, for fixed $b_K = \frac{u_0}{u_K} = 0.6$ and $\lambda = 50$, in figure 6.33. The numerical analysis shown in this figure reveals the presence of a first-order phase transition between the sandwich solution and the baryon solution (hanging from u_J). For the above-mentioned values of the parameters, this happens at $b \approx 0.38$. In the limit where the D8-branes are stacked together, the energy of the sandwich is the smallest, and hence the sandwich is the stable configuration. Then, increasing the distance between the D8-branes (*i.e.* decreasing b), the first-order transition occurs, and the baryons hanging from u_J begin to be stable under this decay.

[26] One can also consider more generally decays of sandwiches with generic n_K, and so they do not satisfy the anyonic relation. These configurations can decay into baryons (plus mesons) if and only if $n_B^2 - 4n_K n_B$ is a perfect square.

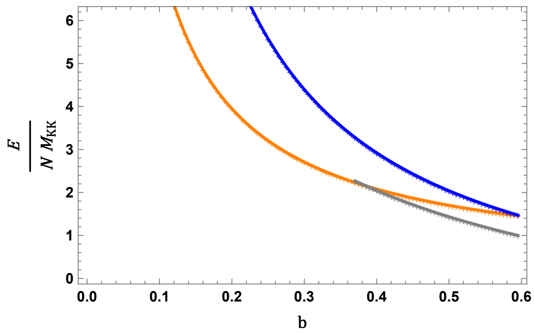

Figure 6.33. The plot shows the energy of the sandwich solution (with $n_K = 0$ and $n_J = 1$) in grey and the energy of its possible decay products: a baryon solution hanging from u_K plus N fundamental strings going from u_J to u_K, shown in blue; or a baryon solution hanging from u_J, shown in orange. We present this plot for fixed $b_K = 0.6$ and $\lambda = 50$.

In terms of the baryon stability, we have found that, for some range of parameters, the one-flavored baryon solution can decay into a sandwich connecting two different flavor branes. Moreover, the baryon solution hanging from u_K plus strings is found to be always more energetic than the other configurations.

We could also have considered a sandwich solution with $n_K = 1$ and $n_J = 0$. In this case, the decay products are: a baryon solution with $n_B = 1$ (plus mesonic radiation) hanging from u_K, or a baryon solution with $n_B = 1$ hanging from u_J, plus N fundamental strings connecting the two flavor branes with direction from u_K to u_J. As for the previous decay, the sandwich solution is almost always less energetic than its competing solutions.

6.5.2 Deconfined phase

As discussed in the introduction of this section, the instabilities in the deconfined phase can be interpreted as "dynamical" instabilities driven by the temperature. The first instability to study for the baryon D6-brane solution is the melting of the baryon vertex into the horizon, which leaves q_s fundamental strings terminating at the horizon. Therefore, focusing on the $n_B = 1$ case for simplicity, we compare the energy of the D6-brane baryon solution (see equation (6.98)) with the energy of $q_s = N$ strings extended from $u = u_J$ to the horizon:

$$E_{\text{f-strings}} = \frac{N}{2\pi l_s^2}(u_J - u_T) = \frac{4\pi}{9}\, N\lambda \frac{T^2}{M_{KK}} \frac{1-\tilde{b}}{\tilde{b}}\,. \tag{6.125}$$

We plot the two energies in figure 6.34. We can see that the energy of the baryons is almost always lower than the energy of a bunch of fundamental strings terminating at the horizon, apart from a small region in parameter space, when λ and $\tilde{b}$ take large values (*i.e.* the temperature is large), for which baryons are more energetic than the strings, so that they are unstable. Let us mention that the same energy comparison for the case of a standard WSS baryon in the deconfined phase has been performed in [195].

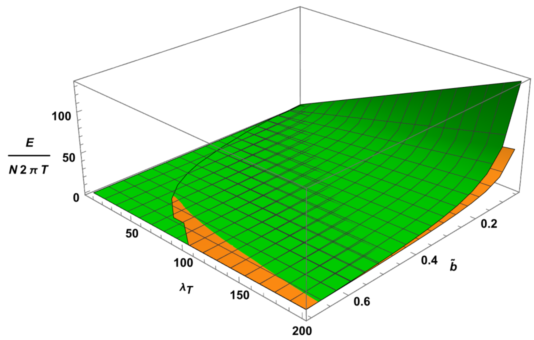

Figure 6.34. The plot shows the energy of baryons (in orange) and the energy of strings connecting the D8-brane to the horizon (in green) as a function of $\tilde{b}$ and λ_T.

The presence of the horizon allows for stable charged string loops, *i.e.* vortons. We have seen that these objects are (meta)stable only if they carry a very large charge $n_B \sim \lambda$; otherwise, they are unstable. At the level of decay channels, they could decay into a bunch of fundamental strings extended from u_J to the horizon u_T, preserving the baryon charge. We checked that the energy of large-charged vortons is always lower than that of fundamental strings (6.125), and therefore these loops are stable under this decay. However, we find that energetically the large-charge vortons are in fact only metastable, since they can decay into a large number (of order λ) of baryons with baryon number $n_B \sim \lambda^0$, conserving the baryon number in the process. Instead, a single large charge (of order λ) baryon could decay into a large charge vorton.

We can also study the decay of sandwich solutions into baryons in the deconfined phase. The derivation of the decay products performed in the confined phase is also applicable to the deconfined phase, and therefore, we are again interested in comparing the energies of a sandwich solution extended between u_J and u_K with the energies of baryon solutions hanging from u_J or u_K (with the addition of the same number of fundamental strings to conserve flavor). We show the energy comparison in figure 6.35. We observe numerically the same pattern as in the confined phase, with the same first-order phase transition and energy comparison between the competing solutions. We can also have a sandwich solution with $n_K = 1$ and $n_J = 0$ (instead of $n_K = 0$, $n_J = 1$), with the same decay products as in the confined phase.

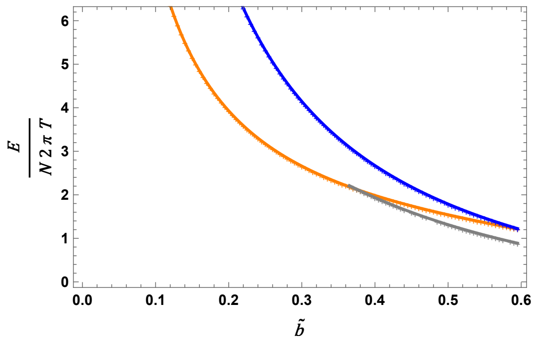

Figure 6.35. The plot shows the energy of the sandwich solution (with $n_K = 0$ and $n_J = 1$) in grey and the energy of its possible decay products: a baryon solution hanging from u_K plus the energy of N fundamental strings going from u_J to u_K, shown in blue; or a baryon solution hanging from u_J, shown in orange. We present this plot for fixed $\tilde{b}_K = u_T/u_K = 0.6$ and $\lambda = 50$.

Chapter 7

Summary and conclusions

In this first part of the thesis, we have put forward a proposal for the string dual, in the context of the WSS model of holographic QCD, of the quantum Hall droplet, or sheet, that should describe the one-flavored baryon at low energies [38]. This object consists of a D6-brane wrapped on the four-sphere of the ten-dimensional background, attached to the flavor D8-brane, with a non-trivial D8-brane gauge field sourced by the D6-brane. Such a construction manifests many of the expected features of the "baryon as quantum Hall droplet" proposal put forward in [38], most importantly the emergence of a $\mathrm{U}(1)_N$ Chern-Simons theory on their worldvolume and the appearance of topological edge modes carrying baryon number. Such a structure emerges naturally in the holographic setup, which lends support for the idea that planar QCD with one flavor admits such pancake-like baryons, despite the absence of a traditional Skyrmion picture. The D6-brane constitutes the hard, gluonic core of the sheet, responsible for the non-analyticity of the η' low-energy action. The D8-brane gauge field provides the soft, mesonic part of the sheet.

We started our journey in chapter 4, in which we constructed two explicit configurations of the sheet. The first configuration corresponds to an infinitely extended sheet without boundaries. The profile of the η', interpolating from 0 to 2π on the two sides of the sheet, has been derived. The holographic construction allows us to calculate precisely the tension and thickness of the sheet, both in the massless and massive-quark cases.

The second configuration we have considered is semi-infinite, with a straight infinite boundary (where the D6-brane terminates on the D8). The boundary constitutes a continuous distribution of magnetic charge for the five-dimensional Maxwell-CS theory (on curved space) on the D8-brane. We solved this interesting problem both in flat space, where an analytic form for the gauge field can be provided, and on the curved Witten background. In the latter case, we have provided a semi-analytic solution. We have derived a four-dimensional effective action for the fluctuating modes and calculated the tension and thickness of the hard and soft parts of the string-like boundary of the sheet.

Finally, we have observed that one can switch on a chiral component of the gauge field on the boundary having zero energy, which is possibly connected to the chiral edge mode one could consider on the boundary of the Hall droplet.

In chapter 5, we adapted the D6/D8-brane system to the deconfined phase of the

WSS model to provide a detailed description of cosmic topological defects within the holographic dual of an SU(N) gauge theory coupled to one massless fundamental flavor at large-N and finite temperature. As we observed in the introduction of chapter 5, at low energies, the effective theory is governed by an axion, which emerges as a pseudo-Goldstone boson associated with the breaking of the global $\mathrm{U}(1)_A$ flavor symmetry. The cosmological evolution of this system can lead to the spontaneous formation of topological defects. These defects arise as non-trivial configurations of the axion field and other mesons, and their properties depend on the specific symmetry-breaking pattern and the thermal history of the Universe.

We examined various topological defects, including straight axionic strings, axionic string loops, axionic vortons, and axionic DWs, through (wrapped) D6-branes in the WSS model. As for a wrapped D6-brane in the confined phase of the WSS model (see chapter 4), a notable feature of this construction is the emergence of a Chern-Simons theory on the (reduced) (2+1)-dimensional world volume of the D6-branes. The interplay between topological field theories like the CS one and axionic defects has been recently explored in [196]. Hereby, our research positions itself at the intersection of recent studies that explore the topological aspects of theories involving an SU(N) gauge group coupled with fundamental flavors.

Our analysis first focused on the D6-brane description of the defects, followed by a description in terms of the flavor degrees of freedom living on the D8-brane. Initially, we studied the straight axionic string configuration, with the D6-brane being the "hard core" of the string. We computed the thickness and the tension of this hard core. Subsequently, we analyzed the D6-brane embedding for string loops and DWs. The embedding of the D6-brane with a circular boundary on the D8-brane revealed the existence of a first-order phase transition[1] between the string loop embedding and the DW embedding. We computed the critical radius (of the D6-brane boundary on the D8-brane) at which this transition occurs, finding that it is a non-trivial function of the background temperature. The WSS model is well known for its rich phase structure, with recent studies addressing phase transitions and bubble nucleation in this model (see, for example, [197, 198, 199]). However, this phase transition has not been considered previously in the literature, as DWs are absent in the deconfined phase of conventional SU(N) gauge theory. The reason can be found in the behavior of the WSS at high temperatures. In this regime, the deconfined phase of the WSS model starts to exhibit properties reflecting the nature of the underlying string theory setup diverging from standard SU(N) gauge theories.[2] This behavior has consequences for axion physics, for example, the axion mass does not go to zero for large temperatures but grows instead [140]. Since in standard phenomenological axion models the appearance of axionic DWs is tied to the emergence of an effective axion mass, one can argue for the presence of axionic DWs in the deconfined phase of WSS to be related to these high-temperature features.

Recent works have also highlighted the relevance of phase transitions seeded by cosmic topological defects [201, 202, 203]. It would be interesting to investigate if

[1] As discussed in chapter 5, this transition is not the typical first-order phase transition between two equilibrium phases.

[2] It has been argued in [200] that the deconfined phase of WSS is not in the same universality class as that of SU(N) Yang-Mills since some discrete symmetries do not match.

and how the D6-brane defects influence the first-order phase transition associated with chiral symmetry breaking in the WSS model.

We further explored uncharged string loops and charged (under the baryon symmetry) string loops, *i.e.* vortons, through the D8-brane gauge field, *i.e.*, through the mesonic modes. Following the results of chapter 4, the D6-brane boundary on the D8-brane acts as a source for the D8-brane gauge field, leading to a non-trivial profile for low-energy mesonic modes. In particular, we derived the mesonic profile and the four-dimensional effective action for the string loop. Then, we turned on the electric potential on the D8-branes, associated with the baryon charge, which gives rise to a Coulomb repulsion mediated by the CS term that can stabilize the loop. A non-trivial electric potential corresponds to non-trivial profiles for the vector mesons. Analyzing the system locally around the D8-brane tip at $u = u_J$, i.e. in a flat limit of the WSS background, we found that the stability radius of string loops with baryon charge $n_B = 1$ and spin $J = N/2$, should be parametrically small in λ. However, the existence of such meta(stable) solutions cannot be verified in the flat space limit. Actually, the analysis of the D6-brane embedding, presented in chapter 6, suggests that vortons with the above quantum numbers cannot be stable. Unfortunately, we are not able to attach the full problem from the D8-brane perspective in curved spacetime.

Finally, in chapter 6, we have provided a concrete, first-principle realization of baryons in single-flavor QCD-like theories as compact, solitonic objects holographically realized as D6-branes ending on flavor D8-branes in the WSS model. Their physical properties, like the energy and the stability radius, computed within the holographic model, are collected in the tables 6.2 and 6.3. The spin-charge relation $J = Nn_B^2/2$, satisfied by these configurations, hints at a deeper underlying structure. It suggests the presence of collective excitations with non-trivial statistics and provides a concrete bridge between solitonic baryons and effective anyonic behavior.

From the string-theory point of view, these charged D6-brane configurations can be seen as formed by a D4-brane, wrapped on the background S^4, representing the baryon vertex in the dual field theory, and by a bunch of fundamental strings attached to it, representing the quark degrees of freedom. Then, the strings are blown up to a D6-brane (with D4 charge) by the angular momentum, as in the standard supertube case [181, 192].

A central element of our construction is the detailed analysis of the DBI-CS theory living on the worldvolume of a D6-brane, which in our setup describes *effectively* a three-dimensional manifold with boundary. The analysis of this theory reveals a rich topological structure supported on the D6-brane, governed by the global properties of the gauge principal bundle. In particular, the D6-brane worldvolume theory supports a non-trivial topological structure encoded in the first Chern number, $\int f/(2\pi)$, which serves as a genuine topological invariant and directly quantifies the baryon number of the configuration. The bulk flux $\int f/(2\pi)$ is closely related to the boundary holonomies $\int \hat{a}/(2\pi)$, defined along the circular edges of the D6-brane, which are sensitive to large gauge transformations in contrast with the baryon number. Physically, these holonomies are associated with winding numbers $n^{(W)} = N \int \hat{a}/(2\pi)$ which precisely count the net number of fundamental strings coming out of the flavor brane. In the field theory interpretation, this is the number of quarks associated with the flavor brane.

The generality of the techniques we made use of allows us to classify and analyze a broad spectrum of solitonic objects, which we refer to as a zoo of configurations, including baryons, vortons, punctured domain walls, and sandwich vortons. Vortons, first presented in chapter 5, correspond to charged D6-branes with a circular boundary on the flavor brane and ending in the horizon. The punctured domain walls correspond to D6-branes ending on the D8-brane along a circular boundary, forming metastable domain walls with holes; these holes can grow and contribute to the decay of extended domain walls, as anticipated in previous studies of defect dynamics in QCD-like theories [41, 43]. Sandwich vortons, on the other hand, are ring-shaped objects corresponding to D6-branes stretched between two D8-branes, whose tips are located at distinct holographic positions. These loops carry both baryon charge and angular momentum and provide a controlled realization of metastable string-like bound states, analogous in spirit to axionic-η' or axionic-pionic vortons discussed in [41], and introduced in chapter 5 in the context of the WSS model.

We have provided explicit numerical solutions for the D6-brane embeddings and gauge connections corresponding to each of these configurations, computing their key physical observables such as mass, size, and charge-to-spin ratio. These solutions are constructed both in the confined and deconfined phases of the WSS model. We mention that the results for the vorton configuration agree with the stability radius and the energy computed in chapter 5 within the D8-brane theory in the flat limit.

Finally, we have explored the possible decay channels of the baryon configuration in both phases. The decay modes are constrained by charge, angular momentum, flavor conservation, and energy considerations. Our analysis suggests the existence of non-trivial phase diagrams in the space of theory parameters in which different solitonic configurations dominate. In particular, focusing on the confined phase, the sandwich solution connecting two different flavor branes can be the decay product of, or it can decay into a baryon solution with some radiated mesons and fundamental strings (*i.e.* multi-flavored mesons). In the deconfined phase, other than the aforementioned decay, the baryon solution can also melt into the horizon and decay into fundamental strings ending at the horizon, *i.e.* deconfined quarks. Finally, the baryon solution, whenever it has a large charge $n_B \sim \lambda$, can decay into large-charged vortons, which themselves can decay into small charge baryons but are stable under the decay into fundamental strings.

There are many extensions that we have left for the future. In chapter 5, we investigated, within the holographic model, the low-energy description of the vorton in terms of the mesonic degrees of freedom that live on the D8-brane worldvolume. However, the holographic Hall droplet baryon is presented from the D6-brane perspective alone (see chapter 6). We plan to explore its description in terms of mesonic degrees of freedom in the near future. Such a description would not only enrich our understanding of baryons as topologically protected excitations, but also extend the holographic picture of these objects to scenarios reminiscent of Hall droplets in Chern-Simons theories. This analogy draws on the idea that baryons, viewed as solitonic objects, could emerge as collective excitations within a topologically non-trivial phase of the gauge theory. This would complete the holographic picture of baryons as *quantum Hall droplets* initiated in [1] and inspired by the seminal ideas in [38].

A delicate issue concerns the stability of the $n_B \sim \mathcal{O}(1)$ baryon solutions we have found in chapter 6. In fact, we found that the size of these particles is parametrically small in λ, both in the Minkowski directions and the holographic direction. As such, the distance of (the center of) the D6-brane from the D8-brane is small in units of $\sqrt{\alpha'}$. In flat space, the system of parallel D6 and D8 branes on top of each other has a tachyonic mode in the spectrum, with mass squared of order $1/\alpha'$, signaling the tendency of the D6-brane to melt into the D8-brane worldvolume. Even if we are considering a non-trivial background, with non-parallel, separated branes, the distance of the D6 and D8 branes could be too small, and keep this mode tachyonic. We plan to investigate this issue in the near future.

Another issue we want to clarify is the emergence of a chiral edge mode, largely studied in the context of FQHE, and its dynamics. We would like to investigate whether the edge dynamics could come from the interactions between the D6-brane and the flavor branes and hence be already present in the model.

A further interesting question to answer is whether it is possible to realize the $N_f \geq 2$ holographic Hall droplet baryon, and how this construction is connected to the standard instantonic baryons in the WSS model, which are the holographic realizations of baryons as Skyrmions. From [38], we expect that on the worldvolume of the $N_f \geq 2$ Hall droplet sheet should live a $\mathrm{U}(N_f)_N$ Chern-Simons theory and this can be realized in the holographic model by considering a stack of N_f D6-branes attached to the stack of N_f flavor branes.

Finally, there has been interest lately [45, 47, 52] in the role played by the Hall droplet sheets and their charged versions at finite density to connect them to physical systems as neutron stars. Therefore, it would be interesting to use holographic methods to investigate these scenarios.

Part II

Original contributions

Chapter 8

Weak rates in strongly coupled cold quark matter

This chapter is devoted to an application of the holographic correspondence to the study of weak reaction rates in strongly coupled, unpaired quark matter, which represents a playground model for the core of neutron stars.

As we have discussed in section 1.5.1, weak interactions play a crucial role in determining the properties of neutron stars and their binary mergers. The equation of state, which dictates the mass and radius of the star, is constrained by the condition of beta-equilibrium. This condition establishes relationships among the relative amounts of different quark (or baryon) and lepton species. When a perturbation in the density drives the matter of the star out of beta-equilibrium, weak processes work to restore it and dampen the perturbation. This results in an effective bulk viscosity that is significantly enhanced when the characteristic time of the perturbation resonates with the timescale determined by the rate of weak processes and the density in the star [57, 58, 59, 60, 61, 62, 63, 64, 65, 66, 67] (see [68] for a review of transport in neutron stars).

Oscillations of a rotating neutron star produce gravitational waves that cause the star to lose angular momentum and spin down, a process that is more pronounced for rapidly rotating stars. Despite this, fast-rotating pulsars with periods of the order of milliseconds are observed within a limited range of temperatures. The effective bulk viscosity induced by beta equilibration is likely necessary to explain the existence and location of this stability window [69, 70, 71]. This viscosity also affects the continuous emission of gravitational waves by a quiescent star [72] and could impact the gravitational wave signal produced during the inspiral [73] and post-merger evolution of a neutron star collision [74, 75, 76, 77, 78, 79, 80].

Although most matter in a neutron star and the remnant of a merger is expected to be primarily composed of hadrons, there are indirect hints of quark matter in the core of heavy neutron stars [54, 55, 56]. Simulations of binary mergers suggest that pockets of quark matter may be produced just after the collision [204, 205]. Therefore, it is interesting to evaluate the bulk viscosity of quark matter induced by weak processes. At the densities involved, QCD cannot be treated perturbatively, and lattice QCD suffers from the sign problem, necessitating other non-perturbative approaches. Holographic models can circumvent these issues and have been applied to the study of dense matter in neutron stars (see [81, 82] for comprehensive reviews). Specifically, the bulk viscosity induced by weak processes was computed using holographic models in [83][1]. However, the bulk viscosity formula involves weak reaction rates that have been computed only perturbatively, so it is not a completely self-contained approach. Furthermore, the existing formulas for weak rates (see section 1.5.1) are obtained through tree-level scattering matrix elements of quarks and leptons [84, 85, 86]. Since the observables obtained from gauge/gravity duality are correlators of gauge-invariant operators, there is no straightforward way to obtain the rates by extrapolating the tree-level formulas. Unfortunately, a main feature of the bulk viscosity, namely its temperature dependence, is highly sensitive to the behavior of the rate. Thus, the present estimation of the bulk viscosity is hindered by significant uncertainty in this respect.

As a step towards improving the bulk viscosity estimates, we will provide a non-perturbative formula for the rates based on correlators of gauge-invariant operators. We will then use it to obtain the temperature dependence of the rates in a simple holographic model of unpaired quark matter. The model, a phenomenological (bottom-up) holographic dual description of QCD [34], has been used extensively, with recent related works including the description of nuclear matter in neutron stars and mergers [208] and the calculation of neutrino emissivities from flavor current correlators [209]. Our goal is not to obtain completely realistic values for the rates, for which more refined models would be needed, but to ascertain possible qualitative changes in the temperature dependence at strong coupling.

We remind the reader that holographic models, despite their utility, come with inherent limitations. They are typically constructed as approximations that capture certain features of QCD, but they do not encompass all the complexities of the theory. One significant limitation is the lack of a first-principles derivation from QCD, leading to uncertainties in their applicability to specific phenomena. Furthermore, these models often rely on large-N, *i.e.* the number of colors, approximations, which may not accurately reflect the behavior of QCD at the finite N relevant to real-world scenarios. The models also face challenges in accurately representing the dynamics at low temperatures and densities, where confinement and chiral symmetry breaking are essential. Therefore, while holographic models provide valuable insights and a non-perturbative framework, their predictions should be interpreted with caution and validated against other approaches and experimental data.

Keeping the above limitations in mind, for direct application to the description of neutron stars and their binary mergers, the rate should be computed in the model used to describe matter in the star. The most employed holographic models so far have been those inspired by top-down brane intersections, namely the D3-D7 [113] and WSS (already introduced in the first part of this thesis work, see sections 3.2, 3.3 of this thesis) models, and a bottom-up model designed to fit lattice QCD data and other known observables, the V-QCD model [37]. The D3-D7 model is the simplest but is limited to describing quark matter in the star [210, 211, 212, 213, 214] and must be combined with other nuclear matter models to construct hybrid equations of state for the matter inside the neutron star. The

[1]The holographic estimate of the QCD contribution to the bulk viscosity was computed previously and found to be much smaller than the expected weak contribution [206, 102, 207].

V-QCD model can describe confined matter but is used primarily at large densities, requiring a hybrid approach to describe matter at lower densities outside the core of the star [215, 216, 217, 218, 219]. Hybrid equations of state have also been constructed with the WSS model [220, 221, 222, 223], but there are proposals to describe nuclear matter in neutron stars at all densities purely holographically [224, 225, 226]. The WSS model has also been used to describe more exotic quark stars [227]. Other proposals to describe dense matter in neutron stars include Einstein-Maxwell-Dilaton theories and other holographic phenomenological models [228, 229, 230]. Computing the weak rate and bulk viscosity to estimate the location of the stability window of rotating pulsars would serve as an additional constraint on these models, as well as on any other phenomenological model for which such a calculation is possible.

This chapter is organized as follows. In Section 8.1, we introduce the weak reaction rates for beta-equilibrium of quark matter and derive a non-perturbative formula in terms of correlators of flavor currents. Next, in Section 8.2, we use a simple holographic model to compute flavor current correlators in a high-density state and study their dependence on frequency and spatial momentum. Finally, in Section 8.3, we combine the results of the previous sections to produce analytical and numerical estimates of the weak rates at low temperatures. We refer to chapter 9 for a comparison of our results with the perturbative results presented in 1.5.1. Technical details regarding the calculation of correlators in the holographic model are provided in the appendices E, F, and G.

8.1 Weak reaction rates

In this section, we derive non-perturbative formulas in the coupling of the strong interactions for the weak reaction rates of quark matter. The formulas correspond to the leading contribution of the electroweak interactions, whose corrections could in principle be computed perturbatively. We also assume that the times and length scales involved are much larger than the scale set by the inverse of the W boson mass.

For the densities expected in the interior of neutron stars and mergers, one should be able to restrict to three quark flavors ($q = u, d, s$) and two lepton flavors ($\ell = e, \mu$). As we have seen in section 1.5.1, the relevant weak processes, or reactions, are produced by a W-boson exchange or emission:

$$u+d \rightleftharpoons u+s, \quad u+\ell^- \to d,s+\nu_\ell, \quad d,s \to u+\ell^- +\bar{\nu}_\ell, \quad \ell_1^- \to \ell_2^- +\nu_{\ell_1}+\bar{\nu}_{\ell_2} \,. \tag{8.1}$$

Assuming neutrinos are not trapped, the beta-equilibrium conditions in quark matter implied by these reactions are

$$\mu_u + \mu_\ell = \mu_d = \mu_s, \qquad \mu_\ell = \mu_e = \mu_\mu \,. \tag{8.2}$$

These relations assume that the different fermion species are at thermal equilibrium. However, that is not the case for neutrinos and for large enough temperatures, the relations among different chemical potentials might be shifted. This was analyzed for baryonic matter in [231, 232, 66].

Even if quarks are confined into hadrons, the same reactions will change their type among protons, neutrons, and hyperons. In this situation, the beta-equilibrium conditions should be given in terms of baryon chemical potentials. See section 1.5.1. Note that in order for any of the species of fermions to be present, it is necessary that the chemical potential is larger than the mass of the corresponding particle.

If a perturbation takes the chemical potentials out of their equilibrium values, the weak reactions will not be in balance, and the densities will change according to the weak rates Γ:[2]

$$\frac{dn_u}{dt} = \sum_{\ell=e,\mu} \left(\Gamma_{d\to u\ell\bar{\nu}} - \Gamma_{u\ell\to d\nu} + \Gamma_{s\to u\ell\bar{\nu}} - \Gamma_{u\ell\to s\nu}\right) , \tag{8.3a}$$

$$\frac{dn_d}{dt} = \Gamma_{su\to ud} - \Gamma_{ud\to su} + \sum_{\ell=e,\mu} \left(\Gamma_{u\ell\to d\nu} - \Gamma_{d\to u\ell\bar{\nu}}\right) , \tag{8.3b}$$

$$\frac{dn_s}{dt} = \Gamma_{ud\to su} - \Gamma_{su\to ud} + \sum_{\ell=e,\mu} \left(\Gamma_{u\ell\to s\nu} - \Gamma_{s\to u\ell\bar{\nu}}\right) , \tag{8.3c}$$

$$\frac{dn_{\ell_1}}{dt} = \Gamma_{d\to u\ell_1\bar{\nu}} - \Gamma_{u\ell_1\to d\nu} + \Gamma_{s\to u\ell_1\bar{\nu}} - \Gamma_{u\ell_1\to s\nu} + \Gamma_{\ell_2\to\ell_1\nu_2\bar{\nu}_1} - \Gamma_{\ell_1\to\ell_2\nu_1\bar{\nu}_2} \, . \tag{8.3d}$$

It is easy to confirm that the total baryon number and electric charge are conserved by these processes

$$n_B = \frac{1}{3}(n_u + n_d + n_s), \quad n_Q = \frac{2}{3}n_u - \frac{1}{3}n_d - \frac{1}{3}n_s - n_e - n_\mu, \quad \frac{dn_B}{dt} = \frac{dn_Q}{dt} = 0 \, . \tag{8.4}$$

Assuming the deviation of the chemical potentials from their beta-equilibrium values $\delta\mu_{f^a}$ is small compared to the baryon chemical potential $\mu_B = \mu_u + \mu_d + \mu_s$, we can expand the rates to linear order in the differences

$$\begin{aligned}
\Gamma_{ud\to su} - \Gamma_{su\to ud} &\approx \lambda_{ds}(\delta\mu_s - \delta\mu_d), && (8.5a)\\
\Gamma_{u\ell\to d\nu} - \Gamma_{d\to u\ell\bar{\nu}} &\approx \lambda^{\ell}_{ud}(\delta\mu_d - \delta\mu_u - \delta\mu_\ell), && (8.5b)\\
\Gamma_{u\ell\to s\nu} - \Gamma_{s\to u\ell\bar{\nu}} &\approx \lambda^{\ell}_{us}(\delta\mu_s - \delta\mu_u - \delta\mu_\ell), && (8.5c)\\
\Gamma_{e\to\mu\nu_2\bar{\nu}_1} - \Gamma_{\mu\to e\nu_1\bar{\nu}_2} &\approx \lambda_{e\mu}(\delta\mu_\mu - \delta\mu_e). && (8.5d)
\end{aligned}$$

In some cases, for instance when quark matter is close to being symmetric, the lepton chemical potential could be below the muon mass $\mu_\ell < m_\mu$. When this happens, muons quickly decay, and the only leptons present are electrons. The equilibration equations simplify somewhat

$$\begin{aligned}
\frac{dn_u}{dt} &= \Gamma_{d\to ue\bar{\nu}} - \Gamma_{ue\to d\nu} + \Gamma_{s\to ue\bar{\nu}} - \Gamma_{ue\to s\nu} \, , && (8.6a)\\
\frac{dn_d}{dt} &= \Gamma_{su\to ud} - \Gamma_{ud\to su} + \Gamma_{ue\to d\nu} - \Gamma_{d\to ue\bar{\nu}} \, , && (8.6b)\\
\frac{dn_s}{dt} &= \Gamma_{ud\to su} - \Gamma_{su\to ud} + \Gamma_{ue\to s\nu} - \Gamma_{s\to ue\bar{\nu}} \, , && (8.6c)\\
\frac{dn_e}{dt} &= \Gamma_{d\to ue\bar{\nu}} - \Gamma_{ue\to d\nu} + \Gamma_{s\to ue\bar{\nu}} - \Gamma_{ue\to s\nu} \, . && (8.6d)
\end{aligned}$$

[2] We have omitted the label on the neutrinos when there is just one lepton involved and put the same numerical sub-index as the corresponding lepton when there are two.

For small deviations from beta-equilibrium, the rates are expanded as (8.5), but taking into account only the electron contribution. Moreover, the coefficient $\lambda_{e\mu}$ does not involve strong coupling physics, so we will ignore it in the following, as it can be computed using the standard methods. Our strategy to derive the other coefficients is to arrive at an expression like (8.3) from Ward identities capturing the non-conservation of flavor currents due to the coupling to the weak sector.

8.1.1 Flavor Ward identities

The theory of strong interactions, QCD, respects flavor symmetries, ensuring that there are no flavor-changing processes. Weak interactions, on the other hand, are not flavor symmetric, and processes such as those in (8.1) are possible. At energy scales much below the W mass, the flavor-changing processes are captured by adding Fermi's interaction term to the effective action

$$\mathcal{L}_{\text{Fermi}} = -2\sqrt{2}G_F(J^\mu_{\text{ch}})^\dagger J_{\text{ch}\,\mu}, \tag{8.7}$$

where the J^μ_{ch} is the left-charged current

$$J^\mu_{\text{ch}} = \overline{\nu}_{e\,L}\gamma^\mu e_L + \overline{\nu}_{\mu\,L}\gamma^\mu \mu_L + \cos\theta_C\,\overline{u}_L\gamma^\mu d_L + \sin\theta_C\,\overline{u}_L\gamma^\mu s_L, \tag{8.8}$$

with G_F Fermi's constant and θ_C the Cabibbo angle giving the change of basis between quark mass and flavor eigenstates. In addition to Fermi's term, flavor symmetry can also be broken by flavor-preserving mass terms and electromagnetic and weak neutral interactions.

In the absence of any flavor-breaking terms, there would be a $\mathrm{SU}(3)_L \times \mathrm{SU}(3)_R$ global symmetry for flavor rotations among quarks and a $\mathrm{SU}(4)_L \times \mathrm{SU}(4)_R$ flavor global symmetry for leptons. To each of these symmetries, we can associate a conserved current $J^\mu_{f\,\chi}$, where $f = l, q$ for leptons or quarks and $\chi = L, R$ for left or right chirality. Since the symmetry is non-Abelian, the current components transform under flavor rotations. Denoting by $T^A_{f\,\chi}$ the generators of the flavor symmetry, the transformation of the current is

$$\delta_{\theta_{f\,\chi}} J^\mu_{f\,\chi} = i\theta^A_{f\,\chi}[J^\mu_{f\,\chi}, T^A_{f\,\chi}]\,. \tag{8.9}$$

We will take the usual normalization for the generators $\mathrm{tr}(T^A_{f\,\chi}T^B_{f\,\chi}) = \frac{1}{2}\delta^{AB}$.

A vector flavor transformation corresponds to a transformation with equal angles for both chiralities $\theta^A_{f\,L} = \theta^A_{f\,R} = \theta^A_f$. In the following, vector currents and generators will be denoted as J^μ_f and T^A_f. If there are flavor-symmetry breaking terms in the action $\mathcal{L}_{\text{br}}$, the Ward identity associated with a vector transformation becomes

$$2\theta^A_f \mathrm{tr}\left(\partial_\mu J^\mu_f\, T^A_f\right) = -\delta_{\theta^A_{f\,L}}\mathcal{L}_{\text{br}} - \delta_{\theta^A_{f\,R}}\mathcal{L}_{\text{br}}\Big|_{\theta^A_{f\,L}=\theta^A_{f\,R}=\theta^A_f}. \tag{8.10}$$

In the following, it will be convenient to introduce the notation for the currents

$$(J^\mu_{f\,\chi})^a{}_b = \bar{f}_{\chi\,b}\gamma^\mu f^a_\chi\,, \qquad f^a = q^a, l^a; \quad q^a = u, d, s;\; l^a = \nu_e, e, \nu_\mu, \mu. \tag{8.11}$$

We are interested in the flavor-changing contributions introduced by Fermi's interaction. We can simplify the analysis by noticing that since Fermi's interaction is symmetric under a rotation between the two lepton generations $(\nu_e, e) \leftrightarrow (\nu_\mu, \mu)$, we can actually restrict lepton transformations to $\mathrm{SU}(2) \times \mathrm{SU}(2) \subset \mathrm{SU}(4)$, with each SU(2) rotating a charged lepton and its corresponding neutrino within each generation. We leave details of the calculation, which is straightforward but tedious, to Appendix E. The Ward identities for the diagonal components of the vector flavor currents are

$$\begin{aligned}
\partial_\mu \langle 0|(J_q^\mu)^u{}_u|0\rangle &= i\sqrt{2}G_F\eta_{\mu\nu}\sum_{\ell=e,\mu}\Big[\cos\theta_C\,\langle 0|(J^\mu_{q\,L})^u{}_d(J^\nu_{l\,L})^d{}_u - (J^\mu_{q\,L})^d{}_u(J^\nu_{l\,L})^{\nu_\ell}{}_\ell|0\rangle \\
&\quad + \sin\theta_C\,\langle 0|(J^\mu_{q\,L})^u{}_s(J^\nu_{l\,L})^\ell{}_{\nu_\ell} - (J^\mu_{q\,L})^s{}_u(J^\nu_{l\,L})^{\nu_\ell}{}_\ell|0\rangle\Big], \qquad (8.12a) \\
\partial_\mu \langle 0|(J_q^\mu)^d{}_d|0\rangle &= i\sqrt{2}G_F\eta_{\mu\nu}\,[\cos\theta_C\sin\theta_C\eta_{\mu\nu}\,\cdot \\
&\quad \cdot\langle 0|(J^\mu_{q\,L})^u{}_s(J^\nu_{q\,L})^d{}_u - (J^\mu_{q\,L})^s{}_u(J^\nu_{q\,L})^u{}_d|0\rangle \\
&\quad \left. - \cos\theta_C\sum_{\ell=e,\mu}\langle 0|(J^\mu_{q\,L})^u{}_d(J^\nu_{l\,L})^\ell{}_{\nu_\ell} - (J^\mu_{q\,L})^d{}_u(J^\nu_{l\,L})^{\nu_\ell}{}_\ell|0\rangle\right], \qquad (8.12b) \\
\partial_\mu \langle 0|(J_q^\mu)^s{}_s|0\rangle &= i\sqrt{2}G_F\eta_{\mu\nu}\,[-\cos\theta_C\sin\theta_C\eta_{\mu\nu}\,\cdot \\
&\quad \cdot\langle 0|(J^\mu_{q\,L})^u{}_s(J^\nu_{q\,L})^d{}_u - (J^\mu_{q\,L})^s{}_u(J^\nu_{q\,L})^u{}_d|0\rangle \\
&\quad \left. - \sin\theta_C\sum_{\ell=e,\mu}\langle 0|(J^\mu_{q\,L})^u{}_s(J^\nu_{l\,L})^\ell{}_{\nu_\ell} - (J^\mu_{q\,L})^s{}_u(J^\nu_{l\,L})^{\nu_\ell}{}_\ell|0\rangle\right], \qquad (8.12c) \\
\partial_\mu \langle 0|(J_l^\mu)^{\nu_\ell}{}_{\nu_\ell}|0\rangle &= i\sqrt{2}G_F\eta_{\mu\nu}\Big[-\cos\theta_C\,\langle 0|(J^\mu_{q\,L})^u{}_d(J^\nu_{l\,L})^\ell{}_{\nu_\ell} - (J^\mu_{q\,L})^d{}_u(J^\nu_{l\,L})^\ell{}_{\nu_\ell}|0\rangle \\
&\quad - \sin\theta_C\,\langle 0|(J^\mu_{q\,L})^u{}_s(J^\nu_{l\,L})^\ell{}_{\nu_\ell} - (J^\mu_{q\,L})^s{}_u(J^\nu_{l\,L})^{\nu_\ell}{}_\ell|0\rangle \\
&\quad - \langle 0|(J^\mu_{l\,L})^{\nu_{\ell'}}{}_{\ell'}(J^\nu_{l\,L})^\ell{}_{\nu_\ell} - (J^\mu_{l\,L})^{\ell'}{}_{\nu_{\ell'}}(J^\nu_{l\,L})^\ell{}_{\nu_\ell}|0\rangle\Big], \qquad (8.12d) \\
\partial_\mu \langle 0|(J_l^\mu)^\ell{}_\ell|0\rangle &= i\sqrt{2}G_F\eta_{\mu\nu}\Big[\cos\theta_C\,\langle 0|(J^\mu_{q\,L})^u{}_d(J^\nu_{l\,L})^\ell{}_{\nu_\ell} - (J^\mu_{q\,L})^d{}_u(J^\nu_{l\,L})^{\nu_\ell}{}_\ell|0\rangle \\
&\quad + \sin\theta_C\,\langle 0|(J^\mu_{q\,L})^u{}_s(J^\nu_{l\,L})^\ell{}_{\nu_\ell} - (J^\mu_{q\,L})^s{}_u(J^\nu_{l\,L})^{\nu_\ell}{}_\ell|0\rangle \\
&\quad + \langle 0|(J^\mu_{l\,L})^{\nu_{\ell'}}{}_{\ell'}(J^\nu_{l\,L})^\ell{}_{\nu_\ell} - (J^\mu_{l\,L})^{\ell'}{}_{\nu_{\ell'}}(J^\nu_{l\,L})^{\nu_\ell}{}_\ell|0\rangle\Big]. \qquad (8.12e)
\end{aligned}$$

Where $(\ell, \ell') = (e, \mu)$ or (μ, e). Note that other terms that break the non-Abelian flavor symmetry, but are diagonal in flavor, do not contribute to the Ward identities of the diagonal components. One can easily confirm that the expressions above are consistent with the conservation of baryon and lepton numbers as well as the electric charge:

$$\begin{aligned}
&\partial_\mu \langle 0|(J_q^\mu)^u{}_u + (J_q^\mu)^d{}_d + (J_q^\mu)^s{}_s|0\rangle = 0, \quad \partial_\mu \langle 0|(J_l^\mu)^{\nu_\ell}{}_{\nu_\ell} + (J_l^\mu)^\ell{}_\ell|0\rangle = 0, \\
&\partial_\mu \langle 0|\frac{2}{3}(J_q^\mu)^u{}_u - \frac{1}{3}(J_q^\mu)^d{}_d - \frac{1}{3}(J_q^\mu)^s{}_s - \sum_{\ell=e,\mu}(J_l^\mu)^\ell{}_\ell|0\rangle = 0.
\end{aligned} \qquad (8.13)$$

The time components of the diagonal components of the flavor vector currents equal the corresponding quark or lepton densities

$$n_u = (J_q^0)^u{}_u,\ n_d = (J_q^0)^d{}_d,\ n_s = (J_q^0)^s{}_s,\ n_\ell = (J_l^0)^\ell{}_\ell. \qquad (8.14)$$

Compared with (8.3) for homogeneous configurations, the rates are determined by the expectation value of a non-diagonal operator quadratic in the flavor currents appearing on the right-hand side of the Ward identities. We can think of such a quadratic operator as obtained from a two-point correlator in the (properly regularized) limit of coincident points. In the absence of flavor-breaking terms, the most general form of the flavor current correlators would be

$$\langle 0|(J^{\mu}_{f\,L})^{a}{}_{b}(J^{\nu}_{f\,L})^{c}{}_{d}|0\rangle = G_1\delta^a_b\delta^c_d + G_2\delta^a_d\delta^c_b\,. \tag{8.15}$$

If there are mass terms in the action of the form $\mathcal{L}_m = \bar{f}_a M_f{}^a{}_b f^b$, or chemical potentials introduced through a background flavor gauge field $A_f{}^a{}_b$, there could also be terms where we replace some or all of the deltas in (8.15) by M_f or A_f, or contractions like $M_f{}^a{}_c M_f{}^c{}_b$, $M_f{}^a{}_c A_f{}^c{}_b$, etc. This potentially can produce many new terms, however, for diagonal mass matrices and chemical potentials, the non-diagonal current correlators appearing on the right-hand side of the Ward identities would still vanish, and similarly for contributions originating from interactions that are diagonal in flavor. Therefore, the non-diagonal current correlators contributing to the Ward identities must be proportional to the flavor-changing coupling G_F. We will derive in the following a closed expression for the $O(G_F^2)$ contribution to the rates in thermal field theory.

8.1.2 Leading contribution in the Fermi coupling

We will assume that the theory is at finite temperature $T = 1/\beta$ and use the real-time formalism to compute the current correlators. See [233] for an introduction to the topic. In general, thermal correlation functions are computed by insertions in a path integral defined along a contour C in complex time. The path-ordered two-point function of two operators $\mathcal{O}_1$ and $\mathcal{O}_2$ is

$$\langle 0|T_C\left[\mathcal{O}_1(x_1)\mathcal{O}_2(x_2)\right]|0\rangle\,. \tag{8.16}$$

The complex time path, or Schwinger-Keldysh path, extends along $C = (t_i, t_f) \cup (t_f, t_f - i\sigma) \cup (t_f - i\sigma, t_i - i\sigma) \cup (t_i - i\sigma, t_i - i\beta)$, with $\sigma > 0$ and $t_i \to -\infty$, $t_f \to +\infty$. We take the point x_1 to be at the first leg of the complex time path on the real axis. Then we have two possible contributions, depending on where the point x_2 is located. If x_2 is on the same leg as x_1, then the thermal correlator coincides with the usual time-ordered Feynman correlator

$$\langle 0|T_C\left[\mathcal{O}_1(x_1)\mathcal{O}_2(x_2)\right]|0\rangle = \langle 0|T\left[\mathcal{O}_1(x_1)\mathcal{O}_2(x_2)\right]|0\rangle = G^F_{\mathcal{O}_1\mathcal{O}_2}(t_1 - t_2, \boldsymbol{x_1} - \boldsymbol{x_2}). \tag{8.17}$$

If, on the other hand, x_2 is on the third leg of the contour C ($\mathrm{Im}\ t' = -\sigma$), the correlator is the Wightman correlator

$$\langle 0|T_C\left[\mathcal{O}_1(x_1)\mathcal{O}_2(x_2)\right]|0\rangle = \langle 0|\mathcal{O}_2(x_2)\mathcal{O}_1(x_1)|0\rangle = G^{<}_{\mathcal{O}_1\mathcal{O}_2}(t_1 - t_2 + i\sigma, \boldsymbol{x_1} - \boldsymbol{x_2}). \tag{8.18}$$

With this in mind, let us find the effect of Fermi's interaction (8.7) when we treat it perturbatively. The thermal expectation value of an operator $\mathcal{O}$ will be, to leading order in the Fermi coupling,

$$\begin{aligned}\langle 0|\mathcal{O}(x)|0\rangle_{G_F} = \langle 0|T_C\left[\mathcal{O}(x)e^{i\int_C \mathcal{L}_{\mathrm{Fermi}}}\right]|0\rangle_0 \approx \langle 0|\mathcal{O}(x)|0\rangle_0 + \\ + i\int_C d^4x'\,\langle 0|T_C\left[\mathcal{O}(x)\mathcal{L}_{\mathrm{Fermi}}(x')\right]|0\rangle_0\,. \end{aligned}\tag{8.19}$$

In the expression above $\langle 0|X|0\rangle_0$ indicates that the expectation value of X is computed in the absence of Fermi's interaction. Since x is in the first leg of the complex time contour and x' runs over its full extent, we have contributions from both the first and third leg of C, which translate into Feynman and Wightman correlators of the operator with the Fermi interaction, respectively

$$\int_C d^4x' \, \langle 0|T_C \left[\mathcal{O}(x)\mathcal{L}_{\rm Fermi}(x')\right]|0\rangle_0 = \\ = \int d^4x' \left[G^F_{\mathcal{O}\mathcal{L}_{\rm Fermi}}(t-t', \boldsymbol{x}-\boldsymbol{x'}) + G^<_{\mathcal{O}\mathcal{L}_{\rm Fermi}}(t-t'+i\sigma, \boldsymbol{x}-\boldsymbol{x'})\right]. \tag{8.20}$$

In the evaluation of the right-hand side of the Ward identities (8.12), $\mathcal{O}$ is quadratic in the flavor currents, as well as $\mathcal{L}_{\rm Fermi}$. Therefore, the leading $O(G_F^2)$ contribution is proportional to correlators of the form

$$\langle 0|\left[(J^\mu_f)^a{}_b(x)(J^\nu_f)^c{}_d(x)\right]\left[(J^\alpha_{f'})^{a'}{}_{b'}(x')(J^\beta_{f'})^{c'}{}_{d'}(x')\right]|0\rangle_0 \approx \\ \delta_{ff'}\Big[\langle 0|(J^\mu_f)^a{}_b(x)(J^\alpha_f)^{a'}{}_{b'}(x')|0\rangle_0 \; \langle 0|(J^\nu_f)^c{}_d(x)(J^\beta_f)^{c'}{}_{d'}(x')|0\rangle_0 + \\ + \langle 0|(J^\mu_f)^a{}_b(x)(J^\beta_f)^{c'}{}_{d'}(x')|0\rangle_0 \; \langle 0|(J^\nu_f)^c{}_d(x)(J^\alpha_f)^{a'}{}_{b'}(x')|0\rangle_0\Big]. \tag{8.21}$$

The factorization above is an approximation. For holographic models dual to a large-N theory, it will happen naturally as part of the large-N expansion. More generally, the non-factorizable contributions would originate from effective eight-fermion interactions, so it is perhaps not unreasonable to assume that they would introduce relatively small corrections even in the finite-N strongly coupled theory.

As we discussed before, in the absence of the Fermi interaction, non-vanishing current correlators should be diagonal in flavor, thus

$$G^{\mu\alpha}_{f;ab,a'b'}(x-x') \equiv \langle 0|(J^\mu_f)^a{}_b(x)(J^\alpha_f)^{a'}{}_{b'}(x')|0\rangle_0 \neq 0, \\ \Rightarrow \quad (a=b \,\wedge\, a'=b') \,\vee\, (a=b' \,\wedge\, a'=b).$$

This limits the number of non-zero contributions to the four-current thermal correlators. We will now write the leading contributions in the Fermi coupling to the Ward identities (8.12) in terms of the Fourier transforms of the Feynman and Wightman correlators of the flavor currents

$$G^{K\,\mu\alpha}_{f;ab,a'b'}(x-x') = \int \frac{d^4k}{(2\pi)^4} e^{ik\cdot(x-x')} G^{K\,\mu\alpha}_{f;ab,a'b'}(k), \qquad K = F, < \,. \tag{8.22}$$

It will be convenient to define

$$\gamma_{f_1^a f_2^b \to f_1^c f_2^d} = \gamma^F_{f_1^a f_2^b \to f_1^c f_2^d} + \gamma^<_{f_1^a f_2^b \to f_1^c f_2^d}, \tag{8.23}$$

with $(K = F, <)$

$$\gamma^K_{f_1^a f_2^b \to f_1^c f_2^d} = \eta_{\mu\nu}\eta_{\alpha\beta} \int \frac{d^4k}{(2\pi)^4} \left[G^{K\,\mu\alpha}_{f_1;ac,ca}(k) G^{K\,\nu\beta}_{f_2;bd,db}(-k) - G^{K\,\mu\alpha}_{f_1;ca,ac}(k) G^{K\,\nu\beta}_{f_2;db,bd}(-k)\right]. \tag{8.24}$$

In terms of these quantities, the leading order contributions in the Fermi coupling to the flavor Ward identities are

$$\partial_\mu \langle 0|(J_q^\mu)^u{}_u|0\rangle \approx -4G_F^2 \textstyle\sum_{\ell=e,\mu} \left(\cos^2\theta_C \gamma_{u\ell\to d\nu} + \sin^2\theta_C \gamma_{u\ell\to s\nu}\right), \quad (8.25a)$$
$$\partial_\mu \langle 0|(J_q^\mu)^d{}_d|0\rangle \approx 4G_F^2 \left(-\sin\theta_C^2 \cos^2\theta_C \gamma_{ud\to su} + \cos^2\theta_C \textstyle\sum_{\ell=e,\mu} \gamma_{u\ell\to d\nu}\right), (8.25b)$$
$$\partial_\mu \langle 0|(J_q^\mu)^s{}_s|0\rangle \approx 4G_F^2 \left(\sin\theta_C^2 \cos^2\theta_C \gamma_{ud\to su} + \sin^2\theta_C \textstyle\sum_{\ell=e,\mu} \gamma_{u\ell\to s\nu}\right), (8.25c)$$
$$\partial_\mu \langle 0|(J_l^\mu)^{\nu_\ell}{}_{\nu_\ell}|0\rangle \approx 4G_F^2 \left(\cos^2\theta_C \gamma_{u\ell\to d\nu} + \sin^2\theta_C \gamma_{u\ell\to s\nu} + \gamma_{\ell\nu'\to\nu\ell'}\right), \quad (8.25d)$$
$$\partial_\mu \langle 0|(J_l^\mu)^\ell{}_\ell|0\rangle \approx -4G_F^2 \left(\cos^2\theta_C \gamma_{u\ell\to d\nu} + \sin^2\theta_C \gamma_{u\ell\to s\nu} + \gamma_{\ell\nu'\to\nu\ell'}\right). \quad (8.25e)$$

Where in the last two rows $(\ell, \ell') = (e, \mu)$ or (μ, ℓ) and ν, ν' are the neutrinos corresponding to ℓ, ℓ' respectively.

8.1.3 Formulas for the rates

A direct comparison of the equilibration equations (8.5) and the Ward identities (8.25) results in the identification of the leading order contribution in the Fermi coupling to the rates as

$$\begin{aligned}
\Gamma_{u\ell\to d\nu} - \Gamma_{d\to u\ell\bar\nu} &\approx 4G_F^2 \cos^2\theta_C \gamma_{u\ell\to d\nu}\,, && (8.26a)\\
\Gamma_{u\ell\to s\nu} - \Gamma_{s\to u\ell\bar\nu} &\approx 4G_F^2 \sin^2\theta_C \gamma_{u\ell\to s\nu}\,, && (8.26b)\\
\Gamma_{ud\to su} - \Gamma_{su\to ud} &\approx 4G_F^2 \sin\theta_C^2 \cos^2\theta_C \gamma_{ud\to su}\,, && (8.26c)\\
\Gamma_{\ell_1\to\ell_2\nu_1\bar\nu_2} - \Gamma_{\ell_2\to\ell_1\nu_2\bar\nu_1} &\approx 4G_F^2 \gamma_{\ell_1\nu_2\to\nu_1\ell_2}\,. && (8.26d)
\end{aligned}$$

With the factors γ defined in (8.23) and (8.24) in terms of thermal correlation functions. We can further simplify the expressions by first noting that, if the system has parity and time reversal invariance, the Feynman correlator satisfies

$$G^{F\,\mu\nu}_{f;ab,ba}(-k_0, -\boldsymbol{k}) = G^{F\,\nu\mu}_{f;ba,ab}(k_0, \boldsymbol{k}). \quad (8.27)$$

A straightforward calculation then shows that $\gamma^F_{f_1^a f_2^b \to f_1^c f_2^d} = 0$ in this case. The Wightman correlator on the other hand is proportional to the spectral function, defined as the imaginary part of the retarded correlator:

$$G^{<\,\mu\nu}_{f;ab,ba}(k_0, \boldsymbol{k}) = n_{f;ab}(k_0)\rho^{\mu\nu}_{f;ab}(k_0, \boldsymbol{k}), \quad \rho^{\mu\nu}_{f;ab} = -2\ \mathrm{Im}\left(G^{R\,\mu\nu}_{f;ab,ba}\right), \quad (8.28)$$

where the factor multiplying the spectral function is the thermal distribution

$$n_{f;ab}(k_0) = \frac{1}{e^{\beta(k_0 + \mu_{f^a} - \mu_{f^b})} - 1}, \quad (8.29)$$

with μ_{f^a} the chemical potential for the fermion species f^a. We now introduce (8.28) in (8.24), and use that

$$n_{f;ab}(-k_0) = -(1 + n_{f;ba}(k_0)), \qquad \rho^{\mu\alpha}_{f;ab}(-k_0, -\boldsymbol{k}) = -\rho^{\alpha\mu}_{f;ba}(k_0, \boldsymbol{k})\,, \quad (8.30)$$

where the last identity follows from time-reversal invariance and parity. After this, one arrives at

$$\begin{aligned}\gamma_{f_1^a f_2^b \to f_1^c f_2^d} &= \gamma^<_{f_1^a f_2^b \to f_1^c f_2^d} = \\ &= \eta_{\mu\nu}\eta_{\alpha\beta} \int \frac{d^4k}{(2\pi)^4} \left[(n_{f_1;ac}(k_0) - n_{f_2;db}(k_0)) \rho^{\mu\alpha}_{f_1;ac}(k_0, \boldsymbol{k}) \rho^{\beta\nu}_{f_2;db}(k_0, \boldsymbol{k}) \right] . \end{aligned} \tag{8.31}$$

This quantity will vanish when the chemical potentials satisfy the relations

$$\mu_{f_1^a} - \mu_{f_1^c} = \mu_{f_2^d} - \mu_{f_2^b}. \tag{8.32}$$

Then, demanding that each of the rates in (8.26) vanish gives the conditions

$$\mu_u - \mu_d = \mu_{\nu_\ell} - \mu_\ell, \tag{8.33}$$

$$\mu_u - \mu_s = \mu_{\nu_\ell} - \mu_\ell, \tag{8.34}$$

$$\mu_u - \mu_s = \mu_u - \mu_d, \tag{8.35}$$

$$\mu_{\nu_{\ell_1}} - \mu_{\ell_1} = \mu_{\nu_{\ell_2}} - \mu_{\ell_2}. \tag{8.36}$$

Setting $\mu_{\nu_\ell} = 0$, it is easy to check that this coincides with the beta-equilibrium conditions in (8.2).

We will now expand (8.24) to the lowest order around the equilibrium values, $\mu_{f^a} = \mu^{eq}_{f^a} + \delta\mu_{f^a}$. The thermal distributions have a pole at small frequencies, that we need to deal with. Let us introduce an arbitrary frequency ω_0 such that $\delta\mu_{f_1^a} - \delta\mu_{f_1^c} \sim \delta\mu_{f_2^d} - \delta\mu_{f_2^b} \ll \omega_0 \ll T$. Then, there is a contribution that we can expand to linear order in the chemical potentials plus a correction from the poles

$$\gamma_{f_1^a f_2^b \to f_1^c f_2^d} \approx \left(\delta\mu_{f_2^d} - \delta\mu_{f_2^b} - (\delta\mu_{f_1^a} - \delta\mu_{f_1^c}) \right) \Lambda^0_{f_1^a f_2^b \to f_1^c f_2^d} + \delta\gamma_{f_1^a f_2^b \to f_1^c f_2^d} , \tag{8.37}$$

where, after defining $\Delta\mu^{eq} = \mu^{eq}_{f_1^a} - \mu^{eq}_{f_1^c} = \mu^{eq}_{f_2^d} - \mu^{eq}_{f_2^v}$, the coefficient Λ is

$$\begin{aligned}\Lambda^0_{f_1^a f_2^b \to f_1^c f_2^d} &= \eta_{\mu\nu}\eta_{\alpha\beta} \int \frac{d^4k}{(2\pi)^4} \rho^{\mu\alpha}_{f_1;ac}(k_0, \boldsymbol{k}) \rho^{\beta\nu}_{f_2;db}(k_0, \boldsymbol{k}) \\ &\times \left[\frac{1}{4T \sinh^2\left(\frac{k_0 + \Delta\mu^{eq}}{2T}\right)} - \frac{T}{(k_0 + \Delta\mu^{eq})^2} \Theta(\omega_0^2 - (k_0 + \Delta\mu^{eq})^2) \right] . \end{aligned} \tag{8.38}$$

We remind the reader that in this formula the fermion species are $f_1, f_2 = q$ (quarks) or l (leptons) and the possible flavors are $q^a = u, d, s$, $l^a = \nu_e, e, \nu_\mu, \mu$. For $k_0 + \Delta\mu^{eq} \gtrsim T$ the function decays exponentially $\sim e^{-(k_0 + \Delta\mu^{eq})/T}$, thus most of the contributions in the frequency integral will come from an interval of width $\sim T$ around $k_0 + \Delta\mu^{eq}$.

The correction to the rate originating from the poles is approximately

$$\begin{aligned}\delta\gamma_{f_1^a f_2^b \to f_1^c f_2^d} =& \eta_{\mu\nu}\eta_{\alpha\beta} \int_{|k_0 + \Delta\mu^{eq}| < \omega_0} \frac{d^4k}{(2\pi)^4} \rho^{eq\,\mu\alpha}_{f_1;ac}(k_0, \boldsymbol{k}) \rho^{eq\,\beta\nu}_{f_2;db}(k_0, \boldsymbol{k}) \\ &\times \left[\frac{T}{k_0 + \Delta\mu^{eq} + \delta\mu_{f_1^a} - \delta\mu_{f_1^c}} - \frac{T}{k_0 + \Delta\mu^{eq} + \delta\mu_{f_2^d} - \delta\mu_{f_2^b}} \right] . \end{aligned} \tag{8.39}$$

We will use the principal value integral

$$\int_{-\omega_0-\Delta\mu^{eq}}^{\omega_0-\Delta\mu^{eq}} \frac{dk_0}{2\pi} \frac{T}{k_0+\Delta\mu^{eq}+\delta\mu} S(k_0) \approx \frac{T}{2\pi} S(-\Delta\mu^{eq}) \log \frac{\omega_0+\delta\mu}{\omega_0-\delta\mu} \approx$$
$$\approx \frac{T}{\pi\omega_0} S(-\Delta\mu^{eq})\delta\mu. \tag{8.40}$$

Thus, we can write

$$\gamma_{f_1^a f_2^b \to f_1^c f_2^d} \approx \left(\delta\mu_{f_2^d} - \delta\mu_{f_2^b} - (\delta\mu_{f_1^a} - \delta\mu_{f_1^c})\right) \Lambda_{f_1^a f_2^b \to f_1^c f_2^d} \,, \tag{8.41}$$

with

$$\Lambda_{f_1^a f_2^b \to f_1^c f_2^d} \approx \Lambda^0_{f_1^a f_2^b \to f_1^c f_2^d} + \eta_{\mu\nu}\eta_{\alpha\beta} \frac{T}{\pi\omega_0} \int \frac{d^3k}{(2\pi)^3} \rho^{eq\ \mu\alpha}_{f_1;ac}(-\Delta\mu^{eq}, \boldsymbol{k}) \rho^{eq\ \beta\nu}_{f_2;db}(-\Delta\mu^{eq}, \boldsymbol{k}). \tag{8.42}$$

If the spectral function vanishes at $k_0 = -\Delta\mu^{eq}$ the last term in (8.42) is zero and one can take the $\omega_0 \to 0$ limit, in which case the expression for the coefficient Λ simplifies

$$\Lambda_{f_1^a f_2^b \to f_1^c f_2^d} \approx \eta_{\mu\nu}\eta_{\alpha\beta} \int \frac{d^4k}{(2\pi)^4} \frac{\rho^{eq\ \mu\alpha}_{f_1;ac}(-\Delta\mu^{eq}, \boldsymbol{k}) \rho^{eq\ \mu\alpha}_{f_2;db}(-\Delta\mu^{eq}, \boldsymbol{k})}{4T \sinh^2\left(\frac{k_0+\Delta\mu^{eq}}{2T}\right)}. \tag{8.43}$$

Combining the expression (8.41) with (8.26) and (8.5), we arrive at the following formulas for the coefficients of the rates

$$\lambda_{ds} \approx 4G_F^2 \sin^2\theta_C \cos^2\theta_C \ \Lambda_{ud\to su}, \tag{8.44a}$$
$$\lambda^{\ell}_{ud} \approx 4G_F^2 \cos^2\theta_C \ \Lambda_{u\ell\to d\nu}, \tag{8.44b}$$
$$\lambda^{\ell}_{us} \approx 4G_F^2 \sin^2\theta_C \ \Lambda_{u\ell\to s\nu}, \tag{8.44c}$$
$$\lambda_{e\mu} \approx 4G_F^2 \ \Lambda_{\mu\nu_e\to\nu_\mu e}. \tag{8.44d}$$

When leptonic contributions can be neglected, as is usually the case in the evaluation of the bulk viscosity in neutron stars, the only relevant coefficient is $\lambda_1 = \lambda_{ds}$, following the conventions in [68]. In the rest of the chapter, we will give an estimate of $\lambda_1 = \lambda_{ds}$ at strong coupling using a holographic model.

8.2 Holographic model

We will use a holographic model dual to a SU(N) gauge theory with N_f flavors to compute the rate. Differently form what we did in the previous parts of this thesis, here we use a bottom-up approach, where we construct a gravitational action with the necessary ingredients to capture the physics of interest, but that does not correspond to a string theory construction where both sides of the duality are known. The glue sector is given by an action consisting of just the Einstein-Hilbert action plus a negative cosmological constant

$$S_c = \frac{1}{16\pi G_5} \int d^5x \sqrt{-g}\,[R - 2\Lambda]\,, \quad \Lambda = -\frac{6}{L^2}\,. \tag{8.45}$$

In the absence of matter, the maximally symmetric solution is an AdS_5 space with radius L. Including the flavor sector will modify the geometry, but it will still asymptote to the same AdS_5, so we can apply the usual holographic dictionary between the fields in the gravity theory and sources and operators in the gauge theory dual (see section 3.1.2).

The flavor sector consists of $\mathrm{U}(N_f)_L \times \mathrm{U}(N_f)_R$ gauge fields, L_M and R_M, dual to the flavor currents, and a complex scalar field X in the bifundamental representation dual to a scalar quark bilinear. The action for the flavor fields is the one commonly used for bottom-up holographic QCD models, originating with [34]

$$S_f = \int d^5x \sqrt{-g}\, \mathrm{Tr}\left[g_X^2\left(-|DX|^2 + \frac{3}{L^2}|X|^2\right) - \frac{1}{4g_5^2}\left(F_{(R)}^2 + F_{(L)}^2\right)\right] . \qquad (8.46)$$

The field strength is defined as $F_{(A)MN} = \partial_M A_N - \partial_N A_M - i\,[A_M, A_N]$. The covariant derivative of the scalar field is defined as follows

$$D_N X = \partial_N X - iL_N X + iXR_N\,, \qquad D_N X^\dagger = \partial_N X^\dagger + iX^\dagger L_N - iR_N X^\dagger\,. \quad (8.47)$$

The mass of the scalar is fixed in such a way that the field is dual to a scalar operator of scaling dimensions $\Delta = 3$, as corresponds to a quark bilinear.

The action is fixed up to an overall normalization of the scalar and gauge fields. In [34, 234] (see also [235]) the normalization was fixed by matching the large Euclidean momentum form of current correlators derived from the holographic model to the OPE of QCD. Then, the matching to QCD in the UV fixes

$$\frac{1}{g_5^2} = \frac{N}{12\pi^2 L}, \quad g_X^2 L^3 = \frac{N}{4\pi^2}\,. \qquad (8.48)$$

The equations of motion for the metric are Einstein's equations with a cosmological constant and the energy-momentum tensor sourced by the gauge fields and the scalars

$$R_{MN} - \frac{1}{2}g_{MN}R + g_{MN}\Lambda = 8\pi G_5 T_{MN}. \qquad (8.49)$$

The equations of motion for the gauge and scalar fields read

$$\frac{1}{\sqrt{-g}}D_M\left[\sqrt{-g}F_{(R)}^{MN}\right] = g_5^2 g_X^2\, j_{(R)}^N\,, \qquad (8.50a)$$

$$\frac{1}{\sqrt{-g}}D_M\left[\sqrt{-g}F_{(L)}^{MN}\right] = g_5^2 g_X^2\, j_{(L)}^N\,, \qquad (8.50b)$$

$$\frac{1}{\sqrt{-g}}D_M\left[\sqrt{-g}D^M X\right] = -\frac{3}{L^2}\,X\,. \qquad (8.50c)$$

where the bulk currents appearing in the equations of the gauge fields are

$$j_{(R)}^M = i\left[\left(D^M X\right)^\dagger X - X^\dagger D^M X\right], \qquad (8.51a)$$

$$j_{(L)}^M = i\left[\left(D^M X\right) X^\dagger - X\left(D^M X\right)^\dagger\right]. \qquad (8.51b)$$

We will look for solutions dual to a deconfined state of the gauge theory at nonzero temperature and baryon density, which are charged black brane geometries. In order to simplify the analysis we will turn off the scalar field, which amounts to having zero quark mass and condensate for all the flavors. In this case, imposing the condition of beta-equilibrium fixes all quark chemical potentials to be equal, since deviations from symmetric quark matter due to nonzero quark masses are absent. Since we are ultimately interested in comparing with QCD results, we will fix the rank of the flavor fields $N_f = 3$.

When the scalars vanish, the charged black brane geometry is the preferred state of the system at large enough values of the chemical potential. There could also be other competing states where the scalar fields or off-diagonal components of the gauge fields acquire a non-trivial profile, corresponding to the spontaneous breaking of flavor symmetries. Since we are interested in comparing with results of unpaired quark matter we will neglect this possibility here.

8.2.1 Background solution

The metric of the charged black brane takes the general form, in Poincaré coordinates,

$$ds^2 = \frac{L^2}{z^2}\left(-f(z)dt^2 + \frac{dz^2}{f(z)} + d\vec{x}^{\,2}\right), \qquad f(z) = 1 - M\frac{z^4}{z_h^4} + Q^2\frac{z^6}{z_h^6}\,. \tag{8.52}$$

The AdS_5 asymptotic boundary is at $z = 0$, and the horizon is at the value where the black body factor vanishes $f(z_h) = 0$. The values of M and Q depend on the background scalar and gauge fields.

As we mentioned above, we will set all quark masses to zero, which allows to have a trivial solution of the scalar $X^{\rm bkg} = 0$. The background gauge fields dual to the quark densities are

$$(L_0^{\rm bkg})^a{}_b = (R_0^{\rm bkg})^a{}_b = \frac{\mu_q}{2}\left(1 - \frac{z^2}{z_h^2}\right)\delta^a{}_b\,. \tag{8.53}$$

Where $\mu_q = \mu_u = \mu_d = \mu_s$ is the quark chemical potential, which is the same for all flavors at beta-equilibrium. Since in this case $\mu_e = 0$, this implies that there is no net electron density, but the processes in (8.1) involving electron absorption or emission would still contribute, although we are neglecting them because they only give subleading corrections in the range of temperatures where the bulk viscosity is largest. The backreaction over the metric is limited to the gauge fields, so the geometry is the AdS Reissner-Nordstrom charged black brane (8.52), with

$$M = 1 + Q^2\,, \qquad Q^2 = \frac{z_h^2\mu_q^2}{2}\,. \tag{8.54}$$

The temperature in the dual field theory is equal to the Hawking temperature, given by

$$T = \frac{1}{\pi z_h}\left(1 - \frac{Q^2}{2}\right)\,. \tag{8.55}$$

One can use these formulas to obtain the position of the horizon as a function of the temperature and quark chemical potential

$$z_h = \frac{2}{\mu_q}\left(\sqrt{1+\left(\frac{\pi T}{\mu_q}\right)^2} - \frac{\pi T}{\mu_q}\right) . \tag{8.56}$$

Later we will often use

$$\bar{T} = z_h T \approx \frac{2T}{\mu_q} . \tag{8.57}$$

8.2.2 Two-point functions of flavor currents

The spectral function entering the formulas for the rates can be obtained from the imaginary part of the retarded correlator of the left flavor currents. Following the usual holographic dictionary [29, 30], we can extract the correlator from the solutions to the linearized equations of fluctuations. We will impose the boundary conditions

$$\lim_{z\to 0} L_\mu(x,z) = l_\mu(x), \quad \lim_{z\to 0} R_\mu(x,z) = 0, \quad \lim_{z\to 0} \frac{1}{z} X(x,z) = 0. \tag{8.58}$$

This turns off the sources for the right flavor currents and the quark bilinears and sets $l_\mu(x)$ as the source for the left flavor currents. The boundary asymptotic expansion of the Fourier transform of the left gauge fields is

$$(L_\mu)^a{}_b(\omega,\boldsymbol{k},z) \sim \left(\delta_\mu{}^\nu + (c_\mu{}^\nu)_{ab} z^2 \log\frac{z}{L} + z^2 (g_\mu{}^\nu)_{ab} + \cdots\right)(l_\nu)^a{}_b(\omega,\boldsymbol{k}), \tag{8.59}$$

where, having set the quark masses to zero,

$$(c_\mu{}^\nu)_{ab} = \frac{1}{2}\left(k_\alpha k^\alpha \delta_\mu^\nu - k_\mu k^\nu\right) . \tag{8.60}$$

The two-point function of the left flavor current can be obtained from the one-point function identifying the coefficient of the source l_μ. The one-point function is extracted from the boundary value of the regularized canonical momentum

$$\begin{aligned}&\langle 0|J^\mu_{q\,L}|0\rangle = \\ &= -\lim_{z\to 0}\frac{1}{g_5^2}\left[\sqrt{-g}F_L^{z\mu} + \left(\log\frac{z}{L} + \log(LB)\right)\left(LD_\alpha\left(\sqrt{-\gamma}F_L^{\alpha\mu}\right) - g_X^2 g_5^2\sqrt{-\gamma}\,j^\alpha_{(L)}\right)\right],\end{aligned} \tag{8.61}$$

where $\gamma_{\mu\nu} = g_{\mu\nu}$ is the induced metric on a radial slice and B is an energy scale of the theory. The additional terms are obtained from the variation of the counterterm action

$$S_{c.t} = \left(\log\frac{z}{L} + \log(LB)\right)\int d^4x\sqrt{-\gamma}\left[\frac{L}{4g_5^2}F_L^{\mu\nu}F_{L\,\mu\nu} + g_X^2 L (D_\mu X)^\dagger D^\mu X\right] . \tag{8.62}$$

The energy scale B, which determines the coefficient of a finite counterterm, can be chosen arbitrarily. Its value is scheme-dependent, depending on how the logarithmic divergence is cancelled. However, as shown in the formulas below, it only enters in contact terms of the real part of the correlators, so it does not affect the calculation of the spectral function. In addition to the terms shown here, one should also introduce a counterterm proportional to a quadratic potential for the scalar that is necessary to cancel further divergences when the quark masses are non-zero. In our case, with massless quarks, it can be safely ignored.

Using the expansion (8.59), the one-point function to linear order in the fluctuation is

$$\langle 0|(J^\mu_{q\,L})^a{}_b|0\rangle = \frac{2L}{g_5^2} G^{\mu\nu}_{ab}(l_\nu)^a{}_b, \qquad G^{\mu\nu}_{ab} = -\eta^{\mu\alpha}\left((g_\alpha{}^\nu)_{ab} - (c_\alpha{}^\nu)_{ab}\log\frac{LB}{e^{1/2}}\right) . \quad (8.63)$$

Taking the variation with respect to the source gives the two-point function

$$\langle 0|(J^\mu_{q\,L})^a{}_b(J^\nu_{q\,L})^{a'}{}_{b'}|0\rangle = \frac{2L}{g_5^2} G^{\mu\nu}_{ab}\delta^a_{b'}\delta^{a'}_b . \quad (8.64)$$

The fit of the model to QCD at large Euclidean momentum (8.48) fixes the normalization constant to the value

$$\mathcal{N} = \frac{2L}{g_5^2} = \frac{N}{6\pi^2} . \quad (8.65)$$

The spectral function is obtained from the imaginary part of the retarded correlator, which can only receive contributions from the coefficient of the $O(z^2)$ term in the boundary expansion (8.59)

$$\rho^{\mu\nu}_{ab,ba} = 2\mathcal{N}\eta^{\mu\alpha}\mathrm{Im}\,(g_\alpha{}^\nu)_{ab} . \quad (8.66)$$

In order to compute the correlators of flavor currents involved in the formulas for the weak reaction rates, we must consider linearized fluctuations of the gauge fields around the background solution. We can restrict to fluctuations that are off-diagonal in flavor, and take into account that the background is diagonal. When the quark masses are zero and the scalar profile is trivial, the energy-momentum tensor of the gauge fields is at least quadratic in the fluctuations. Therefore, metric fluctuations can be turned off. Furthermore, the fluctuations of the left gauge fields decouple from the right gauge field and the scalar, so it is enough to restrict the analysis to the left gauge fields.

8.2.3 Linearized fluctuations

We will work in the radial gauge $L_z = 0$ and expand the fluctuations in Fourier modes

$$L_\mu(x,z) = \int \frac{d\omega}{2\pi}\int \frac{d^3k}{(2\pi)^3} e^{-i\omega x^0 + i\boldsymbol{k}\cdot\boldsymbol{x}} L_\mu(\omega,\boldsymbol{k},z) . \quad (8.67)$$

Our fluctuations correspond to the off-diagonal flavor components $L_\mu \equiv (L_\mu)^a{}_b$, but we will omit flavor indices unless there is some ambiguity.

It will be convenient to rescale coordinates by the horizon position

$$z = z_h Z, \quad x^\mu = z_h X^\mu , \quad (8.68)$$

and work with the dimensionless frequency and momentum

$$\bar{\omega} = z_h \omega, \quad \bar{\boldsymbol{k}} = z_h \boldsymbol{k} \,, (\bar{k} = |\bar{\boldsymbol{k}}|) \,. \tag{8.69}$$

We will also define a dimensionless temperature $\bar{T} = z_h T$. The equations of motion for the linearized fluctuations of the gauge fields in these coordinates are collected in Appendix F.

We are interested in temperatures much smaller than the chemical potential $T/\mu_q \ll 1$. Since the integral over frequencies that determines the rates (8.42) is concentrated on frequencies smaller or of the order of the temperature, we can use a small frequency approximation $\omega/\mu_q \ll 1$.

We will use the approach of [236] to compute low-frequency correlators. When the temperature is zero, the background solution is an extremal black brane that develops an AdS_2 throat at the horizon. One can then divide the geometry into an inner and outer region relative to this throat. When the temperature is non-zero, but very small compared to the chemical potential, there is still a throat, but the inner geometry is a non-extremal AdS_2 with a horizon. From (8.55), we see that the near-extremal solutions correspond to $Q^2 \lesssim 2$. Let us parametrize

$$Q^2 = \frac{2}{Z_*^6}, \qquad Z_* - 1 = |\bar{\omega}| \frac{Z_*^2}{12\zeta_0}, \qquad Z_* - Z = |\bar{\omega}| \frac{Z_*^2}{12\zeta} \,. \tag{8.70}$$

The temperature in units of the horizon position is $\pi \bar{T} = 1 - Z_*^{-6}$. This gives the approximate relation

$$\zeta_0 \approx \frac{|\bar{\omega}|}{2\pi \bar{T}} = \frac{|\omega|}{2\pi T} \,. \tag{8.71}$$

Expanding the metric (8.52) for $|\bar{\omega}| \to 0$ and $Z_* \approx 1$ (since $\bar{T} \ll 1$), one gets

$$ds^2 \approx \frac{L^2}{12\zeta^2} \left(-F(\zeta) d\bar{\tau}^2 + \frac{d\zeta^2}{F(\zeta)} \right) + L^2 d\vec{X}^{\,2} \,, \tag{8.72}$$

where

$$F(\zeta) = 1 - \frac{\zeta^2}{\zeta_0^2}, \qquad \bar{\tau} = |\bar{\omega}| X^0 = |\omega| x^0 \,. \tag{8.73}$$

This is an $AdS_2 \times \mathbb{R}^3$ Schwarzschild geometry with an AdS_2 radius $L^2_{AdS_2} = L^2/12$ and a horizon at $\zeta = \zeta_0$. In the zero temperature limit $Z_* \to 1$, $\zeta_0 \to \infty$ the throat extends to values $\zeta \to \infty$.

The equations for linearized fluctuations can be solved in the inner region, L_μ^{in}, imposing an ingoing boundary condition at the horizon $\zeta \to \zeta_0$, and in the outer region, L_μ^{out}, taking the zero temperature limit where the geometry becomes the extremal AdS_5 Reissner-Nordstrom, (8.52) with $Q = \sqrt{2}$. The calculation of the solutions and connection coefficients up to $O(\omega^2/\mu_q^2)$ corrections is detailed in Appendix G, we summarize here the main results.

In the region towards the end of the AdS_2 throat, $\zeta \to 0$, the solutions have an expansion

$$L_\mu^{\text{in}} \sim A_\mu^- \zeta^{\Delta_-} + A_\mu^+ \zeta^{\Delta_+} \,, \qquad \Delta_+ > \Delta_- . \tag{8.74}$$

This matches with the behaviour of solutions in the outer region close to the horizon $Z \to 1$

$$L_\mu^{\rm out} = C_\mu^- \eta_-(Z) + C_\mu^+ \eta_+(Z), \quad \eta_\pm(Z) \sim (1-Z)^{-\Delta_\pm} , \tag{8.75}$$

which allows the identification

$$C_\mu^\pm = A_\mu^\pm \left(\frac{|\bar{\omega}|}{12}\right)^{\Delta_\pm} . \tag{8.76}$$

The ingoing condition fixes a relation between A_μ^+ and A_μ^- that translates into a relation between C_μ^+ and C_μ^-:

$$C_\mu^+ = \mathcal{G}_L(\omega, k) C_\nu^- , \tag{8.77}$$

with $\mathcal{G}_L(\omega, k)$ usually interpreted as an infrared (IR) Green's function associated with a $0+1$ CFT dual to the AdS_2 gravitational theory. This IR function determines the Green's function of the full theory. In order to see this, we need to translate the above relation between coefficients to the outer normalizable and non-normalizable solutions

$$L_\mu^{\rm out} = l_\mu \phi_{NN}(Z) + g_\mu \phi_N(Z), \tag{8.78}$$

with expansions close to the boundary $Z \to 0$

$$\phi_{NN}(Z) \sim 1 + \frac{\bar{k}^2}{2} Z^2 \log Z + O(Z^4), \quad \phi_N(Z) = Z^2 + O(Z^4) . \tag{8.79}$$

The two sets of outer solutions, $\{\eta_+, \eta_-\}$ and $\{\phi_{NN}, \phi_N\}$, are related by the connection coefficients

$$\eta_\pm(Z) = \alpha_\pm \phi_{NN}(Z) + \beta_\pm \phi_N(Z) . \tag{8.80}$$

Thus, the full solution is

$$\begin{aligned} L_\mu^{\rm out} &= C_\mu^- \left(\eta_-(Z) + \mathcal{G}_L \eta_+(Z)\right) = \\ &= C_\mu^- \left(\alpha_- + \alpha_+ \mathcal{G}_L\right) \phi_{NN}(Z) + C_\mu^- \left(\beta_- + \beta_+ \mathcal{G}_L\right) \phi_N(Z) . \end{aligned} \tag{8.81}$$

Fixing the coefficient of the non-normalizable solution to be the source l_μ, we get that the coefficient of the normalizable term is

$$g_\mu = \frac{\beta_- + \beta_+ \mathcal{G}_L}{\alpha_- + \alpha_+ \mathcal{G}_L} l_\mu . \tag{8.82}$$

More precisely, the connection coefficients and IR Green's function depend on whether the fluctuation is transverse or longitudinal. It turns out that at leading order in ω/T the longitudinal components do not contribute.

8.2.4 Spectral function

Since only the transverse components of the left gauge fields are relevant at low frequencies, the spectral function determined by (8.66) is ($\rho^{00} \approx 0$, $\rho^{0i} \approx 0$),

$$\rho^{ij}_{ab,ba} \approx \mathcal{N} \frac{\mu_q^2}{2} \left(\delta^{ij} - \frac{k^i k^j}{k^2}\right) \rho_L \left(\frac{\omega}{2\pi T}, \bar{k}, \bar{T}\right) , \tag{8.83}$$

where

$$\rho_L\left(\frac{\omega}{2\pi T},\bar{k},\bar{T}\right)=\frac{\beta_+\alpha_- - \beta_-\alpha_+}{\left(\alpha_- + \alpha_+\mathrm{Re}\,\mathcal{G}_L\right)^2+\left(\alpha_+\right)^2\left(\mathrm{Im}\,\mathcal{G}_L\right)^2}\mathrm{Im}\,\mathcal{G}_L\,. \tag{8.84}$$

The IR Green's function of the transverse modes of the left gauge fields is, up to corrections suppressed by factors of T/μ_q,

$$\mathcal{G}_L(\bar{\omega},\bar{k},\bar{T})\approx\frac{\Gamma\left(-\nu_k\right)\Gamma\left(\frac{1}{2}-i\,\frac{\omega}{2\pi T}+\nu_k\right)}{\Gamma\left(\nu_k\right)\Gamma\left(\frac{1}{2}-i\,\frac{\omega}{2\pi T}-\nu_k\right)}\left(\frac{\pi\bar{T}}{12}\right)^{2\nu_k}\,. \tag{8.85}$$

Where we have introduced ν_k for convenience, defined as

$$\nu_k=\sqrt{\frac{1}{4}+\frac{\bar{k}^2}{12}}\,. \tag{8.86}$$

At large spatial momentum the IR Greens' function approaches

$$\mathcal{G}_L(\bar{\omega},\bar{k},\bar{T})\sim-\frac{\cos\left(\frac{\pi\bar{k}}{\sqrt{12}}+i\frac{\omega}{2T}\right)}{\sin\left(\frac{\pi\bar{k}}{\sqrt{12}}\right)}\left(\frac{\pi\bar{T}}{12}\right)^{\frac{\bar{k}}{\sqrt{3}}}\,. \tag{8.87}$$

At low temperatures, there is a strong suppression due to the $\bar{T}$-dependent factor. When $T/\mu_q\to 0$ ($\bar{T}\to 0$), there is a strong suppression of the correlator already at small momenta

$$\mathcal{G}_L\sim\left(\frac{\pi\bar{T}}{12}\right)e^{-\frac{\bar{k}^2}{12}\log\frac{12}{\pi\bar{T}}}\,. \tag{8.88}$$

The support of the Green's function is concentrated on values $\bar{k}\lesssim|\log(T/\mu_q)|^{-1}\ll 1$. In this case, we can approximate the Green's function by

$$\mathcal{G}_L(\bar{\omega},\bar{k},\bar{T})\approx\left(\frac{\pi\bar{T}}{12}\right)e^{-(2\nu_k-1)\log\frac{12}{\pi\bar{T}}}\left(i\frac{\omega}{\pi T}+(2\nu_k-1)\right)+O((2\nu_k-1)^2,i\bar{\omega}(2\nu_k-1))\,. \tag{8.89}$$

The connection coefficients are real and only depend on the momentum. We have computed them numerically and determined their asymptotic behaviour at large spatial momentum (c.f. Appendix G)

$$\alpha_\pm\sim\mp 6^{\mp\frac{\bar{k}}{\sqrt{12}}}\bar{k}^{-1/2}, \tag{8.90}$$

$$\beta_\pm\sim\mp 6^{\mp\frac{\bar{k}}{\sqrt{12}}}\bar{k}^{3/2}\log\bar{k}. \tag{8.91}$$

Considering the large momentum asymptotic behaviour of the IR Green's function (8.87) and connection coefficients (8.90), we see that the spectral function vanishes exponentially fast at large spatial momentum. A special point is $\bar{k}=3$ ($\nu_k=1$), where $\mathcal{G}_L$ diverges and the spectral function has its first zero. For a numerical estimate, one can thus restrict the momentum integral to smaller values.

When $T/\mu_q\to 0$ we can approximate the connection coefficients by their $\bar{k}\to 0$ values, that we can compute analytically

$$\alpha_-\approx 1+O\left(\nu_k-\frac{1}{2}\right),\quad \beta_-\approx-\frac{3}{2}(2\nu_k-1)+O\left[\left(\nu_k-\frac{1}{2}\right)^2\right], \tag{8.92}$$

$$\alpha_+\approx\frac{4}{3(2\nu_k-1)}+O(1),\quad \beta_+\approx 4+O\left(\nu_k-\frac{1}{2}\right). \tag{8.93}$$

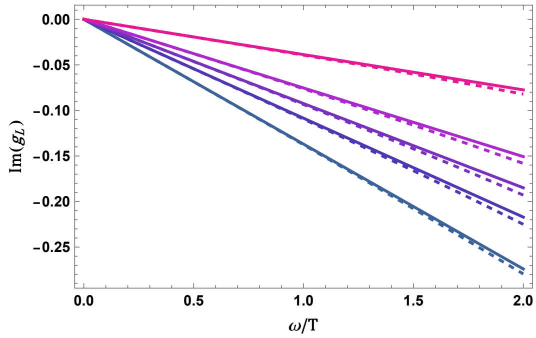

Figure 8.1. Plot of the imaginary part of the full g_L function (dashed) and its leading-order approximation in ω/T (solid) for $\nu_k = 0.6, 0.7, 0.75, 0.8, 0.9$ which correspond to colors from blue to light purple.

Thus $\beta_+\alpha_- - \beta_-\alpha_+ \approx 6$ and

$$\rho_L\left(\frac{\omega}{2\pi T},\bar{k},\bar{T}\right) \approx \frac{6(2\nu_k-1)^2}{(2\nu_k-1)^2+\left(\frac{4A_k(\bar{T})\omega}{3\pi T}\right)^2} A_k(\bar{T})\frac{\omega}{\pi T} \approx 6A_k(\bar{T})\frac{\omega}{\pi T}\,. \tag{8.94}$$

Here we have defined

$$A_k(\bar{T}) = \left(\frac{\pi\bar{T}}{12}\right) e^{-(2\nu_k-1)\log\frac{12}{\pi\bar{T}}}\,. \tag{8.95}$$

Numerically, at low frequencies, the IR Green's function is well approximated by

$$\begin{aligned}\mathcal{G}_L(\bar{\omega},\bar{k},\bar{T}) \approx & \frac{\Gamma(-\nu_k)\,\Gamma\left(\frac{1}{2}+\nu_k\right)}{\Gamma(\nu_k)\,\Gamma\left(\frac{1}{2}-\nu_k\right)}\left(\frac{\pi\bar{T}}{12}\right)^{2\nu_k}\left(1-\frac{i}{2}\tan(\pi\nu_k)\frac{\omega}{T}+\right. \\ & \left.+\frac{\pi^2\tan^2(\pi\nu_k)-\psi^{(1)}\left(\frac{1}{2}-\nu_k\right)+\psi^{(1)}\left(\frac{1}{2}+\nu_k\right)}{8\pi^2}\frac{\omega^2}{T^2}\right)+O\left(\frac{\omega^3}{T^3}\right),\end{aligned} \tag{8.96}$$

where $\psi^{(1)}$ is a polygamma function. In order to see how good is the approximation we plot the real and the imaginary part of the full IR Green function and its approximated expression. We define a reduced IR Green function

$$g_L(\bar{\omega},\bar{k}) = \frac{\Gamma(\nu_k)}{\Gamma(-\nu_k)}\left(\frac{12}{\pi\bar{T}}\right)^{2\nu_k}\mathcal{G}_L(\bar{\omega},\bar{k},\bar{T}), \tag{8.97}$$

so that the plots will be independent of $\bar{T}$. In Figure 8.1 we plot the full imaginary part of g_L (dashed lines) with the approximated formula (solid lines) for some values of ν_k, as a function of $\omega/T \in (0,2)$. Then, we plot the full real part of g_L (dashed lines) with the approximated formula (solid lines), as a function of $\omega/T \in (0,2)$, keeping just the first term in the expansion, Figure 8.2a, and then adding also the quadratic correction, Figure 8.2b. The values of ν_k are $0.6, 0.7, 0.75, 0.8, 0.9$ which correspond to colors from blue to light purple. We observe that as k becomes smaller, the real part becomes better approximated by the leading term.

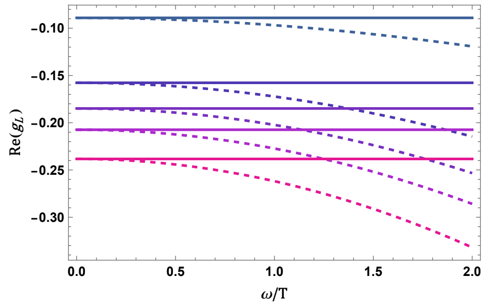

(a) Plot of the real part of the full g_L function (dashed) and its leading order approximation in ω/T (solid) for $\nu_k = 0.6, 0.7, 0.75, 0.8, 0.9$ which correspond to colors from blue to light purple.

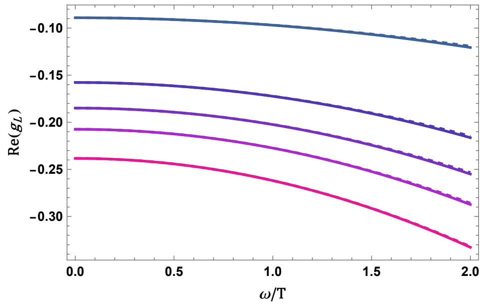

(b) Plot of the real part of the full g_L function (dashed) and its second-order approximation in ω/T (solid) for $\nu_k = 0.6, 0.7, 0.75, 0.8, 0.9$ (colors from blue to light purple).

Figure 8.2. Plots of the real part of the full g_L (dashed lines) and its approximated expressions up to second-order in ω/T (solid lines).

8.3 Estimate of weak reaction rates at strong coupling

We will proceed to estimate the weak rate. Since all the quark chemical potentials are equal at beta-equilibrium and the spectral function (8.83), (8.84) vanishes at zero frequency, we can use the simplified formula (8.43) to compute the rate. Taking into account that only the transverse components contribute to leading order, and rescaling the variables in the momentum integral $\omega = k_0 = 2\pi T s$, $k = \mu_q \bar{k}/2$,

$$\Lambda_{ud\to us} \approx \mathcal{N}^2 \frac{\mu_q^7}{2^7\pi^2} \int_{-\infty}^{\infty} ds \int_0^{\infty} d\bar{k}\, \bar{k}^2 \frac{\rho_L^2(s, \bar{k}, \bar{T})}{\sinh^2(\pi s)} \,. \tag{8.98}$$

Introducing (8.94), and changing variables to $\bar{k}^2 = 3(4\nu^2 - 1)$,

$$\Lambda_{ud\to us} \approx \mathcal{N}^2 \frac{3\sqrt{3}\mu_q^5 T^2}{4} \int_0^{\infty} ds \frac{s^2}{\sinh^2(\pi s)} \int_{1/2}^{\infty} d\nu\, \nu \sqrt{(4\nu^2 - 1)}\, e^{-2(2\nu-1)\log\frac{12}{\pi T}} \,. \tag{8.99}$$

We have

$$\int_0^{\infty} ds \frac{s^2}{\sinh^2(\pi s)} = \frac{1}{6\pi} \tag{8.100}$$

Changing variables $\nu = \frac{1}{2} + u$,

$$\Lambda_{ud\to us} \approx \mathcal{N}^2 \frac{\sqrt{3}\mu_q^5 T^2}{8\pi} \int_0^{\infty} du\, (1 + 2u) \sqrt{u(u+1)}\, e^{-4u\log\frac{12}{\pi T}} \,. \tag{8.101}$$

We use that the main contributions to the integral come from $u \ll 1$:

$$\begin{aligned} &\int_0^{\infty} du\, (1 + 2u) \sqrt{u(u+1)}\, e^{-4u\log\frac{12}{\pi T}} \approx \int_0^{\infty} du\, u^{1/2}\, e^{-4u\log\frac{12}{\pi T}} = \\ &= \frac{\Gamma(3/2)}{\left(4\log\frac{12}{\pi T}\right)^{3/2}} = \frac{\sqrt{\pi}}{2\left(4\log\frac{12}{\pi T}\right)^{3/2}} \,. \end{aligned} \tag{8.102}$$

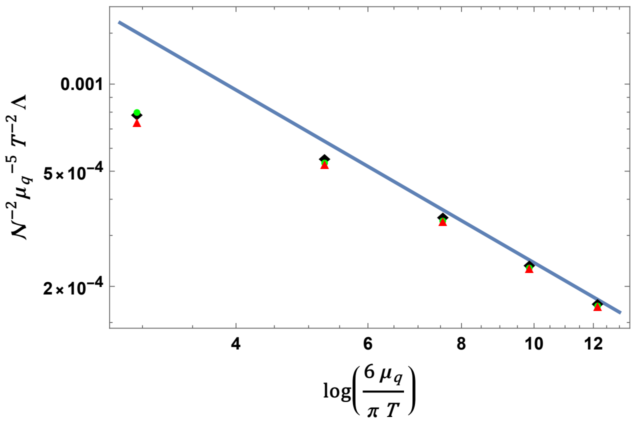

Figure 8.3. Log-log plot of the weak reaction rate multiplied by $\mathcal{N}^{-2}\mu_q^{-5}T^{-2}$ as function of $\log\left(\frac{6\mu_q}{\pi T}\right)$. The solid line described the approximated analytic results of Equation (8.103). The symbols are the results of the numerical integration of the formula (8.98) for $T/\mu_q = 10^{-1}, 10^{-2}, 10^{-3}, 10^{-4}$, taking the leading order approximation of the IR Green function (green dots), the second order approximation (red triangles) and the full result (black diamonds).

Then,

$$\Lambda_{ud\to us} \approx \frac{\mathcal{N}^2}{128}\sqrt{\frac{3}{\pi}}\mu_q^5 T^2 \left(\log\frac{6\mu_q}{\pi T}\right)^{-3/2} . \tag{8.103}$$

We have computed numerically the rate for values of the temperature $T/\mu_q = 10^{-1}, 10^{-2}, 10^{-3}, 10^{-4}$, considering the full dependence of the connection coefficients, and several approximations for the IR Green's function, namely the leading order (8.89), the second order approximation (8.96), and the full result (8.85). In the numerical integration over momentum, we cut the integral at $\nu_k = 1$, where the spectral function has its first zero. The exponential suppression already present at this value of the spatial momentum makes higher momentum contributions to be exceedingly small, so we believe this is a good approximation. We show our numerical results together with the analytic approximation at low temperatures (8.103) in Figure 8.3. We see that indeed the analytic formula approximates well the numerical result at low temperatures, even up to $T/\mu_q \lesssim 10^{-2}$, but for $T/\mu_q \sim 10^{-1}$ the deviations are already sizeable, although the analytic formula still serves as an estimate of the order of magnitude.

Chapter 9

Summary and conclusions

Here we present a summary of the second part of the thesis, together with some conclusive remarks and possible future directions. In this part of the thesis, we addressed the problem of computing the weak rates in (unpaired) quark matter using holography as a tool to overcome the difficulties faced by standard methods in performing computations in finite-temperature and finite chemical potential QCD-like theories.

In particular, in chapter 8, we derived the formulas (8.26) and (8.31) for the weak equilibration rate of quark flavor densities n_a ($a = u, d, s$). These formulas describe the equilibration rates near thermal equilibrium in terms of the spectral function of left-handed currents, to leading order in the Fermi coupling. The result, derived purely through field theory techniques, stems from the modification of Ward identities for flavor currents by symmetry-breaking terms induced by the weak interaction. Up to possible corrections by effective eight-fermion interactions, it is exact in the QCD coupling, with all non-perturbative dynamics of the strongly coupled theory encapsulated in the spectral function. Although we have focused on quark matter, the formulas are derived in an explicitly gauge-invariant way and rely solely on symmetry arguments. Thus, they should be valid for any state of QCD at nonzero temperature, including hadronic (confined) phases. In a confined phase, the natural degrees of freedom are baryons rather than quarks. Baryons are composed of three quarks and can be grouped according to their flavor composition. Therefore, the chemical potential for a baryon $B^{abc} \sim q^a q^b q^c$ would be $\mu_{B^{abc}} = \mu_a + \mu_b + \mu_c$, with $\mu_{a,b,c}$ being the quark chemical potentials corresponding to each flavor. The associated baryon densities should satisfy the conditions

$$n_a = 3n_{B^{aaa}} + 2\sum_{b\neq a} n_{B^{aab}} + \sum_{b,c\neq a} n_{B^{abc}}, \tag{9.1}$$

where the order of the flavor labels is immaterial, and $n_{B^{abc}}$ would, in principle, include all contributions from baryon resonances with the same flavor composition and with a mass below the value of the baryon chemical potential, assuming the decay channels to lower resonances become closed. With these identifications, one can combine the expressions in (8.26) to obtain the rates for the evolution of the density of different baryon species, or rather for the evolution of some combinations of them.

Returning to our analysis, we have used the general formulas for the rates in a particular model of unpaired quark matter with a holographic dual description. Using the holographic dual, we have obtained the leading order low-temperature behavior of the weak reaction rate in a large-density state of strongly coupled matter at beta-equilibrium. For simplicity, we have only considered massless quarks, from which we were able to extract an analytic expression (8.103) for the rate coefficient as defined in (8.5) and (8.44), resulting in

$$\lambda_{ds} \approx G_F^2 \sin^2\theta_C \cos^2\theta_C \frac{\mathcal{N}^2}{32}\sqrt{\frac{3}{\pi}}\mu_q^5 T^2 \left(\log\frac{6\mu_q}{\pi T}\right)^{-3/2} . \tag{9.2}$$

A fit to the large momentum behavior of QCD correlators fixes the normalization constant to $\mathcal{N} = N/(6\pi^2)$, Eq. (8.65). We can compare this with the perturbative result [84, 85, 86] including the leading QCD correction [103]

$$\lambda_{ds} \approx G_F^2 \sin^2\theta_C \cos^2\theta_C \frac{64}{4\pi^2}\mu_q^5 T^2 \left(1 + \frac{4\alpha_s}{9\pi}\log\frac{\kappa\,\alpha_s\mu_q}{T}\right)^4 , \tag{9.3}$$

where $\kappa \approx 0.28(2/3\pi)^{1/2} \approx 0.13$. The logarithmic enhancement of the rate at low temperatures originates from a non-Fermi-liquid behavior of quark matter due to long-range interactions (see also [237, 238]). Although the logarithm should not be too large in order for the perturbative expansion to be valid, the fourth power with which it appears can produce a significant effect on the rate. Considering the strong coupling result, the holographic dual geometry has also been conjectured to describe a non-Fermi ("marginal") liquid [236]. However, the logarithmic factor operates in the opposite way, suppressing the rate. Furthermore, compared to the perturbative result, the logarithm will be much larger, as there are no coupling-dependent factors in the argument suppressing the ratio μ_q/T. As shown in figure 8.3, the analytic formula (9.2) (proportional to (8.103) derived in the previous chapter) provides a good approximation for temperatures T/μ_q below 10^{-2}, but at higher temperatures, corrections to this formula start to become significant. However, their effect is to further suppress the rate.

Several improvements could be applied to the model, with perhaps the most significant being the inclusion of non-zero quark masses [239]. In the perturbative calculation of the rate, the mass enters the dispersion relation of the fermions in the scattering amplitude and removes the low-energy contributions from the massive quarks. In the holographic model, the scalar field dual to the quark bilinears would be non-zero, and its backreaction can change the near-horizon geometry, thus affecting the rate behavior. A generic expectation is that the AdS_2 throat in the near-horizon geometry would be replaced by a hyperscaling Lifshitz geometry (see [240] and references therein), which would probably result in the rate becoming proportional to a different power of the temperature depending on the dynamical exponent and the hyperscaling parameters.

Another extension of the model would be to study phases of paired quark matter, as quark pairing can affect transport properties [60, 62, 63]. A paired state would have a quark condensate with a non-trivial flavor structure, which could be captured by turning on a profile of the scalar field, in the holographic model we used, reproducing the same structure.

In conclusion, our study provides a framework for understanding weak interaction rates in strongly coupled quark matter and highlights the importance of non-perturbative methods in studying dense QCD phases. Future works should focus on refining these models, incorporating more realistic features such as non-zero quark masses and quark pairing, to enhance our understanding of neutron star interiors and their observational signatures.

Appendices

Appendix A

Fractional quantum Hall effect in a nutshell

The quantum Hall effect is one of the best-known examples of a topological phase of matter. It arises in a two-dimensional electron system, *e.g.* Gallium Arsenide, under a strong perpendicular magnetic field B. At very low temperatures ($T \sim 10$ mK) and high magnetic field ($B \sim 10$ Tesla), the transverse (Hall) conductivity, as a function of magnetic field, shows constant plateaux at the values

$$\sigma_H = \frac{e^2}{h}\,\nu, \tag{A.1}$$

where e is the electron charge, and h is the Planck constant. The quantity ν is called *filling fraction*, and it can be an integer number or a rational number. The latter case is known as the Fractional Quantum Hall Effect (FQHE). At the same time, the longitudinal conductivity vanishes, and the system is insulating in the bulk. See [188, 189, 190] for complete reviews on the topic.

The most compelling interpretation of the quantum Hall effect, originally proposed by Laughlin [241], envisions the electron system as an incompressible quantum liquid. In this phase, the electron density remains uniform throughout the bulk, and the system exhibits a finite energy gap that suppresses low-energy density fluctuations. This behavior is particularly transparent in the case of non-interacting electrons occupying a full Landau level, where electron–electron interactions can be safely ignored. The energy gap in such a setting is simply the separation between Landau levels, given by the cyclotron energy, which ensures the stability of the incompressible state.

A.1 Chern–Simons bulk effective theory

The low-energy degrees of freedom of a Hall state can be described by a conserved matter current j^μ, which is dual to a gauge field a_μ,

$$j^\mu = \frac{1}{2\pi}\epsilon^{\mu\nu\rho}\partial_\nu a_\rho. \tag{A.2}$$

This current is topologically conserved, $\partial_\mu j^\mu = 0$, and the U(1) gauge field a is usually referred to as a *hydrodynamic* field, arising from the collective behavior of many underlying electrons.

The effective hydrodynamic action is given by

$$S_{\text{eff}} = \frac{N}{4\pi}\int a\wedge da + \frac{1}{2\pi}\int a\wedge dA + \int a\wedge \mathcal{J}. \tag{A.3}$$

The first term is the Chern-Simons action for a and dominates the low-energy physics. The coupling N in this context is called *level* of the CS theory, and it takes integer values in order for the path integral of the theory to be well-defined. This theory is usually referred to as the $\mathrm{U}(1)_N$ CS theory. Such action is topological and it does not describe any propagating degrees of freedom, but rather it describes global effects occurring at energies below the bulk gap. The CS action violates time reversal and parity symmetry, reproducing what happens in a quantum Hall state in the presence of an external magnetic field.

The second term of (A.3) describes the minimal coupling of the hydrodynamic degrees of freedom with an external electromagnetic field A. Neglecting the third term, or equivalently, setting $\mathcal{J} = 0$, we can integrate out a using the equation of motion to get

$$S_{\text{eff}} = \frac{1}{4\pi N}\int A\wedge dA. \tag{A.4}$$

By taking functional derivatives with respect to A, we compute the induced current

$$J^\mu_{\text{ind}} = \frac{1}{2\pi N}\epsilon^{\mu\nu\rho}\partial_\nu A_\rho, \tag{A.5}$$

from which we can read the quantized Hall conductivity (with $e^2/h = 2\pi$)

$$\sigma_H = \frac{1}{2\pi N} \qquad \Rightarrow \qquad \nu = \frac{1}{N}. \tag{A.6}$$

It is well-known that the CS theory describes the existence of fractional charge and statistics in the system. These are low-energy excitations of the incompressible fluid, known as *anyons*, and their coupling to the hydrodynamic field is described by the third term of (A.3). To see the fractional features of these excitations, let us consider a static source $\mathcal{J}^\mu(x) = n\,\delta^{(2)}(x)\delta^{0\mu}$, where n is U(1) charge coupled to a. Setting $A = 0$, the equations of motion for a are

$$\frac{1}{2\pi}\epsilon^{0ij}\partial_i a_j = \frac{n}{N}\delta^{(2)}(x), \tag{A.7}$$

from which we can see that each excitation is equipped with n/N units of flux. We can compute the electromagnetic response

$$J^0_{\text{ind}}(x) = \frac{n}{N}\delta^{(2)}(x), \tag{A.8}$$

which shows that the electromagnetic charge of these static excitations is the rational number n/N. As anticipated, these quasi-particles have fractional statistics. Recall that the wavefunction of a particle of charge q moving around a flux Φ picks up a phase $\exp(i\,q\,\Phi)$. In the present case, the Aharonov-Bohm phase 2θ of an excitation with charge n_1 for a moving around a flux $\Phi = n_2/N$ generated by another excitation of charge n_2 is

$$2\theta = 2\pi \frac{n_1 n_2}{N} \,. \tag{A.9}$$

This is also known as *braiding phase*, and it is twice the exchange phase that determines the quantum statistics. Among the excitations, the electron has $n = N$, so that for two electrons $\theta/\pi = N$, which is consistent with the Fermi statistics if N is odd.

A.2 The bulk-boundary correspondence

In a finite quantum Hall system, gapless modes necessarily arise at the edge of the sample. These *edge modes* are a direct consequence of the non-trivial topological structure of the bulk. The presence of such edge states can be understood even at the classical level. Consider a charged particle in a uniform magnetic field: the particle undergoes circular motion (*e.g.*, anticlockwise) due to the Lorentz force. Near the boundary of a finite sample, these orbits are truncated, resulting in a skipping motion along the edge. Because the motion is unidirectional, these edge states are said to be *chiral*.

Quantum mechanically, edge states also emerge due to the breaking of Landau level degeneracy near the boundary. For example, in a disc-shaped droplet of radius R, a confining potential near the edge lifts the degeneracy, filling the states up to a Fermi energy. The density profile reveals a Fermi point at the edge, as the bulk remains incompressible. The low-energy excitations around this Fermi point are particle-hole pairs that behave as massless fermions with an approximately linear dispersion relation:

$$E(k) \approx v_F(k - k_F),$$

where $k = m/R$ is the one-dimensional momentum (k_F is the one associated with the Fermi energy), m is the angular momentum, and v_F is the Fermi velocity. These excitations correspond to a (1+1)-dimensional chiral relativistic fermion, known as a Weyl fermion. For a detailed derivation of these results, see [190].

The (1+1)-dimensional theory of the edge modes can arise from the (2+1)-dimensional CS theory as follows. In the absence of an external electromagnetic field, $A = 0$, the equations of motion for a reduce to $a = d\chi$, with χ a scalar field. For a disk geometry $\mathcal{D}$, the action reduces to a boundary term

$$S_{\text{bdry}} = \frac{N}{4\pi} \int dt dx \, \partial_t \chi \partial_x \chi, \tag{A.10}$$

with $x = R\theta$. This is just a symplectic term and leads to a vanishing Hamiltonian. To introduce a dynamic for the edge mode χ, we add a quadratic term in the momenta [190]

$$S_{\text{bdry}} = \frac{N}{4\pi} \int dt dx \, \partial_x \chi \, (\partial_t \chi + v \, \partial_x \chi), \tag{A.11}$$

with v an external parameter. This action is also known as the Floreanini-Jackiw action [112]. The equation of motion for χ is

$$(\partial_t + v \, \partial_x) \partial_x \chi = 0, \tag{A.12}$$

which shows that the edge modes are gapless and chiral.

The chiral boson χ on $\partial\mathcal{D}$ is a periodic field, being the phase of the U(1) gauge field, with period 2π. For the disk geometry, the general solution of the equations of motion is

$$\chi(t,\theta) = \chi_0 - (\theta - v\,t)\alpha_0 + i\sum_{n=0} \frac{\alpha_n}{n} e^{in(\theta - v\,t)}, \qquad \alpha_n^* = \alpha_{-n}\,. \tag{A.13}$$

As a consequence of the periodicity of the scalar field χ, the coefficient $\alpha_0 = m/N$ is quantized for some integer $m \in \mathbb{Z}$. Upon quantization, the coefficients χ_0, α_0, and α_n become operators acting on a bosonic Fock space, whose vacuum is defined by

$$\alpha_n \left|\Omega\right\rangle = 0, \qquad n > 0. \tag{A.14}$$

Imposing the canonical commutation relations between χ and the conjugate momentum $\pi = \delta\mathcal{L}/\delta(\partial_t\chi)$, one can get

$$[\alpha_0, \chi_0] = \frac{1}{iN}\,, \qquad [\alpha_n, \alpha_m] = \frac{n}{N}\delta_{n+m,0}\,. \tag{A.15}$$

In terms of these operators, we can rewrite the Hamiltonian L_0 and its moments L_n as

$$L_0 = \frac{N}{2}\alpha_0^2 + N\sum_{n>0} \alpha_{-n}\alpha_n\,, \qquad L_n = \frac{N}{2}\sum_{m=-\infty}^{+\infty} \alpha_{n-m}\alpha_m\,, \tag{A.16}$$

satisfying the following commutation rules

$$[L_n, \alpha_m] = -m\,\alpha_{n+m}, \quad [L_n, L_m] = (n-m)L_{n+m} + \frac{c}{12}(n^3 - n)\delta_{n+m,0}, \tag{A.17}$$

with $c = 1$. Thus, the chiral boson theory is a conformal field theory with central charge $c = 1$.

We conclude by connecting these results to the bulk physics. The definition of the edge charge should correspond to the bulk expression

$$Q = -\frac{1}{2\pi}\int d\theta\, a_\theta = \alpha_0 = \frac{m}{N}. \tag{A.18}$$

The edge spectrum reproduces the charges of Laughlin quasiparticles. In the bulk, fractional excitations with charge $Q = m/N$ correspond to edge states $|\alpha_0 = m/N\rangle$. This is another aspect of the bulk-boundary correspondence: anyonic excitations in the bulk map to solitonic configurations in the edge conformal field theory. The conformal dimensions of these excitations are determined by the action of the Virasoro generator L_0:

$$L_0 \left|\alpha_0 = \frac{m}{N}\right\rangle = h_m \left|\alpha_0 = \frac{m}{N}\right\rangle, \qquad h_m = \frac{m^2}{2N}. \tag{A.19}$$

In this CFT framework, the eigenstate of α_0 is a highest weight state satisfying $\alpha_n \left|\alpha_0\right\rangle = 0$ for $n > 0$, representing the ground state in a solitonic sector. Excited (descendant) states are generated by the action of the creation operators α_{-n} for

$n > 0$, and have conformal dimensions $n + m^2/(2N)$. Furthermore, the edge excitation with charge $Q = m/N$ and conformal dimension h_m is created by the Fubini-Veneziano vertex operator:

$$\mathcal{V}_m = :e^{im\chi}:, \tag{A.20}$$

where $m \in \mathbb{Z}$ and $\mathcal{V}_m$ inserts a charge $Q = m/N$ at point z on the boundary. This formalism underpins the consistency of the edge CFT with the bulk fractionalized excitations and reflects the deep structure of the quantum Hall state through the lens of conformal field theory.

Appendix B

Green function in duo-polar coordinates

In this appendix, we analyze a more general version of the equation of motion for A_t in flat space which is

$$\frac{1}{r}\,\partial_r\left(r\,\partial_r A_t\right)+\frac{1}{\rho}\,\partial_\rho\left(\rho\,\partial_\rho A_t\right)+\tau\, I(r,\rho)=0\,, \tag{B.1}$$

where $I(r,\rho)$ is a generic instanton density and τ is a constant. We use the Green function method which consists in finding the Green function associated with the operator that acts on A_t and then calculating the convolution with $I(r,\rho)$. In other words, the solution can be written as

$$A_t=\tau\int d^4x'\,G(r,\rho,r',\rho')\,I(r,\rho)\,, \tag{B.2}$$

where G is the Green function satisfying the equation

$$\frac{1}{r}\,\partial_r\left(r\,\partial_r G\right)+\frac{1}{\rho}\,\partial_\rho\left(\rho\,\partial_\rho G\right)=\frac{\delta(\rho-\rho')}{2\pi\rho'}\frac{\delta(r-r')}{2\pi r'}\,. \tag{B.3}$$

One way to solve the above equation is to interpret G as the potential generated by a charge distribution located at $\rho=\rho', r=r'$:

$$\begin{aligned} G&=\int_0^{2\pi}\int_0^{2\pi}\frac{d\psi\,d\theta}{\rho^2+\rho'^2+r^2+r'^2-2\rho\rho'\cos(\psi)-2rr'\cos(\theta)}=\\ &=2\pi\int_0^{2\pi}\frac{d\theta}{\sqrt{(\rho^2+\rho'^2+r^2+r'^2-2rr'\cos(\theta))^2-4\rho^2\rho'^2}}\,. \end{aligned}$$

We use the following trigonometric substitution in the integral:

$$t=\tan\left(\frac{\theta}{2}\right)\,,\quad d\theta=\frac{2}{1+t^2}dt\,,\quad \cos(\theta)=\frac{1-t^2}{1+t^2}\,,$$

that is defined for $\theta\in(-\pi,\pi)$. Therefore, we have to shift the angular variable, and then use the trigonometric substitution. After some calculations, we end up with

$$G=\frac{4\pi}{\sqrt{mp}}\int_{-\infty}^{+\infty}\frac{dt}{\sqrt{\left(t^2+\frac{n}{m}\right)\left(t^2+\frac{q}{p}\right)}}\,, \tag{B.4}$$

where

$$m = (\rho - \rho')^2 + (r - r')^2, \qquad n = (\rho - \rho')^2 + (r + r')^2\,,$$
$$p = (\rho + \rho')^2 + (r - r')^2, \qquad q = (\rho + \rho')^2 + (r + r')^2\,.$$

We can go to the complex plane and solve the integral using the Jordan Lemma taking care of the four simple poles and the two branch cuts. The integral admits an analytic solution in terms of the Elliptic integral of the first kind, which we will indicate as $\mathbf{K}(x)$:

$$\begin{aligned} G &= \frac{4\pi}{\sqrt{mp}} \int_{-\infty}^{+\infty} \frac{dt}{\sqrt{\left(t^2 + \frac{n}{m}\right)\left(t^2 + \frac{q}{p}\right)}} = \frac{4\pi}{\sqrt{mp}} \frac{2}{\sqrt{q/p}} \mathbf{K}\left(1 - \frac{n}{m}\frac{p}{q}\right) = \\ &= \frac{8\pi}{\sqrt{((\rho-\rho')^2 + (r-r')^2)((\rho+\rho')^2 + (r+r')^2)}} \cdot \\ &\quad \cdot \mathbf{K}\left(1 - \frac{(\rho-\rho')^2 + (r+r')^2}{(\rho-\rho')^2 + (r-r')^2} \cdot \frac{(\rho+\rho')^2 + (r-r')^2}{(\rho+\rho')^2 + (r+r')^2}\right)\,. \end{aligned} \tag{B.5}$$

One can check that this is indeed a solution of (B.3). To get the solution for A_t we have to perform the convolution (B.2) with $I(r, \rho; l)$. In general, the convolution will not have an analytic result and the integration has to be performed only numerically. In this work, we have found an analytic solution for the convolution with the instanton density

$$I(r, \rho) = \frac{16\pi\sqrt{2}\mathcal{N}\, r\rho\, l^4}{[(l^2 + \rho^2 + r^2)^2 - 4\rho^2 l^2]^2}\,, \tag{B.6}$$

coming from the definition (5.79). The result of the convolution reads

$$A_t = \frac{2\pi\sqrt{2}\mathcal{N}\,\tau(\rho^2 + r^2)}{(l^2 + \rho^2 + r^2)^2 - 4\rho^2 l^2} + A_t^{(0)}\,, \tag{B.7}$$

where we have the freedom to add the zero modes of the Laplacian operator in duo-polar coordinates:

$$A_t^{(0)} = \frac{c_0}{\sqrt{(l^2 + \rho^2 + r^2)^2 - 4\rho^2 l^2}} + \frac{c_1\, l^2(\rho^2 - r^2 - l^2)}{[(l^2 + \rho^2 + r^2)^2 - 4\rho^2 l^2]^{3/2}}\,. \tag{B.8}$$

Appendix C

Details on the topology of the D6-brane system

In this appendix, we collect the details of the topological properties and theorems used in section 6.1.3. The results exposed here are extracted from [242, 243, 244].

Recall that we are considering a two-dimensional manifold Σ such that $M_3 = \mathbb{R}_t \times \Sigma$, that is, topologically equivalent to a cylinder with its two bounding circles S^1.

We now justify the statement regarding the classification of principal U(1)-bundles used for the baryon number. In the following, we shall work with a general smooth manifold, which we will denote as M. There exists a classifying space named BU(1) such that principal U(1)-bundles over M (up to gauge transformations) are isomorphic to the maps from M to BU(1) (up to homotopy):

$$\{\text{Principal U}(1) - \text{bundle on } M\}/\text{gauge} \cong \{M \to \text{BU}(1)\}/\text{homotopy}\,. \tag{C.1}$$

The classifying space BU(1) is by definition (see [243] for more details) the infinite-dimensional complex projective space $\mathbb{CP}^\infty \equiv S^\infty/\mathrm{U}(1)$. This corresponds to the fibering:

$$S^1 \hookrightarrow S^\infty \twoheadrightarrow \mathbb{CP}^\infty\,. \tag{C.2}$$

Using the long exact homotopy sequence of this fibering (see section 4 of [243] or 17 in [242]), one can show that $\pi_2(\mathbb{CP}^\infty) = \pi_1(\mathrm{U}(1)) = \mathbb{Z}$, and also that every other homotopy group of $\mathbb{CP}^\infty$ vanishes. Path-connected topological spaces that have only one non-trivial homotopy group, like this one, have very useful properties. They are called Eilenberg-Maclane spaces $K(G, n)$ for a group G if:

$$\pi_n(K(G,n)) = G\,, \tag{C.3}$$

and all their other homotopy groups are trivial. Therefore BU(1) verifies:

$$\mathrm{BU}(1) \cong K(\mathbb{Z}, 2)\,. \tag{C.4}$$

As a consequence of a powerful theorem (Brown's representability theorem),[1] the

[1]We are assuming here that M is endowed with a *cellular complex* (CW-complex) that respects nice enough properties, which can always be done for closed manifolds. Remember that a cellular complex is a topological space that is built by gluing together topological balls (so-called cells) of different dimensions in specific ways. See [244] as a useful reference.

maps from M to Eilenberg-Maclane spaces $K(G, n)$ are classified by the nth cohomology group with coefficients in G, therefore in our case, where we have $G = \mathbb{Z}$ and $n = 2$, we get:

$$\{M \to \mathrm{BU}(1)\}/\text{homotopy} \cong \{M \to K(\mathbb{Z}, 2)\}/\text{homotopy} \cong H^2(M; \mathbb{Z}) \,, \qquad \text{(C.5)}$$

i.e. the maps from M to $\mathrm{BU}(1)$ up to homotopy, or equivalently the principal $\mathrm{U}(1)$-bundles over M up to gauge transformations, are classified by the second cohomology group of M with coefficients in $\mathbb{Z}$.

Recall now that given that f vanishes on the two bounding circles, we showed that the relevant manifold to study our setup is in fact the pinched torus $M = \mathbb{PT}$. There, we are using the one-point compactification of the cylinder. In this case, it is equivalent to performing a relative cohomology calculation of the cylinder with respect to the two bounding circles. We proceed by computing its cohomology, which can be done using the long exact sequence:

$$H^*(\mathbb{PT}; \mathbb{Z}) = (\mathbb{Z}, \mathbb{Z}, \mathbb{Z}, 0 \dots) \,. \qquad \text{(C.6)}$$

Then, using the definition of the first Chern class, we get that the integer in $H^2(\mathbb{PT}; \mathbb{Z}) = \mathbb{Z}$ corresponds to the first Chern number of the $\mathrm{U}(1)$-bundle. This last definition also corresponds to our definition of the baryon number.

We now wish to confront this result with the topology of the usual Yang-Mills $\mathrm{SU}(2)$ instanton setup. To reconstruct the statements used in section 6.1.3, the steps are very similar to what we just did. A similar classifying space can be constructed for $\mathrm{SU}(2)$:

$$\{M \to \mathrm{BSU}(2)\}/\text{homotopy} \cong \{\text{Principal } \mathrm{SU}(2) - \text{bundle}\}/\text{gauge} \,, \qquad \text{(C.7)}$$

which, this time, can be seen to be linked with the infinite quaternionic projective group:

$$\mathrm{BSU}(2) = \mathbb{HP}^\infty \equiv S^\infty / SU(2) \,. \qquad \text{(C.8)}$$

$$\mathrm{SU}(2) \hookrightarrow S^\infty \twoheadrightarrow \mathbb{HP}^\infty \,. \qquad \text{(C.9)}$$

This, using the homotopy exact sequence, yields that $\pi_4(\mathbb{HP}^\infty) = \pi_3(\mathrm{SU}(2)) = \mathbb{Z}$, and every other homotopy group of this space vanishes. Therefore, $\mathrm{BSU}(2) = K(\mathbb{Z}, 4)$, which yields by the same theorem the classification of principal $\mathrm{SU}(2)$-bundles by $H^4(M; \mathbb{Z})$. Applying this to $M = S^4$ which is the manifold on which f is defined in the instanton case we have (C.10):

$$H^4(S^4; \mathbb{Z}) = \mathbb{Z} \,. \qquad \text{(C.10)}$$

The last step is to use the properties of the second Chern class instead of the first one, which takes its values in $H^4(S^4; \mathbb{Z}) = \mathbb{Z}$, and corresponds to the instanton number.

Appendix D

Numerical analysis of the D6-brane equations of motion

In this appendix, we present the methods used to numerically solve the equations of motion. We first identify and exploit relations between the physical parameters in order to reduce the parameter space of the numerical study. Then we recall the boundary conditions derived in section 6.1.2 and describe the methods used to solve the differential equations. We start by performing the following coordinate and field redefinition

$$u \to u_J\, u, \qquad \rho \to L\, \rho, \qquad a_\psi \to L\, u_J\, a_\psi, \qquad a_t \to u_J\, a_t\,. \tag{D.1}$$

Let us recall that L has a different expression for the confined and the deconfined phases

$$\text{Confining phase:} \qquad L = \frac{R^{3/2}}{u_J^{1/2}} J(b),$$

$$J(b) = \frac{2}{3}\int_0^1 dv \frac{\sqrt{1-b^3}\,\sqrt{v}}{(1-b^3 v)\sqrt{1-b^3 v-(1-b^3)v^{8/3}}}\,,$$

$$\text{Deconfined phase:} \qquad L = \frac{R^{3/2}}{u_J^{1/2}} J_T(\tilde{b}),$$

$$J_T(\tilde{b}) = \frac{2}{3}\int_0^1 dv \frac{\sqrt{1-\tilde{b}^3}\,\sqrt{v}}{\sqrt{1-\tilde{b}^3 v}\,\sqrt{1-\tilde{b}^3 v-(1-\tilde{b}^3)v^{8/3}}}\,,$$

where we have used the standard notation of the WSS model, $b = u_0/u_J$ and $\tilde{b} = u_T/u_J$. In the following, all the fields and the coordinate u have to be intended as the rescaled ones. With these transformations, the equations of motion become

- Confining phase

$$J^2(b)\,\partial_u\left(\frac{u^4\rho'(u)\rho(u)}{D(u)}\right)-u\,D(u)\left(1-\frac{9}{u^2}\tilde{a}_t^2\right)=0\,, \tag{D.2}$$

$$\partial_u\tilde{a}_\psi+\frac{3}{u}\rho(u)D(u)\,\tilde{a}_t=0\,, \tag{D.3}$$

$$\partial_u\tilde{a}_t+\frac{3}{u}\frac{D(u)}{\rho(u)}\,\tilde{a}_\psi=0\,, \tag{D.4}$$

where

$$f(u)=1-\frac{b^3}{u^3}\,,\qquad D(u)=\sqrt{\frac{J^2(b)\,\rho'(u)^2\,u^3+\frac{1}{f(u)}}{1+\frac{9}{u^2}\left(\frac{\tilde{a}_\psi^2}{\rho^2}-\tilde{a}_t^2\right)}}\,. \tag{D.5}$$

- Deconfined phase

$$J^2(\tilde{b})\,\partial_u\left(\frac{u^4\rho'(u)\rho(u)f_T(u)}{D_T(u)}\right)-u\,D_T(u)\left(1-\frac{9\tilde{a}_t^2}{u^2 f_T(u)}\right)=0\,, \tag{D.6}$$

$$\partial_u\tilde{a}_\psi+\frac{3}{u\,f_T(u)}\rho(u)\,D_T(u)\,\tilde{a}_t=0\,, \tag{D.7}$$

$$\partial_u\tilde{a}_t+\frac{3}{u}\frac{D_T(u)}{\rho(u)}\,\tilde{a}_\psi=0\,, \tag{D.8}$$

where

$$f_T(u)=1-\frac{\tilde{b}^3}{u^3},\qquad D_T(u)=\sqrt{\frac{1+\rho'(u)^2\,u^3 f_T(u)\,J^2(\tilde{b})}{1+\frac{9}{u^2}\left(\frac{\tilde{a}_\psi^2}{\rho^2(u)}-\frac{\tilde{a}_t^2}{f_T(u)}\right)}}\,. \tag{D.9}$$

We adapt the boundary conditions on a discussed in section 6.1.2 to study configurations with generic spin. Recall that in the baryon case, $J=Nn_B^2/2$ holds and therefore the boundary conditions are those indicated in section 6.1.2. For the other cases, we invert equation (6.33) and (6.42):

$$\hat{a}_\psi(u_*)=\frac{n_B}{2}-\frac{J}{Nn_B}\,,\qquad \hat{a}_\psi(u_J)=-\frac{n_B}{2}-\frac{J}{Nn_B}\,. \tag{D.10}$$

After the redefinitions in (D.1), using the holographic dictionary, we obtain

- Confining phase:

$$\tilde{a}_\psi(1)=\frac{2\pi l_s^2}{Lu_J}\left(-\frac{n_B}{2}-\frac{J}{Nn_B}\right)=\frac{6\pi\sqrt{b}}{J(b)\,\lambda}\left(-\frac{n_B}{2}-\frac{J}{Nn_B}\right), \tag{D.11}$$

$$\tilde{a}_\psi(u_*/u_J)=\frac{2\pi l_s^2}{Lu_J}\left(\frac{n_B}{2}-\frac{J}{Nn_B}\right)=\frac{6\pi\sqrt{b}}{J(b)\,\lambda}\left(\frac{n_B}{2}-\frac{J}{Nn_B}\right). \tag{D.12}$$

- Deconfined phase:

$$\tilde{a}_\psi(1) = \frac{2\pi l_s^2}{L\,u_J}\left(-\frac{n_B}{2} - \frac{J}{Nn_B}\right) = \frac{6\pi\sqrt{\tilde{b}}}{J_T(\tilde{b})\,\lambda_T}\left(-\frac{n_B}{2} - \frac{J}{Nn_B}\right), \tag{D.13}$$

$$\tilde{a}_\psi(u_*/u_J) = \frac{2\pi l_s^2}{L\,u_J}\left(\frac{n_B}{2} - \frac{J}{Nn_B}\right) = \frac{6\pi\sqrt{\tilde{b}}}{J_T(\tilde{b})\,\lambda_T}\left(\frac{n_B}{2} - \frac{J}{Nn_B}\right), \tag{D.14}$$

where we have defined the effective 't Hooft coupling constant

$$\lambda_T = \frac{2\pi\,T}{M_{KK}}\,\lambda = \frac{T}{T_c}\,\lambda\,. \tag{D.15}$$

Notably, the deconfined phase expressions are the same as in the confined case, up to replacing $(\lambda, b, J(b)) \to (\lambda_T, \tilde{b}, J_T(\tilde{b}))$. In general, the boundary value problem we are considering depends, a priori, on four parameters: b (or $\tilde{b}$), $\lambda_{(T)}$, n_B, and the angular momentum J.

In the following, we will focus on objects with $J = Nn_B^2/2$. In this case, recall that n_B and $\lambda_{(T)}$ appear only in the ratio

$$\xi_{(T)} \equiv \frac{n_B}{\lambda_{(T)}}, \tag{D.16}$$

effectively reducing the number of parameters by one. The baryon number can be parametrically large in $\lambda_{(T)}$, $n_B = \lambda_{(T)}^{v}$ with $0 \leq v \leq 1$, and we are working in large λ-limit. Therefore, the parameter ξ ranges from zero when $n_B \sim \lambda^0_{(T)}$ to order 1 when $n_B \sim \lambda_{(T)}$.

We will now describe the integration method for this differential problem. The integration domain of the differential equations in the rescaled radial coordinate u is $[b, 1]$ for the confined phase and $[\tilde{b}, 1]$ for the deconfined phase. In section 6.1.2, we have defined two of our boundary conditions in $u = 1$ and two in $u = u_*/u_J$. To find a numerical solution with the correct boundary conditions, we will free the two boundary conditions in $u = u_*/u_J$ and implement two more boundary conditions in $u = 1$, which can be thought of as parameters, $\tilde{a}_t(1)$ and $\rho(1)$. The physical boundary conditions in $u = u_*/u_J$ will then be obtained by varying these two parameters.

These parameter-boundary conditions are not allowed to take any value. Obviously, $\rho(1)$ can only take positive values. A more interesting inequality can be derived for $\tilde{a}_t$. Indeed, for the Lagrangian to be real, the quantity $D^2_{(T)}$ has to be positive or zero. In the confined phase, inside the integration region we are considering, this implies

$$1 + \frac{9}{u^2}\left(\frac{\tilde{a}_\psi^2}{\rho^2} - \tilde{a}_t^2\right) > 0\,. \tag{D.17}$$

A second constraint arises from the equilibrium condition for the D6-brane, which requires that the D6-brane ends orthogonally at the D8-branes' tip. This amounts to having $\rho'(1) = 0$ and, for the lowest energy configuration, to having a concave function. Replacing these values in (6.19) gives the concavity inequality:

$$\frac{u^2}{9} < \tilde{a}_t^2\,. \tag{D.18}$$

The value of the gauge connection component $\tilde{a}_t$ for an equilibrium configuration then has to lie in the window

$$\frac{u^2}{9} < \tilde{a}_t^2 < \frac{u^2}{9} + \frac{\tilde{a}_\psi^2}{\rho^2}\,. \tag{D.19}$$

One can think of exotic solutions, like punctured domain walls, whose profile $\rho(u)$ is a convex function (or there is some interval in which it is convex) for which

$$0 < \tilde{a}_t^2 < \frac{u^2}{9}\,. \tag{D.20}$$

Similar results can be written in the deconfined case for concave solutions

$$f_T(u)\,\frac{u^2}{9} < \tilde{a}_t^2 < f_T(u)\left(\frac{u^2}{9} + \frac{\tilde{a}_\psi^2}{\rho^2}\right), \tag{D.21}$$

and convex ones

$$0 < \tilde{a}_t^2 < f_T(u)\,\frac{u^2}{9}\,. \tag{D.22}$$

In all the cases, we introduce a parameter α to span the window. Our boundary conditions for a baryon become:

- ◇ $\tilde{a}_\psi(1) = -\dfrac{6\pi\, n_B \sqrt{b}}{\lambda J(b)}$ (Confined phase),
  $\tilde{a}_\psi(1) = -\dfrac{6\pi\, n_B \sqrt{\tilde{b}}}{\lambda_T J_T(\tilde{b})}$ (Deconfined phase).
- ◇ $\rho'(1) = 0$, which enforces the equilibrium condition by requiring that the embedding ends orthogonally at $u = u_J$.
- ◇ $\rho(1) = l$ the radius of the D6-brane at the D8-branes' tip is our first parameter-boundary condition. The value of l, which gives the physical boundary conditions in u_*/u_J will be named l_{stable}, the stability radius.
- ◇ $\tilde{a}_t(1)$, our second parameter-boundary condition, which can be given in terms of α as

$$\text{Confined phase:}\quad \tilde{a}_t(1) = \sqrt{\frac{1}{9} + (1-\alpha^2)\left(\frac{(6\pi)^2 b}{\lambda^2 J^2(b)\, l^2}\right)}\,. \tag{D.23}$$

$$\text{Deconfined phase:}\quad \tilde{a}_t(1) = \sqrt{f_T(1)}\sqrt{\frac{1}{9} + (1-\alpha^2)\left(\frac{(6\pi)^2 \tilde{b}}{\lambda_T^2 J_T^2(\tilde{b})\, l^2}\right)}\,. \tag{D.24}$$

Let us observe that the same expression for $\tilde{a}_t$ with a minus sign in front of it gives rise to nonphysical solutions, and hence, we focus on $\tilde{a}_t > 0$. The function $1-\alpha^2$ was chosen heuristically and found to give faster convergence results.

We integrate the equations of motion parametrically using Mathematica. The process depends on the type of solution considered. For baryons specifically, we interrupt the integration process when ρ reaches zero. For punctured domain wall solutions, we also interrupt the process if ρ diverges. This allows us to consider solutions without a predetermined u_*, like domain walls and baryons. For solutions which extend to a fixed u_*, like vortons or sandwich defects, the integration domain is predetermined, so there is no interruption condition.

Specifying the boundary conditions on one side of the integration domain provides the uniqueness of the solution, reducing the problem to finding the parameters l_{stable} and α such that the physical boundary conditions in $u = u_*$ are satisfied. This is achieved by translating the boundary conditions in $u = u_*$ into constraints, finding a Lagrangian functional L_0 for these constraints, and numerically computing its minima over the parameter space:

$$l_{\text{stable}} > 0\,, \quad 0 < \alpha < 1\,. \tag{D.25}$$

Since the different types of solutions we consider correspond to different boundary conditions in $u = u_*$, we need to adjust L_0 to each type of solution. Moreover, the Lagrange multipliers of these constraints also have to be further adjusted to ensure convergence to the desired solution. The constraint functions used for each type of solution are listed in tables D.1, and D.2.

L_0	Confined phase
Baryon	$\tilde{a}_\psi(u_E)^2 + \lambda\rho(u_E)^2$
Punctured domain wall	$\tilde{a}_\psi(u_K)^2 + \frac{1}{\lambda}(u_K - u_*)^2$
Sandwich defect	$\tilde{a}_\psi(u_K)^2 + \frac{1}{\lambda}(u_K - u_*)^2 + \lambda\rho'(u_K)^2$

Table D.1. Constraint functions used for each configuration in the confining phase of the WSS model.

L_0	Deconfined phase
Baryon	$\tilde{a}_\psi(u_E)^2 + \lambda_T\rho(u_E)^2$
Vorton	$\tilde{a}_\psi(u_*)^2 + \tilde{a}_t(u_*)^2 + \frac{1}{\lambda_T}(u_T - u_*)^2$
Punctured domain wall	$\tilde{a}_\psi(u_K)^2 + \frac{1}{\lambda_T}(u_K - u_*)^2$
Sandwich defect	$\tilde{a}_\psi(u_K)^2 + \frac{1}{\lambda_T}(u_K - u_*)^2 + \lambda_T\rho'(u_K)^2$

Table D.2. Constraint functions used for each configuration in the deconfined phase of the WSS model.

It is easy to verify that every solution to the physical boundary problem is at a minimum of this function, and that they are realized for $L_0 = 0$. We will say that the solution is found when the value of L_0 at the minimum is lower than

$$\text{Min } L_0 < \varepsilon \equiv 10^{-10} \tag{D.26}$$

For baryon solutions, the only choice lies in the Lagrange multiplier for each configuration. For the explored range of $\lambda_{(T)}$, this was found to give the best results. For vortons and punctured domain walls, we add a $(u_* - u_K)^2$ term, which controls the coordinate u at which the solution ends, either by entering the horizon (then $u_K = u_T$) or by diverging ($\rho \to \infty$). For the sandwich vortons, we also add a $\rho'(u_*)^2$ term to control the stability at the second D8-brane setup.

Appendix E

Non-conservation equations of flavor currents

With three massless flavors of quarks $q^i = (u, d, s)$ and one flavor of massless leptons $l^a = (\nu_e, e)$ (with only left-handed component for the neutrino), the flavor symmetry group is $\mathrm{SU}(3)_{q_L} \times \mathrm{SU}(3)_{q_R} \times \mathrm{SU}(2)_{l_L} \times \mathrm{U}(1)_{e_R}$. Unequal mass terms for the quarks and the electron break explicitly the flavor group to $\mathrm{U}(1)^5$, where the quarks and electron U(1)s are vector-like.

The EW sector, in particular, W-boson exchange introduces a term in the effective action of the form (Fermi model)

$$\Delta\mathcal{L}_{EW} = -2\sqrt{2}G_F (J^\mu_{ch})^\dagger J_{ch\,\mu}, \tag{E.1}$$

where the J^μ_{ch} is the left-charged current

$$J^\mu_{ch} = \overline{\nu}_{e\,L}\gamma^\mu e_L + \cos\theta_C\, \overline{u}_L \gamma^\mu d_L + \sin\theta_C\, \overline{u}_L\gamma^\mu s_L, \tag{E.2}$$

with θ_C the Cabbibo angle, which gives the change of basis between mass and flavor eigenstates. Let us introduce the notation

$$(J^\mu_q)^i{}_j = \bar{q}_j\gamma^\mu q^i, \quad (J^\mu_l)^a{}_b = \bar{l}_b\gamma^\mu l^a\,. \tag{E.3}$$

Then, in terms of current components,

$$J^\mu_{ch} = (J^\mu_{l\,L})^2{}_1 + \cos\theta_C (J^\mu_{q\,L})^2{}_1 + \sin\theta_C (J^\mu_{q\,L})^3{}_1, \tag{E.4}$$

Where $J^\mu_{l\,L}$ is the current for the $\mathrm{SU}(2)_L$ lepton symmetry and $J^\mu_{q\,L}$ is the current for the $\mathrm{SU}(3)_L$ flavor symmetry. The EW term becomes

$$\begin{aligned}
\Delta\mathcal{L}_{EW} =& -2\sqrt{2}G_F\Big[\cos^2\theta_C (J^\mu_{q\,L})^2{}_1 (J_{q\,L\,\mu})^1{}_2 + \sin^2\theta_C (J^\mu_{q\,L})^1{}_3 (J_{q\,L\,\mu})^3{}_1 \\
&+ \cos\theta_C\sin\theta_C \left((J^\mu_{q\,L})^2{}_1 (J^\mu_{q\,L})^1{}_3 + (J^\mu_{q\,L})^3{}_1 (J^\mu_{q\,L})^1{}_2\right) \\
&+ \cos\theta_C \left((J^\mu_{l\,L})^2{}_1 (J_{q\,L\,\mu})^1{}_2 + (J^\mu_{l\,L})^1{}_2 (J_{q\,L\,\mu})^2{}_1\right) \\
&+ \sin\theta_C \left((J^\mu_{l\,L})^2{}_1 (J_{q\,L\,\mu})^1{}_3 + (J^\mu_{l\,L})^1{}_2 (J_{q\,L\,\mu})^3{}_1\right)\Big]\,.
\end{aligned} \tag{E.5}$$

Let us neglect the terms coupling quarks and leptons. We can rewrite the remaining terms in the following way

$$\begin{aligned}\Delta\mathcal{L}_{EW} =& -2\sqrt{2}G_F\Big[\cos^2\theta_C \,\mathrm{tr}\left(P_{11}J^{\mu}_{q\,L}P_{22}J_{q\,L\,\mu}\right) + \sin^2\theta_C \,\mathrm{tr}\left(P_{11}J^{\mu}_{q\,L}P_{33}J_{q\,L\,\mu}\right) \\ &+ \cos\theta_C\sin\theta_C\left(\mathrm{tr}\left(P_{11}J^{\mu}_{q\,L}P_{32}J_{q\,L\,\mu}\right) + \mathrm{tr}\left(P_{11}J^{\mu}_{q\,L}P_{23}J_{q\,L\,\mu}\right)\right)\Big]\,.\end{aligned} \tag{E.6}$$

Where we have defined the projectors $(P_{kl})^i{}_j = \delta^i_k\delta^l_j$.

By doing $\mathrm{SU}(3)_L\times\mathrm{SU}(3)_R$ rotations of equal angle, we can derive Ward identities for the vector SU(3) flavor currents. The currents transform as

$$\delta_\theta J^\mu_q = i\theta_A[T^A, J^\mu_q] \tag{E.7}$$

Defining $J^\mu_q = J^\mu_{q\,L} + J^\mu_{q\,R}$ and $J^\mu_l = J^\mu_{l\,L} + J^\mu_{l\,R}$. The covariant derivative under a background flavor gauge potential A^f_μ is

$$D_\mu J^\mu_q = \partial_\mu J^\mu_q - i[A^f_\mu, J^\mu_q]\,. \tag{E.8}$$

We will take the normalization for the gauge group generators to be $\mathrm{tr}(T^AT^B) = \frac{1}{2}\delta^{AB}$. Then, the Ward identities are

$$\begin{aligned}&2\mathrm{tr}\left(D_\mu J^\mu_q T^A\right) = \\ &2i\sqrt{2}G_F\Big[\cos^2\theta_C\left(\mathrm{tr}\left(P_{11}[T^A, J^\mu_{q\,L}]P_{22}J_{q\,L\,\mu}\right) + \mathrm{tr}\left(P_{11}J^\mu_{q\,L}P_{22}[T^A, J_{q\,L\,\mu}]\right)\right) \\ &+\sin^2\theta_C\left(\mathrm{tr}\left(P_{11}[T^A, J^\mu_{q\,L}]P_{33}J_{q\,L\,\mu}\right) + \mathrm{tr}\left(P_{11}J^\mu_{q\,L}P_{33}[T^A, J_{q\,L\,\mu}]\right)\right) \\ &+\cos\theta_C\sin\theta_C\left(\mathrm{tr}\left(P_{11}[T^A, J^\mu_{q\,L}]P_{23}J_{q\,L\,\mu}\right) + \mathrm{tr}\left(P_{11}J^\mu_{q\,L}P_{23}[T^A, J_{q\,L\,\mu}]\right)\right. \\ &\left.+\mathrm{tr}\left(P_{11}[T^A, J^\mu_{q\,L}]P_{32}J_{q\,L\,\mu}\right) + \mathrm{tr}\left(P_{11}J^\mu_{q\,L}P_{32}[T^A, J_{q\,L\,\mu}]\right)\right)\Big]\,.\end{aligned} \tag{E.9}$$

Combining the traces and using the cyclic property, we have that

$$\begin{aligned}D_\mu J^\mu_q =& i\sqrt{2}G_F\Bigg(\cos^2\theta_C\left[J_{q\,L\,\mu}\,,\,P_{11}J^\mu_{q\,L}P_{22} + P_{22}J^\mu_{q\,L}P_{11}\right] + \\ &+\sin^2\theta_C\left[J_{q\,L\,\mu}\,,\,P_{11}J^\mu_{q\,L}P_{33} + P_{33}J^\mu_{q\,L}P_{11}\right] + \\ &+\cos\theta_C\sin\theta_C\Bigg(\left[J_{q\,L\,\mu}\,,\,P_{11}J^\mu_{q\,L}P_{23} + P_{23}J^\mu_{q\,L}P_{11}\right] + \\ &+\left[J_{q\,L\,\mu}\,,\,P_{11}J^\mu_{q\,L}P_{32} + P_{32}J^\mu_{q\,L}P_{11}\right]\Bigg)\Bigg)\,.\end{aligned} \tag{E.10}$$

In general, there will also be contributions on the right-hand side depending on the quark masses, but they should vanish for diagonal components.

We can do a similar derivation taking into account the leptons if we introduce projectors

$$(\tilde{P}_{ai})^b{}_j = \delta^b_a\delta^i_j,\quad (\tilde{P}^T_{ia})^j{}_b = \delta^a_b\delta^j_i\,, \tag{E.11}$$

Then

$$\tilde{P} J_q^\mu \tilde{P}^T \sim J_l^\mu, \quad \tilde{P}^T J_l^\mu \tilde{P} \sim J_q^\mu. \tag{E.12}$$

And introduce the $\mathrm{SU}(2)_L \times \mathrm{SU}(2)_R$ rotations of the leptons, such that the diagonal rotations transform the vector currents as

$$\delta_\phi J_l^\mu = i\phi_\alpha [\tau^\alpha, J_l^\mu]. \tag{E.13}$$

With similar normalization for the generators $\mathrm{tr}(\tau^\alpha \tau^\beta) = \frac{1}{2}\delta^{\alpha\beta}$.

Appendix F

Linearized equations of motion of fluctuations

The transverse spatial components of the gauge fields $k^i L_i = k^i R_i = 0$ decouple from the other fluctuations. Their equations are

$$0 = {L_i}'' + \left(\frac{f'}{f} - \frac{1}{Z}\right) {L_i}' + \left(\frac{\bar{\omega}^2}{f^2} - \frac{\bar{k}^2}{f}\right) L_i \, , \tag{F.1a}$$

$$0 = {R_i}'' + \left(\frac{f'}{f} - \frac{1}{Z}\right) {R_i}' + \left(\frac{\bar{\omega}^2}{f^2} - \frac{\bar{k}^2}{f}\right) R_i \, , \tag{F.1b}$$

When the quark masses are nonzero, the time L_0, R_0, and longitudinal $L_\parallel = \frac{k^i}{k} L_i$, $R_\parallel = \frac{k^i}{k} R_i$ components of the gauge fields are coupled to the scalar fluctuations, but they decouple otherwise. The left gauge field equations are

$$0 = {L_\parallel}'' + \left(\frac{f'}{f} - \frac{1}{Z}\right) {L_\parallel}' + \frac{\bar{\omega}^2}{f^2} L_\parallel + \frac{\bar{k}\bar{\omega}}{f^2} L_0, \tag{F.2a}$$

$$0 = {L_0}'' - \frac{1}{Z} {L_0}' - \frac{\bar{k}^2}{f} L_0 - \frac{\bar{k}\bar{\omega}}{f} L_\parallel, \tag{F.2b}$$

$$0 = \bar{\omega} {L_0}' + \bar{k} f {L_\parallel}' \, . \tag{F.2c}$$

The right gauge field equations are

$$0 = {R_\parallel}'' + \left(\frac{f'}{f} - \frac{1}{Z}\right) {R_\parallel}' + \frac{\bar{\omega}^2}{f^2} R_\parallel + \frac{\bar{k}\bar{\omega}}{f^2} R_0, \tag{F.3a}$$

$$0 = {R_0}'' - \frac{1}{Z} {R_0}' - \frac{\bar{k}^2}{f} R_0 - \frac{\bar{k}\bar{\omega}}{f} R_\parallel, \tag{F.3b}$$

$$0 = \bar{\omega} {R_0}' + \bar{k} f {R_\parallel}' \, . \tag{F.3c}$$

The scalar equations are

$$0 = X'' + \left(\frac{f'}{f} - \frac{3}{Z}\right) X' + \left(\frac{\bar{\omega}^2}{f^2} - \frac{\bar{k}^2}{f} + \frac{3}{Z^2 f}\right) X \, . \tag{F.4}$$

We can simplify the equations in the longitudinal sector by introducing the electric fields

$$E_L = \bar{k}L_0 + \bar{\omega}L_\parallel, \qquad E_R = \bar{k}R_0 + \bar{\omega}R_\parallel \,. \tag{F.5}$$

The constraints (F.2c) and (F.3c) fix the time and longitudinal components of the gauge fields in terms of the electric fields and the scalars

$$L_\parallel{}' = \tfrac{\bar{\omega}E_L{}'}{\bar{\omega}^2 - \bar{k}^2 f}\,, \qquad L_0{}' = -\frac{\bar{k}fE_L{}'}{\bar{\omega}^2 - \bar{k}^2 f}\,, \tag{F.6a}$$

$$R_\parallel{}' = \tfrac{\bar{\omega}E_R{}'}{\bar{\omega}^2 - \bar{k}^2 f}\,, \qquad R_0{}' = -\frac{\bar{k}fE_R{}'}{\bar{\omega}^2 - \bar{k}^2 f}\,, \tag{F.6b}$$

The combinations $\bar{\omega}f/Z$ (F.2a) + $\bar{k}/Z$ (F.2b), and $\bar{\omega}f/Z$ (F.3a) + $\bar{k}/Z$ (F.3b) produce the equations for the left and right electric fields respectively

$$0 \;=\; \partial_Z\left(\frac{f}{Z}\frac{E_L{}'}{\bar{\omega}^2 - \bar{k}^2 f}\right) + \frac{1}{fZ}E_L, \tag{F.7a}$$

$$0 \;=\; \partial_Z\left(\frac{f}{Z}\frac{E_R{}'}{\bar{\omega}^2 - \bar{k}^2 f}\right) + \frac{1}{fZ}E_R\,. \tag{F.7b}$$

Appendix G

Solutions in AdS Reissner-Norsdtrom

We want to solve (F.1a) and (F.7a) without the terms depending on the masses, in the charged black brane geometry (8.52) with parameters (8.54). We can solve the equations of motion in the near-extremal AdS_2 throat (8.72) and in the asymptotically AdS_5 metric (8.52). When $|\bar{\omega}| \to 0$ the two sets of solutions have an overlapping region $\zeta \to 0$ in the throat and $Z \to 1$ in the outer region. To leading order in the small $|\bar{\omega}|$ expansion, the equations of motion of the left gauge fields (F.1a) and (F.7a) in the inner region are

$$0 = \partial_\zeta^2 L_i + \frac{F'}{F}\partial_\zeta L_i + \frac{1}{\zeta^2 F^2}\left(\zeta^2 - \frac{\bar{k}^2}{12}F\right) L_i \,, \tag{G.1a}$$

$$0 = \partial_\zeta^2 E_L + \left(\frac{F'}{F} - \frac{2}{\zeta}\frac{\bar{k}^2}{12}\frac{1}{\zeta^2 - \frac{\bar{k}^2}{12}F}\right)\partial_\zeta E_L + \frac{1}{\zeta^2 F^2}\left(\zeta^2 - \frac{\bar{k}^2}{12}F\right) E_L . \tag{G.1b}$$

Outside the AdS_2 throat, we can approximate the geometry by the extremal (zero temperature) Reissner-Norstrom solution, with $f(Z) = 1 - 3Z^4 + 2Z^6$. The equations in the outer region to leading order in the small frequency expansion are

$$0 = \partial_Z\left(\frac{f(Z)}{Z}\partial_Z L_i\right) - \frac{\bar{k}^2}{Z} L_i + O(\bar{\omega}^2) \,, \tag{G.2a}$$

$$0 = \partial_Z\left(\frac{\partial_Z E_L}{Z}\right) - \frac{\bar{k}^2}{Z\, f(Z)} E_L + O(\bar{\omega}^2). \tag{G.2b}$$

G.1 Inner solutions of the transverse components

Let us first find the solutions to the equations in the inner region (G.1). At $T = 0$ ($F = 1$), there is a simple solution to the equation of the transverse components

$$L_{i,I}(\zeta) = \sqrt{\zeta}\,\left(C_i^{(1)}\Theta(\omega) H_{\nu_k}^{(1)}(\zeta) + C_i^{(2)}\Theta(-\omega) H_{\nu_k}^{(2)}(\zeta)\right) \,, \tag{G.3}$$

where the coefficients have been chosen so that the solution satisfies ingoing boundary conditions and we have defined

$$\nu_k = \sqrt{\frac{1}{4} + \frac{\bar{k}^2}{12}} \,. \tag{G.4}$$

These solutions should match with the solutions of the outer region for $\zeta \to 0$. The leading terms in the expansion are

$$L_{i,I}(\zeta) \;\sim\; A_i \zeta^{\frac{1}{2}-\nu_k} + B_i \zeta^{\frac{1}{2}+\nu_k} \;, \tag{G.5}$$

where

$$A_i = -i\frac{2^{\nu_k}\Gamma(\nu_k)}{\pi}\left(C_i^{(1)}\Theta(\omega) - C_i^{(2)}\Theta(-\omega)\right), \tag{G.6}$$

$$B_i = \frac{1}{2^{\nu_k}\Gamma(\nu_k+1)}\left(C_i^{(1)}\Theta(\omega) + C_i^{(2)}\Theta(-\omega) + i\cot(\pi\nu_k)(C_i^{(1)}\Theta(\omega) - C_i^{(2)}\Theta(-\omega))\right) \tag{G.7}$$

In terms of the original coordinate Z, related to ζ through (8.70), the expansion (G.5) is

$$L_{i,I}(\zeta) \;\sim\; A_i \left(\frac{|\bar{\omega}|}{12}\right)^{\frac{1}{2}-\nu_k}\left[(1-Z)^{-\frac{1}{2}+\nu_k} + \mathcal{G}_L(\bar{\omega},\bar{k})(1-Z)^{-\frac{1}{2}-\nu_k}\right) \;, \tag{G.8}$$

where the IR Green's function is

$$\mathcal{G}_L(\bar{\omega},\bar{k}) = \frac{\pi}{2^{2\nu_k}\Gamma\left(\nu_k\right)\Gamma\left(1+\nu_k\right)}\left(-\cot(\pi\nu_k) + i\,\mathrm{sign}(\omega)\right)\left(\frac{|\bar{\omega}|}{12}\right)^{2\nu_k} . \tag{G.9}$$

At non-zero temperatures, it is still possible to find analytic solutions

$$L_{i,I}(\zeta) = A_i\varphi^-_{\nu_k}(\zeta) + B_i\varphi^+_{\nu_k}(\zeta) \;, \tag{G.10}$$

where

$$\varphi^\pm_{\nu_k}(\zeta) = \left(1-\frac{\zeta^2}{\zeta_0^2}\right)^{-\frac{i}{2}\mathrm{sign}(\omega)\zeta_0}\left(\frac{\zeta}{\zeta_0}\right)^{\frac{1}{2}\pm\nu_k} . \tag{G.11}$$
$$\cdot\, {}_2F_1\left(\frac{1}{4} - \frac{i}{2}\mathrm{sign}(\omega)\zeta_0 \pm \frac{\nu_k}{2}\,,\,\frac{3}{4} - \frac{i}{2}\mathrm{sign}(\omega)\zeta_0 \pm \frac{\nu_k}{2}\,,\,1\pm\nu_k\,;\,\frac{\zeta^2}{\zeta_0^2}\right) .$$

The condition that the solution is ingoing fixes

$$B_i = \frac{\Gamma\left(-\nu_k\right)\Gamma\left(\frac{1}{2} - i\,\mathrm{sign}(\omega)\zeta_0 + \nu_k\right)}{2^{2\nu_k}\Gamma\left(\nu_k\right)\Gamma\left(\frac{1}{2} - i\,\mathrm{sign}(\omega)\zeta_0 - \nu_k\right)}A_i \;. \tag{G.12}$$

Using that $Z_* \approx 1$, we arrive at

$$L_{i,I}(\zeta) \;\sim\; A_i \left(\frac{|\bar{\omega}|}{12\zeta_0}\right)^{\frac{1}{2}-\nu_k}\left[(1-Z)^{-\frac{1}{2}+\nu_k} + \mathcal{G}_L(\bar{\omega},\bar{k},\zeta_0)(1-Z)^{-\frac{1}{2}-\nu_k}\right) \;, \tag{G.13}$$

where now

$$\mathcal{G}_L(\bar{\omega},\bar{k},\zeta_0) = \frac{\Gamma\left(-\nu_k\right)\Gamma\left(\frac{1}{2} - i\,\mathrm{sign}(\omega)\zeta_0 + \nu_k\right)}{2^{2\nu_k}\Gamma\left(\nu_k\right)\Gamma\left(\frac{1}{2} - i\,\mathrm{sign}(\omega)\zeta_0 - \nu_k\right)}\left(\frac{|\bar{\omega}|}{12\zeta_0}\right)^{2\nu_k} . \tag{G.14}$$

In terms of temperature the IR Green's function is approximately

$$\mathcal{G}_L(\bar{\omega},\bar{k},\bar{T}) \approx \frac{\Gamma\left(-\nu_k\right)\Gamma\left(\frac{1}{2}-i\,\frac{\omega}{2\pi T}+\nu_k\right)}{2^{2\nu_k}\Gamma\left(\nu_k\right)\Gamma\left(\frac{1}{2}-i\,\frac{\omega}{2\pi T}-\nu_k\right)}\left(\frac{\pi\bar{T}}{6}\right)^{2\nu_k}. \tag{G.15}$$

For frequencies smaller than the temperature, we can expand the IR Green's function as

$$\mathcal{G}_L(\bar{\omega},\bar{k},\bar{T}) \approx \frac{\Gamma\left(-\nu_k\right)\Gamma\left(\frac{1}{2}+\nu_k\right)}{2^{2\nu_k}\Gamma\left(\nu_k\right)\Gamma\left(\frac{1}{2}-\nu_k\right)}\left(\frac{\pi\bar{T}}{6}\right)^{2\nu_k}\left(1-\frac{i}{2}\tan(\pi\nu_k)\frac{\omega}{T}\right)+O\left(\frac{\omega^2}{T^2}\right). \tag{G.16}$$

The imaginary term produces the leading contribution to the spectral function. We can obtain these first terms in the ω/T by first extracting the ingoing factor from the solutions

$$L_{i,I}(\zeta) = \left(1-\frac{\zeta^2}{\zeta_0^2}\right)^{-\frac{i}{2}\mathrm{sign}(\omega)\zeta_0}\psi_i(\zeta), \tag{G.17}$$

and then expanding the equations in powers of ζ_0 and solving order by order. Changing variables to $u = \zeta^2/\zeta_0^2$, the equations for the first two orders $\psi_i = \psi_i^0 + \zeta_0\psi_i^1 + \cdots$ are

$$0 = \partial_u\left(\sqrt{u}(1-u)\partial_u\psi_i^0\right) + \frac{1-4\nu_k^2}{16u^{3/2}}\psi_i^0\,, \tag{G.18}$$

$$0 = \partial_u\left(\sqrt{u}(1-u)\partial_u\psi_i^1\right) + \frac{1-4\nu_k^2}{16u^{3/2}}\psi_i^1 + i\,\mathrm{sign}(\omega)\sqrt{u}\left(\partial_u\psi_i^0+\frac{1}{4u}\psi_i^0\right). \tag{G.19}$$

The solutions to zeroth order are

$$\psi_i^0(u) = A_i^0\varphi_{\nu_k}^{0,-}(u) + B_i\varphi_{\nu_k}^{0,+}(u)\,, \tag{G.20}$$

with

$$\varphi_{\nu_k}^{0,\pm}(u) = u^{\frac{1}{4}(1\pm2\nu_k)}{}_2F_1\left(\frac{1}{4}\pm\frac{\nu_k}{2}\,,\,\frac{3}{4}\pm\frac{\nu_k}{2}\,,\,1\pm\nu_k\,;\,u\right). \tag{G.21}$$

Imposing regularity of this solution when $u\to1$ ($\zeta\to\zeta_0$), *i.e.* removing logarithmic terms, fixes the relation between the coefficients

$$B_i^0 = \frac{\Gamma\left(-\nu_k\right)\Gamma\left(\frac{1}{2}+\nu_k\right)}{2^{2\nu_k}\Gamma\left(\nu_k\right)\Gamma\left(\frac{1}{2}-\nu_k\right)}A_i^0\,. \tag{G.22}$$

The next-order solution can be obtained using a Green's function. First we identify the subleading solution when $u\to0$ ($\zeta\to0$), $\varphi^<$, and the ingoing solution when $u\to1$, $\varphi^>$,

$$\varphi^<(u) = \varphi_{\nu_k}^{0,+}(u)\,,\quad \varphi^>(\zeta) = \varphi_{\nu_k}^{0,-}(u) + \frac{\Gamma\left(-\nu_k\right)\Gamma\left(\frac{1}{2}+\nu_k\right)}{2^{2\nu_k}\Gamma\left(\nu_k\right)\Gamma\left(\frac{1}{2}-\nu_k\right)}\varphi_{\nu_k}^{0,+}(u)\,. \tag{G.23}$$

With these and the Wronskian of the two subleading and ingoing functions we construct a Green's function that maintains the boundary conditions of the leading order solution

$$G(u,u') = -\frac{1}{\nu_k}\left\{ \begin{array}{lcl} \varphi^<(u)\varphi^>(u') & , & u<u' \\ \varphi^>(u)\varphi^<(u') & , & u>u' \end{array} \right. \tag{G.24}$$

Then, taking into account that $\psi_i^0 = A_i^0\varphi^>(u)$, the subleading solution is

$$\psi_i^1(u) = -i\,\mathrm{sign}(\omega)A_i^0\int_0^1 du' G(u,u')\sqrt{u'}\left(\partial_{u'}\varphi^>(u') + \frac{1}{4u'}\varphi^>(u')\right)\,. \tag{G.25}$$

We can now expand the leading and subleading solutions for $u\to 0$. One can check that all contributions from ψ_i^1 are subleading compared to the leading term $\sim u^{\frac{1}{4}(1-2\nu_k)}$. Also, there is just one contribution to the term $\sim u^{\frac{1}{4}(1+2\nu_k)}$, from a total derivative

$$\begin{aligned} &\int_0^1 du' G(u,u')\sqrt{u'}\left(\partial_{u'}\varphi^>(u') + \frac{1}{4u'}\varphi^>(u')\right) \sim \\ &\sim \varphi^<(u)\lim_{u\to 0}\int_u^1 du'\partial_{u'}\left(\sqrt{u'}\frac{(\varphi^>(u'))^2}{2}\right) = \varphi^<(u)\frac{(\varphi^>(1))^2}{2}\,. \end{aligned} \tag{G.26}$$

Taking this into account, the relevant terms in the expansion are

$$\psi_i^0 \sim \left(u^{\frac{1}{4}(1-2\nu_k)} + \frac{\Gamma(-\nu_k)\Gamma\left(\frac{1}{2}+\nu_k\right)}{2^{2\nu_k}\Gamma(\nu_k)\Gamma\left(\frac{1}{2}-\nu_k\right)}u^{\frac{1}{4}(1+2\nu_k)}\right)A_i^0\,, \tag{G.27}$$

$$\psi_i^1 \sim -i\,\mathrm{sign}(\omega)\pi\tan(\pi\nu_k)\frac{\Gamma(-\nu_k)\Gamma\left(\frac{1}{2}+\nu_k\right)}{2^{2\nu_k}\Gamma(\nu_k)\Gamma\left(\frac{1}{2}-\nu_k\right)}u^{\frac{1}{4}(1+2\nu_k)}A_i^0\,. \tag{G.28}$$

It is straightforward to check that this reproduces the first two terms in the ω/T expansion of the IR Greens' function (G.16).

G.2 Inner solutions of the longitudinal components

The equation for the electric field in (G.1) does not have a simple analytic solution, but since we are interested in frequencies $\omega/T \lesssim 1$, we can apply the same expansion as for the transverse components to find the leading contribution to the spectral function.

We first extract the ingoing factor from the solutions

$$E_{L,I}(\zeta) = \left(1-\frac{\zeta^2}{\zeta_0^2}\right)^{-\frac{i}{2}\mathrm{sign}(\omega)\zeta_0}\psi_i(\zeta), \tag{G.29}$$

and then expand the equations in powers of ζ_0 and solve them order by order. Changing variables to $u=\zeta^2/\zeta_0^2$, the equations for the first two orders $\psi_i =$

$\psi_i^0 + \zeta_0 \psi_i^1 + \cdots$ are

$$0 = \partial_u \left(u^{3/2} \partial_u \psi_i^0 \right) + \frac{1-4\nu_k^2}{16 u^{1/2}(1-u)} \psi_i^0 \,, \tag{G.30}$$

$$0 = \partial_u \left(u^{3/2} \partial_u \psi_i^1 \right) + \frac{1-4\nu_k^2}{16 u^{1/2}(1-u)} \psi_i^1 + i \,\mathrm{sign}(\omega) \frac{u^{3/2}}{1-u} \left(\partial_u \psi_i^0 + \frac{3-u}{4u(1-u)} \psi_i^0 \right) . \tag{G.31}$$

The solutions to zeroth order are

$$\psi_i^0(u) = A_i^0 \varphi_{\nu_k}^{0,-}(u) + B_i \varphi_{\nu_k}^{0,+}(u) \,, \tag{G.32}$$

with

$$\varphi_{\nu_k}^{0,\pm}(u) = u^{-\frac{1}{4}(1 \mp 2\nu_k)} {}_2F_1 \left(-\frac{1}{4} \pm \frac{\nu_k}{2} \,, \frac{1}{4} \pm \frac{\nu_k}{2} \,, 1 \pm \nu_k \,; u \right) . \tag{G.33}$$

Imposing regularity of this solution when $u \to 1$ ($\zeta \to \zeta_0$), *i.e.* removing logarithmic terms, fixes the relation between the coefficients

$$B_i^0 = \frac{\Gamma(-\nu_k)\Gamma\left(\frac{3}{2}+\nu_k\right)}{2^{2\nu_k}\Gamma(\nu_k)\Gamma\left(\frac{3}{2}-\nu_k\right)} A_i^0 \,. \tag{G.34}$$

It turns out that this makes the solution vanish at the horizon, something that will be relevant below.

The next-order solution can be obtained in terms of a Green's function. First, we identify the subleading solution when $u \to 0$ ($\zeta \to 0$), $\varphi^<$, and the ingoing solution when $u \to 1$, $\varphi^>$,

$$\varphi^<(u) = \varphi_{\nu_k}^{0,+}(u) \,, \quad \varphi^>(\zeta) = \varphi_{\nu_k}^{0,-}(u) + \frac{\Gamma(-\nu_k)\Gamma\left(\frac{3}{2}+\nu_k\right)}{2^{2\nu_k}\Gamma(\nu_k)\Gamma\left(\frac{3}{2}-\nu_k\right)} \varphi_{\nu_k}^{0,+}(u) \,. \tag{G.35}$$

With these and the Wronskian of the two subleading and ingoing functions we construct a Green's function that maintains the boundary conditions of the leading order solution

$$G(u,u') = -\frac{1}{\nu_k} \left\{ \begin{array}{lcl} \varphi^<(u)\varphi^>(u') & , & u < u' \\ \varphi^>(u)\varphi^<(u') & , & u > u' \end{array} \right. \tag{G.36}$$

Then, taking into account that $\psi_i^0 = A_i^0 \varphi^>(u)$, the subleading solution is

$$\psi_i^1(u) = -i \,\mathrm{sign}(\omega) A_i^0 \int_0^1 du' G(u,u') \frac{u'^{3/2}}{1-u'} \left(\partial_{u'} \varphi^>(u') + \frac{3-u'}{4u'(1-u')} \varphi^>(u') \right) . \tag{G.37}$$

We can now expand the leading and subleading solutions for $u \to 0$. One can check that all contributions from ψ_i^1 are subleading compared to the leading term $\sim u^{-\frac{1}{4}(1+2\nu_k)}$. Also, there is just one potential contribution to the term $\sim u^{-\frac{1}{4}(1-2\nu_k)}$, from a total derivative

$$\begin{aligned} &\int_0^1 du' G(u,u') \frac{u'^{3/2}}{1-u'} \left(\partial_{u'} \varphi^>(u') + \frac{3-u'}{4u'(1-u')} \varphi^>(u') \right) \\ &\quad \sim \varphi^<(u) \lim_{u \to 0} \int_u^1 du' \partial_{u'} \left(\frac{u'^{3/2}}{1-u'} \frac{(\varphi^>(u'))^2}{2} \right) = \varphi^<(u) \lim_{u' \to 1} \frac{(\varphi^>(u'))^2}{2(1-u')} = 0 \,. \end{aligned} \tag{G.38}$$

Taking this into account, the relevant terms in the expansion are

$$\psi_i^0 \sim \left(u^{-\frac{1}{4}(1+2\nu_k)} + \frac{\Gamma\left(-\nu_k\right)\Gamma\left(\frac{3}{2}+\nu_k\right)}{2^{2\nu_k}\Gamma\left(\nu_k\right)\Gamma\left(\frac{3}{2}-\nu_k\right)}u^{-\frac{1}{4}(1-2\nu_k)}\right)A_i^0\,, \tag{G.39}$$

$$\psi_i^1 \sim 0\times A_i^0 u^{-\frac{1}{4}(1-2\nu_k)}\,. \tag{G.40}$$

Thus, the leading ω/T correction actually vanishes for the longitudinal components. This implies that for the calculation of the spectral function, it is enough to compute the transverse contribution.

G.3 Outer solutions of the longitudinal components

Although we will not need these solutions to compute the leading contributions to the rates, it will be useful to study them as they can be found analytically.

We are looking for solutions of the electric field in (G.2). First we will change coordinates $u = Z^2$, so the equations takes the form of a Schroedinger equation

$$E''_{L,O}(u) - \frac{\bar{k}^2}{4u(2u+1)(u-1)^2}E_{L,O} = 0\,. \tag{G.41}$$

We can transform the above equation into a hypergeometric equation by the following change of coordinate and field redefinition

$$E_{L,O}(u) = (1+2u)^{c_\pm}(1-u)^{b_\pm}t_\pm(u), \tag{G.42}$$

$$c_\pm = \frac{1}{2}\pm\nu_k, \qquad b_\pm = 1-c_\pm = \frac{1}{2}\mp\nu_k, \tag{G.43}$$

$$x = \frac{3u}{1+2u}, \qquad u = \frac{x}{3-2x}. \tag{G.44}$$

Then, we get the following hypergeometric equation

$$x(1-x)t''_\pm(x) + (\pm 2\nu_k - 1)x\,t'_\pm(x) - \frac{k^2}{12}\,t_\pm(x) = 0. \tag{G.45}$$

We can compare the above equation to the standard form $x(1-x)t''_\pm(x) + (c_\pm - (a_\pm + b_\pm + 1)x)t'_\pm(x) - a_\pm b_\pm t(x) = 0$, to get

$$c_\pm = 0, \quad a_\pm = \left\{\frac{1}{2}\mp\nu_k, -\frac{1}{2}\mp\nu_k\right\}, \quad b_\pm = \left\{-\frac{1}{2}\mp\nu_k, \frac{1}{2}\mp\nu_k\right\}. \tag{G.46}$$

A general solution can be written as a linear combination of a normalizable and a non-normalizable mode at the boundary. In terms of the original radial variable, they have the form

$$E_O^{(0)} = \alpha\, \phi_{NN}(Z) + \beta\, \phi_N(Z), \tag{G.47}$$

$$\begin{aligned}\phi_{NN}(Z) = {} & (1-Z^2)^{\frac{1}{2}+\nu_k}(1+2Z^2)^{\frac{1}{2}-\nu_k}\Bigg[\Bigg(\left(\frac{1}{2}-2\nu_k^2\right)H_{-\frac{1}{2}+\nu_k} - \nu_k^2(-1+\log 3)+ \\ & + \frac{1}{12}(1+3\log 3)\Bigg)\frac{3Z^2}{1+2Z^2}\,{}_2F_1\left(\frac{1}{2}+\nu_k, \frac{3}{2}+\nu_k, 2, \frac{3Z^2}{1+2Z^2}\right)+ \\ & + \frac{1}{\Gamma\left(-\frac{1}{2}+\nu_k\right)\Gamma\left(\frac{1}{2}+\nu_k\right)} G^{2,2}_{2,2}\left(\frac{3Z^2}{1+2Z^2}\,\middle|\, \begin{matrix}\frac{1}{2}-\nu_k, \frac{3}{2}-\nu_k \\ 0,1\end{matrix}\right)\Bigg],\end{aligned} \tag{G.48}$$

$$\phi_N(Z) = (1-Z^2)^{\frac{1}{2}+\nu_k}(1+2Z^2)^{\frac{1}{2}-\nu_k}\frac{3Z^2}{1+2Z^2}\,{}_2F_1\left(\frac{1}{2}+\nu_k, \frac{3}{2}+\nu_k, 2, \frac{3Z^2}{1+2Z^2}\right), \tag{G.49}$$

where $H_{-\frac{1}{2}+\nu_k}$ is the $(-\frac{1}{2}+\nu_k)^{\text{th}}$ harmonic number and G is the Meijer function.

The non-normalizable and normalizable solutions have been chosen so that their near-boundary expansion is

$$\phi_{NN}(Z) = 1 + \frac{3}{2}(-1+4\nu_k^2)Z^2\log Z + O(Z^4\log Z), \qquad \phi_N(Z) = Z^2 + O(Z^4)\,. \tag{G.50}$$

We want to determine the coefficients α and β for solutions with a selected behaviour close to the horizon $Z \to 1$. The expansion close to the horizon is

$$E_{L,O}(Z) \sim A\,(1-Z)^{\frac{1}{2}+\nu_k} + B\,(1-Z)^{\frac{1}{2}-\nu_k} + \ldots \quad Z \to 1, \tag{G.51}$$

These match with the expansions of the $\varphi^{0,\pm}_{\nu_k}$ inner solutions (G.33) in the $\zeta \to 0$ limit. By requiring that $A = 1$ and $B = 0$, we then determine the value of α and β for the minus mode, while, if we impose $A = 0$ and $B = 1$, we find the coefficients for the plus mode. They turn out to be

$$\alpha_{\mp} = \frac{6^{\pm\nu_k-\frac{1}{2}}\Gamma(\pm\nu_k+1)}{\sqrt{\pi}\,\Gamma\left(\pm\nu_k+\frac{3}{2}\right)}, \tag{G.52}$$

$$\beta_- = -\frac{2^{\nu_k-\frac{5}{2}}3^{\nu_k-\frac{1}{2}}\nu_k\Gamma(\nu_k)\left(\left(6-24\nu_k^2\right)H_{\nu-\frac{1}{2}} - 12\nu_k^2(1+\log(3)) + 1 + \log(27)\right)}{\sqrt{\pi}\,\Gamma\left(\nu_k+\frac{3}{2}\right)}, \tag{G.53}$$

$$\begin{aligned}\beta_+ = {} & -\frac{\pi\nu_k}{2^{-\nu_k+\frac{3}{2}}3^{\nu_k+\frac{1}{2}}\Gamma\left(\frac{1}{2}-\nu_k\right)\Gamma\left(\frac{3}{2}-\nu_k\right)\Gamma(2\nu_k+1)}\cdot \\ & \cdot\Big[\csc(2\pi\nu_k)\left(\left(6-24\nu_k^2\right)H_{\nu_k-\frac{1}{2}} - 12\nu_k^2(\log(3)-1) + 1 + \log(27)\right)+ \\ & + 3\pi\left(4\nu_k^2-1\right)\sec^2(\pi\nu_k)\Big].\end{aligned} \tag{G.54}$$

Since, in order to compute the rates, we have to perform an integral over all momentum, it is interesting to ascertain the behavior of the spectral function at large spatial momentum, which will be in part determined by the behavior of the connection coefficients. From the analytic formulas above, one can see that, for $\nu_k \to \infty$, their asymptotic form is

$$\alpha_- \sim 6^{\nu_k - \frac{1}{2}} (\pi \nu_k)^{-1/2}, \quad \alpha_+ \sim -6^{-\nu_k - \frac{1}{2}} (\pi \nu_k)^{-1/2} \cot(\pi \nu_k), \tag{G.55}$$

$$\beta_- \sim 6^{\nu_k + \frac{1}{2}} \nu_k^{3/2} \log\left(3^{1/2} e^{-1/2} e^{\gamma_E} \nu_k\right), \tag{G.56}$$

$$\beta_+ \sim 6^{-\nu_k + \frac{1}{2}} \nu_k^{3/2} \sqrt{\pi} \left(1 - \frac{\cot(\pi \nu_k)}{\pi} \log\left(3^{1/2} e^{-1/2} e^{\gamma_E} \nu_k\right)\right). \tag{G.57}$$

We can recover this behaviour of the connection coefficients by using a WKB approximation at large spatial momentum. The equation of motion (G.41) is already in Schroedinger form with a potential

$$U_E(u) = \frac{\bar{k}^2}{4u(2u+1)(u-1)^2}. \tag{G.58}$$

We expand the solutions as

$$E_{L,O}(u) = C \exp\left(\bar{k}\, S_0(u) + S_1(u) + O(1/\bar{k})\right). \tag{G.59}$$

The equation for the leading term in the $1/\bar{k}$ expansion is

$$S_0'(u)^2 - \frac{1}{8u^4 - 12u^3 + 4u} = 0, \tag{G.60}$$

which has an analytical solution

$$S_0(u) = \pm \frac{1}{\sqrt{3}} \tanh^{-1}\left(\sqrt{\frac{3u}{2u+1}}\right) + c_0. \tag{G.61}$$

Then, the subleading term is given by

$$S_1(u) = \log\left(\sqrt{2}\sqrt{1-u}\sqrt[4]{u(1+2u)}\right) + c_1. \tag{G.62}$$

Then the solution up to this order reads

$$E_{L,O}(u) \approx \psi(u) = C_\pm \sqrt{1-u}\sqrt[4]{u(1+2u)} \exp\left(\pm \frac{\bar{k}}{\sqrt{3}} \tanh^{-1}\left(\sqrt{\frac{3u}{1+2u}}\right)\right). \tag{G.63}$$

The WKB solution near the boundary has the following expansion

$$\psi(u) \sim C_\pm u^{1/4} e^{\pm \bar{k}\sqrt{u}} \qquad u \to 0.$$

Note that the two terms in the solution directly correspond to the "plus" and "minus" modes at the horizon

$$\psi(u) \sim \widetilde{C}_\pm \left(\frac{1}{1-u}\right)^{\pm \bar{k}/\sqrt{12}} \qquad u \to 1.$$

We have to fix the overall coefficient to properly normalize the WKB solutions in the original coordinate z which are

$$E(z) = C_{\pm}\sqrt{1-z^2}\sqrt{z}\,(1+2z^2)^{1/4}\exp\left(\pm\frac{\bar{k}}{\sqrt{3}}\tanh^{-1}\left(\sqrt{\frac{3z^2}{1+2z^2}}\right)\right). \tag{G.64}$$

Then, the overall coefficients are found to be

$$C_{\pm} = 6^{\mp\frac{\bar{k}}{\sqrt{12}}}. \tag{G.65}$$

Now we have to match these results with the solutions close to the boundary and read the boundary coefficients. Close to the boundary, the potential is to leading order

$$U_E(u) \sim \frac{\bar{k}^2}{4u}.$$

A solution for this approximated potential can be given in terms of modified Bessel functions

$$\psi(u) \approx c_1\sqrt{u}\,K_1\left(\bar{k}\sqrt{u}\right) + c_2\sqrt{u}\,I_1\left(\bar{k}\sqrt{u}\right). \tag{G.66}$$

The expansion for large $\bar{k}$ is

$$\sqrt{u}\,K_1\left(\bar{k}\sqrt{u}\right) \sim \sqrt{\frac{\pi}{2\bar{k}}}u^{1/4}e^{-\bar{k}\sqrt{u}}, \qquad \sqrt{u}\,I_1\left(\bar{k}\sqrt{u}\right) \sim \frac{u^{1/4}}{\sqrt{2\pi\bar{k}}}e^{\bar{k}\sqrt{u}},$$

which is consistent with the WKB solution. We fix the coefficient $c_{1,2}$ with the formulas for $C_{\pm}$ so that the WKB solution for $z \to 0$ and the solution close to the boundary for large $\bar{k}$ coincide. Finally, we can read off from the $z \to 0$ expansion the coefficients $\alpha_{\pm}$ and $\beta_{\pm}$ which are respectively the coefficients of the non-normalizable and normalizable mode. In a compact form, they are

$$\alpha_{\pm} \sim \mp 6^{\mp\frac{\bar{k}}{\sqrt{12}}}\bar{k}^{-1/2}, \tag{G.67}$$

$$\beta_{\pm} \sim \mp 6^{\mp\frac{\bar{k}}{\sqrt{12}}}\bar{k}^{3/2}\log\bar{k}. \tag{G.68}$$

Comparing to (G.55), and taking into account $\nu_k \sim \frac{\bar{k}}{\sqrt{12}}$ in this limit, the WKB approximation captures the leading $\bar{k}$ dependence up to the oscillatory factors.

G.4 Outer solutions of the transverse components

We are looking for solutions of the transverse components in (G.2). We do not have a close analytic solution in this case, so we must resort to numerics. The general solution is a linear combination of two modes $\eta_{L,\mp}(Z)$ which when $Z \to 1$ match with the inner solutions (G.11) for $\zeta \to 0$,

$$\eta_{L,\pm}(Z) \sim (1-Z)^{-\frac{1}{2}\mp\nu_k} + \ldots \qquad Z \to 1. \tag{G.69}$$

There is another basis of solutions we can use to write a general solution, consisting of the normalizable and non-normalizable modes, with a boundary expansion at $Z \to 0$

$$\phi_{NN}(Z) = 1 + \frac{3}{2}(-1+4\nu_k^2)Z^2 \log Z + O(Z^4 \log Z), \qquad \phi_N(Z) = Z^2 + O(Z^4) \tag{G.70}$$

The change of basis is determined by the connection coefficients $\alpha_\pm, \beta_\pm$:

$$\eta_{L,\pm}(Z) = \alpha_\pm \phi_{NN}(Z) + \beta_\pm \phi_N(Z). \tag{G.71}$$

The connection coefficients can be determined from the solutions by matching the $\eta_{L\pm}$ solutions and their first derivative with a linear combination of the normalizable and non-normalizable solutions at any intermediate point $0 < \hat{Z} < 1$:

$$\begin{pmatrix} \alpha_\pm \\ \beta_\pm \end{pmatrix} = \frac{1}{W(Z)} \begin{pmatrix} -\partial_Z \phi_N(Z) & \phi_N(Z) \\ \partial_Z \phi_{NN}(Z) & -\phi_{NN}(Z) \end{pmatrix} \begin{pmatrix} \eta_{L,\pm}(Z) \\ \partial_Z \eta_{L,\pm}(Z) \end{pmatrix} \Bigg|_{Z=\hat{Z}}, \tag{G.72}$$

where $W(Z) = \phi_N(Z)\partial_Z\phi_{NN}(Z) - \partial_Z\phi_N(Z)\phi_{NN}(Z)$. We will obtain the connection coefficients using this formula, by finding numerically the $\eta_{L\pm}$ solutions using shooting from the horizon, and the ϕ_N, ϕ_{NN} solutions using shooting from the boundary. We use $\hat{Z} = 0.2$ as the matching point, but we have checked that changing this value through the interval of numerical integration does not affect the result within our numerical precision.

For the shooting from the boundary, we introduce a cutoff at $Z = 10^{-5}$ and use a series expansion to give initial values for the solution and its first derivative at the cutoff. The expansion is

$$\phi_N(Z) = \sum_{n=1}^{N_a} a_n Z^{2n}, \tag{G.73}$$

$$\phi_{NN}(Z) = b_0 + \sum_{n=2}^{N_b} b_n Z^{2n} + \log(Z) \sum_{n=1}^{N} c_n Z^{2n}. \tag{G.74}$$

Where we take $N_a = 8$, $N_b = 6$ and $N = 7$. The first coefficients of the expansion given that $a_1 = b_0 = 1$ are

$$a_2 = \frac{\bar{k}^2}{8}, \quad a_3 = 1 + \frac{\bar{k}^4}{192}, \quad a_4 = -\frac{1}{2} + \frac{5\bar{k}^2}{24} + \frac{\bar{k}^6}{9216}, \ldots \tag{G.75}$$

$$b_2 = -\frac{3\bar{k}^4}{64}, \quad b_3 = \frac{\bar{k}^2}{6} - \frac{7\bar{k}^6}{2304} \ldots \quad c_1 = \frac{\bar{k}^2}{2}, \quad c_2 = \frac{\bar{k}^4}{16}, \ldots \tag{G.76}$$

For the shooting from the horizon we introduce a cutoff at $Z = 1 - 10^{-5}$. We extract the leading power in the horizon expansion from the solutions

$$\eta_{L,\mp}(Z) = (1-Z)^{-\frac{1}{2}\pm\nu_k}\, p_\mp(Z)\,. \tag{G.77}$$

The equation of motion we solve is

$$\partial_Z^2 p_\mp(Z) + \left(\frac{1+2Z\,(-1\pm\nu_k)}{Z(-1+Z)} + \frac{f'(Z)}{f(Z)}\right)\partial_Z p_\mp(Z) + \frac{\pm\nu_k - 1}{4(Z-1)^2 Z f(Z)} \cdot \tag{G.78}$$
$$\cdot \left[(2 - 5Z \pm 2Z\nu_k)f(Z) + 2(1-Z)Z\left(6(-1+Z)(1\pm 2\nu_k) - f'(Z)\right)\right] p_\mp(Z) = 0.$$

To give initial values at the cutoff, we use the series expansion

$$p_{\mp} = \sum_{n=0}^{N_j} j_{\mp,n} \left(1-Z\right)^n , \tag{G.79}$$

and shooting it from the horizon towards the boundary. We expand up to $N_j = 8$ terms, with the first coefficients in the expansion, given that $j_{\mp,0} = 1$, are

$$j_{\mp,1} = \frac{8\sqrt{3}\sqrt{3+\bar{k}^2} \mp 24 \pm 7\bar{k}^2}{12(\sqrt{3}\sqrt{3+\bar{k}^2} \pm 3)}, \tag{G.80}$$

$$j_{\mp,2} = \frac{\bar{k}^2\left(49\sqrt{3}\sqrt{\bar{k}^2+3} \pm 534\right) - 156\left(\sqrt{3}\sqrt{\bar{k}^2+3} \mp 3\right)}{864\left(\sqrt{3}\sqrt{\bar{k}^2+3} \pm 6\right)}, \ldots \tag{G.81}$$

Although we do not have an analytic formula for the connection coefficients, we can obtain analytic expressions for their asymptotic behaviour at large spatial momentum by applying the same WKB approximation we used for the coefficients of the longitudinal components. First, we should put the equation of motion for L_i in (G.2) in Schroedinger form. This is achieved by the change of variables $u = Z^2$ followed by the redefinition

$$L_i(u) = (1-u)\,(1+2u)^{-1/2}\,\psi_{L_i}(u) \,. \tag{G.82}$$

The equation of motion is now

$$\psi''_{L_i}(u) - U_{L_i}(u)\psi_{L_i}(u) = 0\,, \qquad U_{L_i}(u) = \frac{k^2}{4(1-u)^2u(2u+1)} - \frac{3(u+1)}{(1-u)(2u+1)^2}\,. \tag{G.83}$$

At large $\bar{k}$ the potential is to leading order the same as for the longitudinal modes (G.58)

$$U_{L_i}(u) \sim \frac{k^2}{4(1-u)^2u(2u+1)} = U_E(u)\,. \tag{G.84}$$

Therefore, the large $\bar{k}$ WKB analysis proceeds in the same way as for the longitudinal components, and the connection coefficients have the save asymptotic behaviour given in (G.67).

We have plotted the connection coefficients in Figures G.1a- G.2b. In Figures G.1a and G.1b we plot α_+ and α_-. The coefficient of the non-normalizable mode, α_+, is multiplied by the factor $2(1-\nu_k)(2\nu_k-1)$ in order to remove the divergences in $\bar{k} = 0,\, 3$. We will examine the origin of this divergence in more detail below. In Figures G.2a and G.2b are shown the plots of $2(1-\nu_k)\beta_+$ and $(2\nu_k-1)^{-1}\beta_-$.

G.4.1 Low momentum behavior of connection coefficients

When $\bar{k} = 0$ ($\nu_k = 1/2$) the solutions in the outer region are

$$\eta^0_{L,-}(Z) = 1, \qquad \eta^0_{L,+}(Z) = \frac{2}{1-Z^2} + \frac{4}{3}\log\left[\frac{1+2Z^2}{1-Z^2}\right] - \frac{1}{2} - \frac{4}{3}\log\frac{3}{2}\,. \tag{G.85}$$

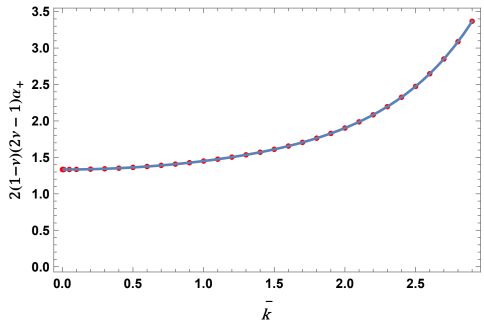

(a) Plot of $2(1-\nu_k)(2\nu_k-1)\alpha_+$ as function of $\bar{k}$.

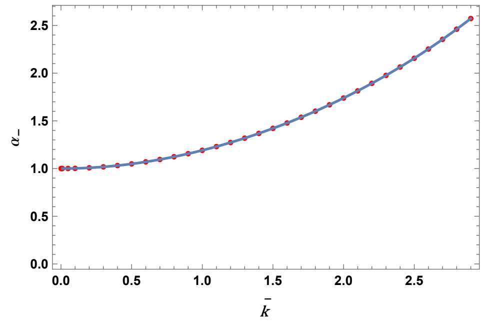

(b) Plot of α_- as function of $\bar{k}$.

Figure G.1. Plots of coefficients $\alpha_\pm$ associated to the non-normalizable mode as functions of $\bar{k}$.

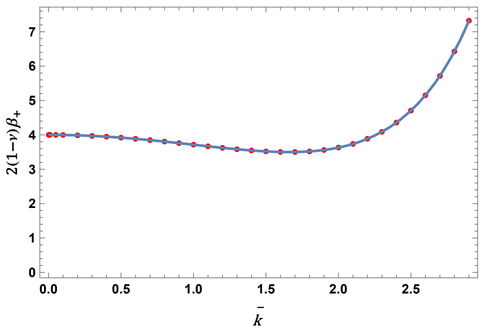

(a) Plot of $2(1-\nu_k)\beta_+$ as function of $\bar{k}$.

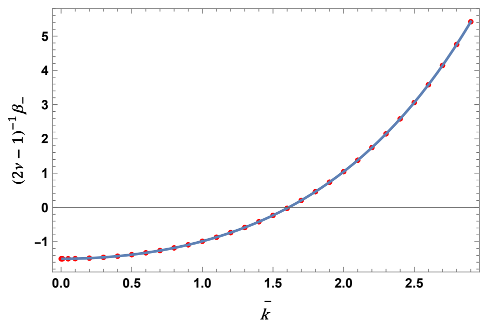

(b) Plot of $(2\nu_k-1)^{-1}\beta_-$ as function of $\bar{k}$.

Figure G.2. Plots of coefficients $\beta_\pm$ associated to the normalizable mode as functions of $\bar{k}$.

The expansions at the boundary and the horizon of the $\eta^0_{L,+}$ solution are

$$\eta^0_{L,+}(Z) \sim \frac{3}{2} - \frac{4}{3}\log\frac{3}{2} + 6Z^2 + \cdots\,, \tag{G.86}$$

$$\eta^0_{L,+}(Z) \sim (1-Z)^{-1} - \frac{4}{3}\log(1-Z) + \cdots\,. \tag{G.87}$$

Therefore, the connection coefficients of these solutions are

$$\alpha^0_- = 1,\ \beta^0_- = 0, \quad \alpha^0_+ = \frac{3}{2} - \frac{4}{3}\log\frac{3}{2},\ \beta^0_+ = 6. \tag{G.88}$$

We can relate these to the $\bar{k} \to 0$ limit of the connection coefficients of the non-zero momentum solutions. First, note that the coefficient $j_{-,n}$ in (G.80) go to zero in the $\bar{k} \to 0$ limit, so $\eta_{L,-} \to \eta^0_{L,-}$. On the other hand $j_{+,1}$ in (G.80) is singular in this limit, but the singularity does not propagate to other coefficients in the expansion, one can already see that it is absent in $j_{+,2}$. In order to remove the singular term we can take the following combination of the solutions

$$\tilde{\eta}_{L,+}(Z) = \eta_{L,+}(Z) - j_{1,+}\eta_{L,-}(Z)\,. \tag{G.89}$$

Expanding this solution at the horizon and for $\bar{k} \to 0$ one can check that it coincides with the expansion in (G.86). We then conclude that $\tilde{\eta}_{L,} \to \eta^0_{L,+}$ in the $\bar{k} \to 0$ limit. This determines the $\bar{k} \to 0$ behaviour of the connection coefficients

$$\alpha_- \sim \alpha^0_-, \quad \beta_- \sim \beta^0_-, \qquad \alpha_+ \sim \alpha^0_+ + j_{+,1}\alpha^0_-, \quad \beta_+ \sim \beta^0_+ + j_{+,1}\beta^0_-\,. \tag{G.90}$$

Since $j_{+,1} \to \infty$ and $\beta_- \to 0$, in order to completely determine β_+ we need to find the non-zero subleading contribution to β_-. We expand

$$\eta_{L,-}(Z) = (1-Z)^{-\frac{1}{2}(1-2\nu_k)}\left(1 + \left(\nu_k - \frac{1}{2}\right)\eta^1_-(Z) + O\left[\left(\nu_k - \frac{1}{2}\right)^2\right]\right)\,. \tag{G.91}$$

The solution for $\eta^1_-(Z)$ can be found explicitly

$$\begin{aligned}\eta^1_-(Z) =& \frac{1}{9}\Big(\log(1-Z)(9 - 12\log(Z)) + 9\log(1+Z) + \pi^2 + 9 - 9\log(2) - 6\mathrm{Li}_2(-2) \\ &+6\log(Z)\left(2\log\left(\frac{1+2Z^2}{1+Z}\right) + \frac{3Z^2}{1-Z^2}\right) + 6\mathrm{Li}_2(-Z^2) - 6\mathrm{Li}_2(Z^2)\Big)\,.\end{aligned} \tag{G.92}$$

The boundary and horizon expansions are

$$\eta^1_{L,-}(Z) \sim \frac{1}{9}\left(9 + \pi^2 - 9\log(2) - 6\mathrm{Li}_2(-2)\right) + 3Z^2(-1 + 2\log Z) + \cdots, \tag{G.93}$$

$$\eta^1_{L,-}(Z) \sim \log(1-Z) + \frac{11}{6}(1-Z) + \cdots\,. \tag{G.94}$$

Therefore

$$\beta_- \sim -\frac{3}{2}(2\nu_k - 1)\,. \tag{G.95}$$

Using now that to leading order

$$j_{+,1} \sim \frac{4}{3(2\nu_k - 1)}, \tag{G.96}$$

We find that when $\bar{k} \to 0$

$$\alpha_- \sim 1 + O\left(\nu_k - \frac{1}{2}\right), \qquad \beta_- \sim -\frac{3}{2}(2\nu_k - 1) + O\left[\left(\nu_k - \frac{1}{2}\right)^2\right], \tag{G.97a}$$

$$\alpha_+ \sim \frac{4}{3(2\nu_k - 1)} + O(1), \quad \beta_+ \sim 4 + O\left(\nu_k - \frac{1}{2}\right). \tag{G.97b}$$

Bibliography

[1] F. Bigazzi, A. L. Cotrone and A. Olzi, *Hall Droplet Sheets in Holographic QCD*, *JHEP* **02** (2023) 194 [2211.05147].

[2] F. Bigazzi, A. L. Cotrone and A. Olzi, *Axionic strings, domain walls, and baryons*, *Phys. Rev. D* **108** (2023) 026019 [2212.09783].

[3] F. Bigazzi, A. L. Cotrone and A. Olzi, *Low energy description of single flavor baryons*, *EPJ Web Conf.* **314** (2024) 00014.

[4] C. Hoyos, A. Olzi and D. Rodriguez-Fernandez, *Weak rates in strongly coupled cold quark matter*, *JHEP* **12** (2024) 058 [2407.21643].

[5] F. Bigazzi, A. L. Cotrone and A. Olzi, *Cosmic topological defects from holography*, *JHEP* **06** (2025) 018 [2411.19302].

[6] F. Bigazzi, A. L. Cotrone, A. Olzi and J.-L. Raymond, *Holographic Baryons as Quantum Hall Droplets*, 2506.16205.

[7] D. J. Gross and F. Wilczek, *Ultraviolet Behavior of Nonabelian Gauge Theories*, *Phys. Rev. Lett.* **30** (1973) 1343.

[8] H. D. Politzer, *Reliable Perturbative Results for Strong Interactions?*, *Phys. Rev. Lett.* **30** (1973) 1346.

[9] D. J. Gross and F. Wilczek, *Asymptotically Free Gauge Theories - I*, *Phys. Rev. D* **8** (1973) 3633.

[10] D. J. Gross and F. Wilczek, *ASYMPTOTICALLY FREE GAUGE THEORIES. 2.*, *Phys. Rev. D* **9** (1974) 980.

[11] K. G. Wilson, *Confinement of Quarks*, *Phys. Rev. D* **10** (1974) 2445.

[12] K. Fredenhagen and M. Marcu, *Confinement criterion for QCD with dynamical quarks*, *Phys. Rev. Lett.* **56** (1986) 223.

[13] E. Epelbaum, H.-W. Hammer and U.-G. Meissner, *Modern Theory of Nuclear Forces*, *Rev. Mod. Phys.* **81** (2009) 1773 [0811.1338].

[14] R. Machleidt and D. R. Entem, *Chiral effective field theory and nuclear forces*, *Phys. Rept.* **503** (2011) 1 [1105.2919].

[15] G. 't Hooft, *A Planar Diagram Theory for Strong Interactions*, *Nucl. Phys. B* **72** (1974) 461.

[16] E. Witten, *Baryons in the 1/n Expansion*, *Nucl. Phys. B* **160** (1979) 57.

[17] S. R. Coleman, *1/N*, in *17th International School of Subnuclear Physics: Pointlike Structures Inside and Outside Hadrons*, 3, 1980.

[18] K. Nagata, *Finite-density lattice QCD and sign problem: Current status and open problems*, *Prog. Part. Nucl. Phys.* **127** (2022) 103991 [2108.12423].

[19] G. Veneziano, *Construction of a crossing-symmetric, regge behaved amplitude for linearly rising trajectories*, *Nuclear Physics B* **10** (1968) 349.

[20] J. Polchinski, *String theory. volume 1, introduction to the bosonic string*, *Cambridge Monographs on Mathematical Physics* (1998) .

[21] J. Polchinski, *String theory. volume ii, superstring theory and beyond*, *Cambridge Monographs on Mathematical Physics* (1998) .

[22] G. 't Hooft, *Dimensional reduction in quantum gravity*, *Conf. Proc. C* **930308** (1993) 284 [gr-qc/9310026].

[23] L. Susskind, *The World as a hologram*, *J. Math. Phys.* **36** (1995) 6377 [hep-th/9409089].

[24] J. M. Maldacena, *The Large N limit of superconformal field theories and supergravity*, *Adv. Theor. Math. Phys.* **2** (1998) 231 [hep-th/9711200].

[25] E. Witten, *Anti de Sitter space and holography*, *Adv. Theor. Math. Phys.* **2** (1998) 253 [hep-th/9802150].

[26] S. S. Gubser, I. R. Klebanov and A. M. Polyakov, *Gauge theory correlators from noncritical string theory*, *Phys. Lett. B* **428** (1998) 105 [hep-th/9802109].

[27] E. Witten, *Baryons and branes in anti-de Sitter space*, *JHEP* **07** (1998) 006 [hep-th/9805112].

[28] H. Hata, T. Sakai, S. Sugimoto and S. Yamato, *Baryons from instantons in holographic QCD*, *Prog. Theor. Phys.* **117** (2007) 1157 [hep-th/0701280].

[29] D. T. Son and A. O. Starinets, *Minkowski space correlators in AdS / CFT correspondence: Recipe and applications*, *JHEP* **09** (2002) 042 [hep-th/0205051].

[30] S. A. Hartnoll, A. Lucas and S. Sachdev, *Holographic quantum matter*, 1612.07324.

[31] E. Witten, *Anti-de Sitter space, thermal phase transition, and confinement in gauge theories*, *Adv. Theor. Math. Phys.* **2** (1998) 505 [hep-th/9803131].

[32] T. Sakai and S. Sugimoto, *Low energy hadron physics in holographic QCD*, *Prog. Theor. Phys.* **113** (2005) 843 [hep-th/0412141].

[33] T. Sakai and S. Sugimoto, *More on a holographic dual of QCD*, *Prog. Theor. Phys.* **114** (2005) 1083 [hep-th/0507073].

[34] J. Erlich, E. Katz, D. T. Son and M. A. Stephanov, *QCD and a holographic model of hadrons*, *Phys. Rev. Lett.* **95** (2005) 261602 [hep-ph/0501128].

[35] U. Gürsoy and E. Kiritsis, *Exploring improved holographic theories for QCD: Part I*, *JHEP* **02** (2008) 032 [0707.1324].

[36] U. Gürsoy, E. Kiritsis and F. Nitti, *Exploring improved holographic theories for QCD: Part II*, *JHEP* **02** (2008) 019 [0707.1349].

[37] M. Jarvinen and E. Kiritsis, *Holographic Models for QCD in the Veneziano Limit*, *JHEP* **03** (2012) 002 [1112.1261].

[38] Z. Komargodski, *Baryons as Quantum Hall Droplets*, 1812.09253.

[39] D. Gaiotto, A. Kapustin, Z. Komargodski and N. Seiberg, *Theta, Time Reversal, and Temperature*, *JHEP* **05** (2017) 091 [1703.00501].

[40] I. I. Kogan, *Axions, monopoles and cosmic strings*, in *International Workshop on Supersymmetry and Unification of Fundamental Interactions (SUSY 93)*, 5, 1993, hep-ph/9305307.

[41] G. Gabadadze and M. A. Shifman, *Vacuum structure and the axion walls in gluodynamics and QCD with light quarks*, *Phys. Rev. D* **62** (2000) 114003 [hep-ph/0007345].

[42] M. M. Forbes and A. R. Zhitnitsky, *Domain walls in QCD*, *JHEP* **10** (2001) 013 [hep-ph/0008315].

[43] D. T. Son, M. A. Stephanov and A. R. Zhitnitsky, *Domain walls of high density QCD*, *Phys. Rev. Lett.* **86** (2001) 3955 [hep-ph/0012041].

[44] G. Gabadadze and M. Shifman, *QCD vacuum and axions: What's happening?*, *Int. J. Mod. Phys. A* **17** (2002) 3689 [hep-ph/0206123].

[45] Y.-L. Ma, M. A. Nowak, M. Rho and I. Zahed, *Baryon as a Quantum Hall Droplet and the Cheshire Cat Principle*, *Phys. Rev. Lett.* **123** (2019) 172301 [1907.00958].

[46] A. Karasik, *Skyrmions, Quantum Hall Droplets, and one current to rule them all*, *SciPost Phys.* **9** (2020) 008 [2003.07893].

[47] Y.-L. Ma and M. Rho, *Dichotomy of Baryons as Quantum Hall Droplets and Skyrmions: Topological Structure of Dense Matter*, *Symmetry* **13** (2021) 1888 [2009.09219].

[48] A. Karasik, *Vector dominance, one flavored baryons, and QCD domain walls from the "hidden" Wess-Zumino term*, *SciPost Phys.* **10** (2021) 138 [2010.10544].

[49] R. Kitano and R. Matsudo, *Vector mesons on the wall*, *JHEP* **03** (2021) 023 [2011.14637].

[50] H. Nastase and J. Sonnenschein, *Charged soliton of the three-dimensional CS+BI Abelian gauge theory*, *Phys. Rev. D* **107** (2023) 125011 [2210.06581].

[51] F. Lin and Y.-L. Ma, *Baryons as vortexes on the η' domain wall*, *JHEP* **05** (2024) 270 [2310.16438].

[52] M. Rho, *The smile of Cheshire Cat at high density*, *J. Subatomic Part. Cosmol.* **1-2** (2024) 100001 [2408.00692].

[53] J. M. Lattimer and M. Prakash, *The physics of neutron stars*, *Science* **304** (2004) 536 [astro-ph/0405262].

[54] E. Annala, T. Gorda, A. Kurkela, J. Nättilä and A. Vuorinen, *Evidence for quark-matter cores in massive neutron stars*, *Nature Phys.* **16** (2020) 907 [1903.09121].

[55] E. Annala, T. Gorda, E. Katerini, A. Kurkela, J. Nättilä, V. Paschalidis et al., *Multimessenger Constraints for Ultradense Matter*, *Phys. Rev. X* **12** (2022) 011058 [2105.05132].

[56] E. Annala, T. Gorda, J. Hirvonen, O. Komoltsev, A. Kurkela, J. Nättilä et al., *Strongly interacting matter exhibits deconfined behavior in massive neutron stars*, *Nature Commun.* **14** (2023) 8451 [2303.11356].

[57] R. F. Sawyer, *Bulk viscosity of hot neutron-star matter and the maximum rotation rates of neutron stars*, *Phys. Rev. D* **39** (1989) 3804.

[58] P. Haensel and R. Schaeffer, *Bulk viscosity of hot-neutron-star matter from direct URCA processes*, *Phys. Rev. D* **45** (1992) 4708.

[59] P. Haensel, K. P. Levenfish and D. G. Yakovlev, *Bulk viscosity in superfluid neutron star cores. I. direct urca processes in npe mu matter*, *Astron. Astrophys.* **357** (2000) 1157 [astro-ph/0004183].

[60] B. A. Sa'd, I. A. Shovkovy and D. H. Rischke, *Bulk viscosity of spin-one color superconductors with two quark flavors*, *Phys. Rev. D* **75** (202107) 065016 [astro-ph/0607643].

[61] B. A. Sa'd, I. A. Shovkovy and D. H. Rischke, *Bulk viscosity of strange quark matter: Urca versus non-leptonic processes*, *Phys. Rev. D* **75** (2007) 125004 [astro-ph/0703016].

[62] M. G. Alford and A. Schmitt, *Bulk viscosity in 2SC quark matter*, *J. Phys. G* **34** (2007) 67 [nucl-th/0608019].

[63] M. G. Alford, M. Braby and A. Schmitt, *Bulk viscosity in kaon-condensed color-flavor locked quark matter*, *J. Phys. G* **35** (2008) 115007 [0806.0285].

[64] M. G. Alford and S. P. Harris, *Damping of density oscillations in neutrino-transparent nuclear matter*, *Phys. Rev. C* **100** (2019) 035803 [1907.03795].

[65] M. Alford, A. Harutyunyan and A. Sedrakian, *Bulk viscosity of baryonic matter with trapped neutrinos*, *Phys. Rev. D* **100** (2019) 103021 [1907.04192].

[66] M. G. Alford, A. Haber and Z. Zhang, *Isospin equilibration in neutron star mergers*, *Phys. Rev. C* **109** (2024) 055803 [2306.06180].

[67] Y. Yang, M. Hippert, E. Speranza and J. Noronha, *Far-from-equilibrium bulk-viscous transport coefficients in neutron star mergers*, *Phys. Rev. C* **109** (2024) 015805 [2309.01864].

[68] A. Schmitt and P. Shternin, *Reaction rates and transport in neutron stars*, *Astrophys. Space Sci. Libr.* **457** (2018) 455 [1711.06520].

[69] M. Alford, S. Mahmoodifar and K. Schwenzer, *Viscous damping of r-modes: Small amplitude instability*, *Phys. Rev. D* **85** (2012) 024007 [1012.4883].

[70] M. G. Alford and K. Schwenzer, *What the Timing of Millisecond Pulsars Can Teach us about Their Interior*, *Phys. Rev. Lett.* **113** (2014) 251102 [1310.3524].

[71] M. G. Alford and S. Han, *Characteristics of hybrid compact stars with a sharp hadron-quark interface*, *Eur. Phys. J. A* **52** (2016) 62 [1508.01261].

[72] M. Sieniawska and M. Bejger, *Continuous gravitational waves from neutron stars: current status and prospects*, *Universe* **5** (2019) 217 [1909.12600].

[73] J. L. Ripley, A. Hegade K. R., R. S. Chandramouli and N. Yunes, "First constraint on the dissipative tidal deformability of neutron stars." 12, 2023.

[74] M. G. Alford, L. Bovard, M. Hanauske, L. Rezzolla and K. Schwenzer, *Viscous Dissipation and Heat Conduction in Binary Neutron-Star Mergers*, *Phys. Rev. Lett.* **120** (2018) 041101 [1707.09475].

[75] D. Radice, S. Bernuzzi, A. Perego and R. Haas, *A new moment-based general-relativistic neutrino-radiation transport code: Methods and first applications to neutron star mergers*, *Mon. Not. Roy. Astron. Soc.* **512** (2022) 1499 [2111.14858].

[76] P. Hammond, I. Hawke and N. Andersson, *Impact of nuclear reactions on gravitational waves from neutron star mergers*, *Phys. Rev. D* **107** (2023) 043023 [2205.11377].

[77] E. R. Most, A. Haber, S. P. Harris, Z. Zhang, M. G. Alford and J. Noronha, *Emergence of Microphysical Bulk Viscosity in Binary Neutron Star Postmerger Dynamics*, *Astrophys. J. Lett.* **967** (2024) L14 [2207.00442].

[78] M. Alford, A. Harutyunyan and A. Sedrakian, *Bulk Viscosity of Relativistic npeμ Matter in Neutron-Star Mergers*, *Particles* **5** (2022) 361 [2209.04717].

[79] M. Chabanov and L. Rezzolla, "Impact of bulk viscosity on the post-merger gravitational-wave signal from merging neutron stars." 7, 2023.

[80] M. Chabanov and L. Rezzolla, "Numerical modelling of bulk viscosity in neutron stars." 11, 2023.

[81] C. Hoyos, N. Jokela and A. Vuorinen, *Holographic approach to compact stars and their binary mergers*, *Prog. Part. Nucl. Phys.* **126** (2022) 103972 [2112.08422].

[82] M. Järvinen, *Holographic modeling of nuclear matter and neutron stars*, *Eur. Phys. J. C* **82** (2022) 282 [2110.08281].

[83] J. Cruz Rojas, T. Gorda, C. Hoyos, N. Jokela, M. Järvinen, A. Kurkela et al., *Estimate for the bulk viscosity of strongly coupled quark matter*, 2402.00621.

[84] H. Heiselberg, J. Madsen and K. Riisager, *Strange Quark Decay Rates in Quark Matter at High Temperatures*, *Phys. Scripta* **34** (1986) 556.

[85] H. Heiselberg, *The Weak conversion rate in quark matter*, *Phys. Scripta* **46** (1992) 485.

[86] J. Madsen, *Rate of the weak reaction s + u to u + d in quark matter*, *Phys. Rev. D* **47** (1993) 325.

[87] F. Gliozzi and P. Provero, *When QCD strings can break*, *Nucl. Phys. Proc. Suppl.* **83** (2000) 461 [hep-lat/9907023].

[88] E. Witten, *Current Algebra Theorems for the U(1) Goldstone Boson*, *Nucl. Phys. B* **156** (1979) 269.

[89] G. Veneziano, *U(1) Without Instantons*, *Nucl. Phys. B* **159** (1979) 213.

[90] E. Witten, *Current Algebra, Baryons, and Quark Confinement*, *Nucl. Phys. B* **223** (1983) 433.

[91] G. H. Derrick, *Comments on nonlinear wave equations as models for elementary particles*, *J. Math. Phys.* **5** (1964) 1252.

[92] T. H. R. Skyrme, *A Nonlinear field theory*, *Proc. Roy. Soc. Lond. A* **260** (1961) 127.

[93] R. Peccei and H. Quinn, *Cp conservation in the presence of instantons*, *Phys. Rev. Lett.* **38** (1977) 1440.

[94] L. Di Luzio, M. Giannotti, E. Nardi and L. Visinelli, *The landscape of QCD axion models*, *Phys. Rept.* **870** (2020) 1 [2003.01100].

[95] J. E. Kim, *Weak interaction singlet and strong cp invariance*, *Phys. Rev. Lett.* **43** (1979) 103.

[96] M. Shifman, A. Vainshtein and V. Zakharov, *Can confinement ensure natural cp invariance of strong interactions?*, *Nucl. Phys. B* **166** (1980) 493.

[97] M. A. Stephanov, *Qcd phase diagram: an overview*, *International Journal of Modern Physics A* (2006) .

[98] K. Fukushima and T. Hatsuda, *The phase diagram of dense qcd*, *Reports on Progress in Physics* **74** (2011) 014001.

[99] G. Baym, T. Hatsuda, T. Kojo, P. D. Powell, Y. Song and T. Takatsuka, *From quarks to neutron stars: A review of dense matter*, *Reports on Progress in Physics* **81** (2018) 056902.

[100] M. Oertel, M. Hempel, T. Klähn and S. Typel, *Equations of state for supernovae and compact stars*, *Reviews of Modern Physics* **89** (2017) 015007.

[101] M. G. Alford, A. Schmitt, K. Rajagopal and T. Schäfer, *Color superconductivity in dense quark matter*, *Reviews of Modern Physics* **80** (2008) 1455.

[102] C. Hoyos, N. Jokela, M. Järvinen, J. G. Subils, J. Tarrío and A. Vuorinen, *Transport in strongly coupled quark matter*, *Phys. Rev. Lett.* **125** (2020) 241601 [`2005.14205`].

[103] K. Schwenzer, *How long-range interactions tune the damping in compact stars*, `1212.5242`.

[104] C. Naya and P. Sutcliffe, *Skyrmions and clustering in light nuclei*, *Phys. Rev. Lett.* **121** (2018) 232002 [`1811.02064`].

[105] D. Gaiotto, Z. Komargodski and N. Seiberg, *Time-reversal breaking in QCD_4, walls, and dualities in 2 + 1 dimensions*, *JHEP* **01** (2018) 110 [`1708.06806`].

[106] D. Gaiotto, A. Kapustin, N. Seiberg and B. Willett, *Generalized Global Symmetries*, *JHEP* **02** (2015) 172 [`1412.5148`].

[107] S. Schafer-Nameki, *ICTP lectures on (non-)invertible generalized symmetries*, *Phys. Rept.* **1063** (2024) 1 [`2305.18296`].

[108] C. Vafa and E. Witten, *Parity Conservation in QCD*, *Phys. Rev. Lett.* **53** (1984) 535.

[109] P.-S. Hsin and N. Seiberg, *Level/rank Duality and Chern-Simons-Matter Theories*, *JHEP* **09** (2016) 095 [`1607.07457`].

[110] S. Zhang, T. Hansson and S. Kivelson, *Effective-field-theory model for the fractional quantum hall effect*, *Physical Review Letters* **62** (1989) 82.

[111] X.-G. Wen, *Theory of the edge states in fractional quantum hall effects*, *International Journal of Modern Physics B* **6** (1992) 1711.

[112] R. Floreanini and R. Jackiw, *Selfdual Fields as Charge Density Solitons*, *Phys. Rev. Lett.* **59** (1987) 1873.

[113] A. Karch and E. Katz, *Adding flavor to AdS / CFT*, *JHEP* **06** (2002) 043 [hep-th/0205236].

[114] G. W. Gibbons and K.-i. Maeda, *Black Holes and Membranes in Higher Dimensional Theories with Dilaton Fields*, *Nucl. Phys. B* **298** (1988) 741.

[115] D. Garfinkle, G. T. Horowitz and A. Strominger, *Charged black holes in string theory*, *Phys. Rev. D* **43** (1991) 3140.

[116] G. T. Horowitz and A. Strominger, *Black strings and P-branes*, *Nucl. Phys. B* **360** (1991) 197.

[117] J. Polchinski, *Dirichlet Branes and Ramond-Ramond charges*, *Phys. Rev. Lett.* **75** (1995) 4724 [hep-th/9510017].

[118] M. Bianchi, D. Z. Freedman and K. Skenderis, *Holographic renormalization*, *Nucl. Phys. B* **631** (2002) 159 [hep-th/0112119].

[119] K. Skenderis, *Lecture notes on holographic renormalization*, *Class. Quant. Grav.* **19** (2002) 5849 [hep-th/0209067].

[120] P. Breitenlohner and D. Z. Freedman, *Positive Energy in anti-De Sitter Backgrounds and Gauged Extended Supergravity*, *Phys. Lett. B* **115** (1982) 197.

[121] P. Breitenlohner and D. Z. Freedman, *Stability in Gauged Extended Supergravity*, *Annals Phys.* **144** (1982) 249.

[122] J. M. Maldacena, *Wilson loops in large N field theories*, *Phys. Rev. Lett.* **80** (1998) 4859 [hep-th/9803002].

[123] J. Polchinski and M. J. Strassler, *Hard scattering and gauge/string duality*, *Phys. Rev. Lett.* **88** (2002) 031601 [hep-th/0109174].

[124] H. Boschi-Filho and N. R. F. Braga, *Qcd/string holographic mapping and glueball mass spectrum*, *Eur. Phys. J. C* **32** (2004) 529 [hep-th/0209080].

[125] L. Da Rold and A. Pomarol, *Chiral symmetry breaking from five dimensional spaces*, *Nucl. Phys. B* **721** (2005) 79 [hep-ph/0501218].

[126] A. Karch, E. Katz, D. T. Son and M. A. Stephanov, *Linear confinement and ads/qcd*, *Phys. Rev. D* **74** (2006) 015005 [hep-ph/0602229].

[127] J. Erdmenger, N. Evans, I. Kirsch and E. Threlfall, *Mesons in Gauge/Gravity Duals - A Review*, *Eur. Phys. J. A* **35** (2008) 81 [0711.4467].

[128] M. Bertolini, P. Di Vecchia, M. Frau, A. Lerda and R. Marotta, *N=2 gauge theories on systems of fractional D3/D7 branes*, *Nucl. Phys. B* **621** (2002) 157 [hep-th/0107057].

[129] M. Grana and J. Polchinski, *Gauge / gravity duals with holomorphic dilaton*, *Phys. Rev. D* **65** (2002) 126005 [hep-th/0106014].

[130] R. C. Myers, *Dielectric branes*, *JHEP* **12** (1999) 022 [hep-th/9910053].

[131] F. Bigazzi, A. L. Cotrone and R. Sisca, *Notes on Theta Dependence in Holographic Yang-Mills*, *JHEP* **08** (2015) 090 [1506.03826].

[132] F. Bigazzi and A. L. Cotrone, *Holographic QCD with Dynamical Flavors*, *JHEP* **01** (2015) 104 [1410.2443].

[133] M. B. Green, J. A. Harvey and G. W. Moore, *I-brane inflow and anomalous couplings on d-branes*, *Class. Quant. Grav.* **14** (1997) 47 [hep-th/9605033].

[134] L. Bartolini, F. Bigazzi, S. Bolognesi, A. L. Cotrone and A. Manenti, *Theta dependence in Holographic QCD*, *JHEP* **02** (2017) 029 [1611.00048].

[135] O. Aharony and D. Kutasov, *Holographic Duals of Long Open Strings*, *Phys. Rev. D* **78** (2008) 026005 [0803.3547].

[136] K. Hashimoto, T. Hirayama, F.-L. Lin and H.-U. Yee, *Quark Mass Deformation of Holographic Massless QCD*, *JHEP* **07** (2008) 089 [0803.4192].

[137] S. Vandoren and P. van Nieuwenhuizen, *Lectures on instantons*, 0802.1862.

[138] S. W. Hawking and D. N. Page, *Thermodynamics of Black Holes in anti-De Sitter Space*, *Commun. Math. Phys.* **87** (1983) 577.

[139] O. Aharony, J. Sonnenschein and S. Yankielowicz, *A Holographic model of deconfinement and chiral symmetry restoration*, *Annals Phys.* **322** (2007) 1420 [hep-th/0604161].

[140] F. Bigazzi, A. Caddeo, A. L. Cotrone, P. Di Vecchia and A. Marzolla, *The Holographic QCD Axion*, *JHEP* **12** (2019) 056 [1906.12117].

[141] R. Argurio, M. Bertolini, F. Bigazzi, A. L. Cotrone and P. Niro, *QCD domain walls, Chern-Simons theories and holography*, *JHEP* **09** (2018) 090 [1806.08292].

[142] E. Witten, *Theta dependence in the large N limit of four-dimensional gauge theories*, *Phys. Rev. Lett.* **81** (1998) 2862 [hep-th/9807109].

[143] S. Dubovsky, A. Lawrence and M. M. Roberts, *Axion monodromy in a model of holographic gluodynamics*, *JHEP* **02** (2012) 053 [1105.3740].

[144] M. Reece, *TASI Lectures: (No) Global Symmetries to Axion Physics*, *PoS* **TASI2022** (2024) 008 [2304.08512].

[145] E. Antonyan, J. A. Harvey, S. Jensen and D. Kutasov, *NJL and QCD from string theory*, hep-th/0604017.

[146] A. Vilenkin and E. P. S. Shellard, *Cosmic Strings and Other Topological Defects*. Cambridge University Press, 7, 2000.

[147] T. W. B. Kibble, *Topology of Cosmic Domains and Strings*, *J. Phys. A* **9** (1976) 1387.

[148] A. Vilenkin, *Cosmic Strings and Domain Walls*, *Phys. Rept.* **121** (1985) 263.

[149] T. Vachaspati and A. Vilenkin, *Formation and Evolution of Cosmic Strings*, *Phys. Rev. D* **30** (1984) 2036.

[150] T. Vachaspati and A. Vilenkin, *Evolution of cosmic networks*, *Phys. Rev. D* **35** (1987) 1131.

[151] B. Carter and X. Martin, *Dynamic instability criterion for circular (Vorton) string loops*, *Annals Phys.* **227** (1993) 151 [hep-th/0306111].

[152] M. Gorghetto, E. Hardy and G. Villadoro, *Axions from Strings: the Attractive Solution*, *JHEP* **07** (2018) 151 [1806.04677].

[153] R. H. Brandenberger, B. Carter, A.-C. Davis and M. Trodden, *Cosmic vortons and particle physics constraints*, *Phys. Rev. D* **54** (1996) 6059 [hep-ph/9605382].

[154] C. J. A. P. Martins and E. P. S. Shellard, *Vorton formation*, *Phys. Rev. D* **57** (1998) 7155 [hep-ph/9804378].

[155] C. J. A. P. Martins and E. P. S. Shellard, *Limits on cosmic chiral vortons*, *Phys. Lett. B* **445** (1998) 43 [hep-ph/9806480].

[156] B. Carter and A.-C. Davis, *Chiral vortons and cosmological constraints on particle physics*, *Phys. Rev. D* **61** (2000) 123501 [hep-ph/9910560].

[157] P. Agrawal, A. Hook, J. Huang and G. Marques-Tavares, *Axion string signatures: a cosmological plasma collider*, *JHEP* **01** (2022) 103 [2010.15848].

[158] M. Ibe, S. Kobayashi, Y. Nakayama and S. Shirai, *On Stability of Fermionic Superconducting Current in Cosmic String*, *JHEP* **05** (2021) 217 [2102.05412].

[159] Y. Abe, Y. Hamada, K. Saji and K. Yoshioka, *Quantum current dissipation in superconducting strings and vortons*, *JHEP* **02** (2023) 004 [2209.03223].

[160] Y. B. Zeldovich, I. Y. Kobzarev and L. B. Okun, *Cosmological consequences of the spontaneous breakdown of discrete symmetry*, *Zh. Eksp. Teor. Fiz.* **67** (1974) 3.

[161] P. Sikivie, *Of axions, domain walls and the early universe*, *Physical Review Letters* **48** (1982) 1156.

[162] A. R. Zhitnitsky, *'Nonbaryonic' dark matter as baryonic color superconductor*, *JCAP* **10** (2003) 010 [hep-ph/0202161].

[163] X. Liang and A. Zhitnitsky, *Axion field and the quark nugget's formation at the QCD phase transition*, *Phys. Rev. D* **94** (2016) 083502 [1606.00435].

[164] O. Bergman and G. Lifschytz, *Holographic U(1)(A) and String Creation*, *JHEP* **04** (2007) 043 [hep-th/0612289].

[165] K. Hashimoto, T. Sakai and S. Sugimoto, *Holographic Baryons: Static Properties and Form Factors from Gauge/String Duality*, *Prog. Theor. Phys.* **120** (2008) 1093 [0806.3122].

[166] M. Kruczenski, R. C. Myers, A. W. Peet and D. J. Winters, *Aspects of supertubes*, *JHEP* **05** (2002) 017 [hep-th/0204103].

[167] D. Freed, J. A. Harvey, R. Minasian and G. W. Moore, *Gravitational anomaly cancellation for M theory five-branes*, *Adv. Theor. Math. Phys.* **2** (1998) 601 [hep-th/9803205].

[168] K. Becker and M. Becker, *Five-brane gravitational anomalies*, *Nucl. Phys. B* **577** (2000) 156 [hep-th/9911138].

[169] A. Boyarsky, J. A. Harvey and O. Ruchayskiy, *A Toy model of the M5-brane: Anomalies of monopole strings in five dimensions*, *Annals Phys.* **301** (2002) 1 [hep-th/0203154].

[170] J. A. Harvey, *TASI 2003 lectures on anomalies*, 9, 2005, hep-th/0509097.

[171] I. S. Gradshteyn, I. M. Ryzhik, A. Jeffrey and D. Zwillinger, *Tables of Integrals, Series, and Products*. Academic Press, USA, 6th ed., 2000.

[172] C. G. Callan and J. M. Maldacena, *Brane death and dynamics from the Born-Infeld action*, *Nucl. Phys. B* **513** (1998) 198 [hep-th/9708147].

[173] L. Thorlacius, *Born-Infeld string as a boundary conformal field theory*, *Phys. Rev. Lett.* **80** (1998) 1588 [hep-th/9710181].

[174] G. W. Gibbons, *Born-Infeld particles and Dirichlet p-branes*, *Nucl. Phys. B* **514** (1998) 603 [hep-th/9709027].

[175] S. Lee, A. W. Peet and L. Thorlacius, *Brane waves and strings*, *Nucl. Phys. B* **514** (1998) 161 [hep-th/9710097].

[176] A. Hashimoto, *The Shape of branes pulled by strings*, *Phys. Rev. D* **57** (1998) 6441 [hep-th/9711097].

[177] M. Fujita, W. Li, S. Ryu and T. Takayanagi, *Fractional quantum hall effect via holography: Chern-simons, edge states and hierarchy*, *Journal of High Energy Physics* **2009** (2009) 066–066.

[178] Y. Hikida, W. Li and T. Takayanagi, *ABJM with Flavors and FQHE*, *JHEP* **07** (2009) 065 [0903.2194].

[179] B. S. Acharya and C. Vafa, *On domain walls of N=1 supersymmetric Yang-Mills in four-dimensions*, hep-th/0103011.

[180] S. Elitzur, G. W. Moore, A. Schwimmer and N. Seiberg, *Remarks on the Canonical Quantization of the Chern-Simons-Witten Theory*, *Nucl. Phys. B* **326** (1989) 108.

[181] D. Mateos and P. K. Townsend, *Supertubes*, *Phys. Rev. Lett.* **87** (2001) 011602 [hep-th/0103030].

[182] D. Tong, *A gauge theory for shallow water*, *SciPost Phys.* **14** (2023) 102 [2209.10574].

[183] H. B. Nielsen and P. Olesen, *Vortex Line Models for Dual Strings*, *Nucl. Phys. B* **61** (1973) 45.

[184] R. Jackiw, K.-M. Lee and E. J. Weinberg, *Selfdual Chern-Simons solitons*, *Phys. Rev. D* **42** (1990) 3488.

[185] S. Bolognesi and S. B. Gudnason, *A Note on Chern-Simons solitons: A Type III vortex from the wall vortex*, *Nucl. Phys. B* **805** (2008) 104 [0711.3803].

[186] D. Tong, *TASI lectures on solitons: Instantons, monopoles, vortices and kinks*, in *Theoretical Advanced Study Institute in Elementary Particle Physics: Many Dimensions of String Theory*, 6, 2005, hep-th/0509216.

[187] P. A. Horvathy and P. Zhang, *Vortices in (abelian) Chern-Simons gauge theory*, *Phys. Rept.* **481** (2009) 83 [0811.2094].

[188] X. G. Wen, *Quantum field theory of many-body systems: From the origin of sound to an origin of light and electrons*. 2004.

[189] D. Tong, *Lectures on the Quantum Hall Effect*, 6, 2016, 1606.06687.

[190] R. Arouca, A. Cappelli and T. H. Hansson, *Quantum Field Theory Anomalies in Condensed Matter Physics*, *SciPost Phys. Lect. Notes* **62** (2022) 1 [2204.02158].

[191] R. Emparan, D. Mateos and P. K. Townsend, *Supergravity supertubes*, *JHEP* **07** (2001) 011 [hep-th/0106012].

[192] D. Mateos, S. Ng and P. K. Townsend, *Tachyons, supertubes and brane / anti-brane systems*, *JHEP* **03** (2002) 016 [hep-th/0112054].

[193] Y. Hamada and W. Nakano, *Gravitational wave spectrum from expanding string loops on domain walls: Implication for nanohertz pulsar timing array signals*, *Phys. Rev. D* **110** (2024) 083513 [2405.09599].

[194] C. G. Callan, Jr. and I. R. Klebanov, *Bound State Approach to Strangeness in the Skyrme Model*, *Nucl. Phys. B* **262** (1985) 365.

[195] S. Seki and J. Sonnenschein, *Comments on Baryons in Holographic QCD*, *JHEP* **01** (2009) 053 [0810.1633].

[196] T. D. Brennan, S. Hong and L.-T. Wang, *Coupling a Cosmic String to a TQFT*, *JHEP* **03** (2024) 145 [2302.00777].

[197] F. Bigazzi, A. Caddeo, A. L. Cotrone and A. Paredes, *Dark Holograms and Gravitational Waves*, *JHEP* **04** (2021) 094 [2011.08757].

[198] F. Bigazzi, A. Caddeo, A. L. Cotrone and A. Paredes, *Fate of false vacua in holographic first-order phase transitions*, *JHEP* **12** (2020) 200 [2008.02579].

[199] F. Bigazzi, A. Caddeo, T. Canneti and A. L. Cotrone, *Bubble wall velocity at strong coupling*, *JHEP* **08** (2021) 090 [2104.12817].

[200] G. Mandal and T. Morita, *Gregory-Laflamme as the confinement/deconfinement transition in holographic QCD*, *JHEP* **09** (2011) 073 [1107.4048].

[201] S. Blasi and A. Mariotti, *Domain Walls Seeding the Electroweak Phase Transition*, *Phys. Rev. Lett.* **129** (2022) 261303 [2203.16450].

[202] S. Blasi, R. Jinno, T. Konstandin, H. Rubira and I. Stomberg, *Gravitational waves from defect-driven phase transitions: domain walls*, *JCAP* **10** (2023) 051 [2302.06952].

[203] S. Blasi and A. Mariotti, *QCD Axion Strings or Seeds?*, 2405.08060.

[204] A. Prakash, D. Radice, D. Logoteta, A. Perego, V. Nedora, I. Bombaci et al., *Signatures of deconfined quark phases in binary neutron star mergers*, *Phys. Rev. D* **104** (2021) 083029 [2106.07885].

[205] S. Tootle, C. Ecker, K. Topolski, T. Demircik, M. Järvinen and L. Rezzolla, *Quark formation and phenomenology in binary neutron-star mergers using V-QCD*, *SciPost Phys.* **13** (2022) 109 [2205.05691].

[206] A. Czajka, K. Dasgupta, C. Gale, S. Jeon, A. Misra, M. Richard et al., *Bulk Viscosity at Extreme Limits: From Kinetic Theory to Strings*, *JHEP* **07** (2019) 145 [1807.04713].

[207] C. Hoyos, N. Jokela, M. Järvinen, J. G. Subils, J. Tarrío and A. Vuorinen, *Holographic approach to transport in dense QCD matter*, *Phys. Rev. D* **105** (2022) 066014 [2109.12122].

[208] L. Bartolini, S. B. Gudnason, J. Leutgeb and A. Rebhan, *Neutron stars and phase diagram in a hard-wall AdS/QCD model*, *Phys. Rev. D* **105** (2022) 126014 [2202.12845].

[209] M. Järvinen, E. Kiritsis, F. Nitti and E. Préau, *Holographic neutrino transport in dense strongly-coupled matter*, *JHEP* **11** (2023) 139 [2306.00192].

[210] M. Aleixo, C. H. Lenzi, W. de Paula and R. da Rocha, *Quark stars in D_3–D_7 holographic model*, *Eur. Phys. J. C* **84** (2024) 253 [2310.17719].

[211] C. Hoyos, D. Rodríguez Fernández, N. Jokela and A. Vuorinen, *Holographic quark matter and neutron stars*, *Phys. Rev. Lett.* **117** (2016) 032501 [1603.02943].

[212] E. Annala, C. Ecker, C. Hoyos, N. Jokela, D. Rodríguez Fernández and A. Vuorinen, *Holographic compact stars meet gravitational wave constraints*, *JHEP* **12** (2018) 078 [1711.06244].

[213] K. Bitaghsir Fadafan, J. Cruz Rojas and N. Evans, *Deconfined, Massive Quark Phase at High Density and Compact Stars: A Holographic Study*, *Phys. Rev. D* **101** (2020) 126005 [1911.12705].

[214] K. Bitaghsir Fadafan, J. Cruz Rojas and N. Evans, *Holographic quark matter with colour superconductivity and a stiff equation of state for compact stars*, *Phys. Rev. D* **103** (2021) 026012 [2009.14079].

[215] N. Jokela, M. Järvinen and J. Remes, *Holographic QCD in the Veneziano limit and neutron stars*, *JHEP* **03** (2019) 041 [1809.07770].

[216] C. Ecker, M. Järvinen, G. Nijs and W. van der Schee, *Gravitational waves from holographic neutron star mergers*, *Phys. Rev. D* **101** (2020) 103006 [1908.03213].

[217] N. Jokela, M. Järvinen, G. Nijs and J. Remes, *Unified weak and strong coupling framework for nuclear matter and neutron stars*, *Phys. Rev. D* **103** (2021) 086004 [2006.01141].

[218] T. Demircik, C. Ecker and M. Järvinen, *Dense and Hot QCD at Strong Coupling*, *Phys. Rev. X* **12** (2022) 041012 [2112.12157].

[219] N. Jokela, M. Järvinen and J. Remes, *Holographic QCD in the NICER era*, *Phys. Rev. D* **105** (2022) 086005 [2111.12101].

[220] S. Pinkanjanarod and P. Burikham, *Massive neutron stars with holographic multiquark cores*, *Eur. Phys. J. C* **81** (2021) 705 [2007.10615].

[221] P. Burikham, S. Pinkanjanarod and S. Ponglertsakul, *Slowly rotating neutron star with holographic multiquark core: I-Love-Q relations*, *Phys. Rev. D* **105** (2022) 104018 [2111.00712].

[222] L. Bartolini and S. B. Gudnason, *Symmetry energy in holographic QCD*, *SciPost Phys.* **16** (2024) 156 [2209.14309].

[223] L. Bartolini and S. B. Gudnason, *Neutron stars in the Witten-Sakai-Sugimoto model*, *JHEP* **11** (2023) 209 [2307.11886].

[224] K. Zhang, T. Hirayama, L.-W. Luo and F.-L. Lin, *Compact Star of Holographic Nuclear Matter and GW170817*, *Phys. Lett. B* **801** (2020) 135176 [1902.08477].

[225] N. Kovensky and A. Schmitt, *Isospin asymmetry in holographic baryonic matter*, *SciPost Phys.* **11** (2021) 029 [2105.03218].

[226] N. Kovensky, A. Poole and A. Schmitt, *Building a realistic neutron star from holography*, *Phys. Rev. D* **105** (2022) 034022 [2111.03374].

[227] P. Burikham, E. Hirunsirisawat and S. Pinkanjanarod, *Thermodynamic Properties of Holographic Multiquark and the Multiquark Star*, *JHEP* **06** (2010) 040 [1003.5470].

[228] K. Ghoroku, K. Kashiwa, Y. Nakano, M. Tachibana and F. Toyoda, *Stiff equation of state for a holographic nuclear matter as instanton gas*, *Phys. Rev. D* **104** (2021) 126002 [2107.14450].

[229] L. A. H. Mamani, C. V. Flores and V. T. Zanchin, *Phase diagram and compact stars in a holographic QCD model*, *Phys. Rev. D* **102** (2020) 066006 [2006.09401].

[230] L. Zhang and M. Huang, *Holographic cold dense matter constrained by neutron stars*, *Phys. Rev. D* **106** (2022) 096028 [2209.00766].

[231] M. G. Alford and S. P. Harris, *Beta equilibrium in neutron star mergers*, *Phys. Rev. C* **98** (2018) 065806 [1803.00662].

[232] M. G. Alford, A. Haber, S. P. Harris and Z. Zhang, *Beta Equilibrium Under Neutron Star Merger Conditions*, *Universe* **7** (2021) 399 [2108.03324].

[233] M. Le Bellac, *Thermal Field Theory*, Cambridge Monographs on Mathematical Physics. Cambridge University Press, 3, 2011, 10.1017/CBO9780511721700.

[234] A. Cherman, T. D. Cohen and E. S. Werbos, *The Chiral condensate in holographic models of QCD*, *Phys. Rev. C* **79** (2009) 045203 [0804.1096].

[235] R. Alvares, C. Hoyos and A. Karch, *An improved model of vector mesons in holographic QCD*, *Phys. Rev. D* **84** (2011) 095020 [1108.1191].

[236] T. Faulkner, H. Liu, J. McGreevy and D. Vegh, *Emergent quantum criticality, Fermi surfaces, and AdS(2)*, *Phys. Rev. D* **83** (2011) 125002 [0907.2694].

[237] A. Gerhold, A. Ipp and A. Rebhan, *Non-Fermi-liquid specific heat of normal degenerate quark matter*, *Phys. Rev. D* **70** (2004) 105015 [hep-ph/0406087].

[238] T. Schäfer and K. Schwenzer, *Non-Fermi liquid effects in QCD at high density*, *Phys. Rev. D* **70** (2004) 054007 [hep-ph/0405053].

[239] C. Hoyos, N. Jokela and A. Olzi, *In preparation.*

[240] M. Taylor, *Lifshitz holography*, *Class. Quant. Grav.* **33** (2016) 033001 [1512.03554].

[241] R. B. Laughlin, *Anomalous quantum Hall effect: An Incompressible quantum fluid with fractionallycharged excitations*, *Phys. Rev. Lett.* **50** (1983) 1395.

[242] R. Bott and L. W. Tu, *Differential Forms in Algebraic Topology*. Springer, 1982, 10.1007/978-1-4757-3951-0.

[243] A. Hatcher, *Algebraic topology*. Cambridge Univ. Press, Cambridge, 2000.

[244] D. J. Simms, *J. milnor, morse theory, annals of mathematics studies 51 (princeton university press, 1963), vi + 153 pp., 24s*, *Proceedings of the Edinburgh Mathematical Society* **14** (1964) 84–84.